Diss. ETH N^o 19124

Hydro-mechanical characterization of rooted hillslope failure: from field investigations to fiber bundle modeling

A dissertation submitted to

ETH ZURICH

for the degree of

Doctor of Sciences

presented by

MASSIMILIANO SCHWARZ

Dott. Forestale ed ambientale, Universitá di Firenze

30.08.1980

citizen of

Uesslingen-Buch TG

accepted on the recommendation of

Prof. Dani Or
Prof. Hans Rudolf Heinimann
Dr. Denis Cohen
Ing. Albert Böll

2011

Aknowledgements

First I want to thank my advisor Prof. Dani Or, who allowed me to come in his group as Ph.D. student from a collaborating external institution (WSL). I consider the time spent at the EPFL and at the ETHZ a unique experience that strongly contributed to my formation as young scientist. It was a special experience to share opinions and knowledge in such a multidisciplinary group. I especially thank Prof. Dani Or for the interest that he shows in my work and for the numerous useful discussion that contribute to my professional development.

The studies discussed in this dissertation would have not been possible without the engagement and the professional work of Dr. Manfred Stähli, who was in chair of my group a the WSL and coordinator of the TRAMM project (of which this Ph.D. work is part). I have appreciated the thrust that he gave to me and his welfare.

A special thank goes to Dr. Denis Cohen. It has been an honor to collaborate with him. I appreciate all his contributions of time, ideas, and passion shared during the time in the office as well as in the free time. I realize the importance of how his approach to the research stimulate our work and made it productive. The joy and enthusiasm he has for his research was contagious and motivating for me, even during tough times in the Ph.D. pursuit. I am also thankful for the excellent example he has provided as a successful and rigorous scientist. Moreover, I appreciate and enjoy his friendship.

The members of the LASEP/STEP group have contributed immensely to my personal and professional time in Lausanne and in Zurich. In particular, I thank the STEP group that kindly shared the special moments of my life in the recent months.The group has been a source of friendships as well as good advice and collaboration. At the time of the LASEP group, I have had the pleasure to meet Prof. Ivan Lunati, who is for me the best example of a coherent science and moreover became an important friend.

In regards to the experimental assistance, I thank infinitely Carlotte Wyron, Gernot Michlmayr, Hans Wunderli and Daniel Breitenstein.

The collaborations within the TRAMM were the origin of nice and interesting contacts. In particular I appreciated the discussion with Cornelia Brönnimann, Amin Askarinejad, Gernot Michlmayr and Catherine Berger.

I want to thank Dr. Filippo Giadrossich that more then a nice scientific collaborator during the Ph.D., is a special friend since almost ten years.

I really appreciate the help of Albert Böll, Dr. Frank Graf and Christian Rickli, who followed me in the first months of the Ph.D. and contributed with important inputs to the definition and pursuit of this Work.

I would like to acknowledge the special meetings with honorary expert on landslides and root reinforcement such as Dr. Chris Phillips, Dr. Kevin Schmidt, Hans Peter Rauch, Prof. Federico Preti, Cristian Rickli, Dr. Paul Hallett, Dr. Luuk Dorren and Prof. Sarah Springmann.

Lastly, I would like to thank my family for all their love and encouragement. For my parents who raised me with a lot of efforts and supported me in my formation. For the presence of my brother Luca and his infinite patience. And most of all for my loving, supportive, encouraging, and patient wife Katharina whose faithful support during the final stages of this Ph.D. is so appreciated, and our daughter Marilie whose smile bring the sun everyday. Thank you.

Summary

The ability to monitor and possibly predict locations and conditions for onset of rapid mass movements are essential for mitigation and risk assessment in mountainous regions such as the Swiss Alps. Despite the ubiquity of such natural hazards, considerable gaps remain in basic understanding of triggering mechanisms and prediction of spatial extent of potentially unstable zones. Vegetation cover plays an important role in slope and bank stabilization through complex interactions between hydromechanics and biotic factors. Plant roots play important role in reducing damage of other natural hazards such as flooding and debris flows as related to slope and bank stability in catchments. This work attempts to improve understanding of triggering mechanisms of shallow landslides in vegetated slopes by proposing and testing a new modeling framework for the quantification of root reinforcement at various spatial scales from the single root to the stand. The study begins with a review of the state of the art of methods and models for quantifying root reinforcement highlighting knowledge gaps the must be addressed to advance understanding and provide more realistic estimates of the role of root reinforcement and modes of failure that are upscalable from the single root to forest stand. The primary knowledge gap lies in the need to consider dynamic mechanical behavior of lateral root reinforcement at different spatial scales requiring explicit estimates of root distribution and dynamic reinforcement.

Formulation of knowledge gaps paved the ways for implementation of mechanical and hydrological concepts within a new modeling framework that is spatially resolved from the tree to the stand scale. The modeling framework is comprised of two main modules: a first is concerned with estimation of root geometrical and distribution information (number per diameter class considering the distance and the dimension of tree stems), and a second module characterizes the mechanical behavior of root bundles (The Root Bundle Model). The numerical results of the model enable isolation of most influential variables on root reinforcement (such as root size distribution, root length, root branching patterns and root tortuousity) and provided guidance for a series of laboratory and field experiments for model calibration and validation. To this end, a novel experimental pullout device was constructed to measure force-displacement behavior of individual and bundles of roots. We used the device to collect data for calibrating the Root Bundle Model in well defined soil and root systems. Subsequently,

we performed field pullout tests using the same set up to determine pullout behavior of natural root bundles in forested soil profiles for model validation under natural conditions. We applied the modeling framework for two case studies illustrating the importance of spatial and dynamic characterization for realistic implementation of root reinforcement in assessment and analysis of shallow landslides triggering mechanisms.

The main outcomes of this work can be resume in three important conclusions:

- In many cases lateral root reinforcement contribute more than basal root reinforcement to the stability of shallow landslides with volumes smaller than 1000-2000 m^2 (depending on the situation).
- It is important to consider the progressive failure of root bundles to obtain realistic force-displacement characterization of root reinforcement, such as the Root Bundle Model does.
- The spatial characterization of root reinforcement at single tree scale is fundamental to understand and predict the triggering mechanisms of shallow landslides in vegetated slopes.

The presented methodology gives the possibility for the first time to upscale the mechanical effects of root reinforcement at the hillslope scale considering a realistic spatial characterization of its force-displacement behaviors. The implementation of such method in models for the simulation and prediction of shallow landslides represents an important advance because it allows the three dimensional quantification of forces redistribution in an unstable slope. Moreover, this methodology may be applied to the quantitative analysis of other important processes related to rooted-soil mechanics such as tree stability and rockfall interactions with trees.

From a practical point of view, the results of this work help to better quantify the role of protection forests. The proposed modeling framework represents for the managers and decision makers an important support tool for the evaluation and management of protection forests. For instance, in specific conditions of slopes subject to shallow landslides, it is now possible to define the minimal dimension of unstable masses and the typologies of forest structures that assure enough local root reinforcement. Based on such informations, the planing of eventual forest interventions can be evaluated quantitatively.

Riassunto

Il monitoraggio e la previsione di rapidi eventi gravitativi sono elementi importanti per la gestione dei pericoli naturali in regioni montane come l'arco alpino. Nonostante la sovente ricorrenza di tali eventi, molte rimangano le incertezze sui meccanismi base di formazione di tali fenomeni e pertanto sulla loro previsione spazio-temporale. I danni dovuti a pericoli naturali come piene e colate di fango sono molto spesso connessi ad altri processi piú a monte, come frane superficiali o stabilitá degli argini. In questo contesto, la vegetazione contribuisce alla stabilitá dei versanti tramite un complessa interazione tra effetti diretti ed indiretti. In questo lavoro vengono presentati risultati volti a migliorare la comprensione e la quantificazione dei meccanismi che portano alla formazione di frane superficiali sotto copertura vegetale e la descrizione di un nuovo metodo per la quantificazione del rinforzo radicale a diverse scale spaziali. Nella prima parte del lavoro viene fatta una revisione dello stato attuale delle conoscenze riguardo i metodi usati per la quantificazione del rinforzo radicale, individuando e discutendo quali sono le conoscenze fondamentali che mancano per lo sviluppo di una metodologia piú avanzata per la stima del rinforzo radicale (dalla singola radice a scala di pendio). La discussione di tale revisione a portato alla conclusione che l'aspetto dinamico del rinforzo laterale delle radici a differenti scale é l'aspetto piú importante che probabilmente é stato trascurato. A tale scopo, nuove funzioni per la stima della distribuzione delle radici e della dinamica di rinforzo sono risultate necessarie. Sulla base di questo primo studio, concetti di meccanica ed idrologia sono stati implementati in una nuova metodologia per la caratterizzazione della dinamica del rinforzo radicale considerando diverse scale di risoluzione. La metodologia presentata é costituita da due gruppi di funzioni: un primo gruppo di funzioni é stato sviluppato per la stima della distribuzione di radici laterali (numero per classe di diametro) considerando la distanza e le dimensioni degli alberi, mentre un secondo gruppo di funzioni é stato concepito per la caratterizzazione della dinamica del rinforzo radicale (il Root Bundle Model). I risultati di questo modello numerico hanno consentito l'individuazione dei parametri che influenzano in maniera fondamentale i risultati (tipo distribuzione dei diametri delle radici, lunghezza delle radici, tipo di biforcazioni delle radici e tortuositá delle radici), e di conseguenza ha consentito di pianificare in maniera oculata una serie di esperimenti di laboratorio ed in campo per la calibrazione e validazione del modello. A

questo punto si é presentata la necessitá di realizzare un nuovo tipo di strumentazione che consentisse di registrare la forza di trazione e lo spostamento di ogni singola radice di un fascio eterogeneo. L' uso di tale apparecchio in condizioni controllate di laboratorio ha consentito la calibrazione del "Root Bundle Model". La validazione del modello é stata fatta con esprimenti *in situ* testando fasci naturali di radici preparate in profili verticali del suolo. Infine, la nuova metodologia é stata testata in due casi di studio per valutarne l' applicazione nella previsione e l'analisi di frane superficiali in bosco. In questo modo si e' mostrato l'importanza di tale tipo di risultati per la gestione delle instabilitá di pendio nella pratica, ma anche l'importanza di quantificare l'influenza della vegetazione a livello scientifico per comprendere i meccanismi di formazione delle frane superficiali. In breve, le conclusioni piú importanti di questo studio possono essere riassunte nei seguenti punti:

- In molti casi il contributo laterale delle radici é piú importante di quello basale, soprattuto per frane con volumi minori di 1000-2000 m^3 (a seconda delle condizioni).
- É molto importante considerare la rottura progressiva di un fascio di radici per ottenere un caratterizzazione della dinamica del rinforzo radicale, come nel caso del "Root Bundle Model".
- La caratterizzazione spaziale del rinforzo radicale alla scala di singolo albero é fondamentale per comprendere e fare previsioni sui meccanismi di formazione delle frane superficiali in pendii vegetati.

La metodologia che viene qui presentata offre oggi la possibilitá per la prima volta di fare un' upscaling degli effetti meccanici del rinforzo radicale a scala di pendio, considerando una caratterizzazione spaziale della dinamica di tale rinforzo. L'implementazione di tale metodo in modelli per la simulazione e la previsione di frane superficiali consente il calcolo della ridistribuzione di forze in tre dimensioni durante la formazione di una frana. Inoltre, questo metodo puó essere applicato nelle analisi quantitative di altri importanti processi legati alla meccanica dei suoli radicati come l'instabilitá degli alberi dovuta all'impatto della caduta di sassi o a forti venti.

Da un punto di vista pratico, i risultati di questo lavoro aiutano a meglio quantificare il ruolo dei boschi di protezione e delle opere di ingegneria naturalistica. In particolare, il tipo di modello proposto rappresenta uno strumento unico per i gestori del territorio e selvicoltori per la valutazione e gestione dei boschi di protezione. Per esempio, in certe condizioni di pendii soggetti a smottamenti e frane, oggi é possibile definire le dimensioni

minime di possibili masse instabili e le tipologie di strutture forestali in grado di garantire localmente un rinforzo radicale sufficiente. Sulla base di tali informazioni é perció possibile pianificare eventuali interventi forestali in modo quantitativo.

.

Contents

Chapter 1

Introduction

Landslide cause many injuries, deaths, and damages around the world, affecting political decisions and management strategies. In mountainous areas, the effects of natural hazards are exacerbated by topography and limited accessibility. In Switzerland, debris flows and landslides occur regularly. About 8% of natural slopes are considered unstable [Romang et al., 2003]. With increases in population and tourism in this alpine region [Wehrli et al., 2007] risks due to natural hazards have increased significantly. On average, landslides in Switzerland cause more than 3 million Swiss francs of damage and kill 6 people per year [BAFU, 2010]. Landslides and related erosional processes have also important impacts difficult to quantify [Brang et al., 2006]. For example, the amount of sediment moved and deposited in a catchment is strongly related to its landslide and erosion activity. Thus, the intensity of debris flows and floods are indirectly related to hillslope and bank-stability processes.

The term landslide is generally used to describe a wide range of processes from large rock slides to small shallow landslides of soil. Various classification schemes based on dimensions, velocity, or source material have been proposed [van Asch et al., 2007]. Herein, we use the term shallow landslide to indicate a rapid mass movement of soil less than 2 meters deep. For those types of mass movements, vegetation is recognized to influence both the hydrology and the mechanics of the slope, affecting the susceptibility of the slope to landsliding.

In the context of slope stability, vegetation can have a positive effect on the hydrology of a hillslope by increasing interception, evapo-transpiration, drainage capacity and field capacity. Negative effects are stem flow, localized infiltration, and the creation of hydrological discontinuities in the soil profile. The positive effect of evapo-transpiration and interception are widely recognized, whereas the effects on drainage capacity are far behind

to be understood and quantified. From a mechanical point of view, vegetation has other positive effects such as root reinforcement, buttressing effects, arching effects, and, in some cases, better soil structure and aggregate stability. Negative effects are increased weight and wind throws solicitations, both not well understood. While negative mechanical effects are not always important or can often be neglected, positive effects such as root reinforcement may play an important role. Traditionally, only basal root reinforcement crossing the slope-parallel failure surface of a landslide was considered. In recent years the importance of lateral root reinforcement on the perimeter of the sliding mass was also recognized. As a general rule it is known that the stabilization effect of lateral root reinforcement is inversely proportional to the volume of the unstable mass. In Switzerland, many landslides are small ($\leq 400\ m^3$) [Rickli and Graf, 2009] and thus one expects vegetation to play a considerable role in lateral reinforcement.

In Switzerland 43% of the forest cover is classified as protection forest and about 15,000 ha of this forest (3.5%) is maintained by government subsidies every year [LFI3, 2010]. Protection forests are defined as forests whose primary function is the protection of people and assets against the impacts of natural hazards or adverse climate [Brang et al, 2007]. The Swiss government is heavily involved in the management of protection forests with investments in research and practical site interventions. In 2008, 97 million Swiss francs were spent for protection against natural hazards, and 60% of that amount was used for the management of protection forests [BAFU, 2010]. Switzerland is one of the first European countries that developed detailed guidelines for the management of protection forests on the basis of state-of-the-art scientific knowledge. Moreover, the interest in bioengineering techniques to stabilize slopes susceptible to landslide or erosion has increased all around the world in the last two decades. These techniques promote friendly environmental protection at low costs [Koch, 2003] and thus are more sustainable than traditional civil engineering techniques. For slope stabilization, bioengineering techniques are based on the use of natural materials such as stones, wood, and live plants. The effects of vegetation in bioengineering are generally considered to be limited to erosion control and stabilization of slopes that are less than 2 meters deep [Florineth, 2004]. Quantifying these effects still remains a difficult problem. Models proposed thus far yield controversial results and are either too crude or too complex for practical applications. For both the management of protection forests and for the planning of protection measures that use live plants, a good estimation of root reinforcement is very important and needs suitable models that can be considered in both academic and practical studies.

In the context of the TRAMM project [CCES, 2010], this Ph.D. fo-

cuses on the spatial and the dynamical quantification of root reinforcement from the scale of single root up to a forest stand (see Figure 1.1). As explained in more details in the introductions of the following chapters, the first important works on this topic were done in the '70 and '80 by Wu et al. [1979] and Waldron and Dekassian [1981] using simple approaches that found widespread applications in science and practice. Only recently, new advanced methods were introduced and discussed [Pollen and Simon, 2005; Mickovski et al., 2009], in particular the "Fiber Bundle Model". This model, first used by the material science community, allows a better estimation of the maximal root reinforcement and, more importantly, is able to characterize the force-displacement behaviors of bundles of roots (see Figure 1.2).

The characterization of the force-displacement behavior of root reinforcement is important because it permits to better understand the role of root networks in the triggering mechanisms of shallow landslides. However, not all experiments required to understand the capability of this new approach have been performed and not all possible extensions of the model have been tested yet. Therefore, new numerical and experimental results are presented in this work aiming to cover these gaps.

The main objective of this work was to extend the knowledge about the triggering mechanisms of shallow landslide on vegetated hillslopes using new experimental and modeling approaches. In particular, we aim to develop a quantitative framework for the characterization of the root dynamical reinforcement at scales that range from the single root to forest stands. In a logical series the fundamental steps to achieve this objective can be summarized as:

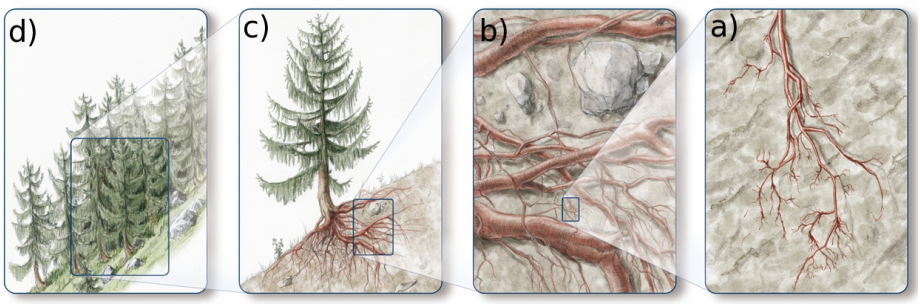

Figure 1.1: Illustration of upscaling sequence of root reinforcement considering scales ranging from a single root to a forest stand: [a] scale of a single root, [b] scale of a bundle of roots, [c] a single tree root system, and [d] scale of a forest stand on a hillslope. Part of Chapter 2.

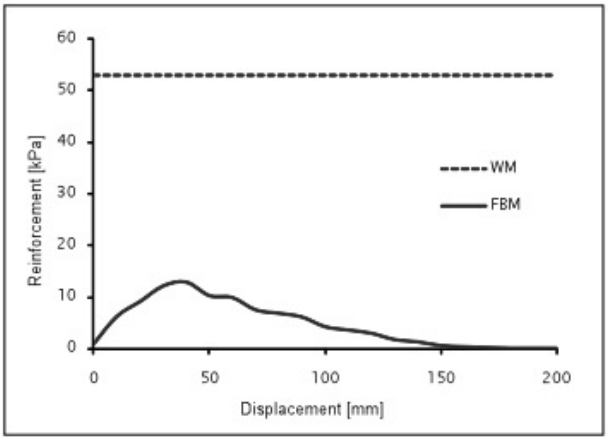

Figure 1.2: Example of tensile strength of a bundle of roots as a function of displacement. The graph shows the difference between Wu's model (WM) and the fiber bundle model (FBM). Part of Chapter 6.

- Highlight knowledge gaps for the upscaling of root reinforcement to the stand scale.
- Develop a new model for the dynamical quantification of root reinforcement.
- Develop an upscaling framework for the spatial characterization of root reinforcement in vegetated hillslopes.
- Calibrate and validate the models with specific laboratory and field experiments.
- Test the developed modeling framework with case studies.

In the following chapters, we present five papers in a logical sequence that starts from the preliminary review and conceptual work (Chapter 2), goes though the modeling (Chapter 3) and experimental work (Chapter 4), and concludes with the application of the modeling framework to two case studies (Chapter 5 and 6).

1.1 References

BAFU, 2010. website: http://www.bafu.admin.ch/umwelt/indikatoren

Brang, P., W. Schnenberger, M. Frehner, R. Schwitter, J. J. Thormann and B. Wasser (2006), Management of protection forests in the European Alps: an overview, *For. Snow Landsc. Res.*, *80(1)*, 2344.

Brooks, S. M., M. J. Crozier, T. W. Glade and M. G. Anderson (2004), Towards Establishing Climatic Thresholds for Slope Instability: Use of a Physically-based Combined Soil Hydrology-slope Stability Model, *Pure and Applied Geophysics*, *161(4)*, 881-905. doi: s10.1007/s00024-003-2477-y

CCES, 2010. website: http://www.cces.ethz.ch/projects/hazri/tramm

Florineth, F., and Molon M. (2004), Dispensa di ingegneria naturalistica, BOKU, Wien, 140 pp.

Koch, D. (2003), Bioengineering, in: SMIA03, sustainable management in action. 4-6 september 2003. University of Geneva.

Mickovski, S. B., P. D. Hallett, M. F. Bransby, M. C. R. Davies, R. Sonnenberg and A. G. Bengough (2009). Mechanical Reinforcement of Soil by Willow Roots: Impacts of Root Properties and Root Failure Mechanism, *Soil Sci. Soc. Am. J.*, *73*, 1276-1285. doi:10.2136/sssaj2008.0172

Pollen, N., and A. Simon (2005), Estimating the mechanical effects of riparian vegetation on stream bank stability using a fiber bundle model *Water Resources Research*, *41*, w07025. doi: 10.1029/2004WR003801.

Rickli, C., and F. Graf (2009), Effects of forests on shallow landslides case studies in Switzerland, *For. Snow Landsc. Res.*, *82 (1)*, 33-44.

Romang, H., B. Tuefen, E. Rick, and C. Wilhelm (2003), Naturgefahren, *Faktenblatt 10 des Amt fr Wald Graubnden*, 12 pp.

van Asch, T. W. J., J. Malet, L. P. H. van Beek, and D. Amitrano (2007), Techniques, issues and advances in numerical modelling of landslide hazard, *Bull. Soc. géol. Fr.*, *178 (2)*, 65-88.

Waldron, L. J., and S. Dakessian (1981), Soil reinforcement by roots: calculation of increased soil shear resistance from root properties, *Soil Science*, *132*, 427-435.

Wehrli, A., P. Brang, B. Maier, P. Duc, F. Binder, E. Lingua, K. Zieg-

ner, K. Kleemayr, and L. Dorren (2007), Schutzwaldmanagement in den Alpen - eine bersicht, *Schweiz Z Forstwes*, *158 (6)*, 142-156.

Wu, T. H., W. P. McKinnell, and D. N. Swanston (1979), Strength of tree roots and landslides on Price of Wales Island, *Alaska Canadian Geotechnology Journal*, *16*, 19-33.

Chapter 2

Quantifying lateral root reinforcement in steep slopes

Autohrs: Schwarz M. [1,2], Lehmann P. [2]. and Or D.[2]

[1] Swiss Federal Institute for Forest, Snow and Landscape Research, 8903 Birmensdorf, Switzerland

[2] Soil and Terrestrial Environmental Physics, Institute of Terrestrial Ecosystems, ETH Zurich, 8092 Zurich, Switzerland

Published in: *Earth Surf. Process. Landforms*, (2010), *35 (3)*, 354 - 367. doi: 10.1002/esp.1927.

2.1 Abstract

A review of present modeling approaches for root reinforcement in vegetated steep hillslopes reveals critical gaps in consideration of plant-soil interactions at various scales of interest for shallow landslide prediction. We propose a new framework for systematic quantification of root reinforcement at scales ranging from single root representation to single tree root system, to reinforcement within a stand of trees. In addition to standard basal reinforcement considered in most approaches, we highlight the critical role of roots in stabilizing slopes through lateral reinforcement. We review primary geometrical and mechanical properties of root systems and their function in reinforcement of soil mass. We consider stress-strain relationships for a bundle of roots using the formalism of the fiber bundle model (FBM) that offers a natural means for up scaling mechanical behavior of root systems. We propose extension of the FBM to consider key root and soil parameters such as root diameter distribution, tortuosity, soil type, soil moisture and friction between soil and root surface. The spatial distribution of root mechanical reinforcement around a single tree is computed from consideration of root diameter and density distributions based on easy to measure properties. Root reinforcement distribution for a stand of trees was obtained from spatial and mechanical superposition of individual tree values considering their positions on a hillslope. Potential applications of the proposed approach are illustrated in a numerical experiment of spatial strength distribution in a hypothetical slope with one thousand trees randomly distributed. The analyses result in spatial distribution of weak and strong zones within the slope where landslide triggering is expected in large and continuous zones with low reinforcement values. Mapping such zones would enhance the quality of landslide susceptibility maps and optimization of silvicultural measures in protection forests.

2.2 Introduction

Landslides and debris flows are common natural hazards in alpine regions [Schmid et al., 2004; Lateltin et al., 2005]. The significant role of vegetation in stabilizing hillslopes and mitigating some of the risks posed by such hazardous mass movements is well established [Wu et al., 1988a; Sidle, 1992; Watson et al., 1999; Montgomery et al., 2000; Osman and Barakbah, 2006;]. Consequently, vegetation plays prominent role in risk mitigation strategies for such natural hazards, for example, by promoting and managing protective forest covers. Notwithstanding the considerable body of re-

search, complex interactions between vegetation and natural slopes present a challenge; even basic questions concerning the extent to which vegetation increases slope stability elude quantification. Nevertheless, efforts to incorporate root reinforcement effects in models for hillslope stability and landslide occurrence must continue.

Several state-of-the-art models for shallow slope stability such as GEOtop [Simoni et al., 2007] and SHETRAN [Bathurst et al., 2007] implement hydrological and mechanical modules to evaluate landslide susceptibility in large catchments. Similar models are also available for small [a few square kilometers] catchments [Montgomery and Dietrich, 1994; Sidle and Wu, 2001]. The role of vegetation in these models is incorporated by introducing an additional cohesion term for the basal failure surface. The effect of vegetation is thus reduced to an apparent cohesion term homogeneously distributed in root zone layer over the landscape. Understandably, a more detailed description might be computationally prohibitive for large catchments, however, for smaller scale applications (e.g., a single hillslope) and even for derivation of a more realistic upscaling of an effective cohesion term, spatial and temporal variations exhibited by root cohesion must be considered (figure 2.1). Recent studies have used Finite Elements to represent detailed cohesion behavior in three-dimensional systems [Kokutse et al., 2006], and in two-dimensional analysis considering basal root reinforcement [Van Beek et al., 2005; Danjon et al., 2007; Genet et al., 2008]. Variations in mechanical reinforcement at the root-zone-scale are particularly important for small and shallow landslides with lateral dimensions of 10 to 2000 m2 [Reneau and Dietrich, 1987]. Naturally, we should expect complexities arising from the distribution of root sizes and details of root-soil mechanical reinforcement [Krogstad, 1995; Schmidt et al., 2001; Sakals and Sidle, 2004; Danjon et al., 2007], however, such interactions also demonstrate that application of uniform cohesion term may represent an oversimplified picture that could overlook susceptibilities emerging when more complete stress-strain relationship of root systems and characteristics of their distribution are included in calculations of slope stability.

The stabilizing effects of vegetation on steep slopes have been addressed in many recent studies [Sidle and Wu, 2001; Pollen et al., 2004; Tosi, 2007]. For shallow bedrock or shallow slip surfaces, the primary mechanical function of roots is enhancement of basal shear strength. For deeper soil bedrock interface and similar scenarios, basal root reinforcement is relatively minor because only a small fraction of roots may reach the depth of a failure plane [Schmidt et al., 2001; Rickli, 2001, Nicoll et al., 2006]. Lateral root reinforcement may affect onset and size of a shallow landslide [Reneau and Dietrich, 1987; Schmidt et al., 2001; Roering et al. 2003; Gray and Barker,

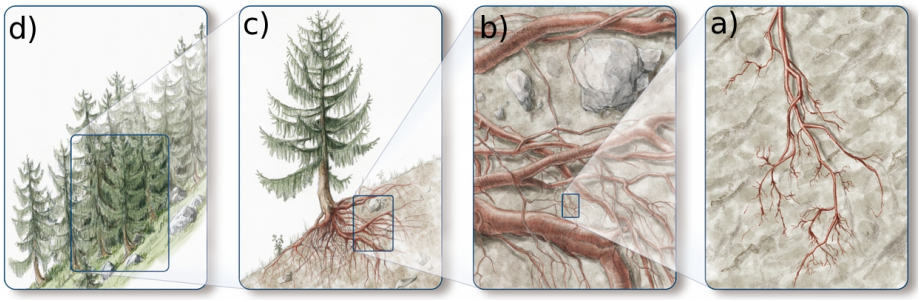

Figure 2.1: Illustration of upscaling sequence of root reinforcement considering scales ranging from a single root to a forest stand: [a] scale of a single root, [b] scale of a bundle of roots, [c] a single tree root system, and [d] scale of a forest stand on a hillslope.

2004]. In the presence of significant lateral root reinforcement, the area that must be destabilized in order to trigger a landslide increases [Reneau and Dietrich, 1987]. Notwithstanding preliminary attempts to quantify lateral root reinforcement [Krogstad, 1995; Zhou et al., 1998; Roering et al., 2003; Sakals and Sidle, 2004] a comprehensive modeling framework for spatial distribution of lateral root reinforcement is urgently needed.

The primary objectives of this study are to review present models for vegetation hydro-mechanical function in steep slopes, to identify conceptual and practical gaps in present models, and to introduce elements of a new modeling framework for quantifying lateral root reinforcement considering scales ranging from a single root to an entire stand. The role of root reinforcement in hillslope stability and landslide triggering would include explicit consideration of root distributions and mechanical properties of bundles of roots, with special focus on tensile root reinforcement (figure 2.2). The study is organized as follows: we first review root properties affecting soil mechanical reinforcement; following a discussion of limitations and gaps we propose tools for quantifying root distribution and derive new methods to estimate mechanical properties [e.g. behavior of bundles of roots]. Finally, we discuss potential extensions of the proposed approach and its suitability for modeling landslide triggering in steep terrain.

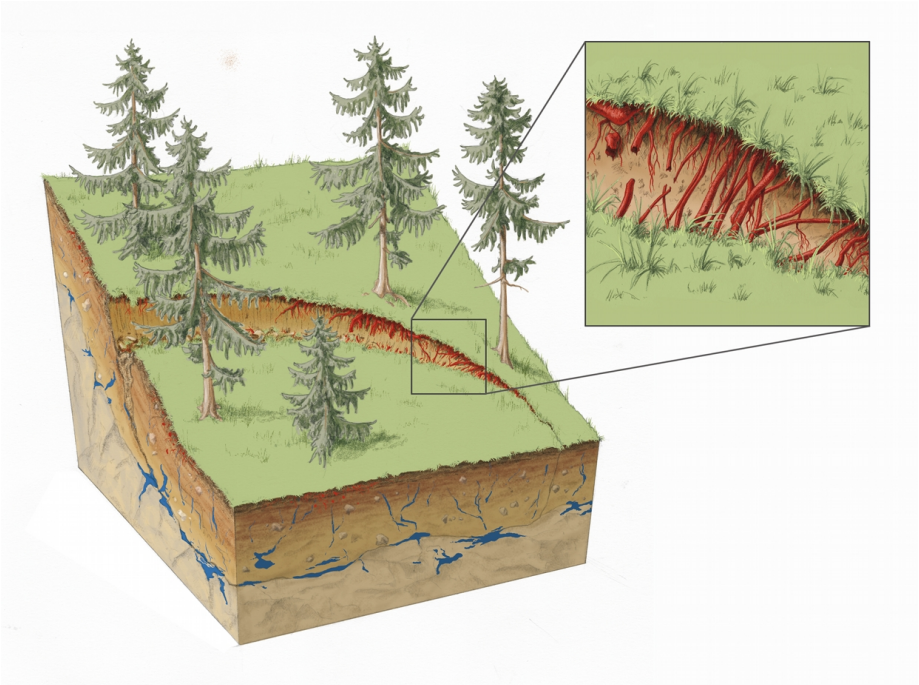

Figure 2.2: Illustration of the activation of root reinforcement during the formation of a tension crack of a shallow landslide.

2.3 Review on Root Properties Relevant for Root Reinforcement

The key properties of roots known to affect mechanical reinforcement of steep hillslopes are root size [diameter, length], spatial arrangement and associated soil root mechanical interactions. In the following we summarize typical values reported in the literature concerning number and size of tree roots and related topological information such as branching and tortuosity [Dupuy et al., 2005a; Hamza et al., 2007; Wu, 2007]. For brevity we provide a summary of the state of the art in root reinforcement modeling at different scales from single root to tree stand, illustrating that a more consistent and encompassing framework for organizing and implementing information is needed. Data from several studies are used to propose a new modeling framework.

Root distribution

Root types

A commonly employed classification of root mechanical function is based on root diameters distinguishing between so called fine and coarse roots [Santantonio, 1990; Tobin et al., 2007]. Fine roots are smaller than 1-2 mm in diameter and typically represent less than 5% of total tree biomass. Fine roots are denoted as tertiary root system and provide more than 90% of the water and nutrient uptake of a root system. Within this class of roots other physio-genetic classes of roots are distinguished [Majdi et al., 2005; Zobel, 2005] exhibiting complex topological features, most prominently root branching order [Wang et al., 2006; Borja et al., 2008]. The mass distribution of fine roots depends on growth and death of individual root tips with relatively high turnover rate [Majdi et al., 2005; Borja et al., 2008] depending on local conditions [Johnsen et al., 2005] and season. Pregitzer et al. [2002] considered the life cycle of lateral fine roots as deciduous elements in the same sense as leaves or needles.

Coarse roots [>2 mm] make up 15-25% of total tree biomass and consist of four classes: taproot, lateral roots, basal roots and adventitious roots [sinkers]. They can be subdivided into primary and secondary roots [Zobel, 2005], with secondary roots originating from the primary roots that are connected directly to the stem. Those root classes have a structural role and their distribution is less influenced by belowground competition. In some cases, coarse roots of neighboring trees may form grafts (Faser et al., 2005].

Root diameter-density distributions and root length

The spatial distribution of root diameters around a tree defines typical root architectures classified as one of three types: heart roots system, plate roots system and tap root system [Kokutse et al., 2006]. Numerous studies report measurements, characterization and visualization of root systems [Drexhage and Gruber, 1999; Danjon et al., 2005; Danjon and Reubens, 2008]. However, only a few provide data regarding root diameter distribution. Experimental results linking root frequency and root diameters obtained for various distances from tree stem are reported by Coutts [1983], Henderson et al. [1983] Wu et al. [1988b], Moroni et al. [2003], Sakals and Sidle [2004] and Kondo et al. [2004]. It is well known that development and structure of root systems under natural conditions are controlled by both genetic characteristics and external factors operating in the rooting environment [Genet et al., 2008]. Root mass distribution around a tree, for example, is seldom

symmetrical under most natural conditions due to heterogeneities in micro-topography, soil physical properties, distribution of nutrients, soil water, below-ground competition [Coutts, 1989; Nicoll and Ray, 1996; Chiatante et al., 2003a, 2003b; Nicoll et al, 2006], light interception by the crown, soil temperature [Steel et al., 1997], site cultivation, prevailing wind direction and soil movement [Reubens et al., 2007].

Measurements of root distributions around individual isolated trees revealed that fine-root biomass (FRB) decreases with increasing distance from the stem [Ammer and Wagner, 2005]. The density of fine roots is assumed to be uniformly distributed in the lateral direction under homogeneous forest canopy [Stober et al., 2000; Puhe, 2003]. The resulting homogeneous fine root density under a stand is due to the fact that overlapping root systems of neighbouring trees may increase fine root density up to maximum value sustainable by below ground resources [Brisson and Reynolds, 1994; Casper et al., 2003]. For intra or interspecific competition, studies have reported vertical niche differentiation [Schmid and Kazda, 2002; Achat et al., 2008], which may modify root density patterns. In contrast with the notion of uniform fine root distribution, several studies reported spatial variations in fine root density [Bedeneau and Auclair, 1989; Mller and Wagner, 2003; Yanai et al., 2006] and total root biomass density [Genet et al., 2008], especially in tree stands where the growth is limited by extreme climatic factors or irregular canopy cover [Puhe, 2003]. Achat et al. [2008] pointed out that variability of fine root distribution is clearly a function of observation surface [high variability for a surface of 0.0025 m^2 and lower variability considering surface of 0.04 m^2]. The distribution and amount of root mass depend also on the season [Babu et al., 2001]. Tree density in a stand seems to be an important factor influencing the mean fine root biomass [Puhe, 2003; Borja et al., 2008].

At the scale of a single tree root system, Roering et al. [2003] have shown a strong correlation between tree stem diameter at breast height [DBH] and root zone effective radius, defined as maximum distance from the stem where coarse roots are found (Figure 2.3). Typically, the lateral extent of a tree root zone is considered to be about 1 to 3 times its crown radius [Kuiper and Coutts, 1992; Drexhage and Gruber, 1998; Casper et al., 2003; Gray and Barker, 2004; Johnsen et al., 2005].

In addition to lateral extent of a root zone, in some cases, the maximum rooting depth is another important factor for root reinforcement function. Root depth is often restricted by bedrock, porosity, moisture, soil structure, nutrients, and by climatic conditions [Tobin et al., 2007]. Laio et al. [2006] presented a model linking mean rooting depth with soil type and climatic conditions. High values of mechanical impedance limit root pen-

etration. Typical values for root penetration pressures are in the range of 0.8 to 1.5 MPa, depending on soil hydration conditions and spatial heterogeneity in soil strength [Clark et al., 2003]. Montagu et al. [2001] show that compensatory growth occurred when roots encountered horizontally compacted layers, but not when they encountered vertically compacted layers. When cracks or old root channels exist, roots clump together and may grow through compacted layers [Clark et al., 2003]. Variations in root density with depth are often expressed in terms of a simple parametric model such as an exponential decay or a gamma function [Abe and Iwamoto, 1990; Abe and Ziemer, 1991; Abernethy and Rutherfurd, 2001; Schenk and Jackson, 2002; Bischetti et al., 2005; Laio et al., 2006; Docker and Hubble 2009] (Figure 2.4). Docker and Hubble [2009] present the results of root system architectural analysis and how the quantity of root material varies both with depth and lateral distance from the tree stem. The advantage in considering the importance of the 2D root distribution for the estimation of root reinforcement is limited by the fact that only information on root cross section area are used, instead of root diameter distributions [as needed for the RBM].

Root length exerts considerable influence on the amount of displacement needed to engage its maximum tensile strength. Studies have found that root length is linearly correlated with root diameter [Waldron and Dakessian, 1981; Wu et al., 1988b]. However the definition of root length is often inconsistent and may be interpreted differently as a function of the root geometry and topology. In this work we define root length as the sum of root segments connecting the considered root cross-section with the furthermost root tip belonging to the main root [length to the end of the root system].

Root geometrical features

Root systems form complex structures of interconnected fibrous elements resulting in diverse root system architectures affecting their hydro-mechanical function. Mechanically important characteristics of root structure are branching order [Wang et al., 2006] and branching intervals along the root. The branching order decreases towards the origins of the root system [tree stem] as branches merge together defining branching points, with the distance between a pair of such points known as root branching distance. Two types of branching geometry are often distinguished: either an apex that continues to grow straight and produces second-order lateral branches, or two terminal apices appear and replace the former single apex at the tip of the root [Dupuy et al., 2005b]. While the number and order of branches is important

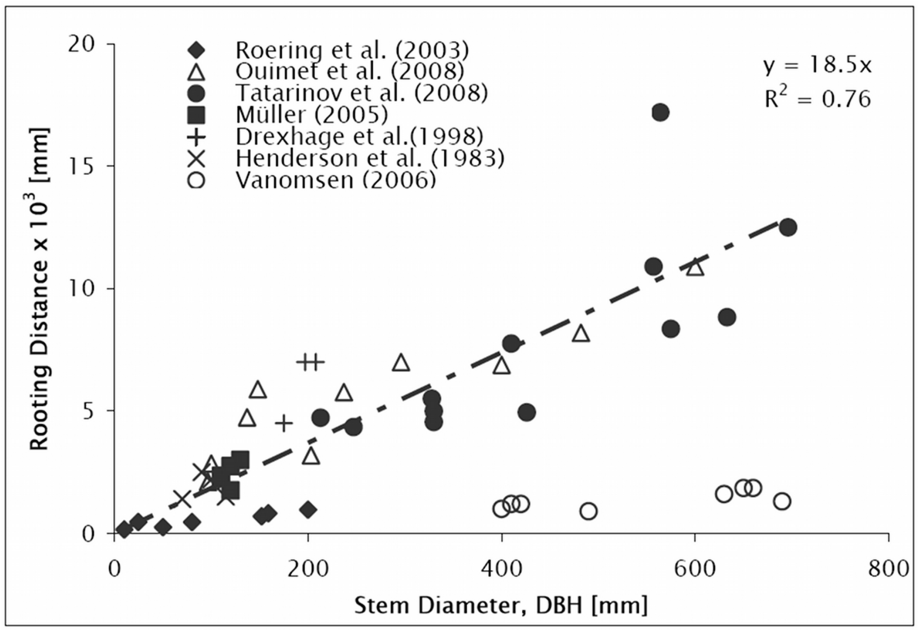

Figure 2.3: Literature-based allometric relations between the maximum extent of lateral roots [down to 1-2 mm in diameter] and tree stem diameter at 1.3 m high [DBH], considering different tree species. Note Vanomsen [2006] considered roots larger than 50 mm in diameter only, these data were not used in the linear regression.

for the pullout resistance, the branching angle has only a limited influence, as it varies during the application of a tensile stress before the maximum resistance is reached [Nilaweera and Nutalaya, 1999; Dupuy et al., 2005a]. Another geometrical factor is the tortuosity defined as the ratio between effective length of a root and the length of a straight line joining both ends of the root. This parameter is considered important in the first part of the strain curve of a root tensile test because it reduces the apparent Youngs modulus of the root tissue to 60%. Theoretically the resisting force produced by each root during a landslide failure, is a function of its orientation and strain. Given the range of possible root orientations and tortuosity, some of the roots will be strained past breaking while others are just beginning to strain and some have not even straightened [Krogstad, 1995]. Gray and Ohashi [1983] have shown from laboratory tests that perpendicular orientations of reinforcing fibers provide comparable reinforcement to random orientated fibers. Analytical calculation [Waldron, 1977] shows that a correction factor for the geometry effects for a single root ranges between 1.1 and 1.3 for shear reinforcement; usually a mean value of 1.2 is used in the

calculations [Bischetti et al., 2005].

Root mechanical properties

Mechanical properties of individual roots

A wealth of information is available regarding tensile strength of roots for different plant species and root diameters [Nilaweera and Nutalaya, 1999; Operstein and Frydman, 2000; Abernethy and Rutherfurd, 2001; Gray and Barker, 2004; Pollen et al., 2004; Bischetti et al., 2005; Mattia et al., 2005; Tosi, 2007; De Beats et al., 2008].

The dependency of the stress-strain relationship on root diameter are attributed to variations in tissue density and cellulose content and are affected by branching order [Genet et al., 2005; Wang et al., 2006]. Considerably less information is available concerning values of Young's modulus or the slope of the stress-strain relationship during root tensile tests. Some information may be found in Operstein and Frydman [2000], Tosi [2007], Fan and Su [2008] and Commandeur and Pyles [1991] (Figure 2.5).

Knowledge of the Young's modulus is important for quantifying processes inducing mechanical activation of the root-soil interface and its shear strength [Mickovski et al., 2007]. For measurements in soils, root tortuosity may affect the apparent Youngs modulus because a tortuous root may stretch with reduced stress transmission to the root tissue [Commandeur and Pyles, 1991].

One of the most challenging mechanical parameters to quantify is the shear strength at the interface between root and soil [Waldron, 1977; Wu et al. 1988a; Gray and Barker, 2004; Dupuy et al., 2005a; Wu, 2007] due to its dependence on soil type, water content [Fan and Su, 2008; Pollen, 2008], root-soil interface cohesive strength, root-soil interface friction angle and root-soil interface shear stiffness [Sivakumar Babu et al., 2008]. Ennos [1989] reported that root hairs and root exudation promote anchoring of young roots due to enhanced contact area between root and soil. Czarnes et al. [1999] observed that increased water content induces longer roothair production in corn seedlings resulting in higher friction in dry soils. The friction between soil and root determines the type of mechanical failure: in cohesive soils, small roots tend to break under dry conditions and slip out under wetter conditions [Pollen, 2008]. When roots break, the observed root strength drops abruptly to zero, whereas when a root slips out, the apparent root strength may drop to lower values that decrease exponentially with slip distance [Mickovski et al., 2007; Docker and Hubble, 2008]. The friction coefficient determines the activated root length during a pull out

test [Waldron and Dakessian, 1981] and influences the apparent tensile stiffness of the root as shown in Hamza et al. [2007]. An additional attribute affecting root-soil friction is the number of branching points. Experimental evidence suggests that increasing the number of branching points increases pullout force [Mickovski et al., 2007] and influences the type of failure [Norris, 2005].

In summary, mechanical properties of individual roots imparting tensile soil reinforcement are related principally to root maximum tensile strength, Youngs modulus of a root, soil compression properties, root tortuosity, dimensions and frequency of root branching points and magnitude of friction coefficient at the root-soil interface. The influence of water content on root mechanical behavior may be lumped into soil compression properties and also into the friction coefficient at the root-soil interface. In the following sections we demonstrate how these parameters fit into the proposed modeling framework for upscaling root reinforcement and mechanical response.

Mechanical properties of root bundles

In recent years, models for mechanical interactions of bundles of roots have been formulated within the formalism of the fiber bundle model [Sornette, 1989; Kun et al., 2007] as alternative building blocks to standard single root models [Wu et al., 1979]. The fiber bundle model (FBM) framework describes stress-strain relationships of populations of fibers linking applied stress to macroscopic displacement of the bundle. The FBM is well established for modeling mechanical fatigue and failure of composite materials, and has recently been employed for describing root reinforcement [Pollen et al., 2004] employing similar concepts to Waldron and Dakessian [1981]. The study of Pollen and Simon [2005] demonstrated that FBM results are in better agreement with laboratory and field tests than the standard single-root model of Wu et al. [1979], which tends to yield overestimates of the stress. The FBM could be used to explain consistent biases and correction factors proposed by various authors [Bischetti et al., 2005; Wu, 2007] that are required to fit the model of Wu et al. [1979] to experimental data.

The application of an FBM approach to root reinforcement modeling enables reliable simulation of global failure behaviors of experimental results reported in the literature [Wu and Watson, 1998; Anderson et al., 1989; Ekanayake and Phillips, 1999; Pollen et al., 2004; Goldsmith, 2006; Mickovski et al., 2007], where stress-strain curves are obtained from highly variable reinforcement subjected to a few centimeters of displacement.

The simplest and classical application of the FBM uses global load sharing [GLS] rules as in Pollen et al. [2004] where stresses are uniformly re-

distributed between all surviving fibers in the bundle, and the stress-strain relations are subsequently calculated considering constant Youngs modulus. Furthermore the thresholds of maximal tensile strength of the different fiber classes are usually estimated using statistical models [such as the Weibull distribution].

Numerous other possibilities are available for extending the FBM approach to consider different failure mechanisms, load sharing, and fiber properties. The modeling of the mechanical behavior in a bundle of roots offers distinct advantages over single root representation where many of the geometrical and mechanical properties of a root system may be represented and accounted (for example the distribution of root classes, estimation of maximum tensile strength, estimation of Youngs modulus, estimation of root length]. More important, the composite behavior of the root system may naturally emerge within such a framework. Finally, progressive failure of soil root systems is accommodated and adds realism to the modeling of such complex processes.

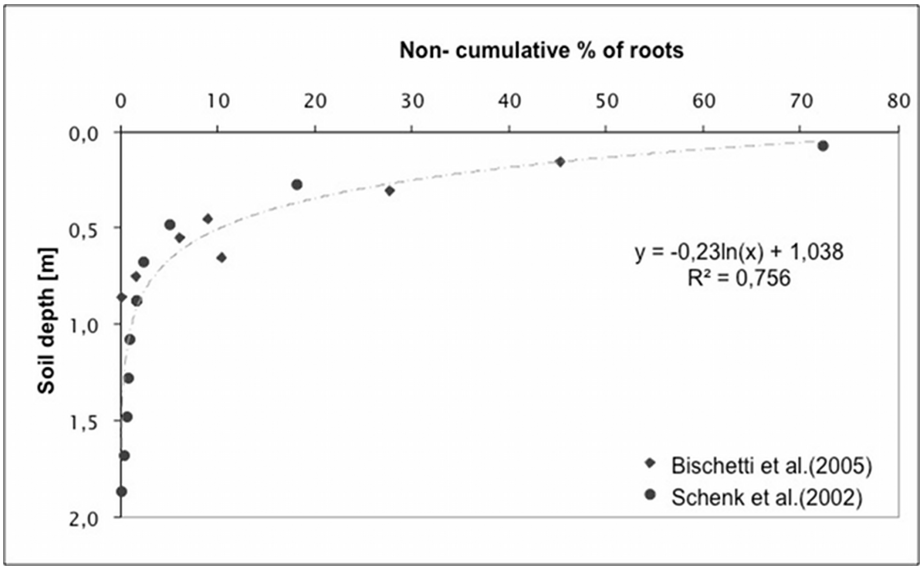

Figure 2.4: Root distribution as a function of soil depth. The data reported in Schenk and Jackson [2002] represent the mean of 33 soil profiles of Boreal forests and 48 soil profiles of cool temperate forests mostly considering percentage weight. The data of Bischetti et al. [2005] are the mean values of root section area of three Norway spruces excavated in north Italy.

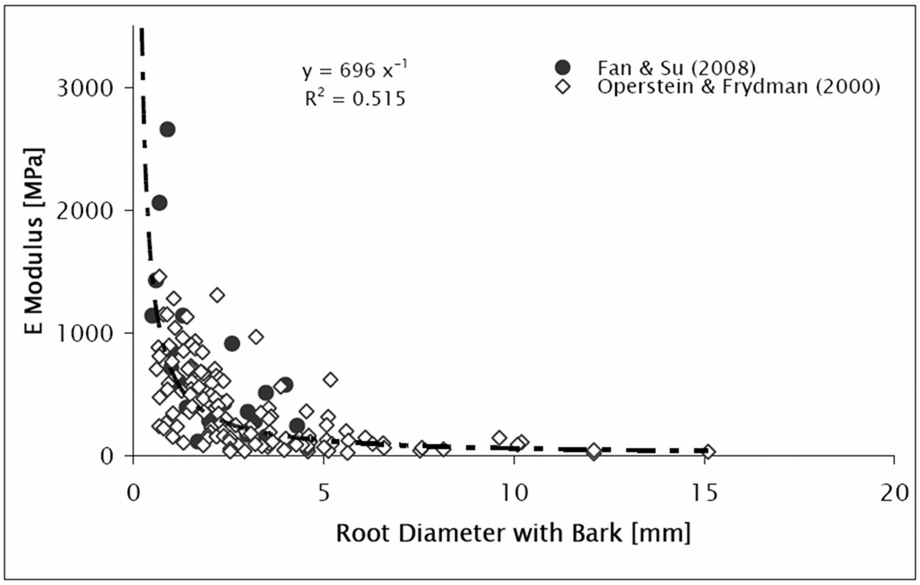

Figure 2.5: Values of elastic modulus versus root diameter [with bark] for different plant species [Sesbania cannabina, Medicago sativa, Rosmarinus officinalis, Pistacia lentiscus and Cistus].

Knowledge gaps in root reinforcement modeling

The key gaps in quantifying root reinforcement and their mechanical behavior in natural systems are best understood by considering the target prediction scale, namely the stand scale and reflecting back on mechanical behavior at the intermediate scales [root zone and single root]. The open questions [and gaps] pertain to how one should systematically consider reinforcement imparted by roots of spatially distributed stands of trees, each with a characteristic root zone with variations of root length, size and strength as a function of distance from the stem, and how to incorporate their progressive mechanical response where not all roots are activated and fail at the same displacement or applied load. Only a few models have thus far considered the spatial distribution of root reinforcement with explicit consideration of the structure of vegetation cover [Sakals and Sidle, 2004; Kokutse et al., 2006; Genet et al., 2008]. Of these only Sakals and Sidle [2004] account for root distribution; however, the basis of their root reinforcement model is the Wu et al. [1979] approach for single root mechanics. Some progress could be gained from consideration of root bundle models such as the FBM [Pollen, 2008] which offers a more realistic means for upscaling and quantifying root reinforcement. A cursory review of the widely

used Wu approach, shows the consistent overestimation of this method.

The importance of considering the spatial distribution of trees in a stand, root system distribution and architecture [at least in a general sense], and the gradual and cooperative activation and failure of bundles of roots, could be addressed [at least partially] by extension of the FBM formalism. Of course, the implementation of such new methodology and framework requires new parameterization and experimental data not considered previously. In the context of the proposed framework in this study, information regarding root distribution and characteristics of failure mechanisms of individual pulled roots is particularly important and limiting.

2.4 A Modeling Framework for Root Reinforcement in Steep Slopes

In this section we propose a modeling framework for quantifying root reinforcement in soils at scales ranging from single root to an entire stand of trees, addressing key knowledge gaps discussed above. Among the novel elements in the proposed framework is the explicit treatment of root distribution effects on mechanical reinforcement, overlapping of root systems, and development of building blocks for integrating mechanical interactions at all scales. We defer detailed tests of various modules and limit the presentation to essential elements and conceptual steps [assumptions and limitations] required for introducing the new framework. A general road map for the proposed root reinforcement framework is depicted in Figure 2.6.

Root distribution model

Recognizing the laborious and prohibitively expensive task of detailed characterization of root distributions, various correlations have been proposed for estimating root-related parameters from above ground and easy-to-measure properties of a tree. For mechanical reinforcement considerations we are particularly interested in quantifying the frequency of roots of different diameter classes at different position in a forest stand. Our modeling approach consists in a static fractal branching model [Tobin et al., 2007], similar to those used by Diggle [ROOTMAP, 1988], Lynch et al. [SimRoot, 1997], Ozier-Lafontaine et al. [FractRoot, 1999] or Pages et al. [Root Typ, 2004]. We propose the use of simple morphogenetic parameters such as mean radial branching distance and root diameter proportionality factor [Van Noordwijk et al., 1994; Ozier-Lafontaine et al., 1999; Vercambre et al.,

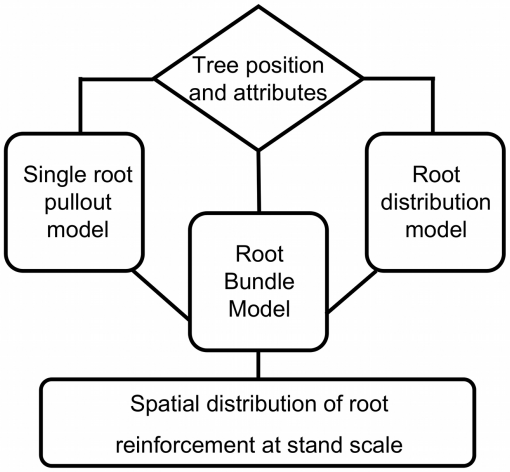

Figure 2.6: A roadmap for the proposed modeling framework. The input parameters needed for the modeling are the position of the tree and other attributes like dimension of the tree [DBH], tree species, soil type and soil water content. These inputs are used to run the single root pullout model and the root distribution model. The outputs of these models flow together in the root bundle model [RBM] for the calculation of displacement dependent root reinforcement in the different zones of a vegetated hillslope.

2003; Collet et al., 2006]. The parameters considered may vary among different tree species and we limited the review and modeling in this study to spruce tree species [*Picea abies*]. Ultimately, we opted for modeling mean root density distribution in three dimensions for different root diameter classes (figure 2.7). The starting point for our modeling of root distribution is the information regarding fine root distribution. The distribution of root diameters associated with primary and secondary root systems is assumed to be strongly correlated with mean fine root distribution and distance from the tree stem. The total number of fine roots associated with an individual tree may be estimated from the sapwood area, crown volume, or other tree properties [Mller and Wagner, 2003; Sakai et al., 2007; Al Alfa et al., 2008; Cermak et al., 2008; Wälder and W"alder, 2008] as follows:

$$N_{fr} = \mu P \tag{2.1}$$

where N_{fr} is the total number of fine roots, μ is a pipe theory coefficient and P is an allometric parameter of a tree such as Leaf Area Index, sapwood area, crown volume or stem basal area. Additionally, the maximal lateral (radial) extent of a root system (d_{max}) may be estimated using empirical relationships such as proposed by Roering et al. [2003] and Ammer and Wagner [2005]. We employed a model similar to that of Ammer and Wagner [2005] to estimate density of fine roots (D_{fr}) as a function of distance from a single tree stem (d_{stem}) as depicted in figure 2.8.

$$D_{fr} = \frac{N_{fr}}{d_{max}} \left[0.6 + 0.4 \frac{d_{stem}}{5DBH} \right] \quad if \quad d_{stem} < 5DBH \tag{2.2}$$

and

$$D_{fr} = \frac{N_{fr}/d_{max}}{2\pi d_{stem}} \quad if \quad d_{stem} > 5DBH \tag{2.3}$$

The importance of fine root distribution is in reflecting conditions of inter and intra-specific competition: we assume that two neighboring root systems may overlap without influencing root distribution if their combined fine root density remains below a threshold value. The maximum fine root density threshold value is considered as a characteristic of the forest stand reflecting climatic and soil factors, notably organic matter, field capacity and specific surface area [Ostonen et al., 1999]. The scarce number of literature values report fine root density values in the range between 10 and 40 roots per vertical square meter for different tree species [Coutts, 1983; Wu et al., 1988b; Moroni et al., 2003].

The density of coarse roots as a function of distance from the stem is deduced by assuming a constant value of branching distance [BD] [Van Noordwijik et al., 1994; OzierLafontaine et al., 1999]. At each branching point a coarse root may split into finer diameter roots, maintaining a constant proportionality factor [PF] between pre-branching crosssectional areas of a coarse root and the sum of cross-sectional areas of finer roots after branching [Van Noordwijik et al., 1994; Wang et al., 2006]. The proportionality factor varies between 0.75 and 1. Maximum root diameter [RDmax] at a prescribed distance from stem can be calculated according to:

$$RD_{max} = [[d_{max} - d_{stem}]/BD]\, CSA_{fr} PF \tag{2.4}$$

where CSA_{fr} is the mean cross-section area of fine roots, $d_{stem,max}$ and d_{stem} are the maximum rooting distance from the stem (figure 2.1) and

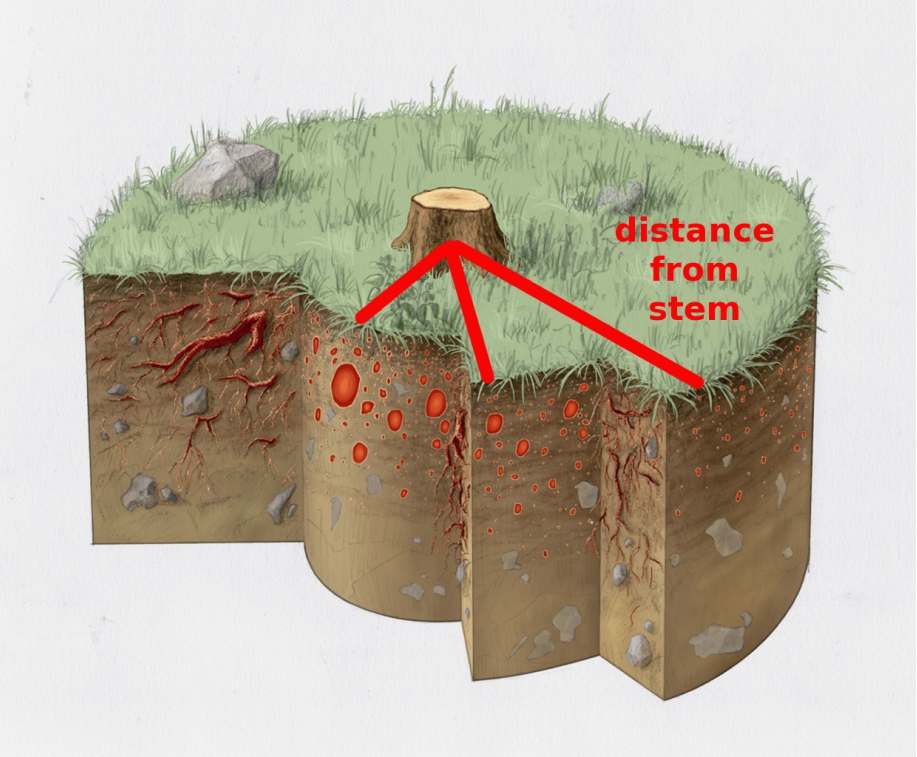

Figure 2.7: Illustration of lateral root distribution at three different distances from tree stem. Note the decrease in maximum root diameter with increasing distance [calculated values for spruce are given in Figures 2.8 and 2.9].

the distance from stem at which RD_{max} is calculated, respectively. For a given maximum lateral root system extent and for a given fine root density the diameter of coarse roots at each branching point is computed defining root diameter as a function of the distance from the stem. Hence, for each distance from a tree, a maximum root diameter [RDmax] is computed as an upper bound for root diameter distribution [assigned a value of zero frequency for convenience]. The fine root frequency at the same distance corresponds to a value shown in Figure 2.8. The number of roots as a function of root diameter for diameter values between fine root size and maximum diameter is calculated on the basis of empirical root distribution data [Waldron and Dakessian, 1981; Wu et al., 1988b; Moroni et al.; 2003]. The resulting root distribution function used for the estimation is the following:

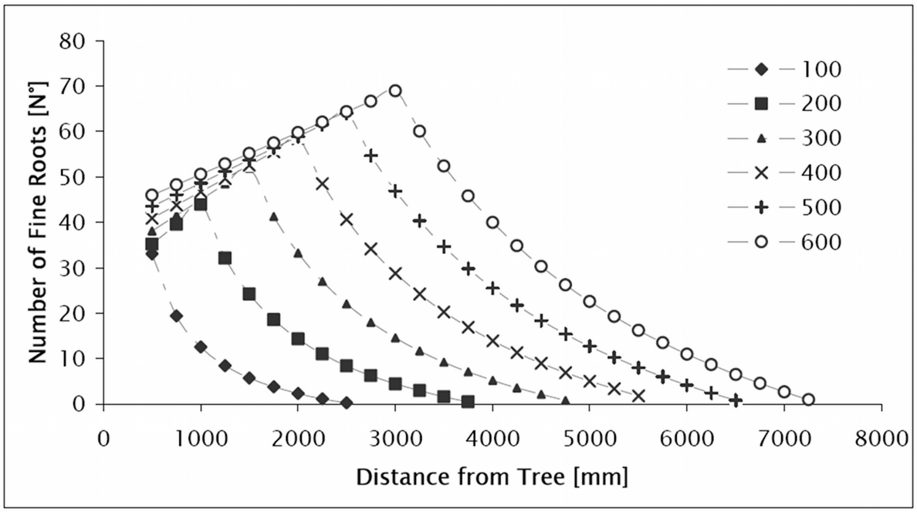

Figure 2.8: Fine root density distribution [crossing a soil vertical profile of 1 m2] as a function of distance from tree stem, for different tree diameters (denoted DBH in [mm]). Fine root density attains a maximum value at a radial distance equal to five times tree diameter.

$$N_{root} = D_{fr}\,[[log[RD_{max}]log[RD]]/log[RD_{max}]]\,RD^{\lambda} \tag{2.5}$$

where λ is the fitted exponent for an empirical set of data as show in Figure 2.9. Based on the relationships presented in Figures 2.8 and 2.9 it is possible to determine the coarse and fine root spatial distribution around a tree. For illustration purposes we calculated the root distribution for a spruce tree with 300 mm DBH under homogeneous soil and environmental conditions (figure 2.10). Although we do not plan to model vertical distribution of roots, this information could be estimated using the statistics of root depth distributions [Nicoll et al., 2006; Schenk, 2008] and maximum rooting depth. Based on the estimation of a maximum rooting depth, which depends on the tree dimension, the eco-hydrological conditions, the pedology of the site and other morphological root parameters, it is possible to extrapolate the root diameter distribution along the soil profile.

Mechanical properties of individual roots

After establishing size and spatial distribution of root diameters, we now focus on other topological attributes important for mechanical reinforcement. The geometry and the main structural elements of the root analogue used for the parameterization in modeling of root mechanical behaviors are

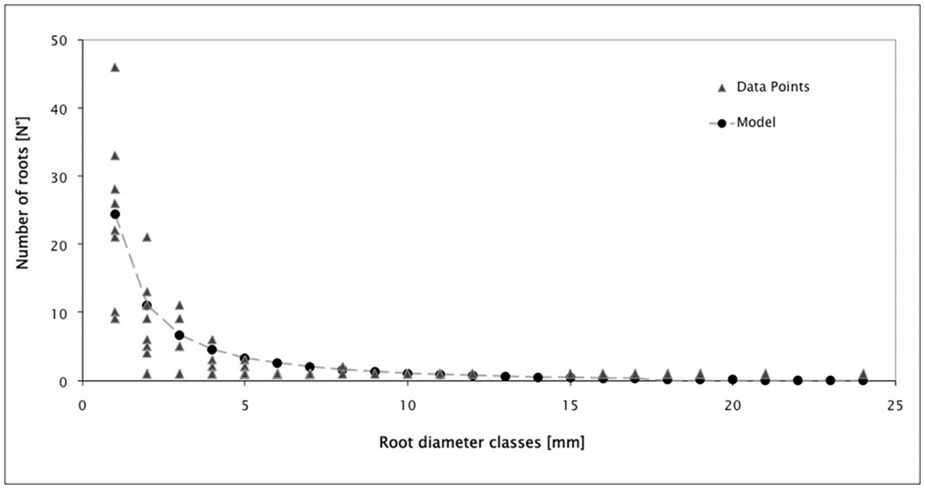

Figure 2.9: Modeled and measured root distribution [in a vertical square meter] determined for a tree with a stem diameter of 200 mm [DBH] at 2.5 m distance from the stem. The data were collected for eight spruces with diameter between 150 and 300 mm in a trench area of 0.25 m2 at 2.5 m distance from tree stem. In this case μ has a value of 08.

shown in figure 2.11. The choice of parameters and applied range of values were based on literature data presented in the review section. In the following section we highlight main derivations used for modeling single root pullout behavior. The mechanical properties of individual roots with different diameters are estimated considering various mechanical and geometrical interactions. For low tensile stresses applied to roots embedded in soil, studies observed lower than average Youngs modulus values [typically for up to 5% strain] attributed to geometrical adjustment of roots from their initially tortuous arrangement as they stretch [Commandeur and Pyles, 1991]. We assume that part of this stretching mechanism is likely to take place in the early stages of tensile crack formation in soil, and it is implemented in the model with the following condition:

$$if \varepsilon < T_t \quad then \quad E_t = Et \tag{2.6}$$

where ε is the strain, E_t is the apparent Youngs modulus of tortuous roots and E is the Youngs modulus of straight roots [equal to Youngs modulus of the root material]. An empirical reduction coefficient t is assumed to vary from 0 to 1. The tortuousity threshold [T_t] is estimated to vary between 0 and 5%. Both the threshold and the reduction coefficient are dependent on root tortuosity of and soil conditions (soil type, confining pressure and water

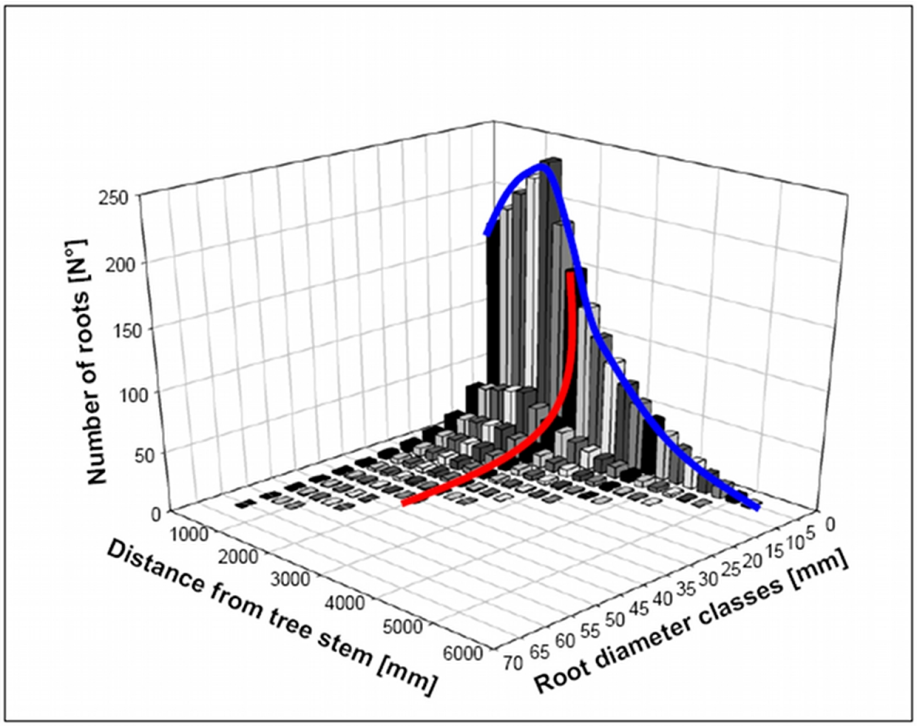

Figure 2.10: Root distribution of a spruce with 300 mm stem diameter (DBH). The thickest roots are close to the tree and the maximum root diameter decreases with increasing distance. The projection of these results on the two vertical planes corresponds to the graphical results shown in Figures 2.5 and 2.6, respectively [blue and red lines].

content). With subsequent increase in applied stress and resulting strain, the load is balanced by root-soil friction along the root surface considering the entire root geometry contributing to friction. During this phase, stress increases without appreciable extension of the root that distributes the load along the rootsoil interface [Waldron and Dakessian, 1981]. Hamza et al. [2007] observed that for such conditions, Youngs modulus initially increases followed by a decrease when the entire root is activated and contributes to friction. This behavior is implemented in the proposed model by varying Youngs modulus with strain according to:

$$E_{app} = E\beta\varepsilon^{-\alpha} \tag{2.7}$$

where E_{app} is the apparent Youngs modulus of progressively activated root length. The coefficient β and α are fitting parameters derived from lab experiments. Owing to the sensitivity to root-soil friction the resulting

stress depends also on the strain rate. This dynamic effect of the root-soil shear interface is reported by Mickovski et al. [2007] and is considered in the new model as a dynamic friction coefficient [f_d]. In addition to root-soil friction, we consider an increase in resistance due to the presence of branching points [τ_{br}], as reported by several studies [Dupuy et al., 2005a; Norris, 2005; Mickovski et al., 2007]. The additional resistance due to this effect ranges from 0.1 to 5 N per branching point depending on soil moisture and branching order. The total slip-out friction of a root [$Frict_{tot}$] is calculated as follows:

$$Frict_{tot} = \{[\tau_{root-soil}\pi RD[RL - \Delta x]] + [\eta_{br}[[RL - \Delta x]/BD]]\}f_d \quad (2.8)$$

where $\tau_{root-soil}$ is the root-soil interface friction (MPa), η_{br} is the additional friction coefficient due to the presence of a single branching point (N), RL is the root length (mm), Δx is the displacement, BD is the branching point distance, and $[RL - \Delta x]$ represents the progressive reduction of the portion of root length on which friction forces are activated. The root length [RL] is estimated as in Pollen [2008]

$$RL = \xi RD^{\gamma} \quad (2.9)$$

where ξ ranges between 200 and 1000 and γ between 0.5 and 1 [Pollen, 2008]. Although Pollen [2008] claims that variations in soil moisture do not affect significantly slip-out behavior of a pulled root, our preliminary calculations lead us to conclude this might be important and should be considered (figure 2.12). To the best of our knowledge, there are no studies providing quantitative information regarding effects of soil water content on friction at the root-soil interface. In this study the friction is considered to change linearly with soil volumetric water content within a range of values between 0.1 and 10 kPa for loamy soils (additional studies of this effect are needed). For calibration of the threshold of maximum root tensile strength it is important to consider that laboratory data obtained from tensile tests [Bischetti et al., 2005] may result in overestimation of the maximum tensile strength under field conditions as shown by Tosi [2007] or Docker and Hubble [2008]. The values of maximal tensile stress from laboratory tensile tests are similar to values of maximum pullout resistance of field experiment considering the root diameter at the point of rupture and not the root diameter at the scarp surface. For illustration purposes, we computed mechanical behavior of two roots differing in diameter (figure 2.12). The calculations for a root with 3 mm diameter and a length of 370 mm predict slip-out under either wet or dry conditions. A root of 7 mm diameter and

with 670 mm length would break under dry conditions and slip out under wet conditions. Note changes in the apparent Youngs modulus under wet conditions due to root tortuosity and soil compression behavior. The results illustrate that roots are more likely to slip out in sands than in cohesive soils.

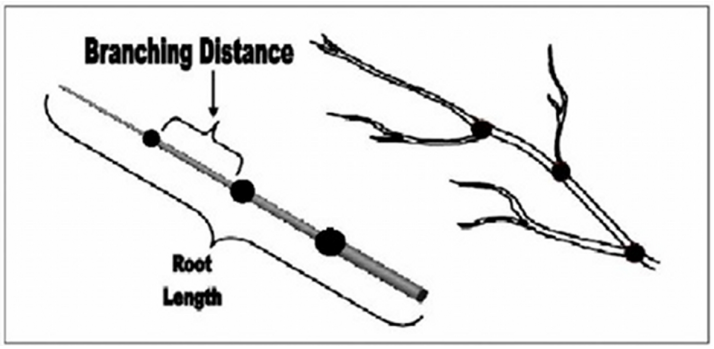

Figure 2.11: Visualization of the root analogue used for parameterization and modeling of tensile strength behavior (left), compared with the geometry of a possible real root. The black dots mark branching points.

Mechanical properties of root bundle model [RBM]

Combining models for root density distribution (figure 2.10) and mechanical behavior for individual roots (figure 2.12) enables calculation of a stress-strain relationship for a bundle of roots. We modified the classical fiber bundle model (FBM) calling it the root bundle model (RBM). While in most applications of FBMs load steps are applied [Pollen and Simon, 2005], we calculated stress-strain behavior for stepwise increase of root bundle displacement using the democratic load sharing FBM rule [Sornette, 1989; Kun et al., 2007]. Geometrical parameters for each root such as root length, tortuosity, and number of branching points are combined with mechanical parameters (Youngs modulus, maximum strength of individual root F_{max}), to obtain the dominant failure mechanism, i.e. stretching due to tortuosity or root-soil mechanical properties, slipping out, or breaking. The main orientation of roots is assumed to be perpendicular to the tension crack. In the actual version of the model we also assume that the mechanical behavior of each single root is dominated from the end of the root present only on one side of the considered tension crack. Stress values for all individual roots are added and contribute to the stress of the bundle as long as individual values are below their respective F_{max} values. For higher displacement

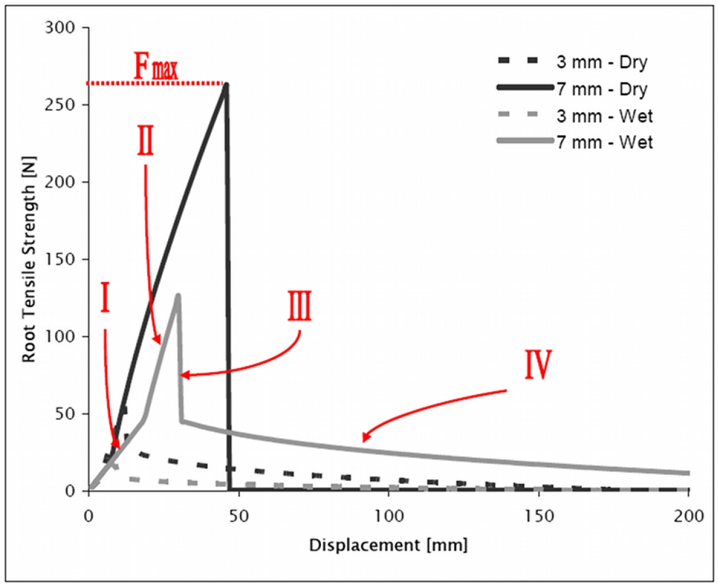

Figure 2.12: Simulated pullout behaviors for single roots with different diameters and moisture conditions in a loamy structured soil [Dry = 01 and Wet = 09 saturation]. In this case the 7 mm diameter root [RD] under dry conditions breaks while the root of the same diameter under wet conditions slips out due to the reduced rootsoil friction. IIV indicate characteristic phases of a failure: [I] tensile strength imparted by geometrical properties of the root pulled apart; [II] the mechanical properties of the root tissue determines this part of the relationship; [III] root slippage and associated abrupt drop in root-soil interface friction; and [IV] residual tensile strength due to friction at rootsoil surface during slipping out.

values broken roots do not contribute to load sharing of the bundle. For roots that are slipping out, however, the residual tensile strength is added to the resulting stress of the bundle. The total force of the bundle (F_{tot}) is a function of displacement (Δx) expressed as

$$F_{tot}(\Delta x) = \sum_{i=1}^{N} F_i(\Delta x) n_i \tag{2.10}$$

where $F_i(\Delta x)$ is the pull-out force of a root belonging to diameter class i, N is the number of diameter classes and n is the number of roots present in the bundle of diameter class i. $F_i(\Delta x)$ is calculated for each root diameter class using the single root pullout model. An example of the force-displacement relationship for a hypothetical bundle of roots in wet and dry loamy soil is

shown in figure 2.13. The variation of the bundle pullout force as a function of the displacement can be expressed with the differential equation

$$\frac{\partial F_{tot}(\Delta x)}{\partial \Delta x} = \sum_{i=1}^{N} F_i(\Delta x_f) n_i - \sum_{i=1}^{N} F_i(\Delta x_0) n_i \tag{2.11}$$

where Δx_f and Δx_0 are displacements at two different loads. Summarizing, we calculate the macroscopic stress-strain behavior of a bundle of roots as the sum of each single root stress-strain curve crossing a tension crack (figure 2.14). The idealized root bundle is composed of different classes of root diameters, which are related to different classes of root length and macroscopic root-soil friction coefficient.

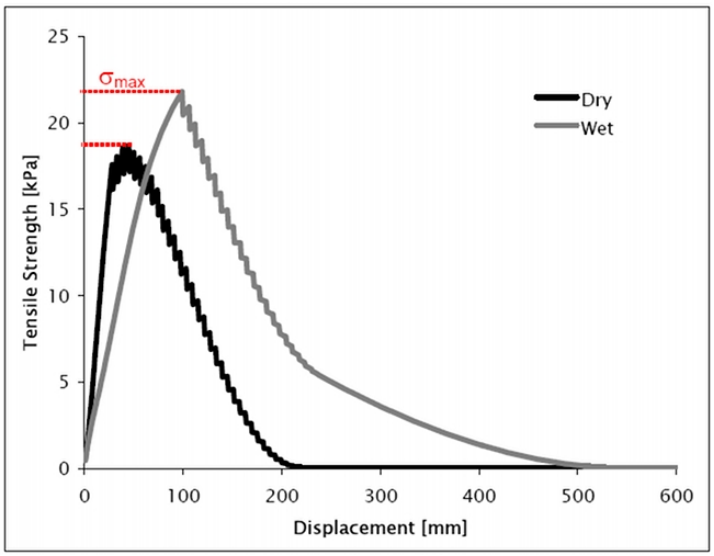

Figure 2.13: Force displacement relationship for a bundle of roots [spruce, 2000 mm distance, DBH = 300 mm] in loamy soil for two different moisture conditions (Dry = 10% saturation and Wet = 90% saturation). The stress-strain relationships of the individual roots are added. For dry conditions the maximum reinforcement is about 15 kPa. For wet conditions more roots do not break but slip out and the residual strain results in higher reinforcement for large displacement values.

Mechanical properties of vegetated hillslopes

Assessing the plant-root contribution to the mechanical behavior of vegetated hillslopes requires upscaling of the contributions from individual roots

to root zone response and then to the stabilizing forces within a heterogeneous stand (figure 2.14). Based on the modeling approach presented in previous sections, for each position in the landscape the root distribution and the stressdisplacement relationship of the bundle can be computed as a function of near-surface distance from the stem. This information can be used, for example, to delineate near-surface weak zones of a hillslope. For that purpose the maximum reinforcement σ_{max} can be determined for each hillslope element in the vicinity of a tree. An example of the calculation of σ_{max} is given in figure 2.13. The maximum reinforcement as a function of distance from the tree is shown in figure 2.15.

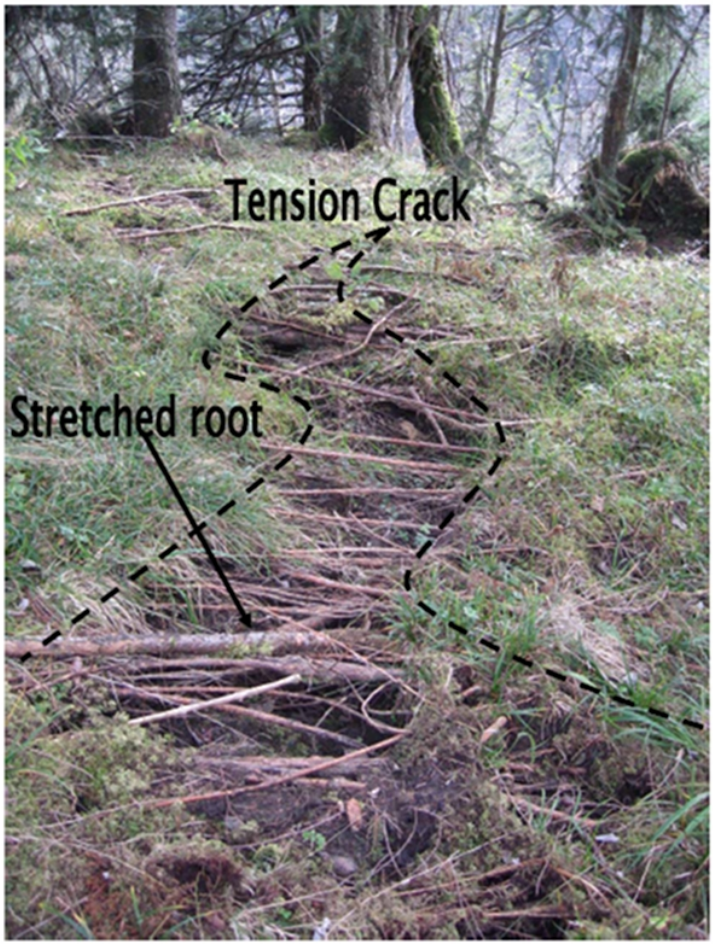

Figure 2.14: Bundle of lateral roots crossing a tension crack of landslide in Herrenboden [Switzerland]. [Photo courtesy of Hunziker U. BELOP, Stalden, Switzerland].

By assigning to each element of the hillslope a maximum stress value according to figure 2.15, the reinforcement distribution can be computed for a natural stand. For elements in the vicinity of several trees the reinforcement of each tree is added. In a numerical experiment shown in figure 2.16, 1000 trees with diameters ranging from 100 to 500 mm and with a minimum distance of 1000 mm, were randomly distributed in a site of 5000 m^2 with a slope gradient of 90% (figure 16a). The grid spacing of the slope was 100 mm and for each grid element the maximum reinforcement was computed (figure 2.16b). To assess the critical load required for destabilizing the slope, we classified the slope into regions that are stronger or weaker than an applied stress (Figure 2.16c, grey zones are stronger and black zones are weaker). For a stress of 5 kPa the zones with weak reinforcement form a continuous weak zone from the left to the right (figure 2.16c). Hence, for a stress of 5 kPa the slope is expected to fail if the lateral and basal boundary conditions of reinforcement are set to zero. Such analyses will enable to determine critical zones and loads for entire hillslopes.

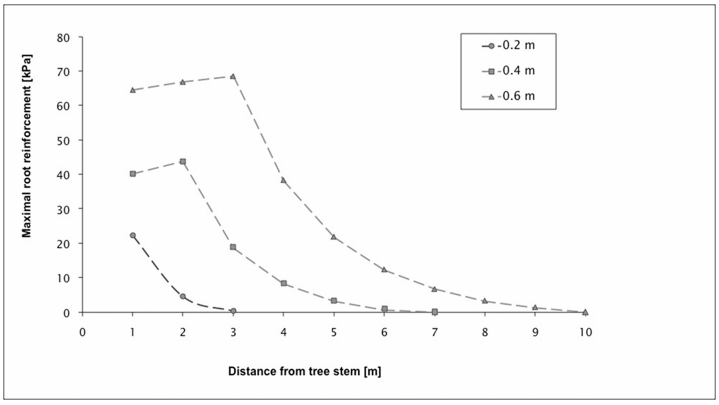

Figure 2.15: Maximum root reinforcement for spruce [Picea abies] as a function of distance from tree stems differing in stem diameter. The reinforcement increases with increasing stem diameter and decreases with increasing distance from the tree.

2.5 Discussion and conclusions

The role of root reinforcement in vegetated hillslopes is an important hydromechanical factor that varies in space (stand, species, soil type and depth) and in time with changes in hydrologic conditions. The addition of a uniform cohesion term may suffice for large landscape-scale applications; how-

ever, it may not reflect conditions prevailing in a particular hillslope and formation of weak zones associated with highly localized landslides. The modeling approach proposed in this study enables determination of root reinforcement at scales ranging from a single root to an entire stand on a hillslope. The proposed root distribution parameterization is far from ideal; however, we rely on literature field data as a starting point pending future validation. Experimental values regarding geometrical factors such as number of branching points or tortuosity are rare and must be verified in future studies. Additionally, the importance and relevance of postulated mechanical effects such as variations of Young's modulus, dynamic root-soil friction, and mobilized increasing root length await experimental verification. The model of root distribution and root reinforcement was based on the properties of individual trees assuming uniform root distributions. In a stand with trees competing for resources within the same soil volume, mechanical and geometrical root properties may be different compared to a single tree. Owing to the complexity of topography, water flow paths and soil formatting processes we should expect considerable deviations in root distributions and mechanical behavior relative to uniform root zones assumed in the derivations. The spatial distribution of root reinforcement must be analyzed in the field and related to hillslope properties and considering overlapping of root zones in a stand. The spatial superposition implicit in the hillslope scale modeling must be verified in experiments and with additional observations. During a landslide, not only tensile stresses but shear and compression stresses are expected to be important and should be considered. In this paper we focus on quantification of tensile strength. The introduction presents evidence of the importance of lateral root reinforcement where tensile strength is a fundamental parameter for inferring root reinforcement for both tensile and shear conditions. Considering potential triggering mechanisms of landslides, local mechanical failure would result in displacement of a soil volume inducing stress on the roots. If the stress is higher than the strength of the roots they may break and the stress must be redistributed to other roots. To model such a cascade of stresses and root failure detailed information on the stress-strain behavior of root reinforcement are needed. The results of the framework presented for the quantification of root reinforcement may be implemented in slope stability models which represent the mechanical forces between neighbored root systems as a bond. The mechanical properties of the bond correspond to the stress-strain behavior of the rooted soil and change as a function of the root distribution, soil condition and displacement. Figure 2.17 shows the representation of a hillslope with a network of bonds. In this study we attempted to balance awkward a fine line between detailed review and

introducing of a new framework based at present on literature information. The limitation of the proposed framework lies in the relatively demanding parameterization and computational burden; hence it would be limited to small-scale applications (forest stand or hillslope) and would not be suitable for an entire catchment. Nevertheless, coupling information on soil thickness, topography and hydrology would make it possible to better define mass and shape of potentially unstable zones. A more practical application consists of field evaluation of the optimal structure of forest cover to maximize slope stabilization. General information of slope stability parameters (steepness, soil cohesion, soil internal angle of friction) will help to assess the contribution of vegetation in slope stabilization [Casadei et al., 2003]. Furthermore, data like those shown in figure 2.15 may be used to define the minimal distance between trees of different dimensions to optimize root reinforcement. The collection of field data on position and attributes of single tree may constitute a big effort even for restricted areas. However, the increasing development of airborne techniques will mean that the collection of those types of data will be less time consuming in the future [Korpela et al., 2007].

2.6 Summary

This study presents a review of quantitative aspects of root distribution and mechanical root properties. To model the tensile root reinforcement more realistically than presently practiced, we consider tortuous root geometry, dynamic friction between root and soil and we implemented these mechanisms into a root bundle model (RBM). The RBM computes the stress-strain relationship as a function of radial distance from a tree stem. To deduce the mechanical properties of an entire stand from individual RBM behavior, we computed maximum reinforcement for each location within the slope. Large and continuous regions of weak reinforcement are expected to be prone to failure and may contribute to the risk of landslide occurrence. These regions could be determined with the proposed modeling approach for various reinforcement threshold values. The model should be extended to describe perturbations emerging when local soil mass becomes unstable. Such an extension would require computation of stress distribution for displacement of a soil volume and the redistribution of resulting loads. With such a completed model approach we will contribute to the optimization of management of protection forests in mountainous regions and to the assessment of unstable slopes.

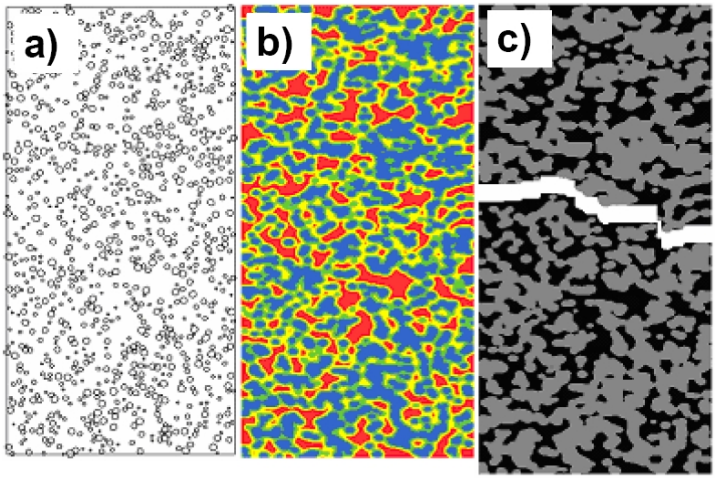

Figure 2.16: Numerical example of a stand (5000 m^2) with 1000 trees. In figure 2.16a the positions of the trees are shown with the radius of the circles indicating the size of the tree (the radius of the circle equals the fourfold of the true radius). In this application of the model no fine root density threshold was considered. In figure 2.16b, the maximum reinforcement at each position is shown with zones with less than 2 kPa in red, 2-5 kPa in yellow, 5-10 kPa in green and higher values in blue. The reinforcement values are segmented into zones that are weaker (black) or stronger (gray) than an applied stress of 5 kPa (figure 2.16c). For a stress of 5 kPa (and all higher values), the weak zone forms a continuous path from the left to the right and may initiate the failure of the slope as indicated by the white intersection.

2.7 Acknowledgements

We thank the CCES [Competence Center Environment and Sustainability] platform of the Swiss Federal Institute of Technology for funding the TRAMM project [Triggering of Rapid Mass Movements], all partners of the project, Manfred Stähli, Christian Rickli and Albert Böll for many constructive discussions.

2.8 References

Abe, K., and M. Iwamoto (1990), Simulation model for the distribution of tree roots application to a slope stability model, *Japanese Forestry Society*, *72*, 375-387.

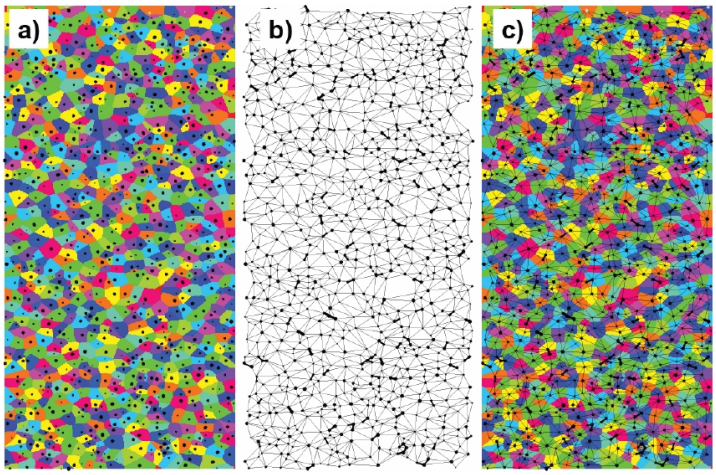

Figure 2.17: Model framework to study landslide triggering. The same slope as shown in Figure 2.16 is discretized into cells according to the root reinforcement of the trees. [a] All elements of a cell belong to one tree and denote the region where the reinforcement of this tree is higher than the effects of neighbored trees. The black dots denote the position of the trees. [b] Each cell is connected to a few other cells and these connections are shown as bonds. The bonds have mechanical properties deduced from the root bundle model. Thicker lines denote strong bonds. c] Superposition of the bond network and the force tessellation.

Abe, K., and R. R. Ziemer (1991), Effects of tree roots on a shear zone: modelling reinforced shear stress, *Canadian Journal of Forest Research*, *21*, 1012-1019.

Abernethy, B., and A. I. Rutherfurd (2001), The distribution and strength of riparian tree roots in relation to riverbank reinforcement, *Hydrological Processes*, *15*, 63-79.

Achat, D. L., M. R. Bakker, and P. Trichet (2008), Rooting patterns and fine root biomass of Pinus pinaster assessed by trench wall and core methods, *Journal of Forest Research*, *13*, 165-175.

Al Alfa, N., N. Marron, C. Cavalloni, and R. Ceulemans (2008), Growth and production of a short-rotation coppice culture of poplar-IV: fine root characteristics of five poplar clones, *Biomass and Bioenergy*, *32*, 494-502.

Ammer, C., and S. Wagner (2005), An approach for modelling the mean fine-root biomass of Norway spruce stands, *Trees*, *19*, 145-153.

Anderson, C. J., M. P. Coutts, R. M. Ritcie, and D. J. Campbell (1989), Root extraction force measurement for Sikta spruce, *Forestry*, *62*, 127-137.

Babu, J., H. N. Pandey, and R. S. Tripathi (2001), Vertical distribution and seasonal changes of fine and coarse root mass in Pinus kesiya Royle Ex. Gordon forest of three different ages, *Acta Oecologica*, *22*, 293-300.

Bathurst, J. C., G. Moretti, A. El-Hames, S. Begueria, and J. M. Garcia-Ruiz (2007), Modelling the impact of forest loss on shallow landslide sediment yield, Ijuez river catchment, Spanish Pyrenees, *Hydrology and Earth System Science*, *11(1)*, 569-583.

Bedeneau, M., and D. Auclair (1989) The study of tree fine root distribution and dynamics using a combined trench and observation window method, *Annalls Science Forests*, *46*, 283-290.

Bischetti, G. B., E. A. Chiaradia, T. Limonato, B. Speziali, B. Vitali, P. Vullo, and A. Zocco (2005), Root strength and root area ratio of forest species in Lombardy [Northern Italy], *Plant and Soil*, *278*, 11-22.

Borja, I., H. A. De Wit, A. Steffenrem, and H. Majdi (2008), Stand age and fine root biomass, distribution and morphology in a Norway spruce chronosequence in southeast Norway, *Tree Physiology*, *28*, 773-784.

Brisson, J., and J. F. Reynolds (1994), The effect of neighbors on root distribution in a Creosotebush [*Larrea tridentate*] population, *Ecology*, *75*, 1693-1702.

Casadei, M., W. E. Dietrich, and N. Miller (2003), Controls on shallow landslide width. In Debris-Flow hazards mitigation: mechanics, prediction, and assessment, Proceedings of the Third International Conference on Debris Flows Hazards Mitigation, Davos Switzerland, Rickermann D, Chen C [eds]. Millpress: Rotterdam; 91102. http://eps.berkeley.edu/ bill/papers/117.pdf

Casper, B. B., H. J. Schenk, and R. B. Jackson (2003), Defining a plants belowground zone of influence, *Ecology*, *84*, 2313-2321.

Cermak, J., N. Nadezhdina, L. Meiresonne, and R. Ceulemans (2008),

Scots pine root distribution derived from radial sap flow patterns in stems of large leaning trees, *Plant and Soil*, *305*, 61-75.

Chiatante, D., S. G. Scippa, A. Di Iorio, and M. Sarnataro (2003a), The influence of steep slopes on root system development, *Journal of Plant Growth and Regulation*, *21*, 247-260.

Chiatante, D., M. Sarnataro, S. Fusco, A. Di Iorio, an dS. G. Scippa (2003b), Modification of root morphological parameters and root architecture in seedlings of *Fraxinus ornus* L. and *Spartium junceum* L. growing on slopes, *Plant Biosystems*, *137(1)*, 47-56.

Clark, L. J., W. R. Whalley, and P. B. Barraclough (2003), How do roots penetrate strong soil?, *Plant and Soil*, *255*, 93-104.

Collet, C., M. Lf, and L. Pages (2006), Root system development of oak seedlings analysed using an architectural model: effects of competition with grass, *Plant and Soil*, *279*, 367-383.

Commandeur, P. R., and M. R. Pyles (1991), Modulus of elasticity and tensile strength of Douglas-fir roots, *Canadian Journal of Forest Research*, *21*, 48-52.

Coutts, M.P. (1983), Root architecture and tree stability, *Plant and Soil*, *71*, 171-188.

Coutts, M. P. (1989), Factors affecting the direction of growth of tree roots, *Annals Science Forests*, *46*, 277-287.

Czarnes, S., S. Hiller, A. R. Dexter, P. D. Hallett, and F. Bartoli (1999), Root:soil adhesion in the maize rhizosphere: the rheological approach, *Plant and Soil*, *211*, 69-86.

Danjon, F., T. Fourcaud, and D. Bert (2005), Root architecture and windfirmness of mature Pinus Pinaster, *New Phytologist*, *168*, 387-400.

Danjon, F., D. H. Barker, M. Drexhage, and A. Stokes (2008), Using three-dimensional plant root architecture in models of shallow-slope stability, *Annals of Botany*, *101*, 1281-1293.

Danjon, F., and B. Reubens (2008), Assessing and analysing 3D archi-

tecture of woody root systems, a review of methods and applications in tree and soil stability, resource acquisition and allocation, *Plant and Soil*, *303*, 1-34.

De Beats, S., J. Poesen, B. Reubens, K. Wemans, J. De Baerdemaeker, and B. Muys (2008). Root tensile strength and root distribution of typical Mediterranean plant species and their contribution to soil shear strength, *Plant and Soil*, *305*, 207-226.

Diggle, A. J. (1988), ROOTMAP a model in three-dimensional coordinates of the growth and structure of fibrous root systems, *Plant and Soil*, *105*, 169-178.

Docker, B. B., and T. C. T. Hubble (2008), Quantifying root-reinforcement of river bank soils by four Australian tree species, *Geomorphology*, *100*, 401-418.

Docker, B. B., and T. C. T. Hubble (2009), Modelling the distribution of enhanced soil shear strength beneath riparian trees of south-eastern Australia, *Ecological Engineering*, *35*, 921-934

Drexhage, M., and F. Gruber (1998), Architecture of the skeletal root system of 40-year-old *Picea abies* on strongly acidified soils in the Harz Montains [Germany], *Canadian Journal of Forest Research*, *28*, 13-22.

Drexhage, M., and F. Gruber (1999), Aboveand below-stump relationships for *Picea abies*: estimation of root system biomass from breast-height diameters, *Scandinavian Journal of Forest Research*, *14*, 328-333.

Dupuy, L., T. Fourcaud, and A. Stokes (2005a), A numerical investigation into factors affecting the anchorage of roots in tension, *European Journal of Soil Science*, *56*, 319-327.

Dupuy, L., T. Foucaurd, A. Stokes, and F. Danjon (2005b), A density-based approach for the modeling of root architecture: application to Maritime pine [*Pinus pinaster* Ait.] root systems, *Journal of Theoretical Biology*, *236*, 323-334.

Ekanayake, J. C., and C. J. Phillips (1999), A method for stability analysis of vegetated hillslopes: an energy approach, *Canadian Geotechnology Journal*, *36*, 1172-1184.

Ennos, A. R. (1989), The mechanics of anchorage in seedlings of sunflower, *Helianthus annuus* L., *New Phytologist*, *113*, 185-192.

Fan, C. C., and C. F. Su (2008), Role of roots in the shear strength of root reinforced soils with high moisture content, *Ecological Engineering*, *33*, 157-166.

Faser, E. C., V. J. Lieffers, and S. M. Landhusser (2005), Age, stand density, and tree size as factor in root and basal grafting of lodgepole pine, *Canadian Journal of Botany*, *83*, 983-988.

Genet, M., A. Stokes, F. Salin, S. B. Mickovski, T. Fourcaud, J. Dumail, and L. P. H. Van Beek (2005), The influence of cellulose content on tensile strength in tree roots, *Plant and Soil*, *278*, 1-9.

Genet, M., N. Kokutse, A. Stokes, T. Fourcaud, X. Cai, J. Ji, and S. B. Mickovski (2008), Root reinforcement in plantation of *Cryptomeria japonica* D. Don: effect of tree age and stand structure on slope stability, *Forest Ecology and Management*, *256*, 1517-1526.

Goldsmith, W. (2006), Soil strength reinforcement by plants. *International Erosion Control*: http://www.ieca.org/membersonly/resources/ proceedings/2006/.

Gray, D. H., and H. Ohashi (1983), Mechanics of fiber reinforcement in sand, *Journal of Geotechnical Engineering*, *109*, 335-353.

Gray, D. H., and D. Barker (2004), Root-soil mechanics and interactions, *Riparian vegetation and fluvial geomorphology, water science and application*, *8*, 113-123.

Hamza, O., A. G. Bengough, M. F. Bransby, M. C. R. Davies, and P. D. Hallett (2007), Mechanics of root-pullout from soil: a novel image and stress analysis procedure. In *Eco and Ground Bio-Engineering*: The Use of Vegetation to Improve Slope Stability, Stokes et al. [eds]. Springer; 213-221.

Henderson, R., E. D. Ford, E. Renshaw, and J. D. Deans (1983), Morphology of structural root system of sikta spruce: analysis and quantitative description, *Forestry*, *56*, 121-135.

Johnsen, K., C. Maier, and L. Kress (2005), Quantifying root lateral distribution and turnover using pine trees with a distinct stable carbon isotope signature, *Functional Ecology*, *19*, 81-87.

Kokutse, N., T. Fourcaud, K. Kokou, K. Neglo, and P. Lac (2006), 3D numerical modelling and analysis of the influence of forest structure on hill slopes stability. In *Disaster Mitigation of Debris Flows, Slope Failures and Landslides*, Interpraevent, September 25-27 2006, Niigata, Japan, Marui H, Marutani T, Watanabe N, Kawabe H, Gonda Y, Rimura M, Ochiai H, Ogawa K, Fiebiger G, Heumader J, Rudolf Miklau F, Kienholz H, Mikos M [eds]. Universal Academy Press, Inc.: Tokyo, Japan; 561-567.

Kondo, K., S. Hayashi, T. Nonoda, S. Numamoto,and Y. Shirakawa (2004), Role of tree roots system for slope failure obtained from two dimensional analysis. In *International Symposion Interpraevent*, 2004, Riva-Trient; 197-207.

Korpela, I., B. Dahlin, H. Schfer, E. Bruun, F. Haapaniemi, J. Honkasalo, S. Ilvesniemi, V. Kuutti, M. Linkosalmi, J. Mustonen, M. Salo, O. Suomi, and H. Virtanen (2007), Single-tree forest inventory using LIDAR and aerial images for 3D treetop positioning, species recognition, height and crown width estimation, *IAPRS*, *36*, 227-233.

Krogstad, F. (1995), A physiology and ecology based model of lateral root reinforcement of unstable hillslopes, *Master thesis*, University of Washington.

Kuiper, L. C., and M. P. Coutts (1992), Spatial disposition and extension of the structural root system of Douglas-fir, *Forest Ecology and Management*, *47*, 111-125.

Kun, F., F. Reischel, R. C. Hidalgo, and H. J. Herrmann (2007), Extensions of fiber bundle models, *Lecture Notes in Physics*, *705*, 57-92.

Laio, F., P. D Odorico, and L. Ridolfi (2006), An analytical model to relate the vertical root distribution to climate and soil properties, *Geophysical Research Letters*, *33*, L18401.

Lateltin, O., C. Haemmig, H. Raetzo, and C. Bonnard (2005), Landslide risk management in Switzerland, *Landslides*, *2*, 313-320.

Lynch, J. P., K. L. Nielsen, R. D. Davis, and A. G. Jablokow (1997), SimRoot: modelling and visualisation of root systems, *Plant and Soil*, *188*, 139-151.

Majdi, H., K. Pregitzer, A. S. Moren, J. E. Nylund, and G. I. Agren (2005), Measuring fine root turnover in forest ecosystems, *Plant and Soil*, *276*, 1-8.

Mattia, C., G. B. Bischetti, and F. Gentile (2005), Biotechnical characteristics of root systems of typical Mediterranean species, *Plant and Soil*, *278*, 23-32.

Mickovski, S. B., A. G. Bengough, M. F. Bransby, M. C. R. Davies, P. D. Hallet, and R. Sonnenberg (2007), Material stiffness, branching pattern and soil matric potential affect the pullout resistance of model root systems, *European Journal of Soil Science*, *58*, 1471-1481.

Montagu, K. D. , J. P. Conroy, and B. J. Atwell (2001), The position of localized soil compaction determines root and subsequent shoot growth responses, *Journal of Experimental Botany*, *52*, 2127-2133.

Montgomery, D. R., and W. E. Dietrich (1994), A physical based model for the topographic control on shallow landsliding, *Water Resources Research*, *30*, 1153-1171.

Montgomery, D. R., K. M. Schmidt, H. M. Greenberg, and W. E. Dietrich (2000), Forest clearing and regional landsliding, *Geology*, *28*, 311-314.

Moroni, M. T., D. Worledge, and C. L. Beadle (2003), Root distribution of *Eucalyptus nitens* and *E. globules* in irrigated and droughted soil, *Forest Ecology and Management*, *177*, 399-407.

Mller, K. H., and S. Wagner (2003), Fine root dinamics in gaps of Norway spruce stands in the German Ore Mountains, *Forestry*, *76*, 149-158.

Nicoll, B. C., and D. Ray (1996), Adaptive growth of tree root systems in response to wind action and site condition, *Tree Physiology*, *16*, 891-898.

Nicoll, B. C., S. Berthier, A. Achim, K. Gouskou, F. Danjon, and L. P. H. van Beek (2006), The architecture of *Picea sitchensis* structural root systems on horizontal and sloping terrain, *Trees*, *20*, 701-712.

Nilaweera, N. S., and P. Nutalaya (1999), Role of tree roots in slope stabilisation, *Bulletin Engineering Geology of the Environment*, *57*, 337-342.

Norris, J. E. (2005), Root reinforcement by hawthorn and oak roots on a highway cut-slope in Southern England, *Plant and Soil*, *278*, 43- 53.

Operstein, V., and S. Frydman (2000), The influence of vegetation on soil strength, *Ground Improvement*, *4*, 81-89.

Osman, N., and S. S. Barakbah (2006), Parameters to predict slope stability soil water and root profiles, *Ecological Engineering*, *28*, 90-95.

Ostonen, I., K. Lohmus, and R. Lasn (1999), The role of soil conditions in fine root ecomorphology in Norway spruce [*Picea abies* [L.] Karst.], *Plant and Soil*, *208*, 283-292.

Ozier-Lafontaine, H., F. Lecompte, and J. F. Sillon (1999). Fractal analysis of the root achitecture of *Gliricidia sepium* for the spatial prediction of root branching, size and mass: model development and evaluation in agroforestry, *Plant and Soil*, *209*, 167-180.

Pages, L., G. Vercambre, J. L. Drouet, F. Lecompte, C. Collet, and J. Le Bot (2004), Root Typ: a generic model to predict and analyse the root system architecture, *Plant and Soil*, *258*, 103-119.

Pollen, N. 2008, Temporal and spatial variability of root reinforcement in streambanks: Accounting for soil shear strength and moisture, *Catena*, *69*, 197-205.

Pollen, N., A. Simon, and A. Collison (2004), Advances in assessing the mechanical and hydrologic effects of riparian vegetation on streambank stability, *Riparian vegetation and fluvial geomorphology, water sciense and application*, *8*, 125-139.

Pollen, N., and A. Simon (2005), Estimating the mechanical effects of riparian vegetation on stream bank stability using a fiber bundle model, *Water Resources Research*, *41*, w07025.

Pregitzer, K. S., J. L. DeForest, A. J. Burton, M. F. Allen, R. W. Ruess, and R. L. Hendrick (2002), Fine root architecture of nine north American

trees, *Ecological Monographs*, *72*, 293-309.

Puhe, J. (2003), Growth and development of the root system of Norway spruce in forest stands a review, *Forest Ecology and Management*, *175*, 253-273.

Reneau, S. L., and W. E. Dietrich (1987), Size and location of colluvial landslides in a steep forested landscape. In *Erosion and Sedimentation in the Pacific Rim*, Proceedings of the Corvallis Symposium, August 1987, *IAHS Publication*, *165*, 39-48.

Reubens, B., J. Poesen, F. Danjon, G. Geudens, and B. Muys (2007), The role of fine and coarse roots in shallow slope stability and soil erosion control with a focus on root system architecture: a review, *Trees*, *21*, 385-402.

Rickli, C. 2001, Vegetationswirkungen und Rutschungen Untersuchung zum Einfluss der Vegetation auf oberflchennahe Rutschprozesse anhand der Unwetterereignisse in Sachseln OW am 15. August 1997. Birmensdorf, Bern. Eidg. Forschungsanstalt WSL, Bundesamt fr Umwelt, Wald und Landschaft.

Roering, J. J., K. M. Schmidt, J. D. Stock, W. E. Dietrich, and D. R. Montgomery (2003), Shallow landsliding, root reinforcement, and the spatial distribution of trees in the Oregon Coast Range, *Canadian Geotechnology Journal*, *40*, 237-253.

Sakai, Y., M. Takahashi, and N. Tanaka (2007), Root biomass and distribution of *Picea abies* stand and *Larix betula* stand in pumiceous Entisols in Japan, *Journal of Forest Research*, *129*, 120-125.

Sakals, M. E., and R. C. Sidle (2004), A spatial and temporal model of root cohesion in forest soils,*Canadian Journal of Forest Research*, *34*, 950-958.

Santantonio, D. (1990), Modeling growth and production of tree roots, In *Process Modeling of Forest Growth responce to Enviromental stress*, Dixon: Portland; 124-135.

Schenk, H. J. (2008), The shallowest possible water extraction profile: a null model for global root distributions, *Vadose Zone Journal*, *7*, 1119-1124.

Schenk, H. J., and R. B. Jackson (2002), The global biogeography of roots, *Ecological Monographs*, *72*, 311-328.

Schmidt, K. M., J. J. Roering, J. D. Stock, W. E. Dietrich, D. R. Montgomery, and T. Schaub (2001), The variability of root cohesion as an influence on shallow landslide susceptibility in the Oregon Coast Range, *Canadian Geotechnology Journal*, *38*, 995-1024

Schmid, I., and M. Kazda (2002), Root distribution of Norway spruce in monospecific and mixed stands on different soils, *Forest Ecology and Management*, *159*, 37-47.

Schmid, F., M. Fraefel, and C. Hegg (2004), Unwetterschden in der Schweiz 19722002 (Financial Damage caused by Flooding and Landslides in Switzerland 19722002]: Verteilung Ursachen, Entwicklung. *Wasser, Energie und Luft*, *12*, 21-28.

Sidle, R. C. (1992), A theoretical model of the effects of timber harvesting on slope stability, *Water Resources Research*, *28*, 1897-1910.

Sidle, R. C., and W. Wu (2001), Evaluation of the temporal and spatial impacts of timber harvesting on landslide occurrence, *Water Science and Application*, *2*, 179-193.

Simoni, S., F. Zanotti, G. Bertoldi, and R. Rigon (2007), Modelling the probability of occurrence of shallow landslides and channelized debris flows using GEOtop-FS, *Hydrological Processes*, *22*, 532-545.

Sivakumar Babu, G. L., A. K. Vasudevan, and S. Haldar (2008), Numerical simulation of fiber-reinforced sand behaviours, *Geotextiles and Geomenbranes*, *26*, 181-188.

Sornette, D. (1989), Elasticity and failure of a set of elements loaded in parallel, *Journal of Physics A: Mathematics and General*, *22*, L243-L250.

Steel, S. J., S. T. Gower, J. G. Vogel, and J. M. Norman (1997), Root mass, net primary production and turnover in aspen, jack pine and black spruce forests in Saskatchewan and Manitoba, Canada, *Tree Physiology*, *17*, 577-587.

Stober, C., E. George, and H. Persson (2000), Root growth and response to nitrogen. In Carbon and Nitrogen Cycling in European Forest Ecosystems, *Ecological Studies*, *142*, 99-121.

Tobin, B., J. Cermak, D. Chiatante, F. Danjon, A. Di Orio, L. Dupuy, A. Eshel, C. Jourdan, T. Kalliokoski, R. Laiho, N. Nadezhdina, B. Nicoll, L. Pages, J. Silva, I. Spanos (2007), Towards developmental modelling of tree root systems, *Plant Biosystems*, *141*, 481-501.

Tosi, M. (2007), Root tensile strength relationships and their slope stability implications of three shrubs species in the Northern Apennines [Italy], *Geomorphology*, *87*, 268-283.

Van Beek, L. P. H., J. Wint, L. H. Cammeraat, J. P. Edwards (2005), Observation and simulation of root reinforcement on abandoned Mediterranean slopes, *Plant and Soil*, *278*, 55-74.

Van Noordwijk, M., L. Y. Spek, P. de Willigen (1994), Proximal root diameter as predictor of total root size for fractal branching models, *Plant and Soil*, *164*, 107-117.

Vanomsen, P. (2006), Der Einfluss der Durchforstung auf die Verankerung der Fichte hinsichtlich ihrer Sturmresistenz. Diss. ETH Nr. 16532, Zürich.

Vercambre, G., L. Pages, C. Doussan, and R. Habib (2003), Architectural analysis and synthesis of plum tree root system in an orchard using a quantitative modelling approach, *Plant and Soil*, *251*, 1-11.

Wälder, O., and K. Wälder (2008), Modeling the fine root biomass dispersion using a special influence function, *iForest*, *1*, 141-144.

Waldron, L. J. (1977), The shear resistance of root-permeated homogeneous and stratified soil, *Soil Science Society of America Journal*, *41*, 843-849.

Waldron L. J., and S. Dakessian (1981), Soil reinforcement by roots: calculation of increased soil shear resistance from root properties, *Soil Science*, *132*, 427-435.

Wang, Z., D. Guo, X. Wang, J. Gu, and L. Mei (2006), Fine root architecture, morphology, and biomass of different branch orders of two Chinese

temperate tree species, *Plant and Soil*, *288*, 155-171.

Watson, A., C. Phillips, and M. Marden (1999), Root strength, growth, and rates of decay: root reinforcement changes of two tree species and their contribution to slope stability, *Plant and Soil*, *217*, 39-47.

Wu, T. H. (2007), Root reinforcement: analyses and experiments. In *Eco and Ground Bio-Engineering: The Use of Vegetation to Improve Slope Stability*, Stokes et al. [eds]. Springer; 21-30.

Wu, T. H., W. P. McKinnell, and D. N. Swanston (1979), Strength of tree roots and landslides on Price of Wales Island, Alaska, *Canadian Geotechnology Journal*, *16*, 19-33.

Wu, T. H., M. McOmber, R. T. Erb, and P. E. Beal (1988a), Study of soil-root interaction, *Journal of Geotechnical Engineering*, *114*, 1351-1375.

Wu, T. H., P. D. Bettadapura, and E. P. Beal (1988b), A statistical model of root geometry, *Forest Science*, *34*, 980-997.

Wu, T. H., and A. Watson (1998), In situ shear tests of soil blocks with roots, *Canadian Geotechnology Journal*, *35*, 579-590.

Yanai, R. D., B. B. Park, and S. P. Hamburg (2006), The vertical and horizontal distribution of roots in northern hardwood stands of varying age, *Canadian Journal of Forest Research*, *36*, 450-459.

Zhou, Y., D. Watts, Y. Li, and X. Cheng (1998), A case study of effect of lateral roots of *Pinus yunnanensis* on shallow soil reinforcement, *Forest Ecology and Management*, *103*, 107-120.

Zobel, R. W. (2005), Primary and secondary root systems. Root and soil management: interaction between roots and the soil, *Agronomy Monograph*, *48*, 3-14.

Chapter 3

Soil-Root Mechanical Interactions During Pullout and Failure of Root Bundles

Autohrs: Schwarz M. [1,2], Cohen D. [2] and Or D.[2]

[1] Swiss Federal Institute for Forest, Snow and Landscape Research, 8903 Birmensdorf, Switzerland

[2] Soil and Terrestrial Environmental Physics, Institute of Terrestrial Ecosystems, ETH Zurich, 8092 Zurich, Switzerland

Published in: *J. Geophys. Res.*, (2010), *115*, F04035. doi: 10.1029/2009JF001603

3.1 Abstract

Roots play a major role in reinforcing and stabilizing steep hillslopes. Traditionally mechanical behavior of roots during slope failure was modeled by upscaling the behavior of static individual roots. Recent studies, however, have shown that much better predictions of slope stability can be made if the progressive failure of bundles of roots are considered. The characteristics of progressive failure depend on interactions between soil deformation and root bundle geometric and mechanical properties. We present a detailed model for quantitative description of mechanical behavior of a bundle of roots under strain-controlled mechanical forcing. The Root Bundle Model (RBM) explicitly considers typical values of root-size spatial distribution (number and dimension of roots), geometric factors (diameter-length proportion, tortuosity, and branching characteristics), and mechanical characteristics (tensile strength, Young's modulus) and interactions under various soil conditions (soil type, confining pressure, and soil moisture). We provide systematic analyses of the roles of these factors on the mechanical response of the bundle and explore the relative importance of various parameters to the macroscopic root-soil mechanical response. We distinguish between increased strength imparted by small roots at small deformations and the resilience imparted by larger roots to growth of large tensile cracks (Figure 3.11) showing that the maximal reinforcement of fine roots is reached within the first 5 cm of displacement whereas a root of 20 mm diameter may reach its maximal pullout force after 10 cm displacement. The model reproduces the gradual straining and ultimate residual failure behavior of root systems often observed in hillslopes with progressive growth of tension cracks (Figure 3.18) allowing a better estimation of the root reinforcement (error of about 20%) than the widely used model of Wu (error of about 50%). These results enhance understanding of root reinforcement mechanisms and enable more realistic implementation of root reinforcement modeling for stability calculations of vegetated slopes, and for guiding ongoing experimental efforts to gather critical root-soil mechanical information.

3.2 Introduction

Roots fulfill a diverse array of functions in plant life ranging from capture and transport of subsurface resources, to mechanical anchoring and stabilizing of trees in support of growth, and to resilience to external stresses such as wind, snow accumulation, rock impact, and soil creep (Coutts, 1983; Schmidt et al., 2001; Rickli, 2001; Casadei et al., 2003; Johnsson et al.,

2006). Roots also stabilize soil on steep slopes by virtue of their extensive proliferation and mechanical properties. Additionaly, plant water uptake by roots decreases soil moisture, thereby increasing matric potential and mechanical strength. Often, these disparate mechanical effects have been lumped into an apparent increase soil cohesion as defined in Mohr Coulomb analysis.

The processes by which roots stabilize slopes depend to a large extent on their size, spatial distribution, and geometry (diameter-length proportion, tortuosity, and branching characteristics). In some cases roots stabilize a slope by bridging across pre-existing weak zones and basal shear planes, and thus become loaded during failures of these zones [Schwarz et al., 2010]. For shallow and laterally extensive root networks, slope stability may increase when sufficient roots cross potential tension cracks (scarp) that define the perimeter of a shallow landslide [Schwarz et al., 2009].

Various methods to quantify effects of root reinforcement along a landslide shear plane have been proposed [e.g., Wu et al., 1979; Ekanayake and Phillips, 1999; Pollen, 2008]. Wu's approach [1979] is widely used as it incorporates data on root and soil mechanical properties in an easy-to-apply model. A limiting assumption in Wu's model is that all roots break simultaneously which is not supported by observations [Pollen et al., 2004; Wu, 2007; Fan and Su, 2008] and results in a consistent over-prediction of actual root reinforcement function. Early models typically did not consider geometrical and stress-strain behavior of root bundles, a necessary element for describing complex interactions between roots and soil matrix. They also overlooked the function of roots of different sizes in reinforcement as discussed in a recent review by Schwarz et al. [2009]. These root size and geometrical characteristics determine how root reinforcement is progressively activated during gradual loading and soil deformation.

Recently, concepts of fiber bundle models (FBM) have been applied to root reinforcement and bank stability problems [Pollen et al., 2004; Pollen, 2008; Mickovski et al., 2009]. The classical FBM model assumes an incremental stress loading in which an imposed tensile force is distributed across unbroken fibers. When a root or fiber breaks, its load is redistributed over the remaining fibers. During each load step, force is redistributed until either equilibrium is reached or the entire bundle fails. Fiber bundle models show better fit to experimental data [Pollen et al., 2004; Pollen, 2008; Mickovski et al., 2009] and rely on simple power-law relationships between root size and mechanical behaviors. However, details of root-soil interactions and root failure mechanisms such as root stretching, size-stiffness relationship, and root-soil friction, which control whether roots slip or fail, are not included. In particular, existing models do not consider the mechanical

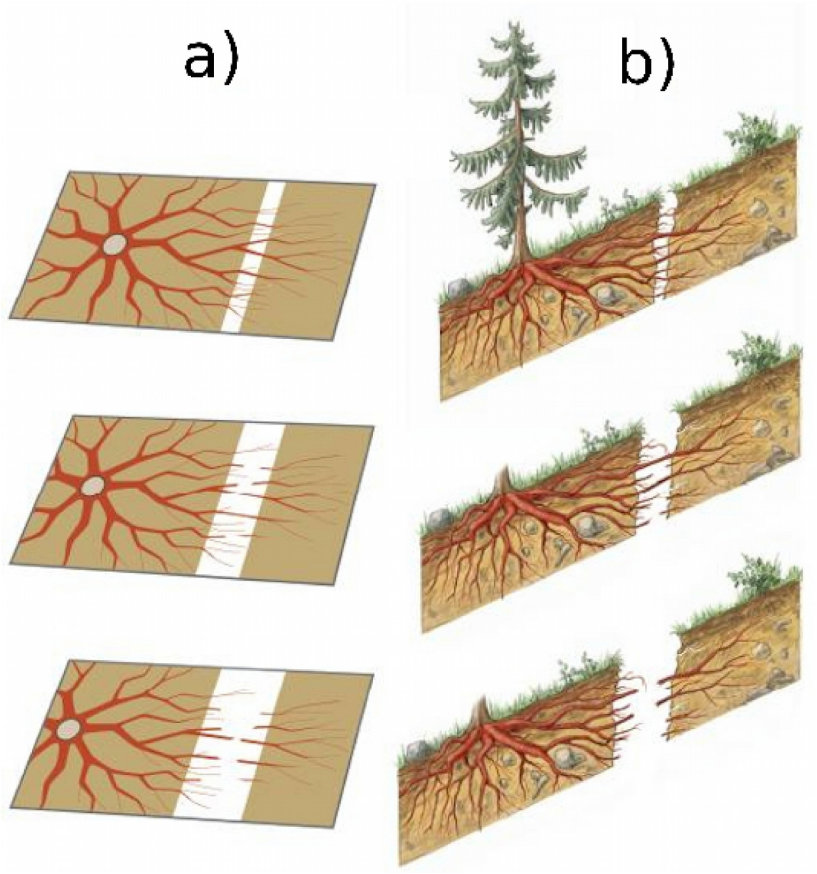

Figure 3.1: Illustration of a pulled bundle of roots modeled by the RBM at three stages of deformation: a) plan view and b) cross-sectional views. The RBM considers root bundle uphill of the transverse failure plane.

properties of soil at all. Present fiber bundle models also do not include models for the estimation of the root size distribution where geometric and mechanical properties vary with root size. Moreover, root reinforcement models are typically not tuned to study lateral reinforcement (with the notable exception of Schmidt et al. [2001]).

The mechanical behavior of pulled roots depends on numerous parameters (detailed below). Previous studies [e.g., Waldron and Dakessian, 1981; Comandeur and Pyles, 1991; Dupuy et al., 2005; Mickovski et al., 2007; Fan and Sun, 2008] provide a basis for identifying first-order control variables that must be included in any root-reinforcement model. One such class of variables is related to root geometry, which is notoriously difficult to characterize precisely [Danjon and Reubens, 2008]. Only a few studies

describe how the various geometrical features of roots (e.g., variation of diameter with length, branching points, tortuosity) contribute to the mechanical behavior of individual roots [Dupuy et al., 2005; Mickovski et al., 2008]. Most research has focused primarily on individual variables such as root diameter or branching pattern [e.g., Stokes et al., 1996; Dupuy et al., 2006; Mickovski et al., 2007]. For example, recent studies have shown the importance of branching points on the stress-strain behavior of pulled roots [Dupuy et al., 2005; Mickovski et al., 2007].

An additional set of key variables is related to the intrinsic mechanical properties of individual roots and bundles. A common measure of root reinforcement is the maximum tensile strength of a root which primarily depends on root diameter. Root stiffness (Young's modulus) is also known to depend on root diameter [Operstein and Frydman, 2000; Tosi, 2007; Fan and Su, 2008]. Commandeur and Pyles [1991] showed that root tortuosity is also an important parameter influencing the macroscopic elastic behavior of a pulled root. Tortuosity should therefore induce an apparent Young's modulus smaller than the root's intrinsic Young's modulus due to frictional interactions between the root and the surrounding soil as the root reconfigures during pulling. Consequently, stiffer roots mobilize more stress than less stiff roots for the same amount of strain. Friction at the root-soil interface is usually considered constant and frictional forces are calculated assuming a constant root diameter [Waldron and Dakessian, 1981; Ennos, 1990]. In reality, root diameter decreases along the root axis, and the activation of root-soil friction depends on the pullout force. Moreover, root-soil friction changes considerably during stretching and slippage but this aspect is neglected.

The primary objective of this study was to quantify the effects of various root geometrical and mechanical parameters on the tensile strength of an individual root and on the mechanical behavior of a bundle of roots under pullout tests. We included the effects of root length, root diameter and its variation along the root, maximum tensile strength, Young's modulus, root-soil interface friction, branching-point frequency, and root tortuosity into a numerical fiber bundle model that describes the mechanical dynamic pullout behavior of roots embedded in a soil matrix during strain-controlled deformation. The model strikes a compromise between complexity arising from root-soil interactions and oversimplifications of previous models by judicious selection of a minimum number of parameters needed to describe key features of the geometry and mechanics of pulled roots. The model considers how a bundle of lateral roots of different diameters contributes to the global reinforcement at different strain increments during the failure of a shallow landslide. Only root sections away from the tree stem are

used in the calculations, with the pullout direction away from the root tip (Figure 3.1). The model is built on a hierarchy of sub-models [Schwarz et al., 2010]: (1) a detailed description of the geometry and mechanics of individual roots; (2) a root frequency-size distribution model; (3) a strain-controlled pullout model of a bundle of roots that includes the effects of root elongation, root-soil friction, and root failure.

The specific objectives of this study are therefore to: (1) Present a new model (termed the Root Bundle Model or RBM) for the calculation of the force-displacement relation for an individual root, (2) Analyze the pullout behavior of a bundle of roots during strain loading, and (3) analyse root reinforcement characteristics of a bundle of roots for different root-size distributions and under various soil conditions.

3.3 Geometrical and Mechanical Model for Individual Roots

Experimental pullout tests on individual roots embedded in a soil matrix show that following initial (elastic) root stretching, roots may then either slip out or simply fail and break [Norris, 2005]. Figure 3.2 shows these different responses on a schematic force-displacement diagram. The first part of the pullout curve is dominated by the elastic properties of root and soil. The non-linear behavior that follows is documented experimentally [Hamza et al., 2007; Mickovski et al., 2007] and is due to the progressive activation of root-soil interfacial friction (details of this effect are described later). The maximum pullout force is reached when either the maximum (intrinsic) tensile strength of the root is exceeded (Figure 3.2, gray dashed line), or when root-soil friction drops reducing the pullout force and the root slips out (Figure 3.2, dark dashed line). Once broken, a root carries no load. During slip, the pullout curve may display complex behavior resulting from interactions between root strength, root elongation, and root-soil friction.

Individual Root Geometry

Single root geometry is characterized by a length-diameter relationship, branching points, and tortuosity. Various empirical relationships [e.g., Wu, 1988; Pollen, 2008] have been proposed for characterizing root length as a function of root diameter (Figure 3.3). Here we use the relation

$$L = L_0 \, d^{L_e}, \tag{3.1}$$

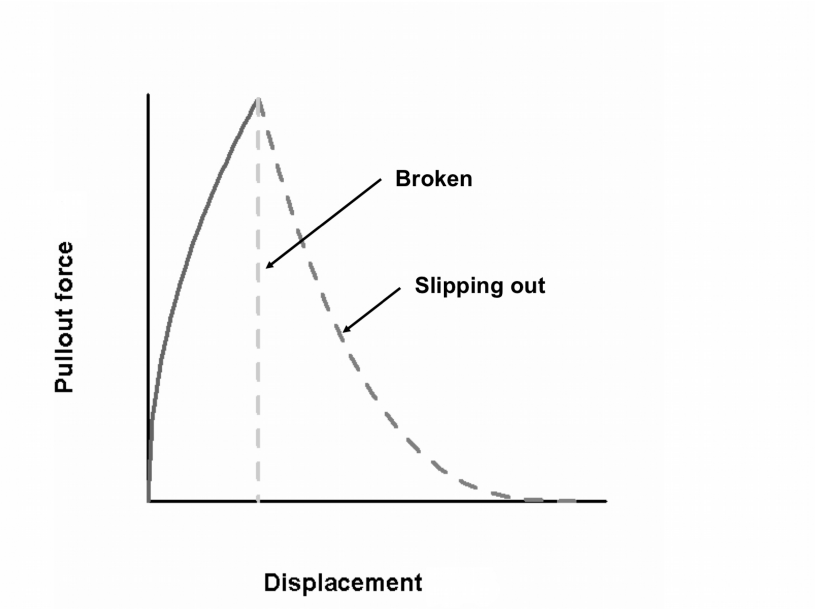

Figure 3.2: Pullout curves of an individual root on a force-strain diagram. The initial elastic stretch of a root (solid line) may be followed by gradual slip out (black dashed line), or abrupt failure and breakage (vertical gray dashed line). [Waldron and Dakessian, 1977].

where L is the length of the root following its axis, L_0 and L_e are empirical coefficients, and d is the root diameter measured where the root is pulled (that correspond to the value of d_n). In subsequent calculations, unless noted otherwise we have used $L_e = 0.63$ and $L_0 = 335$, values that fit data of secondary lateral roots of spruce (*Picea abies* L.) in a forest stand near Zurich, Switzerland [see Vanomsen, 2006, for description of field site].

A root has n branching points and $n + 1$ root segments (Figure 3.4). The mean branching distance or mean segment length (b) is

$$b = L/(n + 1). \tag{3.2}$$

Each root segment is assumend to have a constant diameter. The root diameter is assumed to increase from a minimum of 1 mm at the root tip (d_0) to a maximum value of d_n at the other end.

The variation of root cross sectional area along the root length is calculated as

$$A_i = s_i(i + 1)A_0, \qquad 1 \leq i \leq n, \tag{3.3}$$

where A_i is the cross section area of root segment i, A_0 is the cross sectional area of root segment 0 (equal to $\pi/4$ mm since $d_0 = 1$ mm), and s_i is the

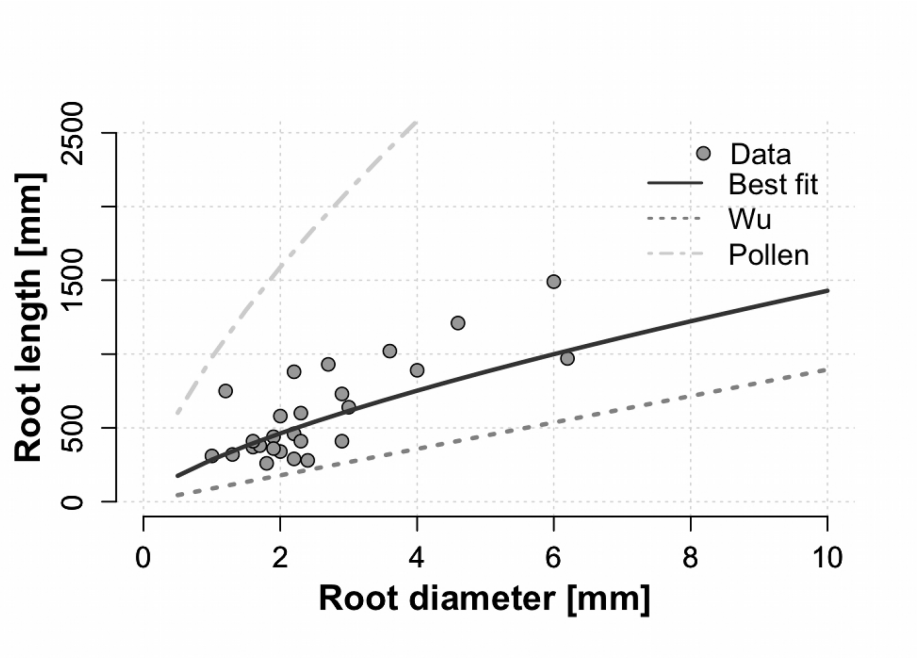

Figure 3.3: Measured data of 27 secondary lateral roots of spruce (*Picea abies* L.) trees (circles) and fitted empirical equation (equation (1), solid black line). Dash and dot-dash gray lines show empirical models used by Wu [1988] for various tree species and of Pollen [2008] for herbaceous species, respectively. The fitting of equation 1 has a residual standard error of 217 on 25 degrees of freedom and a SSE of 216.

scaling factor for root segment i. Since the scaling factor (or so-called root diameter proportionality factor) [Van Noordwijk et al., 1994; Ozier-Lafontaine et al., 1999; Vercambre et al., 2003; Collet et al., 2006] is defined as

$$s_i = \frac{b}{L}\frac{A_i}{A_0}, \qquad 1 \leq i \leq n, \tag{3.4}$$

the root diameter of segment i is given by [Schwarz et al., 2009]

$$d_i = d_0 \sqrt{s_i(i+1)}, \qquad 1 \leq i \leq n. \tag{3.5}$$

Root tortuosity is represented by dividing a root segment into connected sub-segments that meet at an angle γ (Figure 4) given by

$$\gamma = \cos^{-1}\left(\frac{1}{z}\right), \tag{3.6}$$

where z is a tortuosity factor defined as

$$z = \frac{L}{D}, \tag{3.7}$$

and D is the straight distance between the root tip and the pull location (Figure 3.4). For simplicity we assume that tortuosity is identical for all segments.

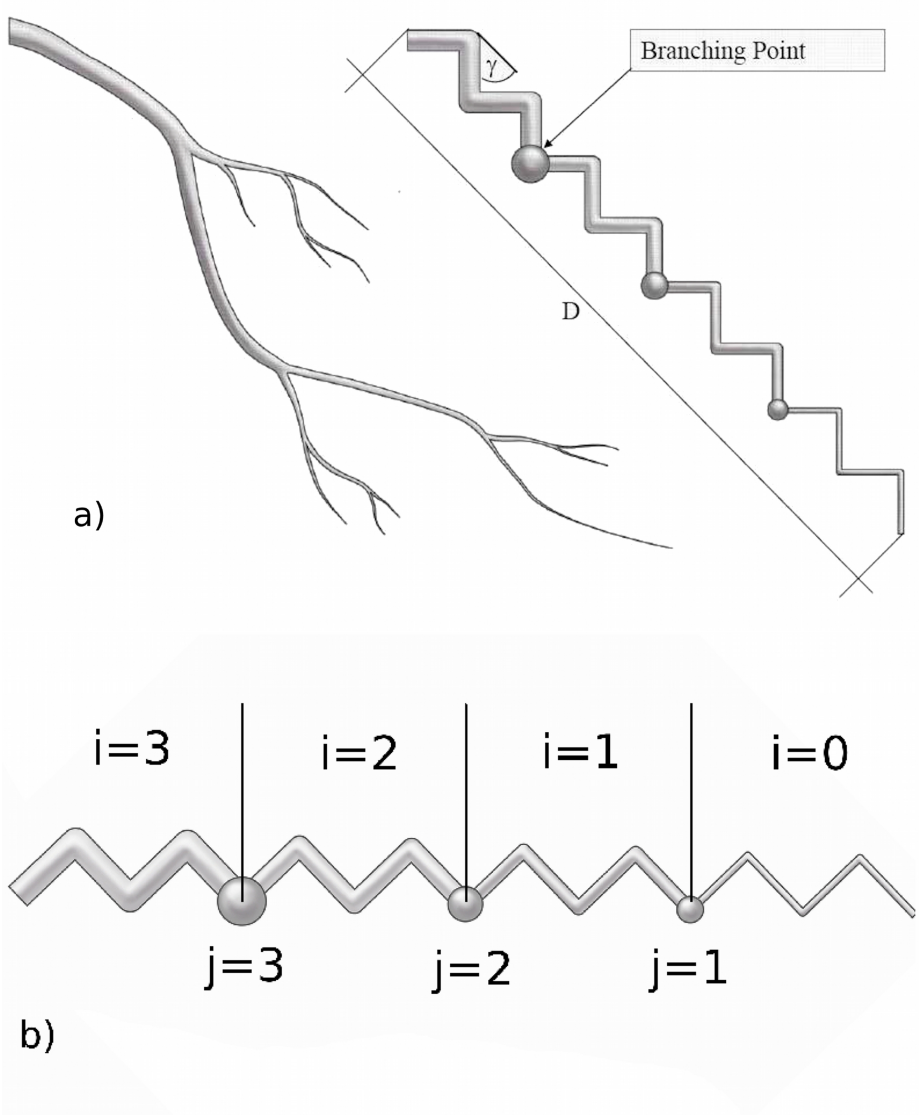

Figure 3.4: (a) Root geometry and root analogue. (b) Notation for a 4-segments root ($n = 3$).

Individual Root Mechanics

Mechanically, each root is characterized by a maximum tensile strength, $T^{\max}$, and intrinsic Young's modulus, E_f, that depend on root diameter. Numerous data indicate that $T^{\max}$ is proportional to the root diameter to some power, viz.,

$$T^{\max} = \alpha\, d^{\beta}, \tag{3.8}$$

where α and β are fitted coefficients. Table 3.1 shows values of these coefficients for spruce species (*Picea* sp.) reported by several authors [Abernethy, 2000; Bischetti et al., 2007; Genet et al., 2008].

Table 3.1: Published values of coefficients α and β in equation 8 for $T^{\max}$ in MPa and d in millimeters.

Reference	α	β
Abernethy [2001]	49.4	-0.8
Bischetti et al. [2007]	28.1	-0.7
Genet et al. [2008]	37.9	-0.5

To estimate Young's modulus, we use the formula of Schwarz et al. [2010] that best fits data found in the literature

$$E_f = 696\, d^{-1}, \tag{3.9}$$

where E_f is Young's modulus in MPa and d is in millimeters. The apparent elasticity of a root results from the combined effects of elasticity of the root itself, tortuosity, and soil properties. While the extension due to the root itself is limited by the maximum tensile strain at strength threshold $T^{\max}$, the extension due to tortuosity may not exceed a strain of $z - 1$, typically around 10–20% [Commandeur and Pyles, 1991]. Considering the common elasticity formulation, we thus define an apparent Young's modulus (E_{app}) as

$$E_{\text{app}} = \frac{\sigma}{\varepsilon} = \frac{F\, D_0}{A_0\, \Delta x}, \tag{3.10}$$

where σ and ε are, respectively, the stress and strain in the root, F is the pullout force, D_0 is the initial distance between the root's two end points, and Δx is the displacement where the root is pulled.

We assume that, in each segment, the resulting strain ε_i is the sum of two strain components due to root stretching and tortuosity,

$$\varepsilon_i = \varepsilon_i^{\mathrm{f}} + \varepsilon_i^{\mathrm{t}} = \frac{f_i^{\mathrm{tot}}}{A_i}\left(\frac{1}{E_{\mathrm{f}}} + \frac{1}{E_{\mathrm{t}}}\right), \tag{3.11}$$

where $\varepsilon_i^{\mathrm{f}}$ and $\varepsilon_i^{\mathrm{t}}$ are strains due to the root material and to tortuosity, respectively, and f_i^{tot} is the pulling force in the segment. Assuming that E_{t} is linearly proportional to E_{f} (where the ratio $\lambda = E_{\mathrm{t}}/E_{\mathrm{f}}$ depends on tortuosity and soil compressibility, the so-called compression index) [Commandeur and Pyles; 1991], equation (11) reduces to

$$\varepsilon_i = \frac{\lambda + 1}{\lambda}\frac{f_i^{\mathrm{tot}}}{A_i E_{\mathrm{f}}}. \tag{3.12}$$

Root–Soil Interfacial Friction

Friction at the root-root interface depends on soil type, soil moisture and confining pressure. We distinguish two major sources of friction: friction at the root-soil interface and friction at branching points. Interfacial friction changes from static friction during the stretching phase of a pullout test, to dynamic friction during the slip out phase. Furthermore, based on studies of fiber-reinforced concrete [e.g., Naaman et al., 1991] static friction may be separated into bonded and debonded friction.

Bonded Friction

In this section we show why bonded friction can be neglected following the approach of Naaman et al. [1991]. Bonded friction is considered a perfectly elastic response to local slip between the fiber and the matrix resulting in a frictional resistance at the fiber-matrix interface of the form

$$\tau_b = kS, \tag{3.13}$$

where τ_b is bonded friction, k is the bond modulus, and S is the local slip which depends on the difference between fiber and matrix Young's moduli, $E_f - E_m$ (for an extended explication of this formulation see Naaman et al. [1991]). When τ_b reaches the critical value of $\tau_b^{\max}$, a debonding crack grows along the fiber-matrix interface (Figure 3.5).

An illustration of how bonded friction varies along a constant diameter root after a debonding crack has begun to grow is shown in Figure 3.6. Integration of friction yields the total frictional force on a root. Even for parameters value that maximize the effect of bonded friction ($k = 10^9$ Pa

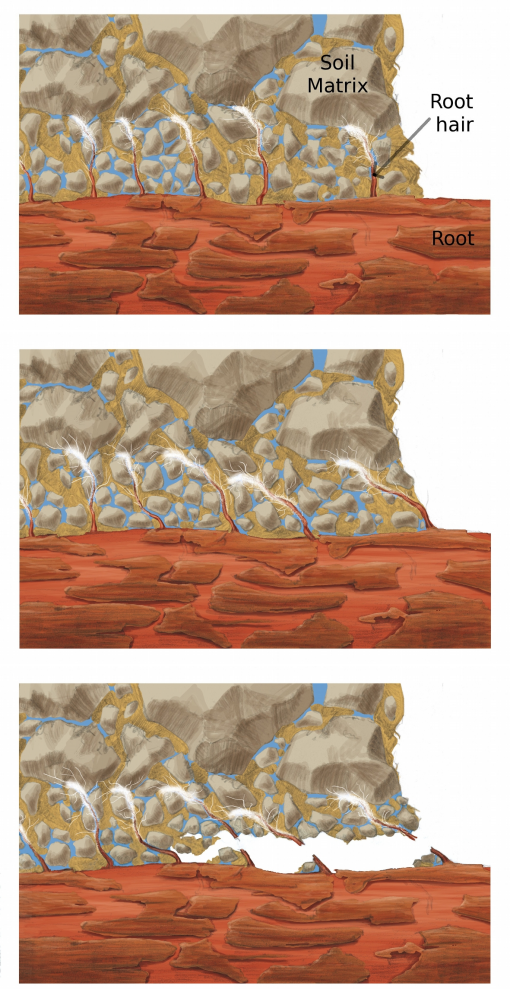

Figure 3.5: Hypothetical illustration of the propagation of a debonding crack at the instance when bonds between the fiber and the surrounding matrix reach a critical shear displacement.

m^{-1}, $\tau_{max} = 50$ kPa, $E_f/E_m = 10^{-3}$) the component of bonded friction to the total frictional force is relatively small (Figure 3.6).

When a root is stretched, its radius is reduced due to radial contraction given by

$$\Delta d = \varepsilon_f \nu_f d, \tag{3.14}$$

where Δd is radial contraction, ε_f is the fiber local strain, and ν_f is Poisson's ratio. Since

$$\varepsilon_f = \frac{F}{\pi (d/2)^2 E_f}, \tag{3.15}$$

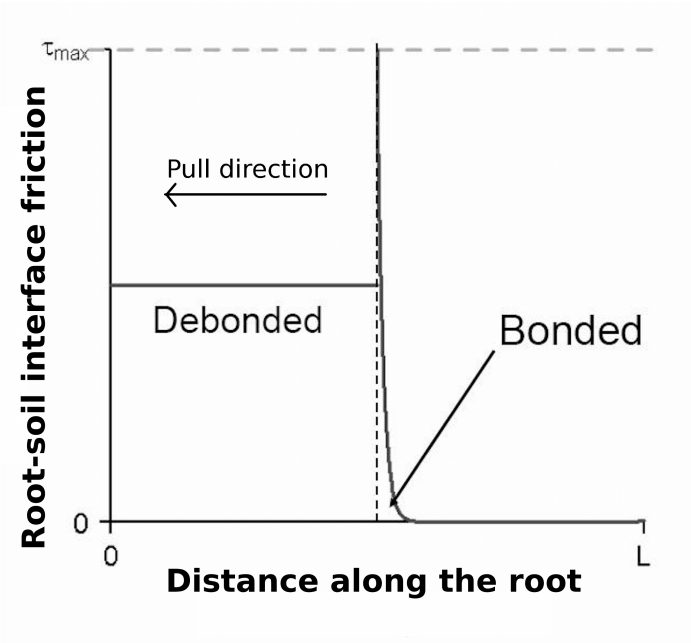

Figure 3.6: Distribution of friction along a root when the debonded crack extends to half the root length. Calculations were done with $k = 10^9$ Pa m^{-1}, $\tau_{max} = 50$ kPa, $E_f/E_m = 10^{-3}$, using the formulation of Naaman et al. [1991].

we can calculate the value of Δd along the root. With $d = 2$ mm, $E_f = 10^6$ Pa [Schwarz et al., 2010], $\nu_f = 0.3$ [Dupuy et al., 2005], and $F = 10$ kN (maximum value of pullout force based on our analysis), the Poisson effect is at most 10% of the root diameter. The decrease in diameter promotes debonding thereby further reducing the bonded zone between the fiber and the matrix. Thus, we can safely neglect bonded friction in our calculations as suggested earlier by Ennos [1990] and Li [1994].

Debonded Friction

Some authors have used a constant value for the root-soil friction (what we call here debonded friction) in the range of 1 to 10 MPa [e.g., Waldron and Dekassian, 1977; Abe and Ziemer, 1991]. In the RBM, the debonded friction is calculated assuming that failure occurs when the Coulomb failure criterion is reached, i.e.,

$$\tau_d = c' + \sigma' \tan \phi, \tag{3.16}$$

where τ_d is debonded friction, c' is the apparent cohesion, σ' is the effective normal stress, and ϕ is the residual root-soil friction angle. The effective normal stress on a root segment depends on tortuosity because the pullout force transferred to a tortuous root has a component which is always perpendicular to the root segment, leading to an asymmetrical local increase of the normal stress. To include this effect, we replace σ' by σ'_{tort}, defined as

$$\sigma'_{\text{tort}} = \sigma' + \left(\frac{f_i^{\text{tot}} \sin\gamma}{\pi\, d_i\, b} \right), \tag{3.17}$$

where f_i^{tot} is the pullout force acting on each root segment (Eq. 28). When only the first root segment is activated, $F = 0$ for all the other segments. For vertical pullout tests, the confining pressure around a root segment also varies as a function of soil depth.

Assuming, for the time being, that all segments of a root are activated and neglecting the effect of tortuosity, the maximum pullout force due to interfacial friction (F^{if}) occurs just prior to slippage and is

$$F^{\text{if}} = \pi\, b\, \tau_d \sum_{i=0}^{n} d_i, \tag{3.18}$$

assuming τ_d is constant in all root segments.

If instead of root segments of different diameters as assumed in the RBM, the root diameter is a continuous function of distance along the root ($d = d(x)$), then equation (18) may be replaced by

$$F^{\text{if}} = \pi\, b\, \tau_d \int_0^l d(x)\, dx, \tag{3.19}$$

where l is distance along the root, and

$$d(x) = d_0 \sqrt{\frac{s}{b} x}. \tag{3.20}$$

Substituting equations (20) into (19) yields

$$F^{\text{if}}(l) = \frac{2}{3} b\, \tau_d\, d_0 \sqrt{\frac{s}{b}}\, l^{3/2}. \tag{3.21}$$

Effect of Soil Saturation

The effect of unsaturated soil conditions is implemented using Bishop's effective stress approach [Lu and Likos, 2006]:

$$\sigma' = \sigma - u_a + \chi(u_a - u_w), \tag{3.22}$$

where σ' is the effective normal stress, σ is the total normal stress, u_a is the air pressure (assumed equal to 0 in our calculations), u_w is the pore water pressure, and χ is the effective stress parameter assumed to be a function of the degree of saturation [Lu and Likos, 2006] with values ranging between 0 (dry) and 1 (fully saturated). Here we assume a linear relation between matric suction $(u_a - u_w)$ and the suction stress $\chi(u_a - u_w)$ as shown in Lu and Likos [2006]. We also assume that once the water content reaches a minimal threshold value (dry condition), suction stress drops to 0 for sandy soil or remains constant for clay and loamy soil at a value corresponding to the effects of cementation. We recognize that the effects of soil saturation are more complex, especially for fine-textured soils. Changes in saturation in fine textured soils modify strength properties as well as deformation characteristics, leading to onset of plasticity as summarized in a recent study by Nuth and Lalouie [2008]. Moreover, it may also introduce time and pull-out rate dependency as described in the rheological framework of Ghezzehei and Or [2000]. For simplicity we defer such constitutive relationships to future studies and focus on standard applications as described next. We use the following equations to calculate the effect of suction on apparent cohesion as a function of water content

$$c' = c'_{\max}\left(\frac{\theta_{\text{sat}} - \theta}{\theta_{\text{sat}} - \theta_{\min}}\right), \qquad \theta \geq \theta_{\min}, \tag{3.23}$$

$$c' = c'_{\text{res}}, \qquad \theta < \theta_{\min}, \tag{3.24}$$

where c' is the apparent cohesion due to suction and cementation effects, c'_{res} is the residual cohesion in dry conditions and $c'_{\max}$ is the maximum value of apparent cohesion that a soil type may reach in optimal water content conditions. For sand $c'_{\max}$ ranges between 1 and 5 kPa [Gouldin, 2006] while for clay $c'_{\max}$ may have a wide range of values which range in the order of tenths of kPa.

Dynamic Friction

If during pullout, the maximum tensile strength of a root is not exceeded, the root slips out and frictional forces are initially reduced due to system dynamics. This decrease is due primarily to breakage and deformation of small lateral root hairs, rearrangement of soil particles, and changes in the value of the confining pressure, but also to the reduction of the length of the root embedded in the soil. To take these latter effects into account, we introduce a frictional decay function which depends on embedded root length, as proposed by Naaman et al. [1991] and Cuhna et al. [2008]. The

dynamic component of the root-soil interfacial friction is then

$$\tau_{\mathrm{dyn}} = c\,\tau_d \left(\frac{D(1+\varepsilon^{\max}) - \Delta x}{L} \right)^{\zeta} + (1-c)\,\tau_d, \tag{3.25}$$

where τ_{dyn} is dynamic friction, $\varepsilon^{\max}$ is the maximum strain a root can sustain, and c and ζ are empirical coefficients. Using literature data of pullout tests of willow's roots in sand [Mikovski et al., 2007], the best fit to equation (25) results in values of c in the range of 0 to 1 (with the range depending on soil type and conditions). The exponent ζ takes on values between 1 and 10. These two coefficients determine the decay of dynamic friction during slip out. For $c = 0$ there is no changes between the static and the dynamic root-soil interfacial friction. For large ζ, root-soil interfacial friction decays exponentially.

Branching Point Friction

Root branching points are represented as spherical elements that increase root-soil interfacial friction. The estimation of this component of friction is based on the following empirical observations and assumptions: (1) The angle between main and side roots at branching point has no influence [Dupuy et al., 2005]; (2) The mean diameter of the branching point is larger than any connected root segments and is a function of the largest root segment diameter; (3) The elasticity of lateral roots is neglected and their activated pullout force is considered constant. Based on information found in the literature [e.g., Stokes et al., 1996; Dupuy et al., 2005], we calculate the friction due to branching point i on segment i as

$$f_i^{bp} = Y\,d_i \tag{3.26}$$

where Y is an empirical branching coefficient.Combining interfacial and branching point friction, the contribution of a root segment to the maximal pullout force is

$$f_i = \pi\,d_i\,b\,\tau_d + Y\,d_i. \tag{3.27}$$

The total pullout force transmitted to the root segment i is

$$f_i^{\mathrm{tot}} = \sum_{j=1}^{i} f_j. \tag{3.28}$$

Again assuming a straight root and activation of all root segments, the maximum pullout force is

$$F_{\max}^{\mathrm{tot}} = \pi\,d_o\,b\,\tau_d + \sum_{i=1}^{n} f_i, \tag{3.29}$$

or, substituting equation 27,

$$F_{\max}^{\text{tot}} = \pi\, d_o\, b\, \tau_d + (\pi\, b\, \tau_d + Y) \sum_{i=1}^{n} d_i \tag{3.30}$$

Force-Displacement Calculation and Modeling Techniques

The complete pullout force as a function of pullout displacement is obtained by simulating a quasi-static pullout experiment where the pullout force is computed during stepwise strain increments. A strain loading approach is necessary to calculate the pullout forces in both the stretching and slip out phases. Stress-loading provoques the complete failure of the bundle at the maximum pullout force and hence cannot model the slip out phase.

Here we describe the algorithm to compute the pullout force in the root bundle as a function of incremental displacement. This algorithm is characterized by two main loops: (1) a stretching and breakage phase loop and (2) a slip out phase loop (Figure 3.7). Initially a root supports no load. During the initial stretching of a root, the pullout force required for matching root strain at a given strain step is calculated through an iterative process that considers progressive increments of activated root lengths. The algorithm used in the model is as follows:

(a) Increment displacement, Δx.

(b) Compute the elongation of the first root segment n, $\Delta D = b\varepsilon_n$, with ε_n given by equation 12 and f_n in equation 12 given by equation 28.

(c) If $\Delta D < \Delta x$ add a root segment and repeat step (b) (i.e., for $n-i$ segments, $\Delta D = b \sum_{j=i}^{n} \varepsilon_j$) otherwise move to the next strain increment (step (a)).

The algorithm is repeated until either the root fails or slips: if cumulative friction exceeds the maximal tensile force of a root segment (estimated using equation (8)), the root breaks. If all root segments have been activated and the maximal tensile strength is not reached, then the root starts to slip out and the algorithm in Figure 3.7 is used. This algorithm calculates the pullout force of the root in the slipping phase considering the progressive reduction of root length embedded in the soil and the axial contraction of the root due to the decreased tensile stress transmitted through the root segments.

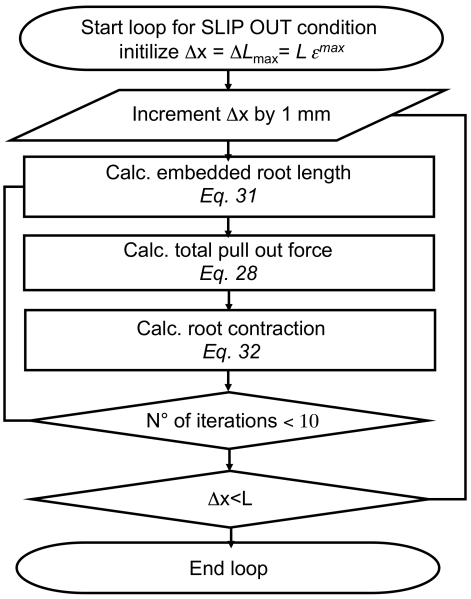

Figure 3.7: Flow chart of the module of the model use to calculate the pullout force in the slip out phase of the force-displacement behavior of an individual root.

The reduction of embedded root length is calculated as

$$\Delta L_{\mathrm{em}} = D(1 + \varepsilon^{max}) - \Delta x, \tag{3.31}$$

where ΔL_{em} is the change of the embedded root length at the displacement Δx, and $\varepsilon^{\max}$ is the maximal strain reached by a root at the instance where slip begins. We assume that prior to root slippage, embedded root length is equal to L (in reality, part of the root is already out of the soil because of tortuosity). Root contraction is calculated using the difference between the strains reached at maximal and minimal pullout force according to

$$\Delta L_{\mathrm{con}} = L(\varepsilon^{\max} - \varepsilon^{\mathrm{slip}}), \tag{3.32}$$

where $\varepsilon_f^{\mathrm{slip}}$ is calculated iteratively using equations (12) and (28), considering an initial number of embedded root segments equal to L_{slip}/b, where at the beginning $L_{\mathrm{slip}} = L - \Delta L_{em}$. The resulting root length along which frictional forces remain active during slippage (L_{slip}) is calculated for a prescribed number of iterations (usually 10), according to

$$L_{\mathrm{slip}} = L - \Delta L_{\mathrm{em}} - \Delta L_{\mathrm{con}} \tag{3.33}$$

With the new embedded root length (L_{slip}), we recalculate friction and total pull out force (equation(29)) over n activated root segments where $n = L_{\text{slip}}/b$. As the total pull out force acting on a root decreases (smaller embedded root length), the root contracts, further decreasing the length of embedded root and thus total friction. The macroscopic consequence of this iterative force balance is also known as stick-slip effect [Dietrich, 1977].

3.4 Root Distribution Model

The global mechanical behavior of a root bundle is strongly influenced by the distribution and size of roots. Data on distribution of roots of different diameter classes are scarce [e.g., Moroni et al., 2003; Wu et al., 1988; Zhou et al., 1998]. Thus, we parametrize root distribution using the non-cumulative Weibull probability function

$$p(d; m, k) = \frac{m}{k^m} d^{m-1} \exp\left[-\left(\frac{d}{k}\right)^m\right] \tag{3.34}$$

with $p(d)$ is the probability that a mapped root in a profile belongs to the root diameter class d, and m and k are the shape and scale parameters of the Weibull probability density function, respectively. We chose the Weibull probability function due to its well-established analytical formulation which may be adapted to various shapes of experimental distributions (in this case better than the lognormal distribution), and because it tends to fit better the distribution of big root diameter classes that are more important for mechanical considerations. For the calculation of the probability of finding a root belonging to a root diameter class within the range of diameter between d_a and d_b, we use the following integral

$$p(d_a - d_b; m, k) = \int_{d_a}^{d_b} \frac{m}{k^m} d^{m-1} \exp\left[-\left(\frac{d}{k}\right)^m\right]. \tag{3.35}$$

This application of the Weibull probability function for the parametrization of the root distribution assume that the shape of the probability function remains identical for roots at different radial distances from the tree stem; the only parameter that changes with distance from the tree stem is the total number of roots found at each distance.

3.5 The Root Bundle Model (RBM)

Recent studies [Pollen and Simon, 2005] show the potential utility of the Fiber Bundle Model (FBM) as a realistic framework for estimation of root

reinforcement in river banks. The classical approach of the FBM consists of simulation of a stress loading step of a bundle of fibers, where each fiber has different maximal tensile strength. In the simplest application, the fibers are considered to have identical length, which makes it possible via a global load sharing rule (uniform transfer of loads of broken fibers to all other fibers in the bundle) to compute analytically the entire stress-strain behavior. However, differences in geometries and in mechanical properties of individual roots may be important and complicate global pullout mechanical behavior of real root bundles. For these reasons, the assumptions of constant Young's modulus and constant root length are unrealistic and may distort the mechanical response of root systems and their failure dynamics as related to triggering a landslide. By calculating mean values of pullout force-displacement behavior of different root diameter classes, we may relax some of the assumptions and consider roots of variable lengths and mechanical properties. The resulting total pullout force of a bundle of roots as a function of displacement can be expressed as a sum of pullout forces of individual roots,

$$F_{\text{bundle}}(\Delta x) = \sum_{j=1}^{N} F_j(\Delta x) n_j \tag{3.36}$$

where $F_j(\Delta x)$ is the pull out force of a root belonging to diameter class j, and n_j is the number of roots present in the bundle of diameter class j. N is the number of diameter classes. $F_j(\Delta x)$ is calculated for each root diameter class using the individual root pullout module. This formulation of the Root Bundle Model (RBM) may be defined as a strain step loading model. In effect, we assume that roots bridging a crack are loaded under tension with no interaction between neighboring roots. We also assume that the orientation of roots has no effect on pullout forces.

3.6 Results

Individual Root Behavior

Pullout Phases

Figure 3.8 shows the different pullout phases calculated for a root without branching points during slip out. In the first part of the force displacement curve the stretching phase is non linear due to the progressive increase of activated root length. This non-linear elastic behavior has also been observed in field and laboratory experiments [e.g., Ennos, 1990; Hamza

et al., 2007]. The point labelled 1 in Figure 3.8 indicates a point when only part of the root-soil interface friction has been activated. At the point labelled 2, all the root is activated and the maximal pull out force is reached. The dotted gray line in Figure 3.8c shows that the maximal tensile strength along the root is never reached, thus the root slips out rather then breaks. Had the black continuous line associated with the point labelled 2 crossed above the gray dotted line, the root would have been broken (this could have happened had the root been longer, root-soil interfacial friction been higher, or root strength been weaker). The gray dotted line is calculated using equations (1), (2), and (8). The force distribution at point labelled 2 shows that root failure is most likely where the root is pulled. Under natural conditions this may not always be true due to heterogeneity of root material, root geometry, and soil interactions. Finally, the point labelled 3 indicates the moment were the embedded root length during the slip out phase is equal to the activated root length at the point labelled 1. Figure 3.8c shows that the total pullout force at these two instances is different. This is because during the stretching phase the diameters of the activated root segments are larger than during the slip out phase; with more root-soil interfacial area, the total friction is larger. The reduction of root diameter along the root partly explains the exponential decay of the pullout force during the slip out phase.

Sensitivity Analyses of Pullout Mechanical Behavior

Theoretical calculations of pullout behaviors of three roots of three different diameter classes (1, 2, and 3 mm) are depicted in Figure 3.9. In Figure 3.9a the force-displacement curves show that small roots tend to slip out while larger roots tend to break. This result, however, depends on the nature of the relations used for estimating root length from root diameter. Figure 3.9b shows force-displacement curves obtained with two different root-length models found in the literature. In the case of Wu's [1988] model (see Figure 3.3), root-length estimates are small and roots do not break. In contrast, Pollen's [2008] model (Figure 3.3) for herbaceous plants yields relatively long roots that tend to break. Figure 3.9 also shows that the maximal pullout force and the displacement at maximal pullout force vary non linearly with root diameters, thus showing that the apparent Young's modulus change as a function of the root diameter.

Figure 3.10 shows the influence of root diameter along its length on the pullout behavior of individual roots. Roots with constant diameters have higher total friction due to their larger surface areas than roots whose diameters decrease toward their tips. This difference in the total root-soil

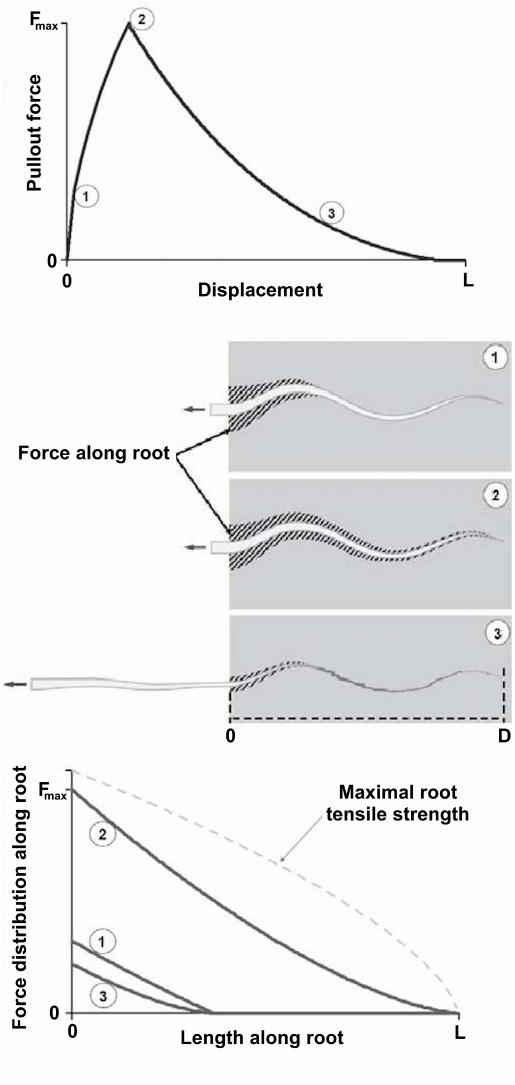

Figure 3.8: Force-displacement behavior of a 2 mm diameter root (top) calculated using the RBM. The three numbered points indicate the position at which correspond the three illustrations of the slipping root (middle) and the three curves (bottom), showing the cumulative force distribution along the root length.

interfacial friction influences both the threshold of the slipping out root diameter class (see the 4 mm diameter root in the Figure 3.10), and the apparent cohesion of the breaking root classes.

To complete the picture of individual root mechanical behavior, we performed sensitivity analyses of some key mechanical and geometrical param-

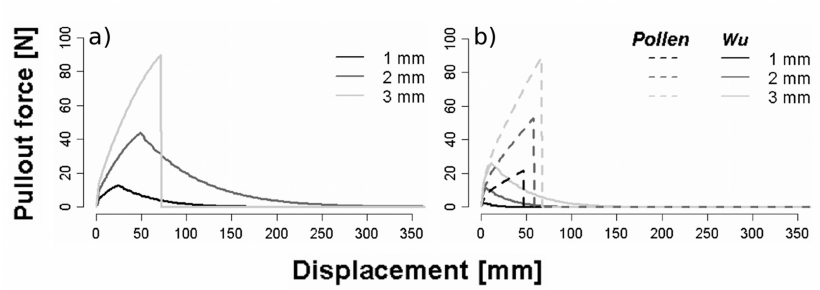

Figure 3.9: Pullout forces versus displacement of representative individual roots with diameters of 1, 2 and 3 mm, used for the calculation of root bundle behaviors. a) results with 2 kPa of confining pressure, 25 ° of root-soil interface friction angle, saturation of 0.9, tortuosity of 1.1, and branching coefficient of 0.4 (also used as standard values in the sensitivity analysis). b) A comparison of pullout behavior of individual roots using two different equations to estimate root length (Wu's [1988] and Pollen's [2008] models) is shown. The diameters of the individual roots are listed in the legend.

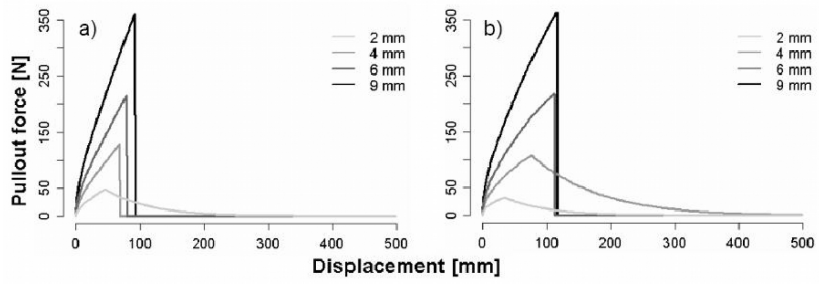

Figure 3.10: Comparison between numerical simulation considering (a) constant or (b) variable root diameter along the root axes. Calculations were done for 2 kPa confining pressure, soil saturation degree of 0.9, root-soil friction angle of 25 ° and factor of tortuosity of 1.1.

eters to identify most sensitive ones. Parameters such as confining pressure and root-soil interface friction angle had low influence on the global pullout behavior of individual roots. The maximal pullout force changed by less than 10% when considering extreme range of values for these two parameters (15–45 ° for the root-soil interface friction angle, and 0–10 kPa for the confining pressure). Results in Figure 3.11 show strong influences of two other parameters: root branching coefficient (Y) and root tortuosity (z). As base values for the calculations we have used 2 kPa for soil confining pressure (equivalent to 10–20 cm soil depth), tortuosity value of 1.1, friction

angle of 25 °, branching point coefficient (Y) of 0.4 (calibrated with field pullout tests of roots with diameters ranging from 1 to 3 mm in diameter), and degree of saturation value of 90% (close to saturation). In Figure 3.11a, we observe that an increase in the value of the branching coefficient leads to an increase of the total friction of the roots. Consequently, the activated root length decreases and so does the apparent elasticity. A strong variation of the global friction influences the type of pullout out behavior, as illustrated in Figure 3.11a: for a branching coefficient greater than 0.4 roots tend to break while for a branching coefficient of 0.1 roots tend to slip out.

Commandeur and Pyles [1991] illustrated the importance of tortuosity on the material (Young's) moduli. Figure 3.11b shows the influence of this parameter on the pullout behavior of individual roots when root-soil interfacial friction is also considered. An increase in tortuosity leads to an increase from 5 to 14 cm of displacement at failure while the maximal pullout force remains constant at 350 N.

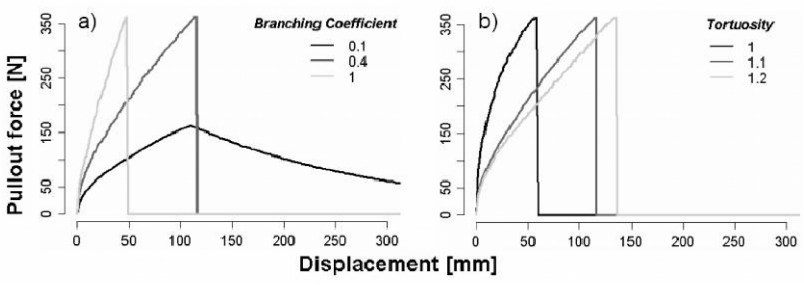

Figure 3.11: Influence of two parameters on pullout behaviors of an individual root (with 9 mm diameter): (a) branching point coefficient and (b) tortuosity.

The influence of soil moisture depends on soil type. For loamy soils the maximal soil cohesion is about 10 kPa at 10% saturation, and residual cohesion is 5 kPa for dry conditions (less than 10% saturation) [Schwarz et al., 2010]. In this case, the variation of maximal pullout force is about 10%, while the variation of displacement at maximal pullout force is about 20%.

Root Bundle Mechanical Response

Comparison between Single and Root Bundle

Erosion mitigation and slope stabilization studies often consider small roots as more effective than larger roots in slope stability [e.g., Reubens et al., 2003]. Results in Figure 3.12 provide new insights into this question and

show that to obtain mechanical reinforcement equivalent to one 20 mm diameter root, 23 roots with diameters of 2 mm are needed. Other differences between the behaviors of the two types of root reinforcement are: (1) the displacement at the maximal pullout force differs by about 50 mm; (2) because a 20 mm diameter root is considerably longer than a 2 mm diameter root (2.5 m against 0.46 m, using our equation (1) with fitted coefficients) the longer root can redistribute forces over greater distances in the soil.

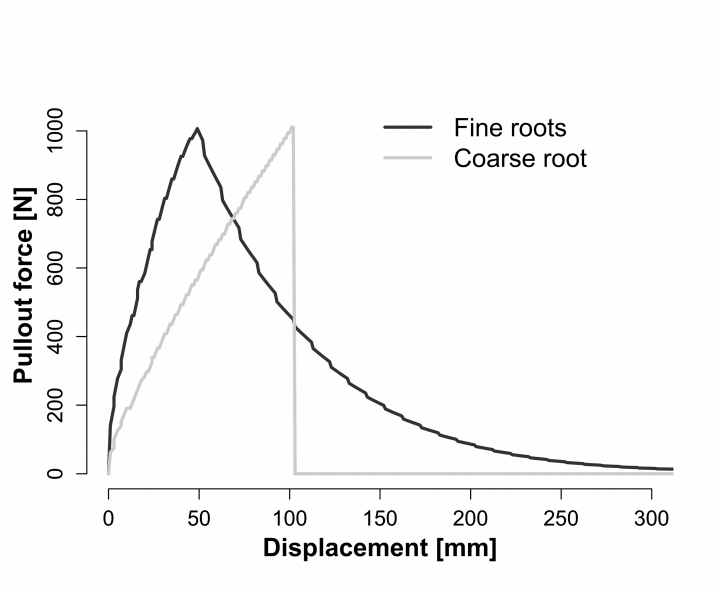

Figure 3.12: Pullout behaviors for the same maximum pullout force for an individual 20 mm diameter coarse root and 23 fine roots with diameters of 2 mm.

Figure 3.13 shows the breakage-slippage threshold on a length-diameter plot for different values of branching coefficient and tortuosity. In general, short roots (small values of L_0) with low friction tend to slip, while long roots with high friction almost always break. Results also show that once the values of branching coefficient and tortuosity are fixed the threshold is determined primarily by root length and does not depend on root diameter.

Effect of Root Size Distributions

Here we compare the influence of different root distributions on root reinforcement of a bundle of roots using measured root distributions and fitted Weibull distributions.

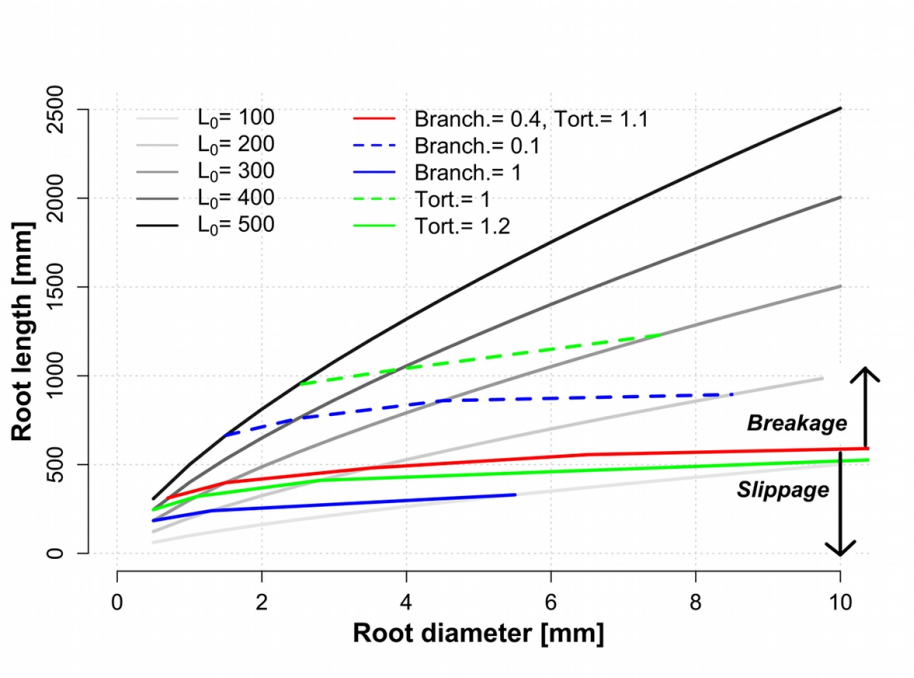

Figure 3.13: Thresholds of root diameter class separating breakage and slippage for different coefficients of root diameter - root length regressions (gray lines in the legend) and for different values of Tortuosity and Branching point coefficient (color lines in the legend).

Measured root distributions were obtained at three different distances from root stems (0.5, 1.5, and 2.5 m) for nine spruce trees (*Picea abies* L.) in the educational forest of ETH Zurich (Switzerland) [Vanmosen, 2006]. Tree stem diameter at 1.3 m height was in the range of 20 to 30 cm. Trenches 50 cm deep and 50 cm wide were dug tangentially to concentric circles around selected trees and the position of the trench was chosen to minimize overlapping root systems with neighboring trees. Figures 3.14 and 3.15 show root size data measured in the field and found in the literature [Wu et al., 1988; Zhou et al., 1998] and Weibull fits. We used the relative percentage of distribution of each root diameter class for each distance from tree stem for the fit of the Weibull distribution. The best fit was found for $m = 1.2$ and $k = 1.9$ using least square error minimization. The variance of the model results is 0.19 with a standard error less than 0.01. Using the same Weibull function, we fitted the data of Wu et al. [1988] and Zhou et al. [1998], obtaining $m = 1$ and $k = 0.8$ for Wu and $m = 1$ and $k = 3.3$ for Zhou (see Figure 3.15).

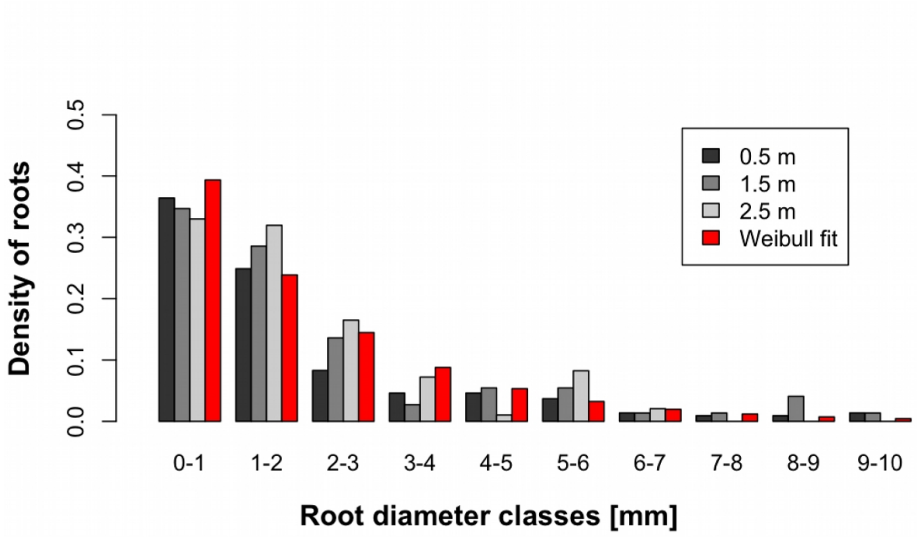

Figure 3.14: Fitted field data of mean root density distribution for 9 spruce trees at three different distance from stem (0.5, 1.5 and 2.5 m) using a Weibull probability function. For this fit the sum of squared errors (SSE) is 0.03.

Field measured root distribution data exhibit a linear relation between distance from tree stem and the total number of roots present in a soil profile. Figure 3.16 shows that (0.5 m away from the tree stem) there were on average 88 roots per square meter in the top 0.5 m of soil profile. The extrapolation of the linear regression indicates that, for trees with 20-30 cm in stem diameter, the maximal rooting distance is about 4.3 m. Such information is important for realistic estimation of root reinforcement at the scale of an individual tree allowing implementation of the RBM at different distances from the tree stem.

Finally, Figure 3.17 shows how maximal root reinforcement varies with distance from the tree stem for a measured field distribution and its Weibull fit. The Weibull fit underestimates the pullout force particularly close to the tree stem. This is because fitted Weibull distribution results in less coarse roots than measured, which contribute most to root reinforcement.

3.7 Discussion

The proposed modeling approach quantifies the influence of key root parameters on the force at failure of an individual root and of a bundle of

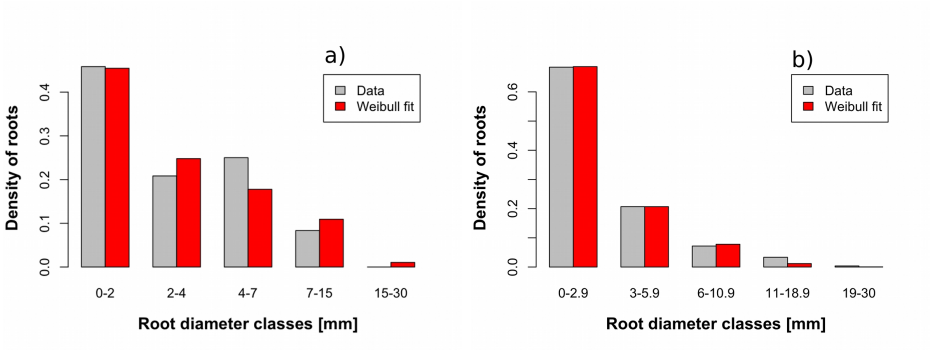

Figure 3.15: Fitting curves using the Weibull probability function for two data sets found in the literature [Wu et al., 1988; Zhou et al., 1998]. The used function parameters are m=1 and k=3.3 (SSE=0.0076) for the data set of Wu et al. [1988] (a) and m=1 and k=2.5 (SSE=0,0005) for the data set of Zhou et al. [1998] (b). To fit the Weibull model to the literature data we use cumulative values of probability of the root diameter classes as used from the authors. In the case of the data of Wu et al. (1988) the root diameter classes are 0-2 mm, 2-4 mm, 4-7 mm, 7-15 mm and 15-30 mm. In the case of the data of Zhou et al. [1998] the classes are 0-1 mm, 1-4 mm, 4-8 mm, 8-14 mm and 14-24 mm.

roots during pullout conditions. The model also yields an estimate of the force-displacement behavior of root reinforcement that could be used in soil strength or slope stability calculations. The innovative elements of this approach are the implementation of natural geometrical factors such as root tortuosity and branching point friction in the analysis of the individual root pullout behavior, the use of an analytical root distribution model, and the use of a fiber bundle model approach to describe the global behavior of a bundle of roots that includes different types of failure mechanisms (stretching, breakage, and slip out), an aspect not considered in other existing models.

Individual Root Behavior

Due to their geometrical and mechanical properties small roots tend to slip out first and then break, while under similar conditions larger roots ($>$ 2 mm diameter) tend to break without slipping out (Figure 3.13). One of the important outcomes of the proposed model is an estimation of the displacement at the maximal tensile force, as discussed in Schwarz et al. [2009], this is particularly important for better understanding how roots contribute to

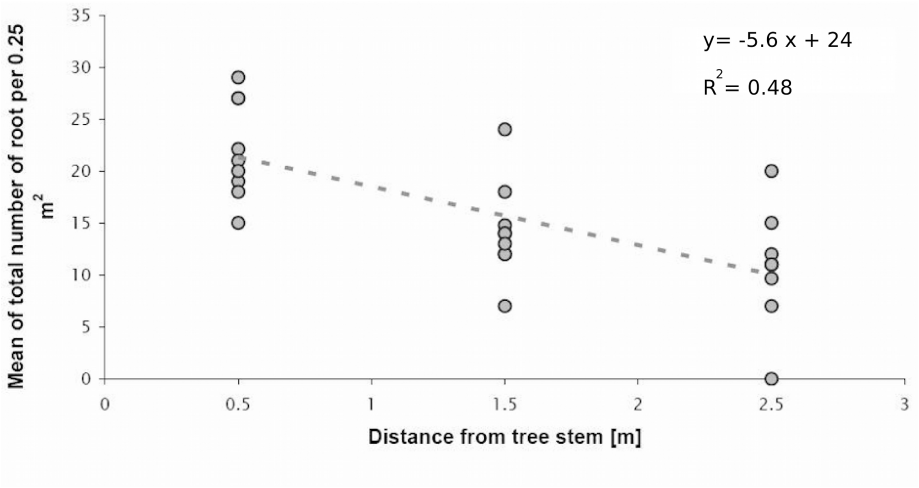

Figure 3.16: Distribution of the total number of roots at different distances form tree stem. (Note that some of the 9 data sets collected for each distance overlap).

the stabilization of a slope and how they influence the triggering of shallow landslides. Results show that the maximal tensile force of a root is attained at different displacements for different root diameter classes. This result represents a fundamental output needed for the application of the Fiber Bundle Model approach to real roots. The estimation of root length has a major influence on model prediction, as already mentioned by Ennos [1990]. The small number of studies on this topic and the wide range of values this parameter can assume depending on plant species and stand, make estimation of root length quite challenging. Nevertheless, the use of empirical relations calibrated fitted to field or literature data still provide plausible estimation of root reinforcement. Results show that including variations in root diameter along its length influences failure mechanisms for smallest root diameter classes and the displacement at which maximal pull out force occurs by about 10%. In general, higher friction (due to either more branching points, increased tortuosity, or enhanced root-soil interfacial friction) leads to an increase in both the maximal pullout force and the displacement at maximal pullout force if a root slips out. When the maximal pullout force exceeds root tensile strength, maximal pullout force remains constant (at breakage threshold) and displacement at maximal pullout force decreases.

The decrease in displacement at maximal pullout force is due to the reduction in activated root length needed to attain total friction equaling

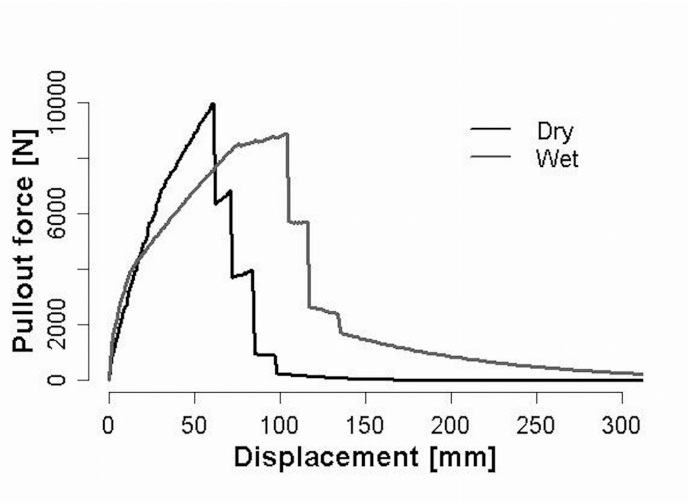

Figure 3.17: Modeled results of root reinforcement behavior for two different soil moisture conditions (20 % degree of saturation for dry and 90 % degree of saturation for wet), based on the root distribution data of Zhou et al. [1998].

maximal root tensile strength. The most sensitive geometrical and mechanical parameters are tortuosity and branching point friction coefficient. While mean tortuosity of roots may be quantified in a consistent way with real values ranging from 1.0 to 1.2, the quantification of branching point friction coefficient is more difficult. Only a few experimental data are reported where attempts to quantify this parameter were made. The work of Stokes et al. [1996], which focused on the influence of insertion angle of lateral root branches on pull out force, showed that for a certain type of branching pattern, a variation of branching angle from 30 ° to 90 ° increased pullout force for an individual branching point by less then 5%. Moreover, the numerical simulation of Dupuy et al. [2005] showed that the most plausible variable for estimation of additional friction due to branching point is the diameter of the root's main axis. In addition, Mickovski et al. [2007] showed that, branching point positions (at different confining pressures) influence friction. Parameters such as confining pressure, water content, and root-soil interface friction angle show a maximal influence on the displacement at maximal tensile force of about 10%, while the influence on maximal tensile force was even less pronounced. The non-linear behaviors of stress-strain curves has also been observed during single-root tensile tests in the laboratory (not embedded in soil) [Commandeur and Pyles, 1991], even if in this case the non-linearity is less accentuated than

when progressively activating roots (such as in a field pullout test). We thus conclude that part of the non-linearity may be attributed to tortuosity and to redistribution of forces between the fibers within the root material.

Slip Out Phase

The approach used for estimating residual root pullout force during slip out phase is characterized by new and potentially important components. First, we introduced the use of a dynamic friction to estimate root-soil interfacial force distribution. Second, we considered an iterative process for root contraction. Finally, we calculated the variation of root surface area along the root axis based on the variation in root diameter. As shown in Figure 3.8, these factors influence the estimation of residual root slip out force. An aspect not explicitly implemented in the model is the capacity of the soil to fill the void left behind big root segments or by large branching points. For plastic soils this mechanism will reduce the residual root-soil interfacial friction force to near zero after a few millimeters of displacement. In granular and cohesionless materials, however, the void left behind slipping roots will be filled by soil grains and the residual-dynamic friction strength will remain constant with a non-zero value. These effects are considered in our calculations for empirically calibrated dynamic coefficient c (equation (25)).

Effect of Soil Moisture

Depending on soil type, soil moisture may have important influence on pullout behavior of root bundles. On the one hand, increased matric potential in wet sand will not only increase sand stiffness by increasing effective stress, but would also modify friction and dilation behavior during shearing [Mickovski et al., 2007]. In natural soils, moisture conditions and the structure of the soil also strongly influence the compressibility of the soil [Lang et al., 2003]. Soil-moisture conditions exert a relatively small influence on the behavior of an individual root in comparison to other parameters. Soil moisture influences both the root-soil interfacial friction and the apparent Young 's modulus. In contrast, soil moisture plays a major role in the global behavior of a bundle of roots. Considering an individual root, the variations of the maximal pull out force and displacement due to soil moisture are at most 10%. However, even a small variation in soil moisture can lead to a change in the type of failure (slipping instead of breaking). In this case, these relative small variations may lead to big differences in the global pull out behaviors of a bundle of roots, particularly when small roots outnum-

ber coarse roots (as is the case in all real situations). Figure 3.18 shows how soil moisture influences global pullout behavior of a typical bundle of spruce roots. Generally speaking, roots in wet soil (60% to 100% degree of saturation) show a smaller resistance to pullout and a higher displacement at maximal pullout force. However, the effect of soil moisture on the global behavior of a bundle is strongly influenced by root size distribution: it is possible that the maximal pullout resistance is higher in wet soil than in dry soil because of the residual strength of small roots.

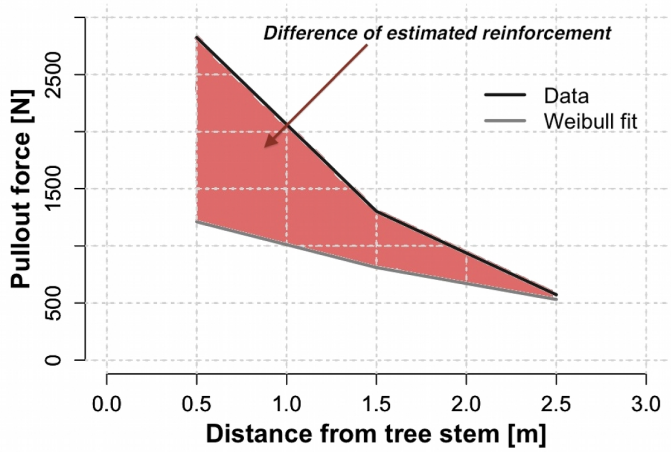

Figure 3.18: Calculated values of maximal root reinforcement as a function of distance from tree stem for two series of root distributions. First, we used mean values of root distribution collected in the field (Uetliberg), second, we used the fitted values of root distribution obtained using the Weibull probability function. The considered soil profile was 50 cm width and 50 cm deep.

The Root Bundle Model (RBM)

One of the interesting results of the application of the RBM is the confirmation that maximal pullout force of different root diameters takes place at different displacements, illustrating the shortcomings of one of the key assumptions in Wu's [1979] model. Furthermore, the RBM allows estimation of mean displacement value at maximal pullout force for different root diameter classes. The result highlights the importance of considering root

diameter distribution (for a single root as well as at the stand level) and shows that the use of Wu's [1979] model, even for relative comparison, may produce large errors due to the different root distributions [De Beats et al., 2008]. In this study, the choice of the Weibull distribution to fit root distribution data is justified on the basis of its mathematical flexibility and its superior performance in estimation of the number of large roots when compared with a log-normal distribution. Large roots have more influence on the global behavior of a root bundle and thus estimating their numbers is critical. The range of Wu's model overestimation is strongly dependent on details of root distribution. Assuming a unique value of maximal root strength, Young's modulus, and root length for each root diameter class still leads to an overestimation (see Figure 3.19). The theory behind the FBM [Sornette, 1989] shows that the variability of these values leads to a lower global maximal strength of the fiber bundle. In the FBM extension proposed in this work, we assumed that no interactions take place between roots of the same bundle. In reality this may be true only if roots are sufficiently far away from each other. Overlapping and interconnections between roots would lead to a more complex mechanism of force redistribution and to a different stress-strain behavior for the bundle. Data indicate that the mean inter-distance of roots ranges between one root every 0.1 to 0.3 meter [Zhou et al., 1998; Wu et al.,1988]. Some studies indicate also that fine roots tend to be clustered [Achat et al., 2008], which means that irrespective of their density, roots would be interacting. Considering that at a certain distance from tree stems, the density of roots decreases exponentially [Ammer and Wagner, 2005], it is reasonable to neglect root interactions in slopes with sparse vegetation. Moreover, field observations and results of numerical simulations show that fine roots play in many cases a central role in slope stabilization. There are two reasons for these conclusions: first, fine roots maximal strength is activated at small displacements suppressing even the smallest of deformations before the system acquires significant kinetic energy, and second, fine roots are more numerous and their distribution on the slope more homogeneous than the distribution of coarse roots. In situations where the growth of lateral coarse root networks can be achieved, slope stabilization will be assured through maximal root reinforcement of coarse roots and through an efficient horizontal redistribution of forces. As showed by Zhou et al. [1998] lateral root reinforcement is displacement dependent, and our numerical simulations show that force-displacement behaviors of a root bundle are strongly dependent on root diameter distribution (Figure 3.19). Therefore, future implementation of root reinforcement in slope stability calculations must consider this aspect, either in an infinite slope approach or in detailed numerical models.

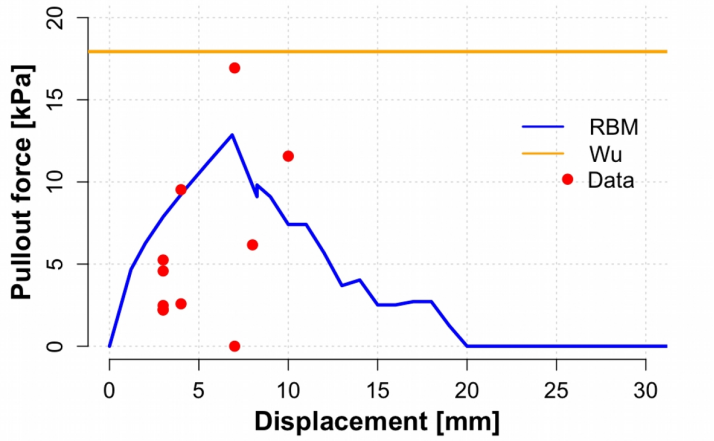

Figure 3.19: Modeled behavior of root reinforcement for the data of Zhou et al. [1998] for one square meter soil profile fitting the mean root distribution with the Weibull distribution function. The calculated maximal reinforcement using the Wu model [Wu et al., 1979] was 18 kPa, while the maximal pullout forces predicted with the RBM is about 13 kPa, which is closer to the measured values (0.22-16.9 kPa). It is important to consider that no root distributions of the single data are reported, and thus just the mean distribution was used for the root reinforcement estimation.

RBM and Slope Stability

Schwarz et al. [2009] highlighted the importance of the force-displacement relations for realistic implementations of root reinforcement in slope stability calculations. Results of our model show that the implementation of vegetation mechanical effects in slope stability calculation must take into account two important aspects. First, not all roots break simultaneously and thus the RBM approach allows a more realistic estimation of root reinforcement. Second, not all resisting forces on a slope act at the same time or amount of displacement. Hence, maximal lateral soil cohesion should not be added to the maximal lateral root reinforcement, because they reach their maximal values at different displacements [Schwarz et al., 2009]. By analogy, root reinforcement at the basal slip surface should be added to the residual shear strength of the soil material and not to the maximal value [Lang et al., 2003]. Moreover, with simple parameterization the model allows estimation of root reinforcement at a high spatial resolution [Schwarz

et al., 2009; Schwarz et al., 2010], and not at only at an average and uniform stand scale values as usually done. In addition, the implementation of the RBM in slope stability model permits a better estimation of the volume of shallow landslides because the information on the force-displacement behavior of the rooted soil allows the simulation of crack propagation during failure. The possibility to better estimate the volume of shallow landslides is an important information for the modeling of sediment transport in a catchment [Bathrust et al., 2007] and debris flow simulations [Christen et al., 2007]. The results of this work and other studies [Casadei et al., 2003; Schwarz et al., 2009], lead to a more general discussion on the role of vegetation in mitigating slope instabilities. Considering mechanical aspects only, one can conclude that even shallow rooted slopes may be stabilized by root networks but the effective contribution of a root network to slope stability is strongly dependent on plant distribution, slope steepness, and the hydro-mechanical properties of soil material.

3.8 Conclusions

In summary, we have presented a model for the estimation of root reinforcement which captures the mechanical behavior of root-soil interactions more realistically and yields force-displacement pullout behavior of a root bundle. Model estimates of tensile strength rely on the following characteristic elements: a) variations of Young's modulus as a function of root diameter along each root, b) consideration of root tortuosity and compression properties of the soil, c) consideration of root deformations d) inclusion of branching points as single friction element, e) incorporating of static and dynamic root-soil friction, f) consideration of root-soil friction variation as a function of soil water content and soil type, and g) accounting for the progressive root-soil friction activation. This study highlights the role of root bundle composition (size and geometry) on macroscopic mechanical behavior of root bundles. The quantification of the stress-strain behavior of a bundle of roots leads to new insights regarding the role of root reinforcement in slope stability. The results show that the overestimation of root reinforcement using the Wu's approach ranges from 0 to 90%, depending on root size distribution. Moreover, the sensitivity analysis of the model highlights key topics for further research. These topics include: the need for more quantitative methods for the estimation of root distribution and root geometrical parameters (like root length, root tortuosity, and branching patterns), the use of probability density functions to describe the variability of the mechanical parameters of roots, implementation of these probability

functions in a system of equations to obtain a mathematical description of the root bundle mechanical behavior, and finally, a better understanding of how roots contribute in space and time to the force redistribution on a vegetated slope.

3.9 Acknowledgments

This work was supported by the CCES platform (Competence Center for Environmental Sustainability) of the ETH domain and is part of the TRAMM project (Triggering of Rapid Mass Movement). We thank Fabian Rüdy for illustrations and Christof Hofer for helpful discussions.

3.10 References

Abe, K., and R. R. Ziemer (1991), Effects of tree roots on a shear zone: modelling reinforced shear stress, *Can. J. For. Res.*, *21*, 1012-1019.

Abernethy, B., and A. I. Rutherfurd (2001) The distribution and strength of riparian tree roots in relation to riverbank reinforcement, *Hydrol. Process*, *15*, 63-79.

Achat, D. L., M. R. Bakker, and P. Trichet (2008), Rooting patterns and fine root biomass of *Pinus pinaster* assessed by trench wall and core methods, *J. For. Res.*, *13*, 165-175.

Ajaz, A., and R. H. G. Parry (1975), Stress-strain behavior of two compacted clays in tension and compression, *Géotechnique 25*, 495-512.

Ammer, C., and S. Wagner (2005), An approach for modelling the mean fine-root biomass of Norway spruce stands, *Trees*, *19*, 145-153.

Bathurst, J. C., G. Moretti, A. El-Hames, S. Begueria, and J. M.Garcia-Ruiz (2007), Modelling the impact of forest loss on shallow landslide sediment yield, Ijuez river catchment, Spanish Pyrenees, *Hydrology and Earth System Science*, *11(1)*, 569583.

Bischetti, G. B., E. A. Chiaradia, T. Limonato, B. Speziali, B. Vitali, P. Vullo, and A. Zocco (2005), Root strength and root area ratio of forest species in Lombardy (Northern Italy), *Plant and Soil*, *278*, 11-22.

Casadei, M., W. E. Dietrich, and N. Miller (2003), Controls on shallow landslide width. In D. Rickermann and C. Chen, Debris-Flow hazards mitigation: mechanics, prediction, and assessment, *Proceedings of the Third International Conference on Debris Flows Hazards Mitigation*, Davos Switzerland, 91-102, Millpress, Rotterdam. http://eps.berkeley.edu/ bill/papers/117.pdf

Christen, M., P. Bartelt, and U. Gruber (2007), RAMMS - a Modeling System for Snow Avalanches, Debris Flows and Rockfalls based on IDL, *Photogrammetrie Fernerkundung Geoinformation*, *4*, 289-292.

Commandeur, P. R., M. R. Pyles (1991), Modulus of elasticity and tensile strength of Douglas-fir roots, *Can. J. For. Res.*, *21*, 48-52.

Coutts, M. P. (1983), Root architecture and tree stability, *Plant and Soil*, *71*, 171-188.

Cuhna, V. M. C. F., J. A. O. Barros, and J. M. Sena-Cruz (2008), Bond-slip mechanisms of hooked- end steel fibers in self-compacting concrete, *Materials science Forum*, *587-588*, 877-881.

De Beats, S., J. Poesen, B. Reubens, K. Wemans, J. De Baerdemaeker, and B. Muys (2008), Root tensile strength and root distribution of typical Mediterranean plant species and their contribution to soil shear strength, *Plant and Soil*, *305*, 207-226.

Dupuy, L., T. Fourcaud, and A. Stokes (2005), A numerical investigation into factors affecting the anchorage of roots in tension, *European Journal of Soil Science*, *56*, 319-327.

Ekanayake, J. C., and C. J. Phillips (1999), A method for stability analysis of vegetated hillslopes: an energy approach, *Can. Geotech. J.*, *36*, 1172-1184.

Ennos, A. R. (1990), The anchorage of leek seedlings: the effect of root length and soil strength, *Annals of Botany*, *65*, 409-416.

Fan, C. C., C. F. Su (2008), Role of roots in the shear strength of root-reinforced soils with high moisture content, *Ecological Engineering*, *33*, 157-166.

Genet, M., N. Kokutse, A. Stokes, T. Fourcaud, X. Cai, J. Ji, S. B. Mickovski (2008), Root reinforcement in plantation of *Cryptomeria japonica* D. Don: effect of tree age and stand structure on slope stability, *Forest Ecology and Management*, *256*, 1517-1526.

Ghezzehei, T.A., and D. Or (2000), Dynamics of soil aggregate coales-

cence governed by capillary and rheological processes, *Water Resour. Res.*, *36*, 367-379.

Goulding, R. B. (2006), Tensile strength, shear strength, and effective stress for unsaturated sand, Dissertation, University of Missouri, Columbia.

Hallett, P. D., K. W. Loades, S. B. Mockovski, A. G. Bengough, M. F. Bransby, M. C. R. Davies, and R. Sonnenberg (2009), An assessment of models that predict soil reinforcement by plant roots, *Geophysical Research Abstracts*, *11*, EGU 8925.

Hamza, O., A. G. Bengough, M. F. Bransby, M. C. R. Davies, and P. D. Hallett (2007), Mechanics of root-pullout from soil: a novel image and stress analysis procedure, In *Eco- and Ground Bio-Engineering: The use of vegetation to improve Slope Stability*, Stokes et al., Springer, 213-221.

Johnsson, M., A. Foetzki, M. Kalberer, T. Lndstrom, W. Amman, and V. Stckli (2006), Root-soil rotation stiffness of Norway spruce (*Picea abies* (L.) Karst) growing in subalpine forested slopes, *Plant and Soil*, *285*, 267-277.

Lang, H. J., J. Huder, and P. Amann (2003), *Bodenmechanik und Grundbau*, 7. Auflage, 317 pp., Springer.

Li, J. X. (1994), Analysis of the pullout of single fibers from low-density polyethylene, *Journal of applied polymer science*, *53*, 225-237.

Lu, N., and W. J. Likos (2006), Suction stress characteristic curve for unsaturated soil, *Journal of geotechnical and geo-environmental engineering*, *2*, 131-141.

Mickovski, S. B., A. G. Bengough, M. F. Bransby, M. R. C. Davies, P. D. Hallet, and R. Sonnenberg (2007), Material stiffness, branching pattern and soil matric potential affect the pullout resistance of model root systems, *European Journal of Soil Science*, *58*, 1471-1481.

Mickovski, S. B., P. D. Hallett, M. F. Bransby, M. C. R. Davies, R. Sonnenberg, A. G. Bengough (2009), Mechanical Reinforcement of Soil by Willow Roots: Impacts of Root Properties and Root Failure Mechanism, *Soil Sci. Soc. Am. J.*, *73*, 1276-1285, doi:10.2136/sssaj2008.0172.

Moroni, M. T., D. Worledge, and C. L. Beadle (2003), Root distribution of *Eucalyptus nitens* and *E. globules* in irrigated and droughted soil, *Forest Ecology and Management*, *177*, 399-407.

Naaman, A. E., G. G. Namur, J. M. Alwan, and H. S. Najm (1991), Fiber pullout and bond slip I: Analytical study, *Journal of Structural Engineering*, *117(9)*, 2769-2790.

Norris, J. N. (2005), Root reinforcement by hawthorn and oak roots on a highway cut-slope in southern England, *Plant and Soil*, *278*, 43-53, doi: 10.1007/s11104-005-1301-0.

Nuth, M., and L. Laloui (2008), Effective Stress Concept in Unsaturated Soils: Clarification and Validation of an Unified Framework, *Int. Journ. of Numerical and Analytical Methods in Geomechanics*, *32*, 771-801.

Operstein, V., and S. Frydman (2000), The influence of vegetation on soil strength, *Ground Improvement*, *4*, 81-89.

Pollen, N., A. Simon, and A. Collison (2004), Advances in assessing the mechanical and hydrologic effects of riparian vegetation on stream bank stability, *Riparian vegetation and fluvial geomorphology, water science and application*, *8*, 125-139.

Pollen, N., and A. Simon (2005), Estimating the mechanical effects of riparian vegetation on stream bank stability using a fiber bundle model, *Water Resources Research*, *41*, w07025.

Pollen, N. (2008), Temporal and spatial variability of root reinforcement in stream banks: Accounting for soil shear strength and moisture, *Catena*, *69*, 197-205.

Reubens, B., J. Poesen, F. Danjon, G. Geudens, and B. Muys (2007), The role of fine and coarse roots in shallow slope stability and soil erosion control with a focus on root system architecture: a review, *Trees*, *21*, 385-402.

Rickli, C. (2001), *Vegetationswirkungen und Rutschungen - Untersuchung zum Einfluss der Vegetation auf oberflchennahe Rutschprozesse anhand der Unwetterereignisse in Sachseln OW am 15. August 1997*, 97 pp., Birmensdorf, Bern. Eidg. Forschungsanstalt WSL, Bundesamt fr Umwelt, Wald

und Landschaft.

Sanborn, S. E., and J. H. Prvost (2008), Discrete modeling of crack bridging by a discontinuous platelet with a controlled interface, *International Journal of Solids and Structures*, *45*, 5059-5073.

Santantonio, D. (1990), Modeling growth and production of tree roots, In *Process Modeling of Forest Growth responce to Enviromental stress*, Dixon, Portland, 124-135.

Schmidt, K. M., J. J. Roering, J. D. Stock, W. E. Dietrich, D. R. Montgomery, and T. Schaub (2001), The variability of root cohesion as an influence on shallow landslide susceptibility in the Oregon Coast Range, *Can. Geotech. J.*, *38*, 995-1024.

Schwarz, M., F. Preti, F. Giadrossich, P. Lehmann, and D. Or (2009), Quantifying the role of vegetation in slope stability: A case study in Tuscany (Italy), *Ecological Engineering*, *36(3)*, 285-291, doi:10.1016/j.ecoleng.2009.06.014.

Schwarz, M., P. Lehmann, and D. Or (2010), Quantifying lateral root reinforcement in steep slopes - from a bundle of roots to tree stands, *Earth Surface Processes and Landforms*, *35(3)*, 354 - 367. doi:10.1002/esp.1927.

Sornette, D. (1989), Elasticity and failure of a set of elements loaded in parallel, *J. Phys. A: Math. Gen.*, *22*, L243-L250.

Tosi, M. (2007), Root tensile strength relationships and their slope stability implications of three shrubs species in the Northern Apennines (Italy), *Geomorphology*, *87*, 268-283.

Vanomsen, P. (2006), Der Einfluss der Durchforstung auf die Verankerung der Fichte hinsichtlich ihrer Sturmresistenz, Diss. ETH Nr. 16532, Zrich, pp 246.

Waldron, L. J. (1977), The shear resistence of root-permeated homogeneous and stratified soil, *Soil Sci. Soc. Am. J.*, *41*, 843-849.

Waldron, L. J., and S. Dakessian (1981), Soil reinforcement by roots: calculation of increased soil shear resistance from root properties, *Soil Science*, *132*, 427-435.

Wu, T. H., W. P. McKinnell,and D. N. Swanston (1979), Strength of tree roots and landslides on Price of Wales Island, Alaska, *Can. Geotech. J.*, *16*, 19-33.

Wu, T. H., P. D. Bettadapura, and E. P. Beal (1988), A statistical model of root geometry, *Forest Science*, *34*, 980-997.

Wu, T. H. (2007), Root reinforcement: analyses and experiments. In *Eco- and Ground Bio-Engineering: The use of vegetation to improve Slope Stability*, Stokes et al., 2007. Springer; 21-30.

Zhou, Y., D. Watts, Y. Li, and X. Cheng (1998), A case study of effect of lateral roots of *Pinus yunnanensis* on shallow soil reinforcement, *Forest Ecology and Management*, *103*, 107-120.

Table 2. List of Terms

Simbol	Unit	Description	Values	Reference
α	[-]	Coeff. eq. 8	Tab. 1	Tab. 1
β	[-]	Coeff. eq. 8	Tab. 1	Tab. 1
γ	$[^o]$	Angle between root sub-segments	24.6	Schwarz et al. [2010]
ΔL_{con}	$[mm]$	Variation of root length due to contraction	Eq. 32	-
ΔL_{em}	$[mm]$	Variation of embedded root length in the soil	Eq. 31	-
Δx	[mm]	Displacement	-	-
Δd	$[mm]$	Root radial contraction	$0.1d$	-
ε	[-]	Strain	-	-
ε_i	[-]	Strain of the root segment i	-	-
ε_i^{f}	[-]	Component of strain due to root material i	-	-
ε_i^{t}	[-]	Component of strain due to root tortuosity i	-	-
ε_f	[-]	Root local strain	-	Naaman et al. [1991]
$\varepsilon^{\max}$	[-]	Maximal strain of a root	-	-
$\varepsilon^{\max}$	[-]	Maximal root strain	-	-
$\varepsilon^{\text{slip}}$	[-]	Root strain due to the slip out friction	-	-
ζ	[-]	Empirical coeff.	-	-
θ	[-]	Volumetric water content	-	-
θ_{sat}	[-]	Volumetric water content in saturated condition	-	-
$\theta_{\min}$	[-]	Volumetric water content corresponding to $c'_{\max}$	-	-
λ	[-]	Empirical ratio between E_{t} and E_{f}	-	Commandeur and Pyles [1991]
ν_f	[-]	Poisson's ratio	0.3	Dupuy et al. [2005]
σ	[kPa]	Stress	-	-
σ'	$[Pa]$	Effective normal stress	-	Lu and Likos [2006]
σ'_{tort}	$[Pa]$	Tortuous effective stress	Eq. 17	-
σ	$[Pa]$	Total normal stress	-	-
τ_b	$[Pa]$	Bonded friction	Eq. 13	Naaman et al. [1991]
τ_d	$[Pa]$	Debonded friction	Eq. 16	-
τ_{dyn}	$[Pa]$	Root dynamic friction	Eq. 25	Cuhna et al. [2008]
ϕ	$[^o]$	Residual root-soil friction angle	35	-
χ	$[-]$	Effective stress parameter	-	Lu and Likos [2006]
A_i	$[mm^2]$	Cross sectional area of root segment i	-	-
A_0	$[mm^2]$	Cross sectional area of root segment 0	$\pi/4$	-
A_n	$[mm^2]$	Maximal cross sectional area of root	-	-
b	$[mm]$	Mean branching distance	10-170	-
c	[-]	Empirical coeff.	-	-
c'	$[Pa]$	Apparent cohesion	Eq. 23-24	Lu and Likos [2006]
$c'_{\max}$	$[Pa]$	Maximum value of apparent cohesion in unsaturated conditions	$1 - 5\,10^3$	Gouldin [2006]
c'_{res}	$[Pa]$	Residual value of apparent cohesion in dry conditions	-	-
d	$[mm]$	Root diameter	> 1	Santantonio [1990]
d_0	$[mm]$	Diameter of root tip	1	Santantonio [1990]
d_i	$[mm]$	Diameter of root segment i	-	-
D	$[mm]$	Straight root length	Eq. 7	Schwarz et al. [2010]
E_f	[MPa]	Young's modulus root material	Eq. 9	Schwarz et al. [2010]
E_t	[MPa]	Young's modulus of tortuous root	-	Commandeur and Pyles [1991]
E_{app}	[MPa]	Apparent Young's modulus of the root	Eq. 10	Commandeur and Pyles [1991]
F	[N]	Pullout force applied to the root	-	-
F^{if}	$[N]$	Maximum pullout force of a root due to interface friction	Eq. 18	-
F^{tot}_{max}	$[N]$	Total maximal friction of a root	Eq. 30	-
f_i^{tot}	[N]	Total pullout force transmitted to root segment i	Eq. 28	-
f_i	[N]	Pullout friction due to root segment i	Eq. 27	-
f_i^{bp}	$[N]$	Branching point friction	Eq. 26	-
i	[-]	Root segment index	-	-
k	$[Pa/m^2]$	Bond modulus	10^9	-
k	[]	Scale parameter of the Weibull distribution	0.8-3.3	-
L	$[mm]$	Tortuous root length	Eq. 1	Commandeur and Pyles [1991]
l	$[mm]$	Tortuous length along root	-	-
L_0	[-]	Coeff. eq. root length	100-500	Pollen et al. [2004]
L_e	[-]	Exponent eq. root length	0.7	Pollen et al. [2004]
L_{slip}	$[mm]$	Root length embedded in the soil during slippage	Eq. 33	-
m	$[-]$	Shape parameter of the Weibull distribution	1-1.2	-
N	$[-]$	Number of root diameter classes	-	Schwarz et al. [2010a]
n	[-]	Number of branching points	Eq. 2	-
S	$[m]$	Local root-soil interface slip	10^{-5}	-
s	[-]	Scaling factor	0.75	Collet et al. [2006]
$T^{\max}$	[MPa]	Maximum tensile strength	Eq. 8	-
u_a	$[Pa]$	Pore air pressure	0	-
u_w	$[Pa]$	Pore air pressure	0	-
Y	$[N/m]$	Empirical braching coeff.	0-1	Schwarz et al. -
z	[-]	Root tortuosity	1.1	Schwarz et al. [2010a]

Chapter 4

Pullout tests of root analogs and natural root bundles in soil

Autohrs: Schwarz M. [1,2], Cohen D. [2] and Or D.[2]

[1] Swiss Federal Institute for Forest, Snow and Landscape Research, 8903 Birmensdorf, Switzerland

[2] Soil and Terrestrial Environmental Physics, Institute of Terrestrial Ecosystems, ETH Zurich, 8092 Zurich, Switzerland

In Press: *J. Geophys. Res.*, doi:10.1029/2010JF001753. (accepted 7 February 2011).

4.1 Abstract

Root-soil mechanical interactions are key to soil stability on steep hillslopes. Motivated by new advances and applications of the Root Bundle Model (RBM), we conducted a series of experiments in the laboratory and in the field to study the mechanical response of pulled roots. We systematically quantified the influence of different factors such as root geometry and configuration, soil type, and soil water content considering individual roots and root bundles. We developed a novel pullout apparatus for strain-controlled field and laboratory tests of up to 13 parallel roots measured individually and as a bundle. Results highlight the importance of root tortuosity and root branching points for prediction of individual root pullout behavior. Results also confirm the critical role of root diameter distribution for realistic prediction of global pullout behavior of a root bundle. Friction between root and soil matrix varied with soil type and water content and affected the force-displacement behavior. Friction in sand varied from 1 to 17 kPa, with low values obtained in wet sand at confining pressure of 2 kPa, and high values obtained in dry sand with 4.5 kPa confining pressure. In a silty soil matrix, friction ranged between 3 kPa under wet and low confining pressure (2 kPa) and 6 kPa in dry and higher confining pressure (4.5 kPa). Displacement at maximum pullout force increased with increasing root diameter and with tortuosity. Laboratory experiments were used to calibrate the RBM that was later validated using six field measurements with natural root bundles of Norway spruce (*Picea abies* L.). These tests demonstrate the progressive nature of root bundle failure under strain-controlled pullout force and provide new insights regarding force-displacement behavior of root reinforcement, highlighting the importance of considering displacement in slope stability models. Results show that the magnitude of maximum root pullout forces (1–5 kPa) are important for slope stability. The force-displacement relations characterized in this study are fundamental inputs for quantifying the resistive force redistribution on vegetated slopes and may provide explanation for abrupt loss of strength during landslide initiation and deformation.

4.2 Introduction

The study of root-soil mechanical interactions, often motivated by questions related to slope stability or tree stability, has evolved from an early focus on reinforcement and strength imparted by roots crossing a slip surface [Wu et al., 1979; Waldron and Dakessian, 1981] or vertical root reinforcement along

a profile [Abe and Ziemer, 1991], to considerations of lateral reinforcement and dynamic aspects of root-soil interactions [e.g., Schwarz et al., 2010b,c]. Traditionally, studies focused on maximum tensile strength of individual roots as basic input information for the estimation of root reinforcement along a soil profile [Nilaweera and Nutalaya, 1999; Watson et al., 1999; Operstein and Frydman, 2000; Tosi, 2007; De Beats et al., 2008; Docker and Hubble, 2008]. Some studies also recognized the role of lateral distribution of roots on the horizontal redistribution of forces on a slope [Reneau and Dietrich, 1987; Schmidt et al., 2001; Roering et al., 2003; Casadei et al., 2003; Schwarz et al., 2010c], and later considered the horizontal distribution of root reinforcement [Sakals and Sidle, 2004; Schwarz et al., 2010c]. Shewbridge and Sitar [1990] showed analytically how reinforcement affects the width of a shear zone and how the larger tensile strength of root-reinforced soils exceeds bending stresses by an order of magnitude. Schwarz et al. [2010c] showed in a case study of a shallow landslide on a vegetated slope that the contribution of lateral root reinforcement was the only mechanical contribution of vegetation to slope stability. This scenario is supported by other observations of rainfall-triggered landslides in Switzerland [Rickli and Graf, 2009]. These and other results indicate that for both shear and tensile reinforcement one should focus on the root pullout behavior.

Numerous engineering studies on soil-nailing techniques and concrete reinforcement have identified several key factors in the pullout behavior of single or multiple soil nails or fibers [Wang et al., 1988; Naaman et al., 1991a,b; Li, 1994; Teixeira et al., 2007; Cunha et al., 2008; Yang et al., 2008]. Hong et al. [2003] showed that the friction at the soil-nail interface was dependent upon the surface roughness of the nail and the confining pressure; Su et al. [2008] reported that peak pullout shear resistance of soils reinforced by nails was not significantly different for two different degrees of soil-water saturation (38% and 75%). Some of these results may be useful in the context of root pullout behavior, but the relatively complex geometry and the mechanical heterogeneities of natural root systems necessitate specific considerations requiring new experimental data and models of root-soil interactions. For example, some studies [Anderson et al., 1989; Czarnes et al., 1999; Abernethy and Rutherfurd, 2001; Hamza et al., 2007; Mickovski et al., 2007] have shifted from the standard measurement of the maximum tensile strength of roots to the characterization of the force-displacement behavior of pulled roots in a soil matrix, thus taking into account displacement and root-soil interactions for the description of the pullout process and root reinforcement in relation to various factors. Studies have also discussed the importance of factors such as root length, root branching pattern and tortuosity, and how these factors affect the pullout behavior of natural

roots [Stokes et al., 1996; Abernethy and Rutherfurd, 2001; Mattia et al., 2005; Stokes et al., 2009; Mickovski et al., 2010].

There are only a few analytical or numerical studies that have addressed the pullout behavior of individual roots [Ennos, 1990; Stokes et al., 1996; Dupuy et al., 2005], and among these only one model is capable of predicting the force-displacement behavior of a pulled root [Ennos, 1990]. In one of the rare studies aimed at experimentally evaluating dynamic aspects of reinforcement for a bundle of roots, Zhou et al. [1998] back-calculated the global contribution of lateral root reinforcement as the difference between the shearing resistance of rooted soil blocks and the shearing resistance of soil blocks without roots. The progressive nature of root bundle failure under a tensile or shear stress was recognized and discussed previously [Waldron and Dakessian, 1981; Zhou et al., 1998; Schmidt et al., 2001; Docker and Hubble, 2008; Cohen et al., 2009; Hubble et al., 2010], leading to the recognition that Wu et al. [1979] root-area-ratio calculation of root-cohesion often used for slope stability assessment must be revised [Docker and Hubble, 2008; Stokes et al., 2009; Hubble et al., 2010; Mickovski et al., 2010]. A recent study by Pollen et al. [2004] introduced the concept of the fiber bundle model (FBM) for the estimation of root reinforcement. As reviewed in detail by Schwarz et al. [2010a], the FBM provides quantitative consideration of geometrical and dynamic aspects of root reinforcement with model parameters, providing more realistic root reinforcement estimates. Two approaches have been used for studying root reinforcement with the FBM. One, first presented by Pollen et al. [2004], imposes a stress on a bundle or roots. During a stress loading step, some roots break and their loads are redistributed to intact roots according to some predefined rules [Thomas and Pollen-Bankhead, 2010]. Depending on the redistribution rule, roots may or may not have identical displacements, unless assumptions are made regarding the geometry or mechanical properties of the roots, for example a constant elastic modulus independent of root diameter. Also, with stress loading, the bundle residual pullout forces past the maximum force cannot be calculated because the bundle breaks at the maximum load.

A second approach, introduced by Schwarz et al. [2010b] and implemented in the Root Bundle Model (RBM) [Schwarz et al., 2010a], loads the bundle by a sequence of strain steps and the total pullout force is simply calculated as the sum of pullout forces of individual roots in the bundle. No assumptions are needed about load redistributions. Because all roots have identical displacements, a complete description of root mechanics and geometry can be included, yielding a more realistic distribution of stresses among roots of the bundle. Also, calculations of forces can go beyond the maximum force and thus estimate the bundle's residual force at large dis-

placements. Yet, the parametrization and calibration of the FBM remains a challenge due to the complexity and heterogeneity of root-soil systems. For improved understanding of the force-displacement behavior of a bundle of roots and for a realistic prediction of root reinforcement, new types of experiments and input data are required. Specifically, there is a need to quantify key factors and parameters also identified in recent numerical and analytical studies [Ennos, 1990; Dupuy et al., 2005; Schwarz et al., 2010a] such as: root length, root branching distance, decrease of root diameter past a branching point (using a scaling factor), root tortuosity, variation of Young's modulus, and maximum tensile strength as a function of diameter and along the root length.

The primary objectives of this study were to improve estimation of lateral root reinforcement by identifying and quantifying parameters controlling root bundle mechanical behavior by means of laboratory and field measurements and use these data to calibrate and validate the Root Bundle Model of Schwarz et al. [2010a].

4.3 Materials and Methods

The Pullout Apparatus

We designed a novel apparatus to obtain experimental data on the pullout behavior of a root bundle composed of a heterogeneous population of roots. The apparatus is capable of measuring simultaneously the pullout force and displacement of single elements of the bundle. The device was designed to conduct displacement-controlled experiments and can pull up to 13 roots/fibers simultaneously (Figure 4.1). The pullout apparatus consisted of a rigid structure (400 x 600 x 800 mm) where a rigid plate (400 x 600 x 25 mm) moved along four parallel guides with circular cross sections (diameter 30 mm). On the stiff plate we installed 13 load cells (Omega engineering, LCL-040) to which individual roots/fibers were attached, so that the measurements of each pullout force is independent of the friction between the rigid plate and the guides. The load cells have a maximum load capacity of about 180 N (with a safe overload of 150%) and an accuracy of $\pm$ 0.25% at full scale. The load cells were connected to a data logger (Campbell Scientific, CR3000) which collected force and displacement data every second. The displacement of the plate was measured using a Linear Variable Differential Transformer (LVDT, SigmaEpsilon, AS-630) which had a linear accuracy of $\pm$ 0.3%. The plate was pulled with an electric motor positioned at the back of the machine. The pullout apparatus was designed

and constructed to remain stiff with negligible internal elastic deformations. In laboratory tests, roots or fibers were embedded in soil or sand within a horizontal wooden box (600 x 600 x 1300 mm) (Figure 4.1) and attached to the loading plate. In the field, roots prepared on the vertical face of a soil profile were attached directly to the plate of the machine.

Field Experiments

Study Area

The study area is located at Uetliberg near Zürich, Switzerland (Long. 8.470631, Lat. 47.366211; UTM/WGS 84) at an altitude of 630 m a.s.l. The site is on a flat ridge in the northern part of the Albis range. The geological substratum is a limestone and the Uetliberg rise consists of glacial sediments deposited during the Wurm period [Vanomsen, 2006]. The climate is continental with mean annual precipitation of 1100 mm and mean annual temperature of 8 °C [Vanomsen, 2006]. The soil in the area is an Inceptisol with a mollic surface horizon (Ah, 0.1–0.2 m depth) and a cambic subsurface horizon (Bh, > 0.2 m depth) [Soil Survey Staff, 2010]. The soil of the mollic horizon is classified as a silty loam [Soil Survey Staff, 2010]. The upper layer of the soil was well structured with aggregate sizes ranging from

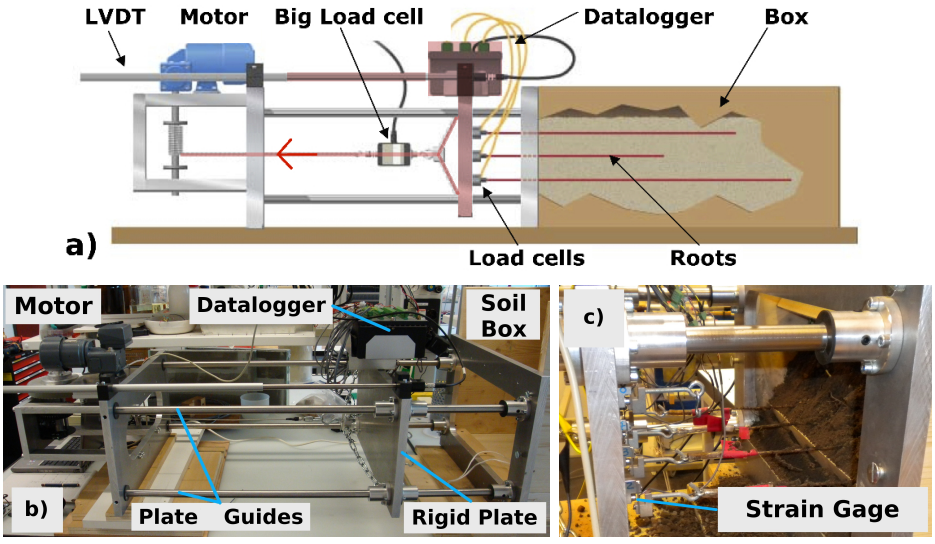

Figure 4.1: (a) Schematic of the pullout machine. Moving parts are shown in red. (b) Photo of the pullout machine in the laboratory. (c) Detail of the rigid plate with attached strain gages.

1 to 20 mm. Gravels and cobbles with diameters between 5 and 100 mm constituted only 5% of the soil material. Soil samples were taken from the mollic horizon (Ah) to measure water retention and grain-size distribution on dispersed and aggregated samples (Figure 4.2). The fitting parameters of the water retention curve are typical of a loamy soil and indicate a high porosity of almost 60%. To measure the grain-size distribution of the dispersed soil, 5 kg of soil was dried and wet sieved for particle sizes from 0.1 to 10 mm. For the aggregated soil, an additional 5 kg of soil was dry sieved for particles greater than 2 mm (10 min throw-action sieving with amplitude of 3 mm with a sieve shaker (Retsch, AS 300)) to illustrate the effect of aggregation on the particle-size distribution (Figure 4.2b). The smallest fraction of the soil (< 0.1 mm) was analyzed with the laser diffraction technique after treatment with H_2O_2 (2 ml on 2 g soil), Calgon (sodium hexametaphosphate), and UV (for 1 min).

The canopy of the forest stand is a single layer dominated by Norway spruce trees (*Picea abies* L.) (about 90% of trees) with stem diameters between 200 and 300 mm at 1.3 m height. The mean stem density is 400 to 500 trees ha^{-1} and the mean tree height measured with a hypsometer is about 23 m. The spruce trees were planted and are regularly distributed. The autochthonous vegetation typically consists of a deciduous forest dominated by beech trees (*Fagus silvatica* L.) and belongs to the phyto-sociological class of the *Fagetum typicum*. The regeneration layer is composed of beech (*Fagus silvatica* L.) and Sycamore maple (*Acer pseudoplatanus* L.) species.

Soil Trenches

In order to investigate the pullout resistance of natural root bundles of spruce, 6 rooted soil profiles near spruce trees were used as test samples. Trees with average dimensions of about 300 mm in diameter at breast height were chosen, avoiding trees growing below the forest canopy. Trenches were dug 2.5 m from the center of the tree stem. Each trench was 2 m long, 0.8 m in width, and 0.5 m deep. The orientation of the trench was chosen to minimize interactions with root systems of other trees. Before the excavation, roots of spruce trees were carefully cut along the trench line with a garden shear to prevent mechanical stresses before the test.

Field Experimental Setup

Roots intersecting the profile (Figure 4.3) were selected based on their diameters (between 1 and 3 mm) and their locations on the profile (to allow for a good connection to the pullout plate). Strain gages were positionned

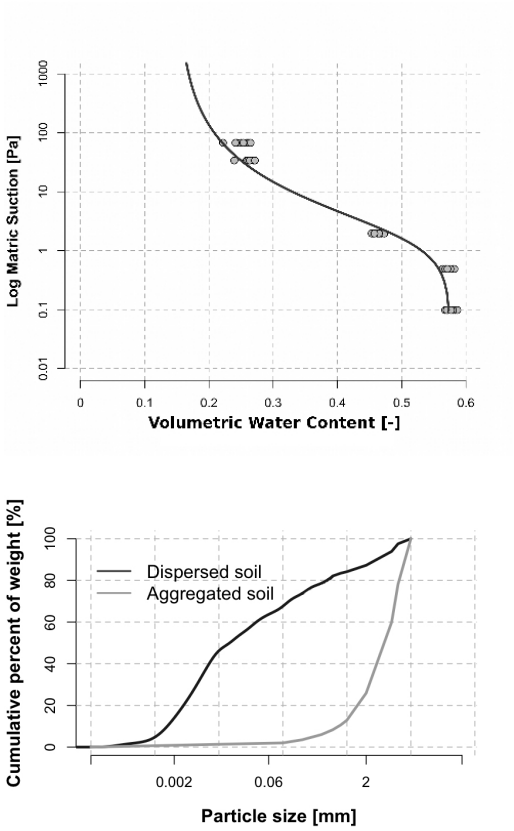

Figure 4.2: Characteristics of Uetliberg soil used for the laboratory experiments: (a) Water retention curve of the fine component of soil (aggregates < 2 mm) and van Genuchten [1978] model fit with parameters $\alpha = 5.2$ [10^{-1} mm], $n = 1.5$, $\theta_r = 0.15$, and $\theta_s = 0.575$; (b) grain size distribution (aggregated and dispersed).

on a 40 mm squared mesh to ensure that the sensors were lined up with the axis of the pull direction. Roots were glued to metal rings equipped with a screw that overlapped the de-barked end of the root. The length of the overlapping segment was proportional to the diameter of the root and embedded in a rubber tube in which liquid glue was injected (see Figure 4.3). Prepared roots with glued metal rings were attached to strain gages on the pullout plate and pre-tensioned using a screw system to a load between 0 and 2 N. The pre-tensioning activated all roots at the same time once the plate started to move. After the experiment, *in situ* volumetric water content of the soil was measured using a handheld TDR (Time Domain Reflectometry) instrument (Hydrosense, Campbell Scientific).

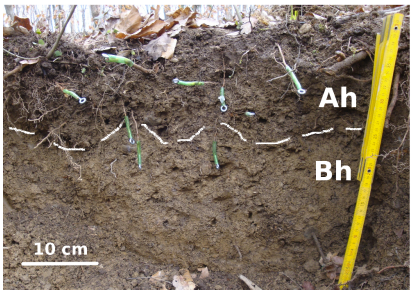

Figure 4.3: Field soil profile showing roots of spruce (*Picea abies*) with metal rings ready for a pullout experiment.

Laboratory Experiments

Laboratory experiments consisted of three types of tests (Table 4.1): i) cotton threads as root analogs, ii) field-sampled root segments of spruce trees, and iii) field-sampled natural roots of spruce trees. These materials are described in the next subsection. Cotton fibers were embedded in wet or dry sand to investigate the influence of tortuosity and branching points on the global pullout behavior of individual fibers in homogeneous conditions. To simulate tortuosity, fibers were laid in sand in a zig-zag pattern consisting of 200 mm long segments at 90 degree angle (Figure 4.4). Branching points were simulated by crimping 4-mm diameter lead fishing beads at 200 mm intervals along the fiber. Straight natural root segments were pulled out from sand or soil under different moisture and confining pressure conditions. These tests aimed at quantifying root-soil friction under different conditions. Finally, we tested natural roots in reconstituted soil matrix using straight and tortuous roots and roots with and without branching points (branching points removed). Tortuosity, defined as the ratio of length along the root axis and the straight distance between the two end points of the root, was measured in the laboratory and was 1.4 for cotton fibers and ranged between 1.0 and 1.2 with a 1.1 average for natural roots.

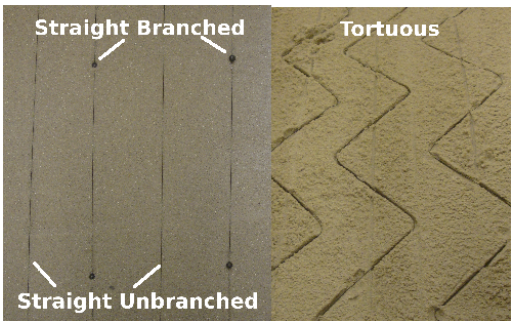

Figure 4.4: Laboratory set up of experiments with tortuous cotton fibers in sand.

Table 4.1: Summary of Field (F) and Laboratory (L) experiments with cotton fibers (A) roots (R) and roots segments (RS) in sand (SA) or soil (SO) under dry (D) or wet conditions (W). Fibers and roots are also grouped into straight (S), tortuous (T), branched (B) or a combination of these groups.

Field/Lab.	Fibers/Root/Root Seg.	Soil/Sand	Wet/Dry	St./Tor./Br.	N° of repetitions
L	A	SA	D	S	5
				SB	5
				T	5
				TB	5
			W	S	5
				SB	5
				T	5
				TB	5
	R	SO	W(15% VWC)	S	9
				T	9
				SB	9
	RS	SO	W(20% VWC)	S	25
			W(10% VWC)	S	25
			D	S	25
		SA	W(10% VWC)	S	15
			W(5% VWC)	S	15
			D	S	15
F	R	SO	W		36 (in 6 bundles)

Roots and Cotton-Thread Root Analogs

Cotton Fibers

Cotton fibers were used to study pullout behavior without the geometrical and mechanical variability found in roots. Cotton was selected due

to the similarity of its apparent elastic properties to those of fine roots. Cotton fibers had mean diameters of 0.2 mm (±10%) and were 1 m long. Dry fibers had a maximum tensile force of about 25 N (0.8 N standard deviation) and an elastic (Young's) secant modulus of ∼ 42 GPa (6.8 GPa standard deviation). Wet cotton fibers had a maximum tensile force of 22 N (1.5 N standard deviation) and an elastic (Young's) secant modulus of ∼ 31 GPa (3 GPa standard deviation).

Natural Root Segments

In order to characterize friction between the root surface and the soil matrix (root-soil interfacial friction), we collected 5 root segments with diameters between 4 and 6 mm. These straight segments were cut from large secondary [Santantonio, 1990] lateral spruce (*Picea abies* L.) roots sampled from the first 400 mm of the top soil layer. The diameter of each root segment was measured every 100 mm to calculate the root surface area used to convert measured pullout forces to frictional stresses. All root segments had lengths between 60 and 1000 mm with a fairly constant diameter (±6%).

Natural Roots

Twenty seven roots of spruce (*Picea abies* L.) were collected and stored in a solution with 10% ethanol at 4^oC to prevent the deterioration of the root material following procedures outlined in Bischetti et al. [2003]. Root diameters ranged between 1 and 4 mm. Roots were sampled from the uppermost 400 mm of the top soil layer and can be classified as secondary lateral roots [Santantonio, 1990]. The experiments were carried out within two weeks of collection. Before the experiments, roots were hand washed gently under water to remove residual soil and root hairs. Fine root tips were also removed. For each root, we measured root diameter at its base, tortuous and straight length, diameter at each branching point, and branching distances (Figure 4.5). The straight length of a root was measured by gently stretching it on a table. A branching point was defined when a lateral root was larger than 0.5 mm in diameter.

A power-law fit of tortuous length, L, versus base diameter, d_b, yielded

$$L = 335\, d_b^{0.63}, \tag{4.1}$$

where L and d_b are both in millimeters. Data show that the number of branching points (n_{bp}) increases nearly linearly with base root diameter ($n_{bp} = 2.8\, d_b$; see Figure 4.6).

Dividing the tortuous root length by the number of branching points we obtain the value of the mean branching distance. The mean branching distance, associated with the mean lengths of root segments with constant cross-sectional diameters, is a parameter in the root bundle model. Mean

branching distances, however, were normally distributed and highly variable, between 30 and 187 mm with a standard deviation of 43.3 mm. For modeling purpose we assumed a mean value of 90 mm based on the average of 23 measurements.

Previous studies on root growth and root distribution have used a scaling factor (also called a proportionality factor) to characterize the variation of diameter along root length [van Noordwijk et al., 1994; Ozier-Lafontaine et al., 1999; Vercambre et al., 2003; Collet et al., 2006]. This scaling factor is the ratio of the main root cross-sectional area before and after the branching point, including cross-sectional areas of any branching lateral roots. We used the geometrical model of Schwarz et al. [2010a] to compute root diameter as a function of length along the root:

$$d(l) = 2\sqrt{\frac{l}{b}\frac{f^2}{4}s}, \tag{4.2}$$

where d is the root diameter at a distance l from the root tip, b is the mean branching distance, f is the mean diameter of fine roots (in our calculation assumed to be 1 mm, following the classification of fine roots in Santantonio [1990]), and s is the scaling factor. For $d(L) = d_b$, substituting equation (1) into equation (2) and rearranging, we obtain

$$s(d_b) = \frac{b}{335}d_b^{1.4}, \tag{4.3}$$

where s, d_b and b are in millimeters. Measured values of scaling factor fit well with values computed using equation (3) (see Figure 4.7). Thus, equation (3) was used as an input in the Root Bundle Model [Schwarz et al., 2010a].

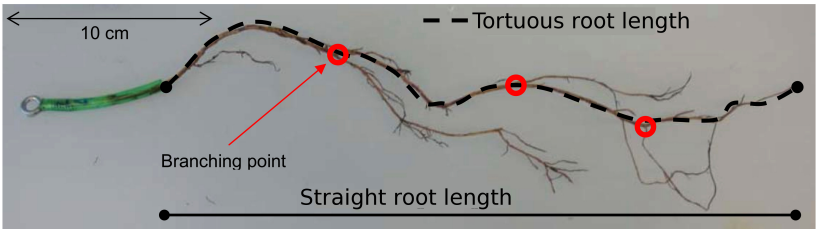

Figure 4.5: Characterization of geometrical parameters of a root. The red circles indicate branching points. The drawings show the geometrical meaning of tortuous and straight root length.

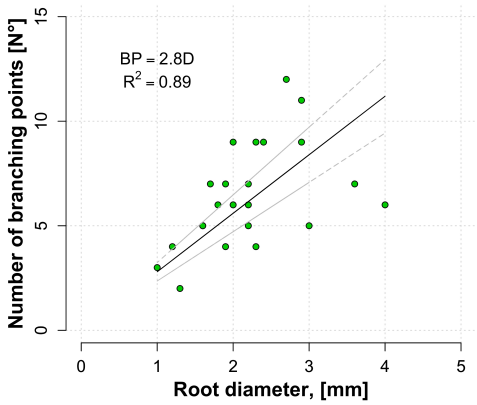

Figure 4.6: Number of branching points versus root diameter. The black line shows the linear regression with intercept at 0 and a slope of 2.8. The gray lines show the confidence interval of the regression at the 5% of probability.

Experimental Setup

Laboratory Experimental Setup

In the laboratory experiments we used the same apparatus as in the field experiments except that in the laboratory roots were embedded in a soil/sand matrix contained in a wooden box. The setup was designed to operate horizontally to avoid overburden gradients along the roots. As soil matrix we used a uniformly graded silica sand (D_{50}= 0.6 mm) or a silty loam collected in the study area (see Figure 4.2). The fine soil material was sieved in the field with a 20 mm mesh and kept dry in the laboratory. The roots/fibers were embedded in the soil matrix adding the soil material layer by layer and retaining an approximate bulk density of 1.0 throughout the vertical column. The upper surface of the soil matrix was leveled to equalize weight distribution. The confining pressure was determined by adding weights on top of the soil surface over a wooden board. We used weights of 120 and 270 kg to simulate upper confining pressures of 2 and 4.5 kPa, respectively. The preparation of different moisture conditions was performed by adding the amount of water needed to obtain the desired gravimetric water content and mixing the mass manually. The matrix mass was then left to equilibrate for a few hours prior to setting into the wooden box. The soil was characterized by standard laboratory drained direct shear tests on recon-

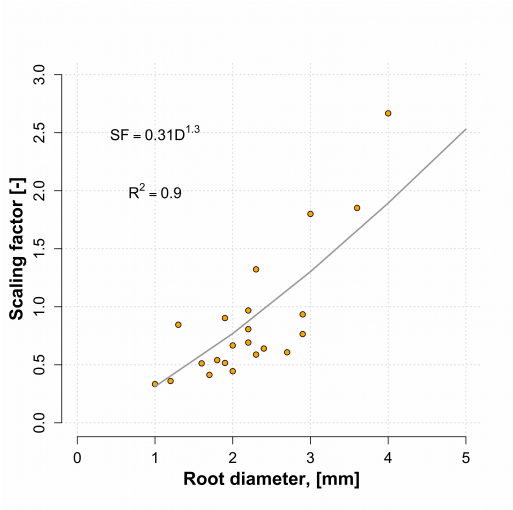

Figure 4.7: Root diameter versus calculated scaling factor of tested roots. The nonlinear regression model is shown to be significant with a p-value less than 0.001 and a residual standard error of 0.32 on 22 degrees of freedom.

structed saturated samples with material from the Ah horizon at confining pressures of 50, 100, 150, and 200 kPa (see parameters in Table 4.2). Although confining pressures in the standard shear tests were higher than under real conditions (0.5–1 m soil depth), they yielded standard parameters that could be compared with other soils.

Table 4.2: Soil properties of the Ah horizon.

Property	Symbol	Value	Unit
Bulk density	ρ_b	1000	$[kg\,m^{-3}]$
Porosity	n	63	[%]
Residual friction angle	ϕ_r	25 (SD=2)	[°]
Cohesion	c	17.5 (SD=5)	[kPa]

The Root Bundle Model (RBM)

Experimental force-displacement pullout curves were compared with RBM predictions. The RBM [Schwarz et al., 2010a] is an extension of the fiber bundle model [e.g., Sornette, 1989; Pollen et al., 2004; Raischel et al. 2006; Cohen et al., 2009] that takes into account failure mechanisms of individual roots (i.e., slip and breakage) and root-soil friction. The model calculates the pullout force of a root bundle as a function of displacement during displacement-controlled loading of the bundle. Key parameters of the model are: root length, root tortuosity, branching point coefficient (a coefficient that describes how much a branching point influences the maximum and the residual pullout force of a root), root-soil friction angle (derived from the root-soil interfacial friction forces measured at different confining pressures), water content, and confining pressure. Based on a sensitivity study of the RBM [Schwarz et al., 2010a], the most sensitive parameters were the coefficients used to describe root length (equation (1)) and the branching point coefficient.

4.4 Results and Discussion

Experiments using Cotton Fibers

Figure 4.8 displays the pullout behavior of cotton fibers averaged over 5 replicates for straight fibers (S), tortuous fibers (T), straight fibers with branching points (SB), and tortuous fibers with branching points (TB), placed in wet (5% VWC) and dry sand.

Results show that, in wet sand, S fibers had the smallest maximum pullout force (about 5 N), and peak strength occurred at a relatively small displacement (within the first 10 cm in this case). Also, friction during the slip-out phase decayed exponentially. SB fibers showed a higher maximum pullout force (about 10 N) also within the first 10 cm of displacement (corresponding to 10% strain). In contrast with SB fibers, the slip-out phase of S fibers was more gradual and linear. T and TB fibers showed similar pullout behaviors with maximum pullout force of about 15 N at displacement of 25–30 cm. The slip-out phase also followed exponential frictional decay. For tortuous fibers, the effect of branching points was negligible.

The pullout curves of fibers in dry sand (Figure 4.8b) showed, in general, lower maximum forces than in wet sand. T and TB fibers reached maximum pullout forces at larger displacement than S and SB fibers. Moreover, in contrast to wet sand, the behavior of T and TB fibers differed considerably, suggesting that the presence of branching points in tortous roots had a

larger influence in dry sand than in wet sand. The lower secant elastic modulus of cotton fibers does not justify the different measured pullout behaviors of cotton fibers in wet and dry sand. Water, however, appears to have the most influence on interfacial friction and hence on the pullout force.

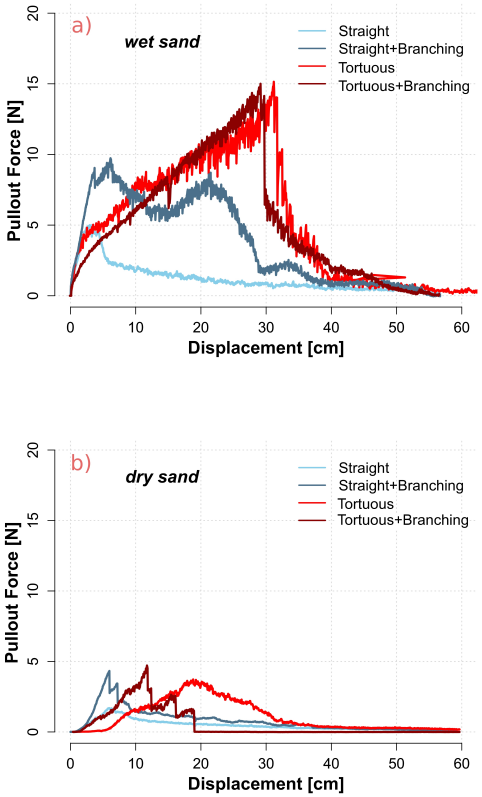

Figure 4.8: Pullout tensile forces versus displacement for four different classes of cotton fibers (straight fiber (S), tortuous fiber (T), straight fiber with branching points (SB), and tortuous fibers with branching points (TB)), in (a) wet sand (15% VWC) and in (b) dry sand (0% VWC). Curves are averages of 5 experiments. The slip out phase begins at the displacement at which the maximum pullout force is reached.

Experiments using Root Segments

Effects of Soil Type and Water Content on Friction Traditionally, the effects of lateral branching roots and root hairs are considered as

an integral part of the global root-soil interfacial friction. To better understand root-soil interfacial friction, however, we focused on friction due to interactions between the roughness of the root bark and the soil matrix by performing pullout experiments in the laboratory with natural root segments sampled from the field (no branching points and no root hairs). To quantify systematically the effects of confining pressure and soil water content, we repeated experiments with different combinations of these factors. In total we performed 24 experiments, each time using the same 5 root segments (pseudo-replicates), for a total of 120 force-displacement curves (see Table 4.1). A possible variation of root-soil interfacial friction due to wear of the samples caused by the angular sand could not be observed between the first pullout test and successive tests. In fact, the variability of the pullout behaviors between the replicated tests did not show a decreasing trend and it was probably more influenced by local packing condition of the sand/soil matrix than by wear of the root-soil interface. Figures 4.9 and 4.10 show force-displacement results of 5 specific pullout experiments in soil and sand, respectively, with root segments of different diameters. In soil, maximum pullout force and displacement at maximum pullout force were nearly identical for the dry and wet cases (Figure 4.9a,b). Pullout forces for the dry soil (Figure 4.9b), however, showed large, rapid, oscillations of up to 25 N for the large root segments, while wet soil force-displacement curves in Figure 4.9a were smoother, indicating a more uniform friction. In contrast, maximum pullout forces in dry sand (Figure 4.10b) were three to five times larger than in wet sand (Figure 4.10a). Pullout forces decayed rapidly after a sharp peak in dry sand while they plateaued in wet sand. For sand, the dry cases showed only slightly more oscillations than the wet cases.

Figures 4.11 and 4.12 show the values of root-soil interfacial friction under various combinations of moisture and confining pressure for soil and sand, respectively. For soil, results in Figure 4.11 show that volumetric water content in soil causes a small but perceptible decrease of root-soil friction. A possible explanation for the decrease of friction with increasing water content is the decrease of soil aggregate stiffness with water: under wet conditions, individual aggregates are more plastic (less stiff) and deform more easily, resulting in a lower root-soil interfacial friction angle and thus lower friction. The data of Figure 4.11 were used to calibrate the root-soil interfacial friction parameters of the RBM such as the angle of friction (42°) and the cohesion (ranging between 0 kPa in the dry case, and 2 kPa in the wet case with 20% VWC). The discrepancy between the values of cohesion obtained for the soil (17.5 kPa, Table 4.2) and for the root-soil interface is likely due to the different types of test (drained saturated shear test for the

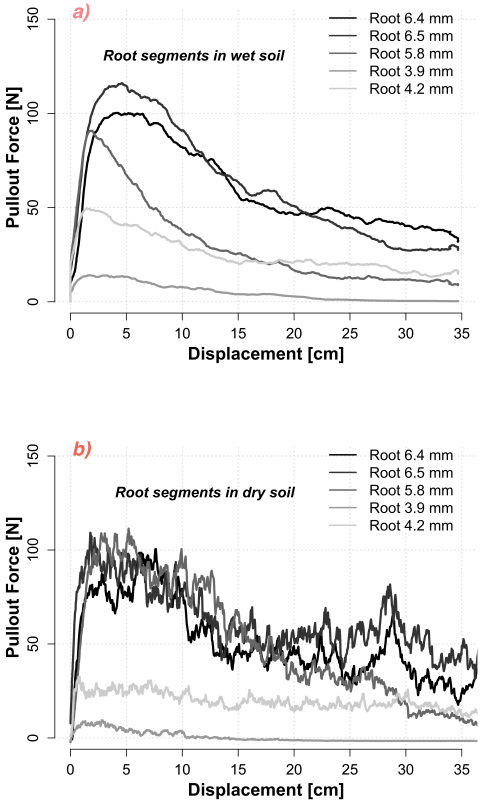

Figure 4.9: Pull out behavior of root segments in wet (a) and dry soil (b). Volumetric water contents are, respectively, 20% and 0%, and confining pressure is 4.5 kPa in both cases.

soil at confining pressure of 50, 100, 150, and 200 kPa, and pullout tests for the roots with low confining pressures between 2 and 4.5 kPa) and method: for soil, cohesion is extrapolated from the residual shear force, while for pulled roots we consider the maximum pullout force. The influence of the type of test and of the confining pressure on the derived angle of internal friction has been discussed by Fannin et al. [2005]. They showed that the maximum angle of shearing resistance in cohesionless soils is stress-dependent and exhibits a linear relation with the logarithm of effective stress. In our case, we observed a similar behavior if we consider separately each pair of shear test data at different confining pressures (50-100 kPa, 100-150 kPa, and 150-200 kPa). In particular, we obtained that the angle of internal friction for the three combinations of confining pressures decreases

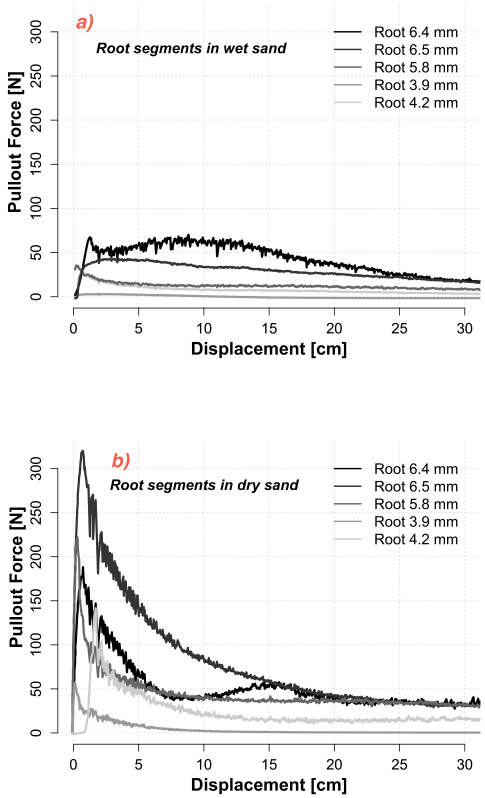

Figure 4.10: Pull out behaviors of root segments in wet (a) and dry sand (b). Volumetric water contents are, respectively, 10% and 0%, and confining pressure is 4.5 kPa in both cases.

with increasing confining pressure (28°, 26°, and 24°, respectively), whereas cohesion increases (10.5 kPa, 15.1 kPa, and 20.9 kPa, respectively).

In natural soils, root hairs, root exudates, pressure due to root growth and overall adaptation of the root to the pore structure of the soil should increase root-soil shear strength in comparison with measured laboratory values. Under field conditions, soil bulk density increases with soil depth. In our study area [Vanomsen, 2006], a bulk density of 1400 kg m^{-3} is exceeded at depth ranging between 200 and 600 mm. This range of depths provides an indication of the possible root zone depths for spruce trees (*Picea abies* L.) [Brady and Weil, 2007] where most of root reinforcement would take place. Thus, for the soil mechanical characterization, we sampled soil at the Ah horizon with a soil bulk density of 1000 kg m^{-3} (Table 4.2) representing

realistic conditions of the soil in the rooted zone. At such low confining pressure (0–8.5 kPa), structured soils in the laboratory should offer a lower surface of contact between roots and soil aggregates than in a natural setting thus explaining the lower friction between roots and soil.

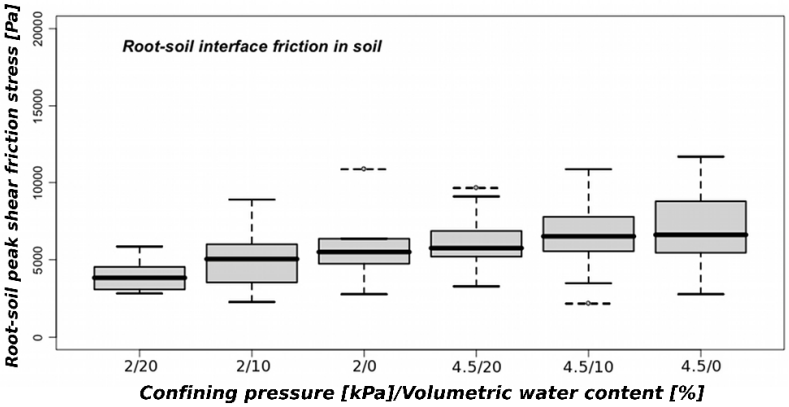

Figure 4.11: Box plot of maximum pullout friction stress of roots in soil (in [Pa]) for different combinations of confining pressures/water contents ([kPa]/[%]). For each cases, a minimum of five tests were performed. For each cases is shown the median (bold black line segment), the 75% percentile (gray box), and the 100% percentile. An isolated circle indicates that one data point was outside the 95% percentile.

Root-soil interfacial friction for sand was highly correlated with confining pressure for dry sand, but not for wet sand. We hypothesize that, since root segments were neither perfectly straight nor smooth, wet unsaturated sand does not transmit confining pressure homogeneously to the root because the matrix is self-supporting at the onset of root segment slip (Figure 4.10a). In contrast, we expect that dry sand would fill the void space left behind a slipping root segment (Figure 4.10b). Confining pressure is thus more homogeneously transmitted to the root-matrix interface resulting in higher interfacial friction. Mickovski et al. [2007] measured higher interfacial friction in wet sand, in apparent contradiction with our measurements. We hypothesize that this apparent contradiction is due to the different experimental setup. In the case of Mickovski et al. [2007], root analogues are pulled vertically, whereas in our case the natural root segments are pulled horizontally. Other pullout tests on stem segments of purple willow (*Salix purpurea* L.) [Bischetti et al., 2009] gave root-soil interfacial friction stress between 0 and 5 kPa for a confining pressure of 3.9 kPa in a poorly graded sand with a soil moisture of 5–10 %, in accord with our own measurements.

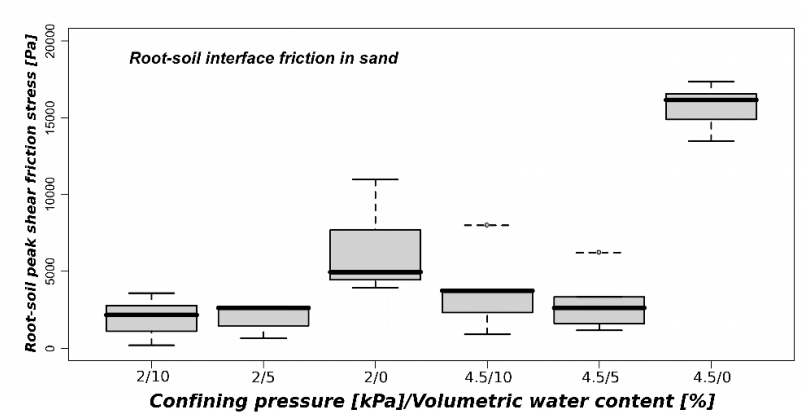

Figure 4.12: Box plot of maximum pullout friction stress of roots in sand (in [kPa]) for different combinations of confining pressures/water contents ([Pa]/[%]). For each case, a minimum of five tests were performed. For each case is shown the median (bold black line segment), the 75% percentile (gray box), and the 100% percentile. A lone circle indicates that one data point was outside the 95% percentile.

Effect of Fiber Type We observed different behaviors between cotton fibers and root segments of spruce (*Picea abies* L.) in pullout experiments in sand with different moisture contents (Figures 4.8 and 4.10). Under wet conditions, friction is highest for cotton fibers but lowest for root segments. We explain this opposite behavior by the difference in diameter of cotton fibers and roots relative to the grain size and by the difference in material properties: in the case of cotton fibers, their diameters are smaller than the grain size of the sand particles and the material is highly deformable, thus contacts between fibers and soil matrix are limited in dry conditions and confining pressure in the matrix is only partially transmitted to the fiber-matrix contacts. Under wet conditions, capillary water forming pendular bridges between the cotton fibers and the grains increase the surface contact and the apparent cohesion between fibers and matrix.

Effect of Fiber Length Although the effect of the root length-diameter relationship (also known as root aspect ratio) on the pullout force were not studied in the present experiments, root length has a major effect on the root mechanical behavior, as has been widely recognized [Waldron and Dakessian, 1981; Ennos, 1990; Michovski et al., 2007; Michovski et al., 2010] and demonstrated in the Root Bundle Model [Schwarz et al., 2010a]. Our measurements of root geometry confirm that root tortuous length increases with increasing root diameter for spruce trees (*Picea abies*

L.) (see equation(2)). Different tree species or root types would yield different parameters that would likely modify significantly the pullout forces of individual roots and root bundles.

Laboratory Experiments with Natural Roots

To quantify the influence of tortuosity and branching points on the pullout behavior of natural roots taken from the study area, we performed pullout tests with 3 roots of different diameters (1, 2 and 3 mm). The experiments were repeated 3 times for each case considered (unbranched, branched, and tortuous-unbranched), and the results are shown in Figure 4.13.

Effect of Branching Points Comparison between data in Figures 4.13a and 4.13b highlights the importance of root branching pattern on global pullout behavior, as was previously shown for cotton fibers (Figure 4.8). The maximum pullout force was twice as large for branched samples than for unbranched samples, while the displacement at maximum pullout force was in both cases similar. For both cotton and natural root experiments, the presence of branching points doubles the value of the maximum pullout force. The larger displacement at maximum pullout force observed for branched roots is attributed to the additional root-soil friction of branching points that increases root pullout force. With branching points, the mobilization of tensile strength along anchored root branches is also included and is manifested primarily at larger displacement. The initial part of the force-displacement curve (root stretching) is similar for branched and unbranched roots.

Predictions with the RBM confirm the need to introduce a branching point coefficient [Schwarz et al., 2010a] that explicitly considers this additional friction to improve estimation of root mechanical behavior. Other studies [Stokes et al., 1996; Dupuy et al, 2005; Mickovski et al., 2007] have also recognized the importance of branching pattern in pullout behavior of roots, but the parametrization of branching points in a model and the use of experimental data to validate it is novel. The assumption of the RBM to neglect the influence of the branching angle is based on results reported by Stokes et al. [1996] which showed that for a certain type of branching pattern, a variation of branching angle from 30 to 90 degrees increased pullout force for an individual branching point by less then 5%.

Effect of Tortuosity Figure 4.13c shows that for tortuous roots, both the maximum pullout force and the displacement at maximum reinforcement were higher than for straight roots without branching points. The larger values of pullout forces measured for tortuous roots can be attributed to the increase in root-soil interfacial friction due to the increased normal

stress at the root-soil interface caused by the component of the pullout force perpendicular to the root. The increase in displacement is attributed to a lower global (effective) Young's modulus caused by the low bending resistance of a root embedded in soil. The magnitude of the effective Young's modulus depends on the bending properties of the tortuous root as well as on the plasticity of the soil. Different soil stiffness will also modulate the effects of tortuosity on root mechanical behavior. For stiff soil, tortuosity has little or no effect on the effective Young's modulus whereas for more compliant soils the effects of tortuosity will vary as a function of the compression and shearing properties of soil. The calibration of the tortuosity coefficient in the RBM with laboratory data resulted in an effective Young's modulus one-third the value of the root material modulus [see Schwarz et al., 2010a].

Previous numerical simulations [Schwarz et al., 2010a] have shown that root tortuosity has a major impact on the mechanical behavior of pulled roots. Predicted curves in Figure 4.13c were obtained using measured tortuosity of 1.1. The implementation of a tortuosity factor in modeling root reinforcement is a new element that explains the range of displacements at which roots reach their maximum pullout force.

Pullout Tests in the Field

We performed a total of 6 pullout field experiments using a total of 36 roots with diameters ranging from 1 to 3 mm. Figure 4.14 shows the mean behavior of different root diameter classes (the mechanical behavior of individual roots showed a high degree of variability in terms of maximum pullout force (standard error of 30%) and displacement (standard error of 25%)). We observed that small roots tended to slip out whereas larger roots (in this case $\geq$ 2 mm) tended to break. The volumetric soil water content for these experiments was between 15 and 20%.

Figure 4.15 shows the global pullout behavior of one of the five root bundles from a field test and comparison with a model run. The global pullout force increases continuously during the first part of the force-displacement curve until the first root (or class of root diameters) breaks or slips out (point A in Figure 4.15). In many cases, in both models runs and field tests, it is possible to observe the presence of multiple peaks before the pullout force starts to decrease gradually (point B in Figure 4.15). The breakage of a root or a class of roots that dominates the bundle may result in an abrupt decrease in the global pullout force (point C in Figure 4.15). The high variability of individual root behavior strongly influences the global behavior of a root bundle when considering a limited number of

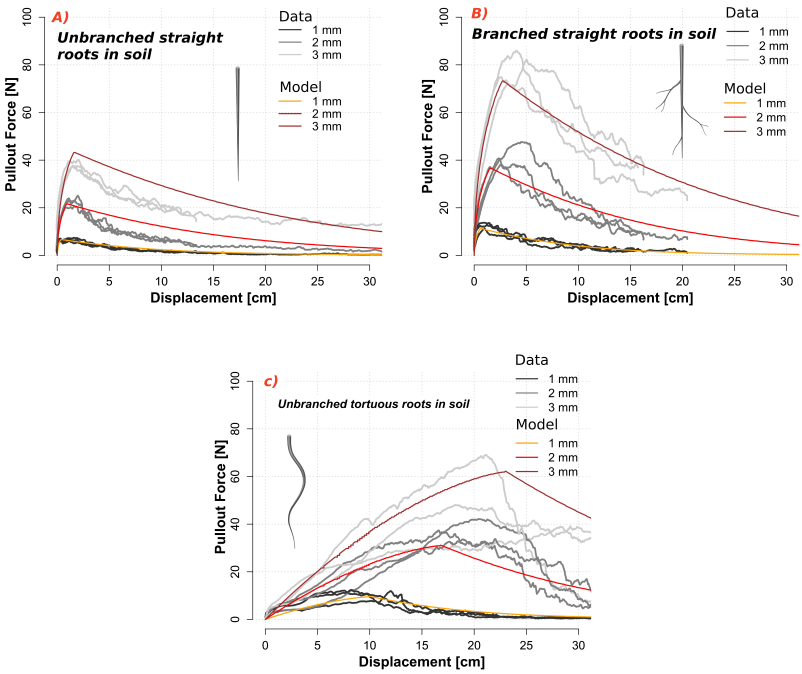

Figure 4.13: Comparison between unbranched straight roots (a), branched straight roots (b), and unbranched tortuous roots (c) in soil. The soil used in these tests is from Uetliberg and had a volumetric water content of 15%. Confining pressure was 2 kPa and tortuosity was 1.1 (in the case of tortuous roots). For the RBM, the value of the branching point coefficient was set to 0.1.

roots. The prediction of the pullout forces with the RBM shows a peak value which is about 16% less than the measured maximum peak. Moreover, the predicted displacement at maximum reinforcement is about 30 % more than measured values (3.8 cm measured and 4.9 cm modeled). For the same bundle of roots, the use of Wu's model [Wu et al., 1979] for the estimation of root reinforcement would result in a constant value of 464 N, an overestimation of about 60% in root reinforcement.

Figure 4.16 shows the difference between two modeling approaches and six field pullout tests for quantifying the maximum root reinforcement. The first approach considers the maximum root reinforcement calculated with the sum of the maximum forces as in the approach of Wu [Wu et al., 1979]. The second approach is the application of the RBM [Schwarz et al., 2010a] (Table 4.3). Results show that the RBM tends to underestimate with a

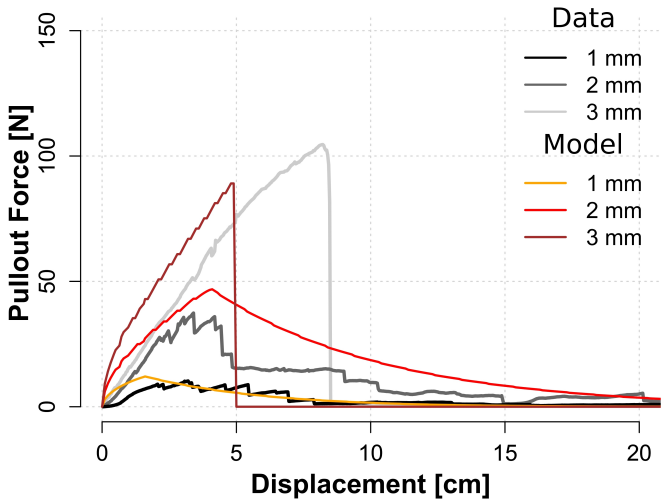

Figure 4.14: Field pullout forces versus displacement for three classes of root diameter. Data shown are mean values of respectively 12 roots of 1–2 mm, 9 roots of 2–3 mm and 1 root of 3 mm.

relative standard error of 16%, whereas the sum of maximum forces overestimate peak strength by 60%. For this application, the RBM yields more realistic values of maximum root reinforcement and, in addition, provides the full stress-strain behavior of root bundles. The causes of the commonly observed overestimation of peak forces of Wu's approach are often attributed to the lack of consideration of progressive failure of roots [Pollen, 2007]. In contrast, the RBM takes into account progressive failure in addition to other geometrical and mechanical factors discussed above. A certain degree of peak force underestimation by the RBM could be explained by the fact that the pullout curves of natural roots exhibit local force peaks due to numerous irregularities that are not captured by a model based on mean forces.

Displacement and Failure Dynamics of Root Bundles

To highlight the importance of failure dynamics of root bundles, we present in Figure 4.17 calculations of displacement at maximum pullout force for assumed distributions of root bundles, using the pullout data of individual roots measured in the field and those modeled with the RBM. These results show that total displacement to failure was between 20 and 80 mm, and

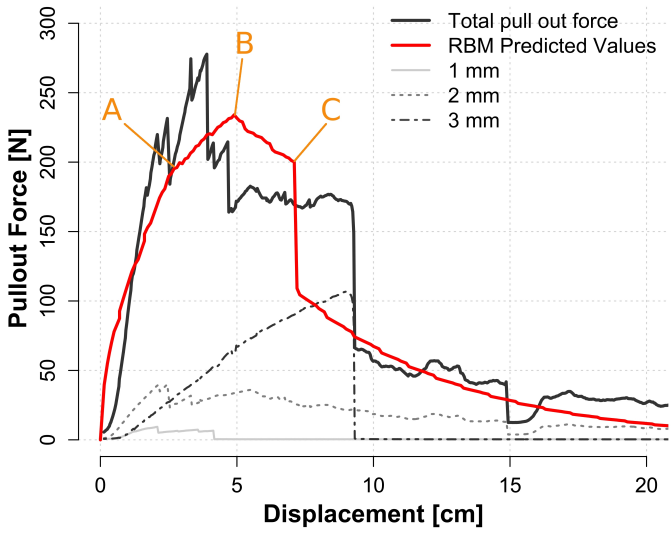

Figure 4.15: Pullout forces versus displacement of a field experiment showing the global behavior versus the model behavior, and the single root behaviors. Capital letters letters indicate the three failure phases which follow the failure of the three classes of root diameter (A = 1 mm, B = 2 mm, C = 3 mm).

displacement was strongly dependent on the distribution of root diameters in the bundle. Moreover, we confirm that the displacement at maximum pullout force increases with increasing size of the dominant root diameter in a bundle.

The computed displacement at maximum pullout force for the 6 tested root bundles (Table 4.3) was constant at 4.9 cm. This result is attributed to the dominance of 2-mm roots in all tested bundles. Hence, the displacement at maximum pullout force of the bundle corresponds to that of the 2-mm diameter class (see Figure 4.13). Estimating root-bundle displacement at failure is one of the most important feature of the RBM. In particular, the RBM allows the simulation of different modes of global failure of root bundles that may be characterized by continuous decay of residual pullout force or by abrupt breakage of a class of root diameter (such as in Figure 4.14). The RBM implements a quantitative approach for explicit consideration of the effects of root tortuosity and soil mechanical properties on the displacement and failure of a bundle of roots. For root bundles with few roots, the prediction of the displacement of maximum pullout force or

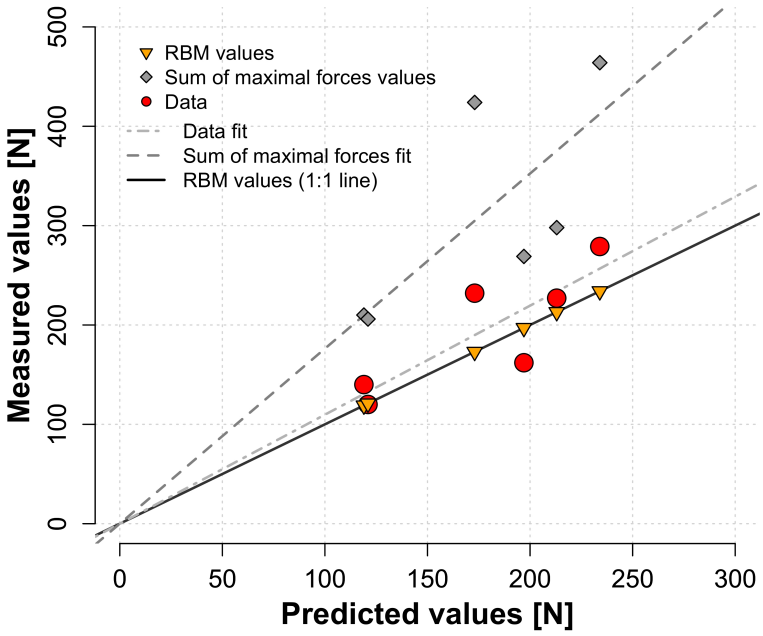

Figure 4.16: Measured maximum root reinforcement versus predicted root reinforcement with the RBM and with the sum of maximum forces [Wu et al., 1979]. Each data point correspond to the maximum pullout force of bundles tested in the field experiments.

the displacement at which the most significant decrease in pullout force occurs is challenging. However, the possibility of estimating the displacement even within an order of magnitude represents a reasonable approximation in many applications. For root bundles with a large number of roots, the RBM provides a better prediction for two reasons: (1) for a broad distribution of root diameters [Schwarz et al., 2010a], an abrupt decrease in pullout force is unlikely due to the balanced contributions of individual root diameter classes, and (2) heterogeneities of maximum pullout forces and displacements of individual roots are statistically compensated for roots of similar diameters. In general, the distribution of root diameters and the number of roots exert a significant influence on the displacement at maximum pullout force of a root bundle.

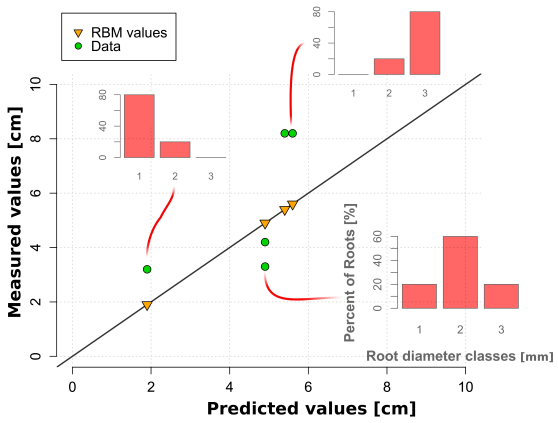

Figure 4.17: Displacement at maximum root reinforcement for different types of root distributions in a bundle. The data are obtained using pullout field data and RBM predicted values. The three bar plots inserts show the percentage composition of the root bundle for three of the six bundles. Some of the modeled data points are overlapping due to the dominant effect of a root diameter class. Thus only four triangles are shown instead of six.

Implications of the model on slope stability calculations

Results of this study highlight the importance of two mechanical variables for slope stability calculations: (a) amount of displacement, and (b) variation of root reinforcement as a function of displacement. Calculations of factor of safety using infinite slope approaches consider lateral root reinforcement as a cohesion term added to the soil intrinsic cohesion. Our measurements clearly demonstrate that these calculations overestimate slope stability because these two components of the stabilizing force are activated at different displacements and hence can not be simply additive. Moreover, Schwarz et al. [2010c] have shown that lateral root reinforcement plays an important role in the stabilization of small shallow landslides ($\leq$ 1000 m^3) where roots do not cross the basal shear plane, and that a realistic implementation of root reinforcement in a slope stability calculation is possible only by considering the spatial distribution of all trees and deriving the value of lateral root reinforcement in the stand based on the spatially resolved calculation of root reinforcement at the scale of an individual tree.

Table 4.3: Summary of maximum pullout force and displacement at maximum pullout force measured and predicted for the 6 root bundles tested in the field. The root distributions are expressed as number of roots and percent of the total.

Bundle Nº	**Nº of Roots**			**Displacement** [**cm**]		**Max.Force** [**N**]	
	1 mm	2 mm	3 mm	Data	Model	Data	Model
1	4 (50%)	3 (37.5%)	1 (12.5%)	3.8	4.9	279	234
2	4 (57%)	2 (29%)	1 (14%)	6.7	4.9	227	213
3	3 (60%)	2 (40%)	0 (0%)	2.3	4.9	140	121
4	3 (60%)	2 (40%)	0 (0%)	4.9	4.9	120	121
5	1 (20%)	4 (80%)	0 (0%)	1.4	4.9	162	197
6	3 (50%)	3 (50%)	0 (0%)	2.6	4.9	232	173

With the RBM, a complete description of root reinforcement evolution, from progressive to abrupt failure, can be obtained that links root mechanical behavior with triggering mechanism of shallow landslide in vegetated slopes.

4.5 Conclusions

This study presents results of laboratory and field experiments aimed at quantifying influences of different geometrical and mechanical attributes on pullout of individual roots and bundles of roots. In particular, the experiments focused on effects of root tortuosity, root branching patterns, root geometry, soil type, and soil moisture on the pullout behavior of an individual root, as well as root diameter distribution on the global behavior of a root bundle. The results show that:

1. Branching pattern strongly influences the value of maximum pullout force of individual roots, whereas root tortuosity has an effect on both the maximum pullout force and the displacement at maximum pullout force.

2. Root-soil interfacial friction varies with different soil types.

3. Soil water content does not exert a significant influence on friction but friction decreases slightly with increasing water content in natural soil.

4. Pullout behavior of different classes of root diameters exhibits large variability, however, the effect of this variability is limited when a bundle of roots is considered.

5. The RBM provides a reasonable prediction of global pullout behavior of root bundles in the field with a mean underestimation of 16%, while the application of the approach of Wu leads to a mean overestimation of 60% (the magnitude of the overestimation is strongly related to the distribution of roots).

The application of the RBM provides important information regarding root-bundle (and reinforced soil) stress-strain behavior. This information is particularly important for slope stability calculations and for consideration of the interactions of different forces (friction, cementation, suction). As discussed in Schwarz et al. [2010c], implementation of a strain-stress function in standard slope stability modeling approaches such as finite element or discrete element models, as well as classical force or momentum equilibrium calculations, offers considerable advantages. In particular, highly resolved spatial calculations of force-displacement of root reinforcement behavior would improve estimation of triggering mechanisms for shallow landslides with volumes smaller than 1000 m^3 [Schwarz et al., 2010c]. The results contribute to a better estimation of variations of root reinforcement as a

function of distance from tree stem which is an important practical application for optimizing planting or thinning of protection forests [Schwarz et al., 2010b]. Finally, results demonstrate that for simulation of pullout mechanical behavior of root bundles, a strain loading approach is necessary to model slip of individual roots and to obtain realistic force-displacement pullout curves.

4.6 Acknowledgments

This work was supported by the CCES platform (Competence Center Environment and Sustainability) of the ETH domain and is part of the TRAMM project (Triggering of Rapid Mass Movements in Steep Terrain). We thank Charlotte Wirion for her important contribution to the laboratory and field experiments, Gernot Michlmayr for helping with field experiments, and Daniel Breitenstein and Hans Wunderli for technical support. We thank Dr. Kevin Schmidt and two anonymous reviewers for a thourough review of this paper.

4.7 References

Abe, K. and R. R. Ziemer (1991), Effects of tree roots on a shear zone: modelling reinforced shear stress, *Can. J. For. Res.*, *21*, 1012–1019.

Abernethy, B. and A. I. Rutherfurd (2001), The distribution and strength of riparian tree roots in relation to riverbank reinforcement, *Hydrol. Process*, *15*, 63–79.

Anderson, C. J., M. P. Coutts, R. M. Ritcie, and D. J. Campbell (1989), Root extraction force measurement for Sikta spruce, *Forestry*, *62*, 127–137.

Bischetti, G. B., F. Bonfanti, and M. Greppi (2003), Misura della resistenza alla trazione delle radici: apparato sperimentale e metodologia d'analisi, *Quaderni di Idronomia Montana*, *21/1*, (in Italian).

Bischetti, G.B., E. A. Chiaradia, V. D'Agostino, and T. Simonato (2009), Quantifying the effect of brush layering on slope stability, *Ecol. Eng.*, *in press*, doi:10.1016/j.ecoleng.2009.03.019.

Brady, N. C. and R. R. Weil (2007), The nature and properties of soil, *Pearson international edition*, 961 pp.

Casadei, M., W. E. Dietrich, and N. Miller (2003), Controls on shallow landslide width, In D. Rickermann and C. Chen, *Debris-Flow hazards mitigation: mechanics, prediction, and assessment*, Proceedings of the Third International Conference on Debris Flows Hazards Mitigation, Davos Switzerland, p. 91–102, Millpress, Rotterdam.

Cohen, D., P. Lehmann, and D. Or (2009), Fiber bundle model for multiscale modeling of hydromechanical triggering of shallow landslides, *Water Resources Res.*, *45*, W10436, doi:10.1029/2009WR007889.

Collet, C., M. Löf, and L. Pages (2006), Root system development of oak seedlings analysed using an architectural model: effects of competition with grass, *Plant and Soil*, *279*, 367–383.

Cunha, V. M. C. F., J. A. O. Barros, and J. M. Sena-Cruz (2008), Bond-Slip Mechanisms of Hooked-End Steel Fibers in Self-Compacting Concrete, *Material Science Forum*, *587-588*, 877–881.

Czarnes, S., S. Hiller, A. R. Dexter, P. D. Hallett, and F. Bartoli (1999), Root:soil adhesion in the maize rhizosphere: the rheological approach, *Plant and Soil*, *211*, 69–86.

De Beats, S., J. Poesen, B. Reubens, K. Wemans, J. De Baerdemaeker, and B. Muys (2008), Root tensile strength and root distribution of typical Mediterranean plant species and their contribution to soil shear strength, *Plant and Soil*, *305*, 207–226.

Docker, B. B. and T. C. T. Hubble (2008), Quantifying root-reinforcement of river bank soils by four Australian tree species, *Geomorphology*, *100*, 401–418.

Dupuy, L., T. Fourcaud, and A. Stokes (2005), A numerical investigation into factors affecting the anchorage of roots in tension, *European Journal of Soil Science*, *56*, 319–327.

Ennos, A. R. (1990), The anchorage of leek seedlings: the effect of root length and soil strength, *Annals of Botany*, *65*, 409–416.

Fannin, R. J., A. Eliadorani, and J. M. T. Wilkinson (2005), Shear strength of cohesionless soils at low stress, *Géotechnique*, *55*, 467–478.

Hamza, O., A. G. Bengough, M. F. Bransby, M. R. C. Davies, and P. D. Hallett (2007), Mechanics of root-pullout from soil: a novel image and stress analysis procedure. In *Eco- and Ground Bio-Engineering: The use of vegetation to improve Slope Stability*, Stokes et al., Springer; 213–221.

Hong, Y. S., C. S. Wu, and Yang S. H. (2003), Pullout resistance of single and double nails in a model sandbox, *Can. Geotech. J.*, *40*, 1039–1047, doi: 10.1139/T03.048.

Hubble, T. C. T., B. B. Docker, and I. D. Rutherfurd (2010), The role of riparian trees in maintaining riverbank stability: A review of Australian experience and practice, *Ecological Engineering*, *36*, 292-304, doi:10.1016/j.ecoleng.2009.04.006.

Li, J. X. (1994), Analysis of the pullout of single fibers from low-density polyethylene, *Journa of applied Polymer Science*, *53*, 225-237.

Mattia, C., G. B. Bischetti, and F. Gentile (2005), Mechanical characteristics of root systems of typical Mediterranean species, *Plant and Soil*, *278*, 23–32.

Mickovski, S. B., A. G. Bengough, M. F. Bransby, M. R. C. Davies, P. D. Hallet, and R. Sonnenberg (2007), Material stiffness, branching pattern and soil matric potential affect the pullout resistance of model root systems, *European Journal of Soil Science*, *58*, 1471–1481.

Mickovski, S. B., M. F. Bransby, A. G. Bengough, M. C. R. Davies, and P. D. Hallett (2010), Resistance of simple plant root systems to uplift loads, *Can. Geotech. J.*, *47*, 78–95.

Naaman, A. E., G. G. Namur, J. M. Alwan, and H. S. Najm (1991a), Fiber pullout and bond slip I: Analytical study, *Journal of Structural Engineering*, *117(9)*, 2769–2790.

Naaman, A. E., G. G. Namur, J. M. Alwan, and H. S. Najm (1991b), Fiber pullout and bond slip II: Experimental validation, *Journal of Structural Engineering*, *117(9)*, 2791–2800.

Nilaweera, N. S. and P. Nutalaya (1999), Role of tree roots in slope sta-

bilization, *Bull. Eng. Geol. Env.*, *57*, 337–342.

Operstein, V. and S. Frydman (2000), The influence of vegetation on soil strength, *Ground Improvement*, *4*, 81–89.

Ozier-Lafontaine, H., F. Lecompte, and J. F. Sillon (1999), Fractal analysis of the root architecture of *Gliricidia sepium* for the spatial prediction of root branching, size and mass: model development and evaluation in agroforestry, *Plant and Soil*, *209*, 167–180.

Pollen, N. (2007), Temporal and spatial variability in root reinforcement of streambanks: Accounting for soil shear strength and moisture, *Catena*, *69*, 197–205.

Pollen, N., A. Simon, and A. Collison (2004), Advances in assessing the mechanical and hydrologic effects of riparian vegetation on streambank stability, *Riparian vegetation and fluvial geomorphology*, *8*, 125–139, in *, water science and application*, edited by S. Bennett and A. Simon, AGU, Washington, D. C.

Raischel, F., F. Kun, R. C. Hidalgo, and H. J. Herrmann (2006), Statistical damage models: Fiber bundle models, in Damage and Its Evolution in Fiber-Composite Materials: Simulation and Non-destructive Evaluation, edited by G. Busse, B. H. Kröplin, and F. K. Wittel, pp. 443–471, ISD, Stuttgart, Germany.

Reneau, S. L. and W. E. Dietrich (1987), Size and location of colluvial landslides in a steep forested landscape, *In Erosion and sedimentation in the Pacific Rim, proceedings of the Corvallis Symposium, August 1987, IAHS Publ.*, *165*, 39–48.

Rickli, C., and F. Graf (2009), Effects of forests on shallow landslides case studies in Switzerland, *For. Snow Landsc. Res.*, *82(1)*, 33–44.

Roering, J. J., K. M. Schmidt, J. D. Stock, W. E. Dietrich, and D. R. Montgomery (2003) Shallow landsliding, root reinforcement, and the spatial distribution of trees in the Oregon Coast Range, *Can. Geotech. J.*, *40*, 237–253.

Sakals, M. E. and R. C. Sidle (2004), A spatial and temporal model of root cohesion in forest soils, *Can. J. For. Res.*, *34*, 950–958.

Santantonio, D. (1990), Modeling growth and production of tree roots, *Process Modeling of Forest Growth respons to Enviromental Stress*, 124–135.

Schmidt, K. M., J. J. Roering, J. D. Stock, W. E. Dietrich, D. R. Montgomery, and T. Schaub (2001), The variability of root cohesion as an influence on shallow landslide susceptibility in the Oregon Coast Range, *Can. Geotech. J.*, *38*, 995–1024.

Schwarz, M., D. Cohen, and D. Or (2010a), Soil-root mechanical interactions during pullout and failure of root bundles, *J. Geophys. Res.*, , *115*, F04035. doi:10.1029/2009JF001603..

Schwarz, M., P. Lehmann, and D. Or (2010b), Quantifying lateral root reinforcement in steep slopes - from a bundle of roots to tree stands, *Earth Surface Processes and Landform*, *35*, 354–367. doi: 10.1002/esp.1927.

Schwarz, M., F. Preti, F. Giadrossich, P. Lehmann, and D. Or (2010c), Quantifying the role of vegetation in slope stability: A case study in Tuscany (Italy), *Ecological Engineering*, *36*, 285–291.

Shewbridge, S. E. and N. Sitar (1990), Deformation-based model for reinforced sand, *Journal of Geotechnical Engineering*, *116*, 1153-1170.

Soil Survey Staff (2010), Keys to Soil Taxonomy, 11th ed. USDA-Natural Resources Conservation Service, Washington, DC. *ftp://ftp-fc.sc.egov.usda.gov/NSS*

Sornette, D. (1989), Elasticity and failure of a set of elements loaded in parallel, *Journal of Physics*, *22*, L243L250.

Stokes, A., C. Atger, A. G. Bengough, T. Fourcaud, and R. C. Sidle (2009), Desirable plant root traits for protecting natural and engineering slopes against landslides, *Plant and Soil*, *324*, 1–30, doi: 10.1007/s11104-009-0159-y.

Stokes, A., J. Ball, A. H. Fitter, P. Brain, and M. P. Coutts (1996), An experimental investigation of the resistance of root model systems to uprooting, *Annals of botany*, *78*, 415–421.

Su, L. J, T. C. F. Chan, J. H. Yin, Y. K. Shiu, and S. L. Chiu (2008), Influence of overburden pressure on soil-nail pullout resistance in a compacted

fill, *Journal of Geotechnical and Geoenvironmental Engineering*, *134(9)*, 1339–1347, doi: 10.1061/(ASCE)1090-0241(2008)134:9(1339)

Teixeiria, S. H. C., B. S. Bueno, and J. G. Zornberg (2007), Pullout resistance of individual longitudinal and transverse geogrid ribs, *Journal of Geotechnical and Geoenvironmental Engineering*, *133*, 37–50.

Thomas, R. E. and N. Pollen-Bankhead (2010), Modeling root-reinforcement with a fiber-bundle model and Monte Carlo simulation, *Ecological Engineering*, *36*, 47–61. doi:10.1016/j.ecoleng.2009.09.008

Tosi, M. (2007), Root tensile strength relationships and their slope stability implications of three shrubs species in the Northern Apennines (Italy), *Geomorphology*, *87*, 268–283.

van Genunchten, R. (1978), Calculating the unsatured hydraulic conductivity with a new, closed-form analytical model, *Research Report 78-WR-08* Department of Civil Engineering, Priceton University.

van Noordwijk, M., L. Y. Spek, and P. de Willigen (1994), Proximal root diameter as predictor of total root size for fractal branching models, I. Theory, *Plant and Soil*, *164*, 107–117.

Vanomsen, P. (2006), Der Einfluss der Durchforstung auf die Verankerung der Fichte hinsichtlich ihrer Sturmresistenz, Diss. ETH Nr. 16532, Zürich, 246 pp.

Vercambre, G., L. Pages, C. Doussan, and R. Habib (2003), Architectural analysis and synthesis of plum tree root system in an orchard using a quantitative modelling approach, *Plant and Soil*, *251*, 1–11.

Waldron, L. J. and S. Dakessian (1981), Soil reinforcement by roots: calculation of increased soil shear resistance from root properties, *Soil Science*, *132*, 427–435.

Wang, Y., V. C. Li, and S. Bacjer (1988), Modelling of fibre pull-out from a cement matrix, *The international Journal of Cement Composites and Lightweight Concrete*, *10(3)*, 143–149.

Watson, A., C. Phillips, and M. Marden (1999), Root strength, growth, and rates of decay: root reinforcement changes of two tree species and their

contribution to slope stability, *Plant and Soil*, *217*, 39–47.

Wu, T. H., W. P. McKinnell, and D. N. Swanston (1979), Strength of tree roots and landslides on Prince of Wales Island, Alaska, *Can. Geotech. J.*, *16*, 19–33.

Yang, S., Z. Wu, X. Hu, and J. Zheng (2008), Theoretical analysis on pullout of anchor from anchor from anchor-mortar-concrete anchorage system, *Engineering Fracture Mechanics*, *75*, 961–985.

Zhou, Y., D. Watts, Y. Li, and X. Cheng (1998), A case study of effect of lateral roots of *Pinus yunnanensis* on shallow soil reinforcement, *Forest Ecology and Management*, *103*, 107–120.

Chapter 5

Spatial characterization of interacting root systems - theory and case study

Autohrs: Schwarz M. [1,2], Cohen D. [2] and Or D.[2]

[1] Swiss Federal Institute for Forest, Snow and Landscape Research, 8903 Birmensdorf, Switzerland

[2] Soil and Terrestrial Environmental Physics, Institute of Terrestrial Ecosystems, ETH Zurich, 8092 Zurich, Switzerland

In preparation for: *Geomorphology*.

5.1 Abstract

We propose a new upscaling approach for the quantification of root reinforcement based on the Root Bundle Model for the characterization of the pullout force-displacement behavior and on a simple approach for the estimation of root distribution at stand scale. We compared model results with measurements of root distribution along the scarp of an artificially rainfall-triggered landslide in a vegetated hillslope. The results show that the model tend to overestimate the density of small roots (1, 2 and 3 mm diameter), leading to an error in the estimation of maximal root reinforcement. Variability of maximal root reinforcement within the forest stand is high, ranging from 0 up to 20 kPa. However, most soil reinforcement by roots occurs close to the tree stem or in zones where root systems overlap. We think that the presented method is important for practical and scientific application, since a detailed description of maximal root reinforcement in a slope is fundamental for the prediction of shallow landslides and the management of protection forests.

Key words: Root Reinforcement, Shallow Landslide, root distribution modeling, root bundle model.

5.2 Introduction

Plant roots strongly influence the morphology, spatial distribution, and triggering mechanisms of shallow landslides in vegetated slopes [Schmidt et al., 2001; Roering et al., 2003]. Typical parameters such as canopy index, stem diameter distribution and species composition of forested stand are used qualitatively to define strategies for protection forest management [Brang et al., 2006]. The mechanical effects of vegetation on the stability of shallow landslide is widely recognized [Sidle and Ochiai, 2006], and is usually defined as root reinforcement. Despite considerable progress in this area, realistic description and analysis of the spatial distribution of root reinforcement in vegetated hillslopes remain lacking. Many studies on the stability of vegetated slopes consider root reinforcement as a constant homogenously distributed basal apparent cohesion [Montgomery and Dietrich, 1994, (TOPOG, SHALSTAB); Sidle and Wu, 2001, (dSLAM); Bathrust et al., 2005, (SHETRAN); Simoni et al., 2007, (GEOtop)]. Few models implement heterogeneities due to tree distribution [Sakals and Sidle, 2004; Genet et al., 2008] and none consider the dynamics of root reinforcement.

Root-soil mechanical properties and interaction have been studied intensively and recently reviewed in the context of triggering of rapid mass

movements [Schwarz et al., 2010b]. Proper quantification of root reinforcement involves upscaling of reinforcement mechanisms from the individual root, to root bundle, to interacting neighboring root systems [Schwarz et al., 2010b]. Previous work highlighted the importance of including the progressive failure of roots within a bundle. Experiments indicate that the activation of roots or bundles of roots along a tension crack is not simultaneous, and must be considered in evaluating and quantifying root reinforcement in a vegetated slope. In recent years the use of the fiber bundle model concept (FBM) was introduced for the calculation of progressive root reinforcement in single soil profiles [Pollen and Simon, 2005; Schwarz et al., 2010a; Cohen et al., *in review*], but was not applied to larger scales such as a forest stand. In addition to progressive failure, the upscaling of root reinforcement requires knowledge of the spatial root distribution. Schmidt et al. [2001] showed with detailed measurements in several landslide scarps that values of root reinforcement must be compiled at the landslide scale because the vegetation and root reinforcement vary at that scale. An example of variation of root distribution at the stand scale is shown in figure 5.1.

Recent studies recognized the importance of lateral root reinforcement particularly for protection function against shallow landslides [Schmidt et al., 2001; Roering et al., 2003; Schwarz et al., 2010c]. In many cases, the effects due to the lateral root reinforcement is higher then those due to the basal root reinforcement. This consideration is explained basically by the fact that most of the roots in a forest stand are confined in the first 1 m of soil and that deep roots reach only locally a shear plane of a shallow landslides that is usually located at 1-2 m depth [Schmidt et al., 2001, Danjon et al., 2007]. For this reason the implementation of the lateral root reinforcement is important for a realistic analysis of shallow landslides. Studies such as done by Schmidt et al. [2001] and Kukotse et al. [2006] were the first to introduce 3D analysis of root reinforcement considering constant lateral and basal root reinforcement for different forest structure. Kukotse et al. [2006], however, assumed a homogenous root reinforcement within the same root system and did not consider the lateral interactions of neighboring root systems and the spatial variability of root reinforcement within the same root system.

The approach of Schwarz et al. [2010b] is one of the first modeling framework for the estimation and characterization of root distribution at stand scale that allow a realistic upscaling of lateral root reinforcement at the stand scale.

The primary objective of this work is to present a quantitative method for the characterization of the distribution of lateral root reinforcement on a

vegetated slope (apparent E modulus, displacement at maximal reinforcement and maximal root reinforcement), and validate it in a case study. Building up on the outcomes of previous studies such as Sakals and Sidle [2004] and others [Wu and Sidle, 1995; Dhakal and Sidle, 2003], we tested a model framework [Schwarz et al., 2010b] that combined the spatial distribution of root with the force-displacement characterization of root reinforcement at stand scale. In a first step we used the model to characterize the theoretical spatial distribution and the dynamic of root reinforcement within single tree root system and between interacting root systems. Secondly, we present the field characterization and the calibration of the model for a case study. Finally, we compared the results of the model with the data on root distribution collected in the landslide scarp present in the study area. These results help to define the limits and the potentialities of root reinforcement in the triggering of shallow landslides and expand the knowledge needed to optimize the management of protection forests.

Figure 5.1: Soil profile showing the variability of root distribution at stand scale (Patagonia, South America).

5.3 A model of root reinforcement for interacting root systems

We model the spatial distribution of root reinforcement by upscaling the mechanical behavior of a single root and its spatial extension to a large number of roots distributed in a forest stand [Schwarz et al., 2010b]. The framework combines two independent models: a) a root distribution model for secondary lateral roots and b) a single root pullout model. We assume that:

1) Root distribution of an individual tree is not influenced by concurrence of neighboring trees and is symmetrical.

2) The pullout behavior of a single root is not influenced by neighboring roots.

3) Lateral root reinforcement is isotropic.

The motivations for these assumptions are discussed in the following sections.

Root distribution of interacting root systems

The model to estimate root distribution of a single tree is based on four parameters [Schwarz et al., 2010a]: 1) Pipe coefficient (empirical coefficient used to estimate the distribution of fine roots as a function of tree size, specie and stand characteristics). 2) Maximum lateral rooting distance (estimated with empirical formulas). 3) Scaling factor or proportionality factor (empirical coefficient used to calculate the maximum root diameter (ϕ_{max}) at a prescribed distance from stem). 4) Exponent λ (empirically fitted exponent used to calculate the density of coarse roots as a function of fine root frequency). The maximum root diameter at a certain distance from a tree was derived by an empirical function considering the number of branching points along the root [Schwarz et al., *in review*]. The calibration of this correlation was done using the only reported data available for spruce trees (*Picea abies*).

In Schwarz et al. [2010b] we showed how these parameters may be obtained from literature data and how this approach allows an estimation of root distribution for spruce trees (*Picea abies*).

Following the model of Schwarz et al. [2010b], the number of roots N in 1 m width vertical soil profile (considering a theoretical infinite depth), for the root diameter class ϕ at a position x, due to the vicinity of the tree t, is calculated as

$$N_{\phi,x,t} = D_{fr}\frac{(log(1+\phi_{max}) - log(1+\phi))}{log(1+\phi_{max})}\phi^{\lambda} \tag{5.1}$$

where D_{fr} is the density of fine roots ($\leq$ 1 mm diameter) which depends on the tree stem diameter and the distance from tree stem, ϕ_{max} is the maximum root diameter at a prescribed distance from stem, and λ is the fitted exponent for an empirical set of data. In this study these parameters are calibrated considering class-diameters sizes of 1 mm. We employed a model similar to that of Ammer and Wagner [2005] to estimate density of fine roots (D_{fr}) as a function of distance from a single tree stem, and we assume a constant value of branching distance [Van Noordwijik et al., 1994; Ozier- Lafontaine et al., 1999] for the calculation of maximum root diameter ϕ_{max} at a prescribed distance from stem, as reported in Schwarz et al. [2010b]. The distribution of fine roots is mostly influenced by below-ground competition and we partly considered this aspect by the calibration of two parameters: 1) the pipe theory coefficient [Schwarz et al., 2010b] which has to be calibrated for different stands and tree species; 2) the maximal threshold of fine root density which is characteristic of each forest stand.

The upscaling of the root distribution at the stand scale is done considering a linear superposition of single root systems. The root distribution at position x for a root diameter class ϕ is calculated as

$$N_{\phi,x} = \sum_{t=1}^{T} N_{\phi,x,t} \tag{5.2}$$

where t is the tree numbering index and T is the total number of trees in the stand.

Mechanical reinforcement of interacting root systems

To estimate mechanical reinforcement, we use a modified version of the root bundle model (RBM) [Schwarz et al., 2010a]. The RBM is an extension of the Fiber Bundle Model [e.g., Sornette, 1989; Kun et al. 2007; Cohen et al., 2009] that takes into account geometrical and mechanical characteristics of roots such as length and tortuousity. The model calculates the pullout force of a root bundle as a function of displacement during displacement controlled loading of the bundle (see Figure 5.2). The simplification of this version of the RBM is based on the assumption that all roots break instead of slipping out. This simplification is justified by the fact that field observations during the pullout tests indicate that most roots break,

and omitting slip reduce the computation time of the numerical simulations considerably. Moreover, based on the study of Schwarz et al. [2010a], one of the most sensitive parameters of the RBM is the coefficient used to estimate root length.

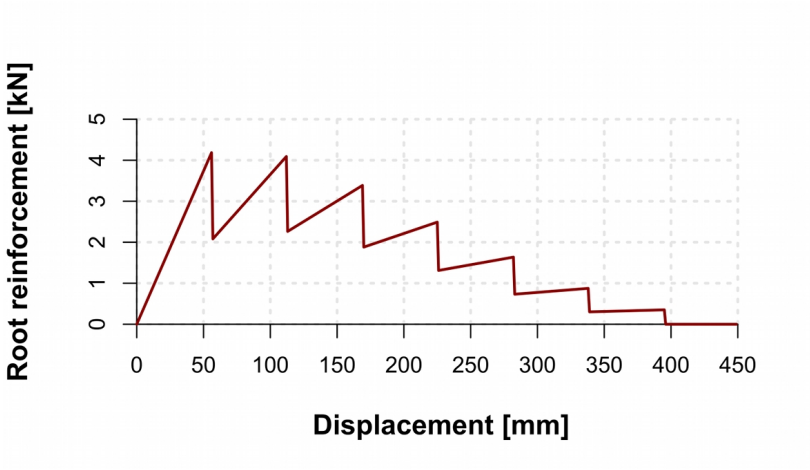

Figure 5.2: Typical force-displacement behavior of a root bundle modeled with the simplified version of the RBM.

The geometrical and mechanical characteristics of each root are expressed in the model by the following empirical equations

$$L(\phi) = L_0 \left(\frac{\phi}{\phi_0} \right)^{\gamma} \tag{5.3}$$

where $L(\phi)$ is the tortuous root length in [mm], L_0 is an empirical characteristic length in [mm], ϕ is root diameter in [mm], ϕ_0 is a reference diameter (in order to obtain a dimensionless value), and γ is an empirical power-law exponent. The effect of the apparent Young's model was implemented in the simplified model as

$$E(\phi) = E_0 \left(\frac{\phi}{\phi_0} \right)^{-\beta} r \tag{5.4}$$

where $E(\phi)$ is the Young's modulus [MPa], E_0 is an empirical characteristic modulus in [MPa], β is an empirical power-law exponent, and r is a dimensionless coefficient introduced to consider the effects of root tortuousity on the tensile behavior of a root [Schwarz et al., 2010a]. The threshold of maximal tensile force for each root diameter class is then calculated as

$$F_{max}(\phi) = F_0 \left(\frac{\phi}{\phi_0} \right)^{\xi} \tag{5.5}$$

where $F_{max}(\phi)$ is the maximal tensile force [N] F_0 is an empirical characteristic modulus in [N], ξ is an empirical power-law exponent.

The parameters of the RBM are in part calibrated using literature data (see Table 5.1) and in part using field data (see section 5.5).

Table 5.1: Values of the calibrated parameters for the RBM.

Symbol	**Parameter**	**Value**	**Unit**
-	Pipe coefficient	0.09	[−]
b	Mean branching distance	90	[mm]
L_0	characteristic length	285	[mm]
γ	exponent root length	0.7	[-]
E_0	characteristic Young's modulus	600	[MPa]
β	exponent Young's modulus	1	[-]
r	tortuosity coefficient	0.3	[-]

5.4 Model Application

The following section shows examples of results obtained with the proposed simplification of the RBM. The presentation of these results follows the upscaling approach from the root distribution and root reinforcement within a root bundle, to the reinforcement at single root system scale, and finally to the stand minimal lateral root reinforcement.

Roots distribution of interacting root systems

The parameters used in the RBM for the calculation presented in this section were set considering typical literature values [Schwarz et al., 2010a] and are reported in Table 5.1 in the following section.

The calculated values of root distribution within two interacting root systems show that the frequency of fine roots reach values of 250 roots per vertical square meter only in cases of high tree density (for example 600 trees/ha with stem diameters of 60 cm). These data are comparable with those reported in literature [Schmid and Kazda, 2002; Bischetti et al., 2005]. Figure 5.3 shows the simulated spatial root distribution of fine roots (1 mm diameter) between two trees of 0.3 m stem diameter at different distance from each other (10, 5, 2 m). In this case, root systems start to interact at distances lower then 9 m and the maximal root frequency per square meter reached is less than 200 roots. The distribution of coarse roots is derived as a function of the fine root distribution and the distance from tree stem. The results show that the range of possible maximal root diameter goes from 10 to 50 mm for root systems belonging to 10 and 60 cm tree stem diameter, respectively.

Lateral root reinforcement of a single root system

From the combination of the root distribution model and the RBM we can characterize the mechanic of root reinforcement within a single root system. The plots in Figure 5.4 show the distribution of the maximal root reinforcement, the displacement at maximal root reinforcement and the secant modulus of elasticity in function of the distance from tree stem.

Nearby the tree stem, root reinforcement slightly increase due to the increasing number of fine roots (within a radius 5 times the tree stem diameter); further away from the tree stem, root reinforcement decrease exponentially down to 0 at a distance that corresponds to the maximal lateral rooting extension. From this plot we can see that the maximal lateral

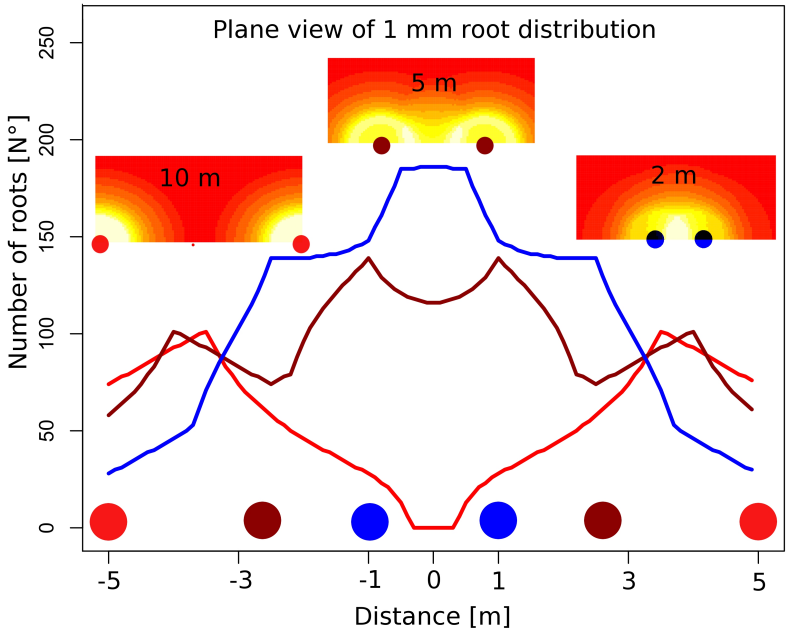

Figure 5.3: Calculated distribution of 1 mm roots within the interaction of two trees at different distances. Colored circles indicate the position of the tree stems. In this example we considered trees with 0.3 m DBH.

extension of the root systems range between 2 m for a 0.1 m tree stem diameter and 6.5 m for a 0.5 m tree stem diameter.

The Figure 5.4b shows that the displacement at maximal root reinforcement for the three stem diameters considered is characterized by three values: 56 mm, 112 mm and 169 mm. These values correspond to the displacement thresholds of maximal tensile force for the three smallest classes of root diameters (1, 2 and 3 mm). Thus, the plot shows that in zones near the tree stem of 0.4-0.5 m diameter the mechanical behavior of the root bundle is dominated by the 3 mm diameters whereas with increasing distance from the stem or decreasing stem diameter the root bundle behaviors are dominated by smaller root diameters (2 and 1 mm).

The secant modulus of elasticity is the quotient between the maximal tensile force of the root bundle and the corresponding displacement. The values of plot 4c show that the stiffness of root reinforcement decrease with increasing the distance from tree stem.

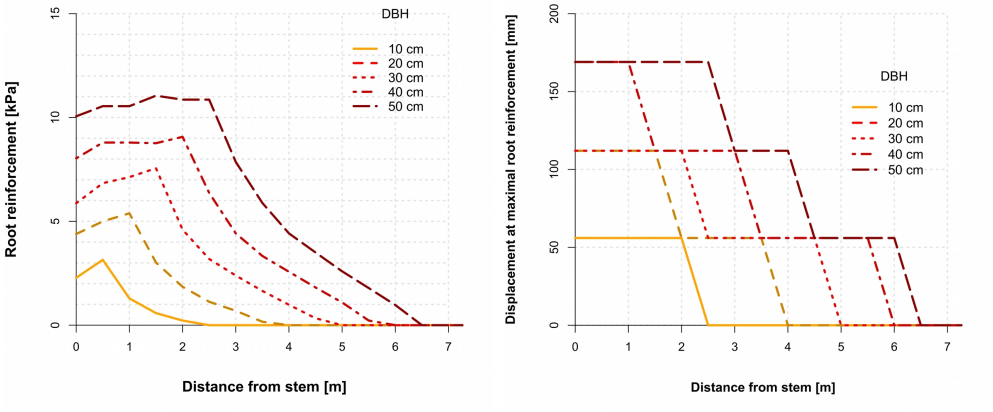

Figure 5.4: Calculated maximal root reinforcement and displacement at maximal root reinforcement as a function of the distance from tree stem.

Lateral root reinforcement between interacting root systems

The calculations of root reinforcement between the root systems show distributions similar to those of the fine roots (Figure 5.3). Figure 5.5 shows that in the case of trees with 0.3 m stem diameter the minimal root reinforcement may vary from 0 (10 m distance) to 15 kPa (when trees are a 2 m distance from each other). For a distance of 5 m the root reinforcement result in a more or less constant reinforcement of 7 kPa.

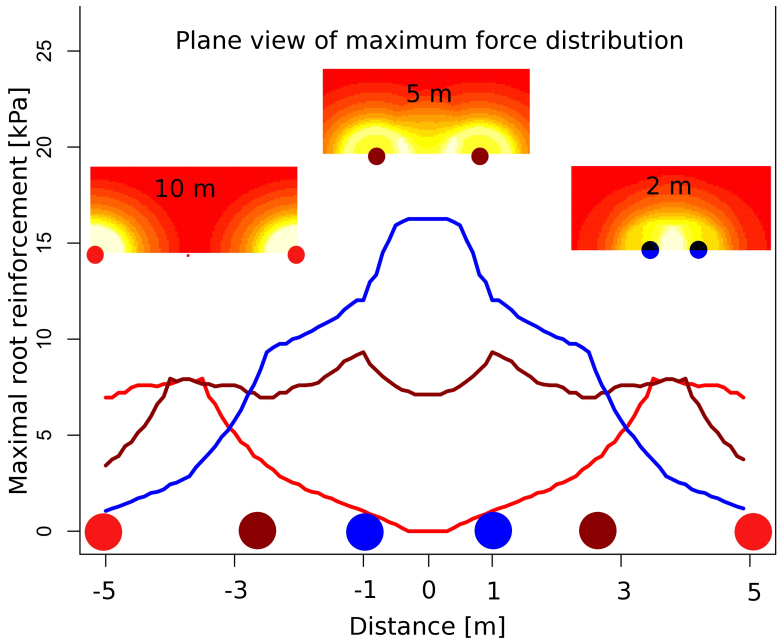

Figure 5.5: Calculated distribution of maximal root reinforcement within the interaction of two trees at different distances (as Figure 5.3). In this example we considered trees with 0.3 m DBH.

Distribution of lateral root reinforcement at stand scale

At stand scale the zones of minimal root reinforcement are generally localized in areas between the trees, where the density of roots is low. Figure 5.6 shows how the minimal root reinforcement within a homogeneous unit cell of a stand can vary in function of the dimension of the trees and their set distances. The results show that for a inter-distance of 4 m trees of 0.1,

0.3, 0.5 and 0.7 m stem diameter, the minimal lateral root reinforcement is about 0, 10, 20 and 30 kPa respectively. This density of trees corresponds to a stand density of about 600 tree/ha, that mean a stand basal area of 4, 42, 117, 230 m^2/ha, respectively. In the case of low tree density (like 100 trees/ha) it results that only trees with diameter bigger than 0.7 m are present and assure a minimal lateral root reinforcement of about 7 kPa.

Surprisedly, the values calculated for the two different types of tree distribution in stand (hexagonal or squared) result to be similar, with a maximal difference from each other of less then 10%. Moreover, the minimal root reinforcement decay exponentially with increasing distance between the trees. In all the cases considered here, the maximal density of fine roots was always less then 300 roots/m^2, which is below the values of maximal phisiological threshold reported in literature [Schwarz et al., 2010b].

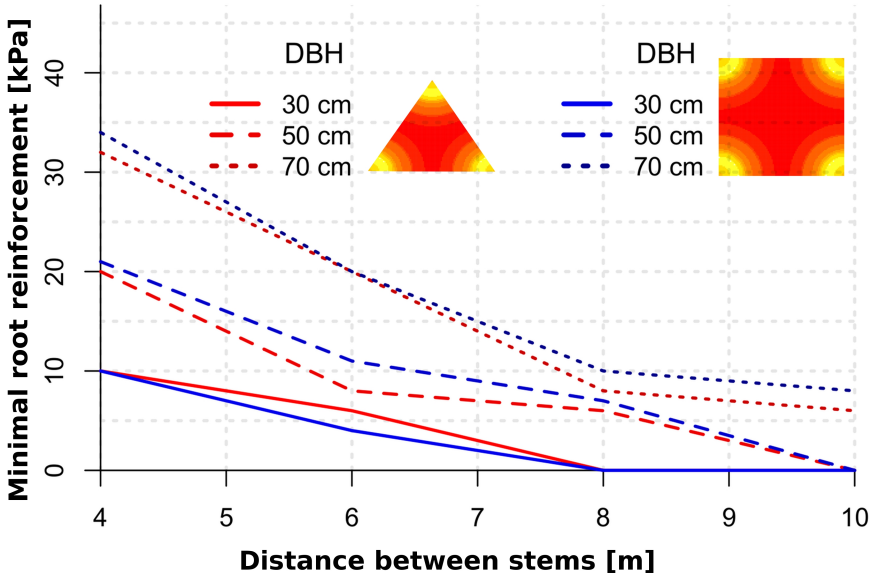

Figure 5.6: Plot of minimal lateral root reinforcement in function of distance (bottom axis) between trees for 2 types of trees distributions (triangle (red lines) and squared (blue lines)).

5.5 Case study: the Rüdlingen experiment

Field site

The study area is situated on the upper part of the Rhine river bank with a S-E exposition near Buchberg (Swiss midland). This area consists mainly of molasse with a lithology composed of sandstone. Soils are shallow and under the forest cover they developed in the form of a brown earth. The stand is located on a slope (37^o-40^o) at circa 350 m altitude. The horizontal profile is slightly concave. The vegetation cover is composed of three layers: a single layer of trees (covertures of circa 80%, high from 5-20 m), a lower layer with shrubs (1-5 m) and finally a herb layer. The species composition of each layer is quite heterogeneous thus we decided to do the root reinforcement characterization based on the data of the most present species that is the ash tree (*Fraxinus excelsior*). The site is classified as $Aceri - Fraxinetum$. The location is humid due to the vicinity of the river, and the reaction of the soil-stone substrate is basic. The slope is generally well drained (no signs of reduction in the soil profiles) and the soil biological activity is high, forming a mull humus layer. The soil is good aggregated in the upper layers (crumbs,

diameter aggregates circa 1-10 mm), but shows increased density at circa 50-70 cm depth. The upper layers of the soil profile in some zones of this area are the deposit material of a recent shallow landslide that failed in the upper part of the slope. Damages on the tree trunks and the age of young trees growing on the sediment indicate that the event was about 6 years ago (2002-2003). The position, dimension and species of the present trees were collected *in situ* using a meter-band, a compass and an inclinometer. This study area was chosen because it was the location of a landslide experiments coordinated from the IGT group of the ETH Zurich within the TRAMM multidisciplinary project (www.cces.ethz.ch/projects/hazri/tramm).

Root distribution measurements

We characterized the root distribution considering root diameter classes and frequency. First we used 2 soil profiles at 1.5 and 2.5 m from the stem of an ash tree with a diameter of 31 cm in order to calibrate the model of Schwarz et al. [2010b] (pipe coefficient) and we calibrated the pipe coefficient considering the minimal Sum of Squared Errors (SSE). After the landslide experiment occurred the 18 March 2009 (Figure 5.7), we collected the distribution of root along the scarp and compared the results with the model. We mapped only live roots (following criteria reported in Schmidt et al. [2001]) of tree species. The length of the scarp was divided in sub-sectors of 1 m width and within each sub-sector the diameter of the roots was measured with a digital caliper. As data we obtained the number of roots of each root diameter class (1 mm classes) in each sub-sector. For semplicity the sub-sector are grouped in 4 bigger sector (see Figure 5.7).

Calibration of the root distribution function

The results of the root distribution mapped in the field for the calibration of the root distribution model (Figure 5.8) show that the number of fine roots decrease with increasing distance from the tree stem (52 roots of 1 mm diameter at 1.5 m distance from the tree stem versus the 30 roots at 2.5 m distance from the stem). Moreover, the data show that the maximal root diameter present in the profile is higher at 1.5 m than at 2.5 m with values of 9 and 6 mm, respectively. The decay exponent λ used in eq. 5.1 was set equal to -1 for the best fit of the data. Field observation on the root orientation with respect to the vertical plane of the soil profile show that most of the roots in the top layers of the soil were oriented parallel to the slope with high variable parallel orientations. The vertical distribution of roots in the soil profile confirmed the observation done from previous

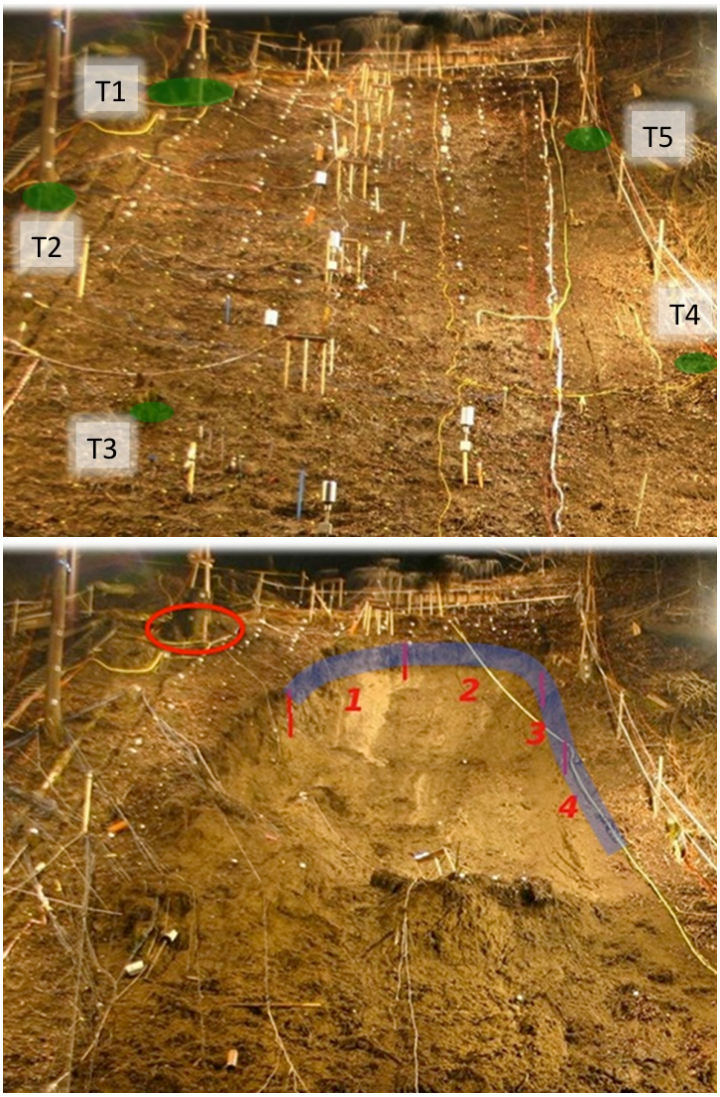

Figure 5.7: Plan view of the landslide experiment side in Rüdlingen before (a) and after the failure (b). The green points and labels T1-T5 in figure a indicate the position of some tree on the slope present also in figure 5.13. Red numbers in figure b indicate the sector of the scarp where roots were mapped.

studies that most part of the root biomass is confined in the first meter of soil depth and that decay exponentially with soil depth [Abe and Iwamoto, 1990; Abe and Ziemer, 1991; Abernethy and Rutherfurd, 2001; Schmidt et al., 2001; Schenk and Jackson, 2002; Bischetti et al., 2005; Laio et al., 2006; Docker and Hubble 2009].

In order to compare these results with other literature data [Schmid and Kazda, 2002; Bischetti et al., 2005] we calculated the cross sectional area, the correspondent root area ration (RAR = cross section area of roots / area of the mapped soil profile), and the biomass of the roots (considering a density of 0.6 g/cm^3 and a length-diameter relation as showed in Schwarz et al. [*in review*]). The resulting total cross section area at 1.5 m distance was 1317 mm^2 m^{-2} (that correspond to a RAR of 0.13%) , whereas at 2.5 m distance was 1004 mm^2 m^{-2} (that correspond to a RAR of 0.1%). The estimated biomass would correspond to 1209 and 693 g m^{-2}, respectively.

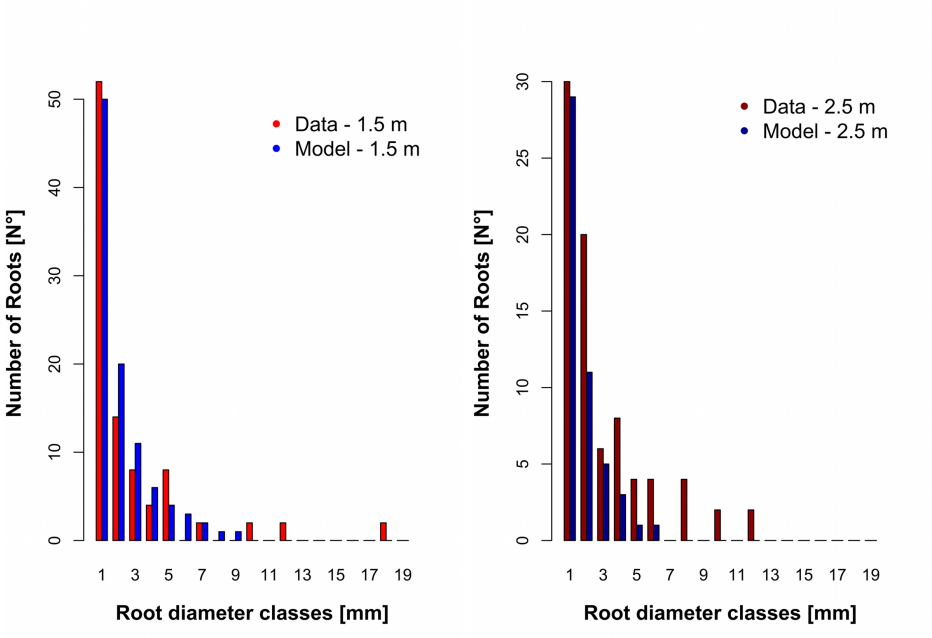

Figure 5.8: Calibrated root distribution function with the field data of two soil profiles at 1.5 and 2.5 m from the stem of a ash tree (*Fraxinus excelsior*).

Root distribution along the landslide scarp

In this section we present the comparison between the predicted value of root distribution and the data collected along the landslide scarp in the field area (Figure 5.9). Additionally to the root distribution, we characterized the mechanical behaviors of root reinforcement along the scarp and at stand scale.

The Landslide area was 8 m width and about 15 m long with a mean depth of 1.5 m (varying between 0.8 and 1.7 m). Most of the tree roots

Figure 5.9: Pictures of the landslide scarp. The big beech (*Fagus silvatica*) stump in the red circle can be used as reference and corresponds to the big tree in the top-left position of the plan view (Figure 5.13).

along the 24 m long mapped scarp were localized in the first 0.6 m of soil depth, whereas the root network of the grass plants was confined in the first 0.2 m of soil depth. In the following results we considered only the distribution of tree roots. In order to facilitate the presentation of the results we considered 4 central sectors of the scarp each one with a length of 5 m (Figure 5.10) and root diameter class up to 20 mm. The roots of 1-2 mm diameter (that corresponds to the diameter class of the fine roots) represented the 81 % of the total number of roots. In term of cross section area, fine roots represent the 23 % of the total roots cross section area. The most important diameter class as percent of cross section is the 2 mm class with a total of 2176 mm^2 on a total of 15242 mm^2, that corresponds to the 14% of the total root cross section area. The total RAR results to be 0.04 %.

The results of the predicted root distribution in each single sectors show that the model tend to overestimate the number of roots (Figure 5.10). Considering all the roots, the model has an average error of 18%, derived from high variable errors within each single sector (25 %, 5%, 58% and 7%, respectively). This variability leads to an error in the calculation of the maximal root reinforcement of about 28%; in particular we notice that 65% of this error is due to the overestimation of the number of roots with diameter less then 5 mm. The total root reinforcement at 50 mm displacement calculated using the measured root distribution was 83 kN, whereas using the modeled root distribution we obtain a value of 106 kN.

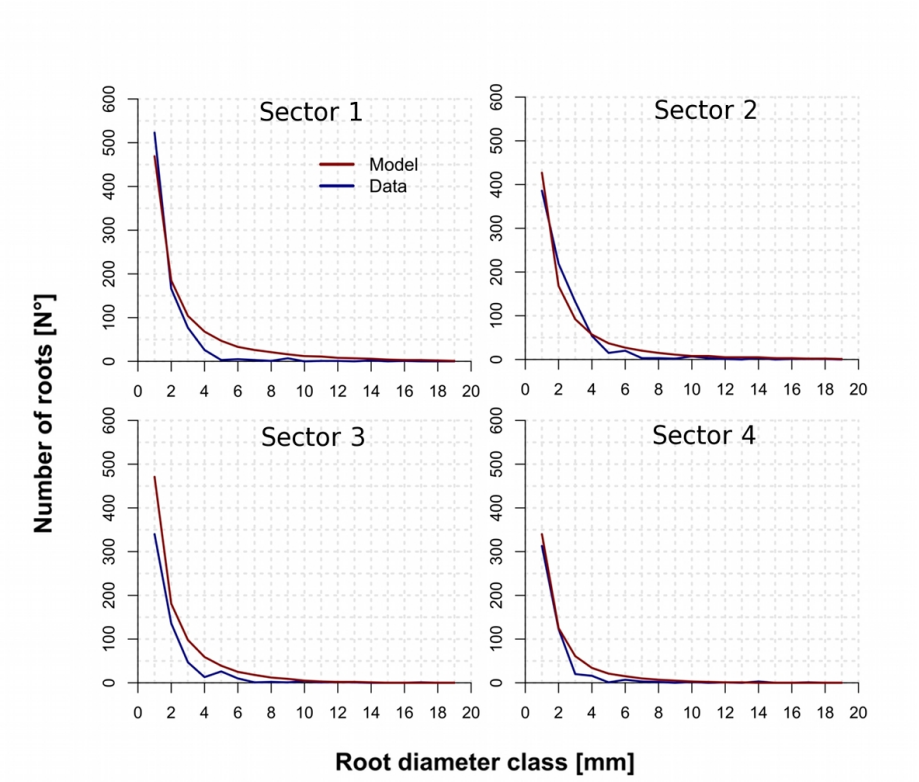

Figure 5.10: Measured and predicted distribution of roots of different diameter classes (x axis) in the 4 sectors of the landslide scarp.

Pullout measurements and calibration of the RBM for individual tree roots

We carried out a total of 27 root pullout tests for thread diameters up to 5.5 mm for Ash tree roots (*Fraxinus excelsior*). After the excavation of a soil profile at 1.5 and 2.5 m from the tree we chose living roots and we set up the pullout tests, as described in Schwarz et al. [*in press*]. The first 5-10 cm of the roots exiting the soil profile was debarked and a metal ring was attached to it using a commercial glue injected in a plastic tube that covered the root and the screw of the metal ring. After 1-2 hours, when the glue was solidified, we performed the manual pullout tests using a digital force gauge (IMADA, ZPS-DPU). In all cases the roots break; most of the times within the space between the glued metal ring and the soil profile surface, in only few cases the roots break within the soil matrix (few centimeters behind the

soil profile surface). All the root diameter with bark were measured before the tests. Regression curves of the thread strength versus root diameter data were subsequently used to extrapolate root tensile strength for roots >5.5 mm in diameter.

The fitting of the non linear regression was done using the nls package in R [Ihaka and Gentleman, 1996; see http://www.r-project.org/].

The data and the non linear fitting confirm the trend of the results reported in previous work in Europe [Bischetti et al., 2005] (Figure 5.11). However, it results that our measured maximal pullout forces are in general lower then the forces fitted with second-order polynomial regression by Schmidt et al. [2001] for the data of plant species in the Oregon Coast Range. The fitted curve obtained from the field pullout test was used to calibrate the RBM [Schwarz et al., 2010a].

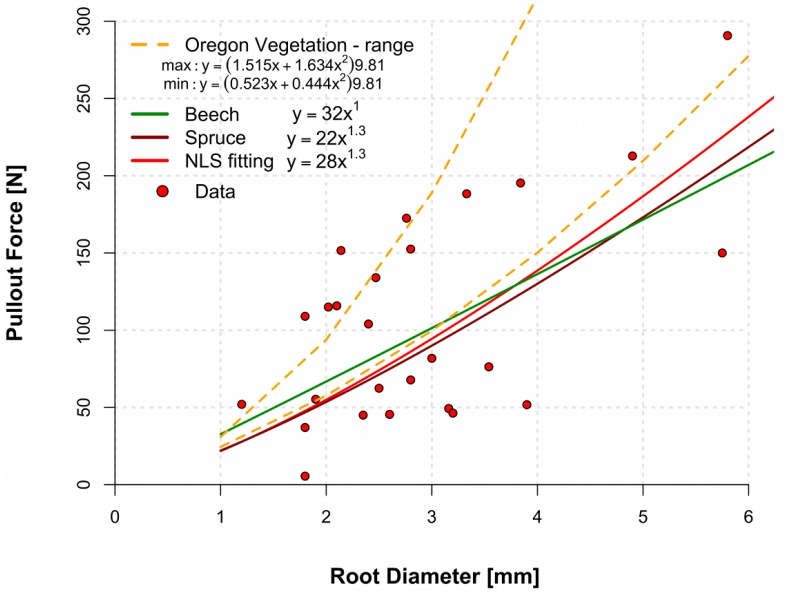

Figure 5.11: Measured maximal tensile force of roots with different diameter. The non linear fitting line (red) is compared to the fitting equations reported in Bischetti et al. [2005] for spruce (violet line) and beech (green line), and with range of value reported by Schmidt et al. [2001] for 12 plant species in Oregon (yellow dashed lines).

Estimating spatial lateral root reinforcement

The calculation of the maximal root reinforcement with the RBM along the scarp gives values that range between 2 and 14 kPa, with a mean value of 7 kPa. However, considering that this is overestimated, the real values should be about 25% lower. The comparison between the calculated root reinforcement and the distribution of roots along the scarp in Figure 5.12 shows that there is a good correspondence between the frequency distribution of roots and the variation of the maximal root reinforcement. Moreover, the peaks on root reinforcement corresponds quite well to the presence of maximal root diameter. For orientation we can observe that the first peak of reinforcement (at about 5 m distance along the scarp in sector 1) corresponds to the position near the big tree circled in Figure 5.9. The calculation of the root reinforcement using the Wu method [Wu et al., 1979] gives higher values than the simplified RBM (the root reinforcement would be 27.8 kPa

in sector 1, 22.2 kPa in sector 2, 17.4 kPa in sector 3 and 10.6 kPa in sector 4).

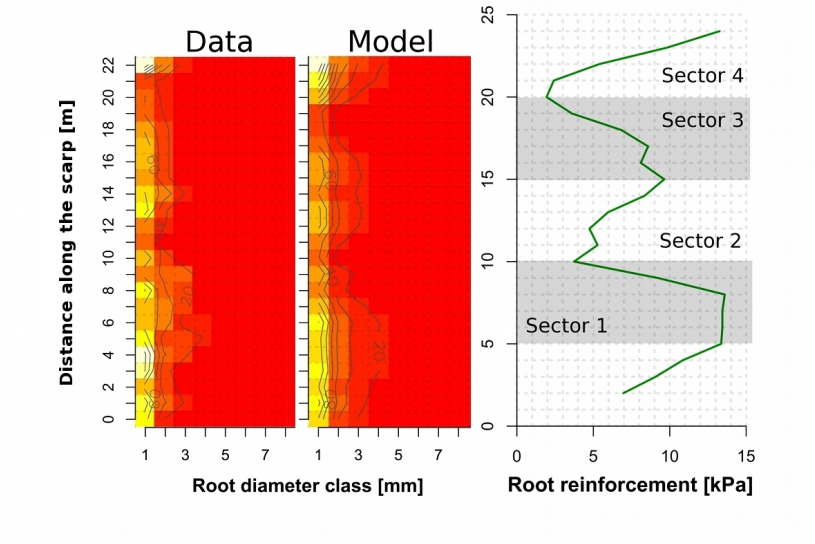

Figure 5.12: a) Measured and predicted distribution of roots of different diameter classes (x axis) along the landslide scarp (y axis). The isolines indicate the number of roots present in the soil profile per linear meter along the scarp (red indicates density of less than 40 roots/m, orange indicates root density between 40 and 80 roots/m, and yellow color indicates root density higher than 80 roots/m). b) Distribution of calculated maximal lateral root reinforcement along the scarp using the measured root distribution and the simplified version of the RBM.

We highlight the presence of few roots bigger then 20 mm diameter along the scarp. In total, we mapped 19 of these big roots with diameter between 20 and 45 mm, that are not predict by the model. However, root reinforcement calculations show that their mechanical contribution to the reinforcement represents less the 1.5 % of the total reinforcement (which correspond to 1200 kN along all the scarp at maximal reinforcement).

The maps in Figure 5.13 not only show the maximal root reinforcement (that corresponds to the maximal value of the force-displacement curve in Figure 5.2), but also the displacement needed to reach the maximal reinforcement. The quotient between this two values (maximal force and displacement) represents the secant Young's modulus, that can be use to characterize the distribution of stiffness due to the presence of roots. The three peaks of reinforcement shown in Figure 5.12 correspond in the map to the position of the three trees along the landslide scarp (blue line in

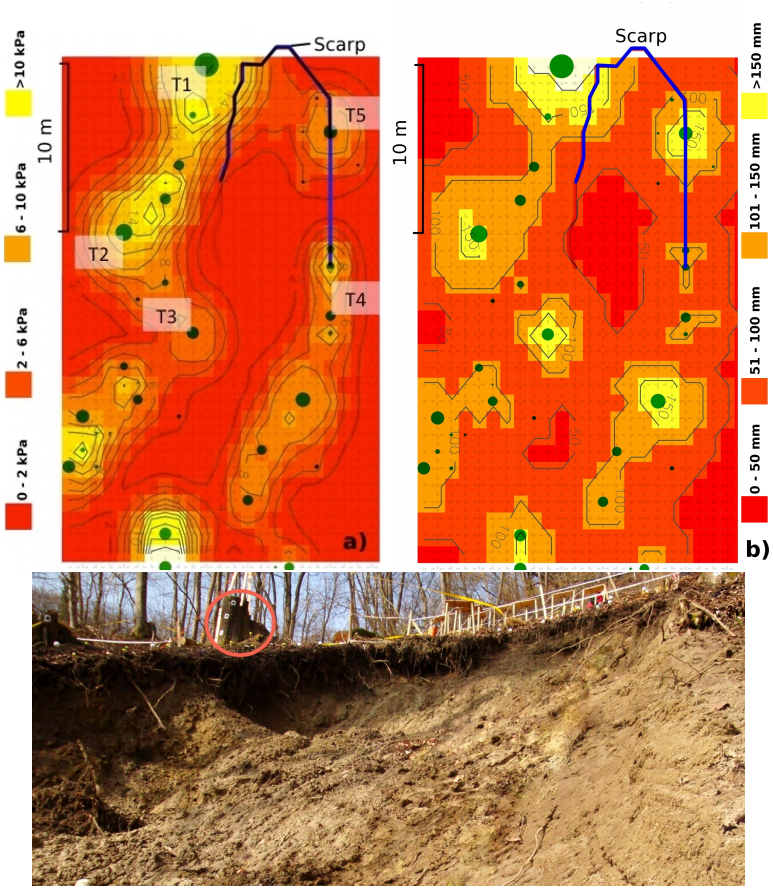

Figure 5.13: Map of maximal root reinforcement (a) and displacement at maximal root reinforcement (b) in the study area of Rüdlingen. Green points indicate tree positions and dimensions. See figure 5.7 for tree location on the slope.

the Figure 5.13). The map of displacement at maximal root reinforcement shows that the critical displacement on the slope correspond to the three characteristic distances shown in Figure 5.4 (that correspond to the values of 56 mm , 112 mm and 169 mm). In fact, we can interpret this map saying that rooted soil is more stiff near tree stems than areas with low root frequency. Moreover, we can say that the roots of 1 mm diameter dominated the mechanical behavior of root bundles in areas with displacement values lower than 56 mm, whereas areas with values between 56 and 112 mm are dominated by the 2 mm root diameter and so forth. The distribution of the secant Young's modulus has a distribution of values between 0 and 150 kPa.

5.6 Discussion

Modeling of lateral root distribution

The prediction of root distribution is an important element for the quantification and spatial characterization of root reinforcement. We highlight the importance to characterize the distribution of root distribution in term of frequency and dimension of roots, instead of more common quantities such as root biomass or cross section area. This type of data input are fundamental for the characterization of the dynamic behaviors of root reinforcement, which was never considered in previous landslide analysis.

Our approach for the quantification of root reinforcement is explicitly a compromise between the need of a complex set of equations and parameters to run a model and the use of easy to measure parameters measurable in the field or with remote sensing. However, one of the limitation of the present application is that only few data for the calibration and validation of the model exist. Nevertheless, we obtain an acceptable agreement between the modeled and measured distribution of roots along the landslide scarp. However, it is difficult to delineate a list of the main sources of errors, considering the controverse bibliography informations. For instance, Bolte et al. [2004] show that the relationship between DBH and coarse root biomass is not moderated by tree species (spruce or beech), and Puhe et al. [2003] suggested that root distribution is more influenced by stand location than species composition. However, some authors show that root systems of different species show different characteristic shapes [Polomski and Kuhn, 1998; Tatarinov et al., 2008] and plasticity [Schmid and Kazda, 2002]. In the particular case of alpine spruce stands, we consider that the aboveground competition for light represents the most important limiting factor for growth, whereas the underground competition for water and resources is less important. Similarly, the competition in our study area could be considered driven by light. Based on these consideration we deduce that for the modeling of root distribution of tree stand where water or underground resources are not the main factor of competition, a simple superposition approach for interacting root systems gives satisfactory results for slope stability calculations.

During the calibration of the root distribution function no roots bigger then 20 mm were found, whereas in the landslide scarp some sporadic roots reach dimension of 45 mm. The fact that the model did not predict the presence of few outstanding bigger roots is probably due to the condition that our model is based on concepts valid only for secondary lateral roots and for a monopodial root branching pattern. As shown in Schwarz et al.

[2010a], a good approximation of the maximal root diameter in a root bundle is important because it has a major influence on the root reinforcement calculation.

Literature values show that an empirical calibration of the equation used for the calculation of the maximal lateral root extend is difficult due to the high variability of data. However, Schwarz et al. [2010b] show that a simple linear regression (such as the one used in this study) could reasonably fit a wide range of reviewed datasets. We consider this aspect an important field of research that need more future studies.

The overestimation of predicted root distribution may arise for different reasons: a) more trees are needed for the calibration of the model. b) Root frequency distribution are not the only data-set calibration needed, and other parameters should be implemented in the model. c) Fine roots have a strong seasonality, hence there are less fine roots in winter (when the landslide occurred) than in summer (when the calibration was done). To answer to this questions more work is needed in future validation research. Moreover, other aspects such as the seasonal decay of fine roots in tree species should be considered. We consider also that roots of grass plants shouldn't be taken into account at the scale of hillslope, because these roots are present only for limited periods of the year and are not homogeneously distributed.

Characterization of lateral root reinforcement

The characterization of the type of failure of a root bundle is important for the understanding of the triggering mechanisms of shallow landslides. For instance, abrupt failure of the bundle in a tension crack would lead to a rapid redistribution of forces in the surrounding crack zones with a dynamic that is driven by the stiffness of the root reinforcement (in stiff zones the forces will be redistributed more widely, whereas in less stiff zones forces are redistributed locally), similar to a domino effect. In the case of root bundles that fail more progressively, the combination of the local residual root reinforcement and the stiffness of the reinforced soil assure a more homogeneous distribution of destabilization forces, and thus increase the stability of a slope.

In the case of ideally homogeneous forest stands such as shown in Figure 5.6, the small variation in minimal lateral root reinforcement between the two different geometrical assets could be interpreted by the fact that at a certain distance from trees (tails of the curves in Figure 5.4a) the variation of root reinforcement is small for a big interval of distances (within 2 m there is a variation of 3 kPa of reinforcement). Thus, the differences are

remarkable only for high tree density, where the distances between stems are lower than 2 or 3 m. In this case, both the increased reinforcement and stiffness assure the stability of large steep areas.

Along the scarp in the study area, the use of the simplified RBM predicts a total reinforcement of 106 kN using the modeled root distribution, or 83 kN using the measured root distribution. In comparison, the approach of Wu et al. [1979] leads to values of 470 kN in the case of the modeled root distribution and of 251 kN for the case of measured root distribution. The overestimation of 23 kN using the RBM is due to the overestimation of root frequency, especially in the diameter classes of 1, 2 and 3 mm. Moreover, it must be considered that generally the use of the RBM leads to a underestimation of the pullout force of a bundle (between 10 and 20 %) [Schwarz et al., *in review*]. Thus, It seems that these two types of errors tends to compensate each other. However, This range of errors are less important if compared with the 100% error obtained using the Wu approach [Wu et al., 1979] .

Distribution of dynamic root reinforcement under heterogeneous vegetation cover

We show that the presence of roots strongly change the local stiffness of the soil, thus under the same stress condition the slope responds locally in different ways either to lateral shearing, compression or tension.

Like in other scarps of shallow landslides, also in this case we observed that the line of the scarp, and thus the tension crack, goes through areas of high values of root reinforcement nearby the lower side of tree stems. From the visual analysis of the failure, we conclude that the instability of the slope is triggered in the central-upper part of the landslide, where the root reinforcement is low and the stiffness of the rooted soil is low too. Then, due to the compressive pressure (which is much higher then the tensile stress) the crack develop following the path where the balance between compression and tension/shearing forces allow the triggering or not of the neighbor areas, hence ideally where stiffness and reinforcement are lower (see Figure 5.14). In this case of study the location of the weak zone that triggered the failure was strongly influenced by the high heterogeneity of the bedrock surface and by the artificial rainfall distribution; hence, it is difficult to clearly quantify the role of the spatial distribution of roots on the development of the tension crack. Future work will focus on this aspect and clarify the role of hydrogeology too. The analysis of the crack propagation in this case of study leads to other interesting questions related

to the mechanisms of root reinforcement. For instance, it is assumed that the reinforcement of the same bundle of roots pulled out from the upper part of the crack or from the bottom part of the crack behave in the same way. However, we believe that this is not true and that roots pulled out from a stable soil mass show higher tensile forces than roots pulled out from a sliding mass of soil (in which the pore ratio change during the displacements and consequently also the root-soil frictional behaviors). Hence, we believe that soil in the downslope side of a stem is less reinforced by roots than the upslope side, and that these differences could be the reason why usually tension crack develop preferably nearby the downslope side of the trees present on a slope. Further ongoing research is also focusing on this aspect.

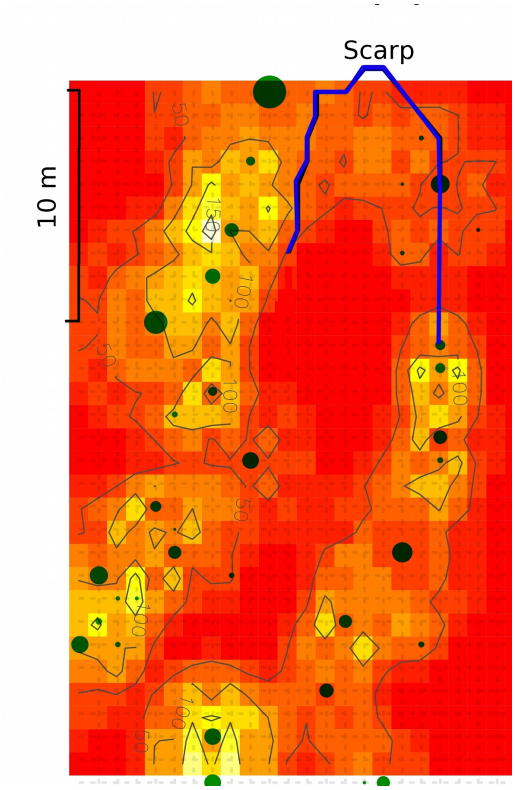

Figure 5.14: Map of the apparent secant elastic modulus in the study area of Rüdlingen. Isolines in MPa. The yellow areas indicate values bigger than 150 MPa, orange areas indicate values between 100 and 150 MPa, and red areas indicate values lower than 100 MPa.

5.7 Conclusions

We presented the theoretical and practical application of a modeling framework for the spatial characterization of root reinforcement at stand scale. With relative few inputs (position and dimensions of trees) we showed that it is possible to realistically estimate the variability of the reinforcing effect of roots within a forest stand. The possibility to quantify the dynamics of root reinforcement represent a big improvement for the implementation of root reinforcement in slope stability models. Moreover, it gives the possibility to better understand the mechanisms of shallow landslide triggering in vegetated hillslope using advanced models such as finite element method (FEM) [Merodo et al., 2004], discrete element methods (DEM) [van Asch et al., 2007] or cell automata techniques [Segre and Deangeli, 1995]. This

framework can also be extended in the future for the characterization of the temporal variability of root reinforcement in function of different forest managements in space and time. Moreover, new studies are needed to understand the dynamic of shallow landslides failures and to quantify the real contribution of roots to the force redistribution during the propagation of a tension crack in a vegetated slope. Such kind of models are strongly needed for a more realistic prediction of landslides and sediment mobilization at catchment scale, but also for the planning in protection forests management and bioengineering.

5.8 Aknowledgement

This work was supported by the CCES platform (Competence Center for Environmental Sustainability) of the ETH domain and is part of the TRAMM project (Triggering of Rapid Mass Movement). We thank Francesca Gambazzi, Christian Rickli and Gernot Michlmayer for the field assistance and the IGT group of Prof. Sarah Springmann at the ETH-Zurich for the set up of the Rüdlingen field experiment.

5.9 References

Abe, K., and M. Iwamoto (1990), Simulation model for the distribution of tree roots application to a slope stability model, *Japanese Forestry Society*, *72*, 375 - 387.

Abe, K., and R. R. Ziemer (1991), Effects of tree roots on a shear zone: modelling reinforced shear stress, *Canadian Journal of Forest Research*, *21*, 1012 - 1019.

Abernethy, B., and A. I. Rutherfurd (2001), The distribution and strength of riparian tree roots in relation to riverbank reinforcement, *Hydrological Processes*, *15*, 63 - 79.

Ammer, C., and S. Wagner (2005), An approach for modelling the mean fine-root biomass of Norway spruce stands, *Trees*, *19*, 145 - 153.

Bathurst, J. C., G. Moretti, A. El-Hames, S. Begueria, and J. M. Garcia-Ruiz (2007), Modelling the impact of forest loss on shallow landslide sediment yield, Ijuez river catchment, Spanish Pyrenees, *Hydrology and Earth*

System Science, *11(1)*, 569 - 583.

Bischetti, G. B., E. A. Chiaradia, T. Limonato, B. Speziali, B. Vitali, P. Vullo, and A. Zocco (2005), Root strength and root area ratio of forest species in Lombardy (Northern Italy), *Plant and Soil*, *278*, 11 - 22.

Bolander, J. E., S. Choi, and S. R. Duddukuri (2008), Fracture of fiber-reinforced cement composites: effects of fiber dispersion, *Int. J. Fract.*, *154*, 73 - 86. doi: 10.1007/s10704-008-9269-4

Bolte, A., T. Rahmann, M. Kuhr, P. Pogoda, D. Murach, and K. GAdow (2004), Relationships between tree dimension and coarse root biomass in mixed stands of European beech (*Fagus sylvatica* L.) and Norway spruce (*Picea abies* [L.] Karst.), *Plant and Soil*, *264*, 1 - 11.

Brang, P., W. Schnenberger, M. Frehner, R. Schwitter, J. J. Thormann and B. Wasser, 2006, Management of protection forests in the European Alps: an overview, *For. Snow Landsc. Res.*, *80 (1)*, 23 - 44.

Brisson, J., and Reynolds J. F. (1994). The effect of neighbors on root distribution in a creosotebush (*Larrea tridentata*) population, *Ecology*, *75(6)*, 1693 - 1702.

Cohen, D., P. Lehmann, and D. Or (2009), Fiber bundle model for multiscale modeling of hydromechanical triggering of shallow landslides, *Water Resources Research*, *45*, W10436. doi:10.1029/2009WR007889.

Cohen, D., M. Schwarz, and D. Or (*in review*), An analytical fiber bundle model for pullout mechanics of root bundles, *J. Geophys. Res.*, *in review.*

Cruickshank, M. G., D.J. Morrison, and A. Lalumiére (2009), The interaction between competition in interior Douglas-fir plantations and disease caused by *Armillaria ostoyae* in British Columbia, *Forest Ecology and Management*, *257*, 443 - 452. doi:10.1016/j.foreco.2008.09.013

Danjon, F., D. H. Barker, M. Drexhage, and A. Stokes (2007), Using three- dimensional plant root architecture in models of shallow-slope stability, *Annals of Botany*, *101*, 1281 - 1293.

Dhakal, A. S., and R.C. Sidle (2003), Long term modeling of land-

slides for different forest management practices, *Earth Surface Processes and Landforms*, *28*, 853 - 868.

Docker, B. B., and T. C. T. Hubble (2009), Modelling the distribution of enhanced soil shear strength beneath riparian trees of south-eastern Australia, *Ecological Engineering*, *35*, 921 - 934.

Dupuy, L., P. J. Gregory, and A. G. Bengough (2010), Root growth models: towards a new generation of continuous approaches, *J. Exp. Bot.*, *61(8)*, 2131 - 2143. doi: 10.1093/jxb/erp389

Fraser, E. C., V. J. Lieffers, and S. M. Landhäusser (2005), Age, stand density, and tree size as factors in root and basal grafting of lodgepole pine, *Can. J. Bot.*, *83*, 983 - 988. doi: 10.1139/B05-048

Fleischer, F., S. Eckel, I. Schmid, V. Schmidt, and M. Kazda (2006), Point process modelling of root distribution in pure stands of *Fagus sylvatica* and *Picea abies*, *Can. J. For. Res.*, *36*, 227 - 237. doi:10.1139/X05-232

Genet, M., N. Kokutse, A. Stokes, T. Fourcaud, X. Cai, J. Ji, and S. B. Mickovski (2008), Root reinforcement in plantation of Cryptomeria japonica D. Don: effect of tree age and stand structure on slope stability, *Forest Ecology and Management*, *256*, 1517 - 1526.

Ihaka, R., and R. Gentleman (1996), R: a language for data analysis and graphics, *Journal of Computational and Graphical Statistics*, *5*, 299 - 314.

Kokutse, N., T. Fourcaud, K. Kokou, K. Neglo, and P. Lac (2006), 3D Numerical modelling and analysis of the influence of forest structure on hill slopes stability. In: Marui, H., Marutani, T., Watanabe, N., Kawabe, H., Gonda, Y., Kimura, M., Ochiai, H., Ogawa, K., Fiebiger, G., Heumader, J., Rudolf-Miklau, F., Kienholz, H., Mikos, M., (Eds), Interpraevent 2006, *Disaster Mitigation of Debris Flows, Slope Failures and Landslides*, 2527 September, 2006, Niigata, Japan. Universal Academy Press, Inc., Tokyo, Japan, ISBN 4-946443-98-3, pp. 561 - 567.

Kun, F., F. Raischel, R. C. Hidalgo, and H. J. Herrmann (2007), Extensions of Fibre Bundle Models, *Lect. Notes Phys.*, *705*, 57 - 92. doi: 10.1007/3-540-35375-5 3

Laio, F., P. DOdorico, and L. Ridolfi (2006), An analytical model to relate the vertical root distribution to climate and soil properties, *Geophysical Research Letters*, *33*, L18401.

Meinen, C., C. Leuschner, N. T. Ryan, and D. Hertel (2009), No evidence of spatial root system segregation and elevated fine root biomass in multi-species temperate broad-leaved forests, *Trees*, *23*, 941 - 950. doi: 10.1007/s00468-009-0336-x

Merodo, J. A. M., M. Pastor, P. Mira, L. Tonni, M.I. Herreros, E. Gonzalez, and R. Tamagnini, (2004), Modelling of diffuse failure mechanisms of catastrophic landslides, *Comput. Methods Appl. Mech. Engrg.*, *193*, 2911 - 2939.

Messier, C., L. Coll, A. Poitras-Lariviere, N. Belanger and J. Brisson (2009), Resource and non-resource root competition effects of grasses on early- versus late-successional trees, *Journal of Ecology*, *97*, 548 - 554.

Montgomery, D. R, and W. E. Dietrich (1994), A physical based model for the topographic control on shallow landsliding, *Water Resources Research*, *30*, 1153 - 1171.

Ozier-Lafontaine, H., F. Lecompte, and J. F. Sillon (1999), Fractal analysis of the root architecture of *Gliricidia sepium* for the spatial prediction of root branching, size and mass: model development and evaluation in agroforestry, *Plant and Soil*, *209*, 167 - 180.

Pollen, N., and A. Simon (2005), Estimating the mechanical effects of riparian vegetation on stream bank stability using a fiber bundle model, *Water Resources Research*, *41*, W07025. doi: 10.1029/2004WR003801

Polomski, J., and N. Kuhn (1998), Wurzelsysteme. WSL, Birmensdorf, 290 pp.

Puhe, J. (2003), Growth and development of the root system of Norway spruce (*Picea abies*) in forest stands: a review, *Forest Ecology and Management*, *175*, 253 - 273.

Reneau, S. L., and W. E. Dietrich (1987), Size and location of colluvial landslides in a steep forested landscape, *In Erosion and sedimentation in the Pacific Rim, proceedings of the Corvallis Symposium, August 1987,*

IAHS Publ., *165*, 39 - 48.

Rewald, B., and C. Leuschner (2009), Belowground competition in a broad-leaved temperate mixed forest: pattern analysis and experiments in a four-species stand, *Eur. J. Forest. Res.*, *128*, 387 - 398. doi: 10.1007/s10342-009-0276-4

Rodriguez, R., M. Espinosab, G. Hofmannc, and M. Marchantd (2003), Needle mass, fine root and stem wood production in response to silvicultural treatment, tree size and competitive status in radiata pine stands, *Forest Ecology and Management*, *186*, 287 - 296. doi:10.1016/S0378-1127(03)00300-1

Roering, J. J., K. M. Schmidt, J. D. Stock, W. E. Dietrich, and D. R. Montgomery (2003), Shallow landsliding, root reinforcement, and the spatial distribution of trees in the Oregon Coast Range, *Can. Geotech. J.*, *40*, 237 - 253.

Sakals, M. E., and R. C. Sidle (2004), A spatial and temporal model of root cohesion in forest soils, *Can. J. For. Res.*, *34*, 950 - 958.

Santantonio, D. (1990), Modeling growth and production of tree roots, *Process Modeling of Forest Growth responce to Enviromental stress*, 124 - 135.

Schenk, H. J., and R. B. Jackson (2002), The global biogeography of roots, *Ecological Monographs*, *72*, 311 - 328.

Schmid, I., and M. Kazda (2002), Root distribution of Norway spruce in monospecific and mixed stands on different soils, *Forest Ecology and Management*, *159*, 37 - 47.

Schmidt, K. M., J. J. Roering, J. D. Stock, W. E. Dietrich, D. R. Montgomery, and T. Schaub (2001), The variability of root cohesion as an influence on shallow landslide susceptibility in the Oregon Coast Range, *Can. Geotech. J.*, *38*, 995 - 1024.

Schwarz, M., D. Cohen, and D. Or (*in press*), Pullout tests of root analogs and natural root bundles in soil - experiments and modeling, *J. Geophys. Res.*, *in press.*

Schwarz, M., D. Cohen, and D. Or (2010a), Soil-root mechanical interactions during pullout and failure of root bundles, *J. Geophys. Res.*, *115*, F04035. doi:10.1029/2009JF001603.

Schwarz, M., P. Lehmann, and D. Or (2010b), Quantifying lateral root reinforcement in steep slopes - from a bundle of roots to tree stands, *Earth Surface Processes and Landform*, *in press*, doi: 10.1002/esp.1927.

Schwarz, M., F. Preti, F. Giadrossich, P. Lehmann, and D. Or (2010c), Quantifying the role of vegetation in slope stability: A case study in Tuscany (Italy), *Ecological Engineering*, *36*, 285 - 291.

Segre, E., and C. Deangeli (1995), Cellular automaton for realistic modelling of landslides, *Nonlinear Processes in Geophysics*, *2*, 1 - 15.

Shewbridge, S. E., and N. Sitar (1989), Deformation characteristics of reinforced sand in direct shear, *Journal of Geotechnical Engineering*, *115 (8)*, 1134 - 1147.

Sidle, R. C., and H. Ochiai (2006), Landslides: Processes, Prediction, and Land Use,, Water *Resources Monograph*, *18*, 312 pp.

Sidle, R. C., and W. Wu (2001), Evaluation of the temporal and spatial impacts of timber harvesting on landslide occurrence, *Water Science and Application*, *2*, 179 - 193.

Simoni, S., F. Zanotti, G. Bertoldi, and R. Rigon (2007), Modelling the probability of occurrence of shallow landslides and channelized debris flows using GEOtop-FS, *Hydrological Processes*, *22*, 532 - 545.

Sornette, D. (1989), Elasticity and failure of a set of elements loaded in parallel, *Journal of Physics A: Mathematics and General*, *22*, L243 - L250.

van Asch, T. W. J., J. Malet, L. P. H. van Beek, and D. Amitrano (2007), Techniques, issues and advances in numerical modelling of landslide hazard, *Bull. Soc. géol. Fr.*, *178 (2)*, 65 - 88.

Van Noordwijk, S. L. Y, and P. de Willigen (1994), Proximal root diameter as predictor of total root size for fractal branching models, *Plant and Soil*, *164*, 107 - 117.

Wehrli, A., P. Brang, B. Maier, P. Duc, F. Binder, E. Lingua, K. Ziegner, K. Kleemayr, and L. Dorren, (2007), Schutzwaldmanagement in den Alpen eine bersicht. *Schweiz Z. Forstwes.*, *158(6)*, 142 - 156.

Wu, T. H., W. P. McKinnell, and D. N. Swanston (1979), Strength of tree roots and landslides on Price of Wales Island, *Alaska Canadian Geotechnology Journal*, *16*, 19 - 33.

Wu, W., and R. C. Sidle (1995), A distributed slope stability model for steep forested basins, *Water Resour. Res.*, *31*, 2097 - 2110.

Chapter 6

Quantifying the role of vegetation in slope stability

Autohrs: Schwarz M. [1,2], Preti F. [3], Giadrossich F. [3], Lehmann P. [2] and Or D.[2]

[1] Swiss Federal Institute for Forest, Snow and Landscape Research, 8903 Birmensdorf, Switzerland

[2] Soil and Terrestrial Environmental Physics, Institute of Terrestrial Ecosystems, ETH Zurich, 8092 Zurich, Switzerland

[3] Dipartimento di Ingegneria Agraria e Forestale, Universitá di Firenze, Via S. Bonaventura 13, 50145 Firenze, Italy

Published in: *Ecological Engineering*, (2010), *36*, 285 - 291. doi: :10.1016/j.ecoleng.2009.0

6.1 Abstract

Vegetation significantly affects hillslope hydrological and mechanical properties related to shallow landslide triggering. In view of the complexity of soil plant hydrological interactions, the quantification of root mechanical reinforcement remains a challenge. Herein we present a back analysis of mechanical stability criteria related to a well-characterized vegetated shallow landslide in Italy, focusing on the quantification of lateral and basal root reinforcement. Lateral root reinforcement is included in slope stability estimates by adding a stabilizing force proportional to the scarp surface and root distribution. This stabilizing force is added to the force balance equation for the infinite slope model for different landslide shapes and dimensions. To quantify root reinforcement, we use the Wu model and the fiber bundle model (WM and FBM, respectively). Implementation of the latter model allows the quantification of the stressstrain behaviour of a bundle of roots for different root distributions and mechanical properties. Results of these models are compared highlighting key differences between the two approaches. Calculations using the FBM can explain the overestimation of lateral root reinforcement using WM and the commonly observed overestimation in the factor of safety. The model also quantifies the displacement-dependent behaviour of root reinforcement on vegetated slopes. Lateral root reinforcement can strongly influence the stability of slopes up to a certain area (1000 - 2000 m^2). The magnitude of this stabilizing effect depends on parameters such as inclination, soil mechanical properties, and root distribution.

6.2 Introduction

Understanding and quantifying the mechanical effects of vegetation on steep slopes remains an unresolved problem. Modelling approaches span a wide range of spatial scales, from modelling of a single root to modelling the stability of an entire vegetated slope. The combination of different spatial and temporal scales and the various processes and elements present in a vegetated system make quantitative description complex and sometimes contradictory. A growing number of models are employed for quantifying root reinforcement; however, direct comparisons between model predictions and data remain sketchy. Recently, the application of the fiber bundle model (FBM) for the estimation of root reinforcement proposed by Pollen and Simon [2005] has emerged as a useful representation of mechanical and geometrical characteristics of plant root systems. The model has previ-

ously been used extensively in engineering and material sciences to study the breakdown of complex heterogeneous materials [Peires, 1926; Kun et al., 2007]. In addition to other well-known methods and techniques used to study root reinforcement, like shear, pullout, or centrifuge tests [Anderson et al., 1989; Zhou et al., 1998; Fan and Su, 2008], back analysis offers a useful approach to understand the potential contribution of root reinforcement to mechanical stability of a natural slope. Usually, the effects of roots on slope stability at the slope or catchment scale are implemented in two-dimensional models where lateral effects are neglected and reinforcement is considered only if roots cross a slip surface (Sidle and Wu, 2001; Bathurst et al., 2007). In many instances, the root reinforcement effect is homogenized and added as a uniform cohesion term at the stand scale, neglecting inherent geometrical distribution and local variability. Only a few examples treat lateral effects of roots in three-dimensional models [e.g., Schmidt et al., 2001; Kokutse et al., 2006]. Casadei et al. [2003], Casadei and Dietrich [2003] and Dietrich et al. [2008] were the first to introduce the aspect of lateral root reinforcement in slope stability calculation and to discuss the influence of this parameter on the dimension of landslides. In this work we apply a similar concept for a specific case study. The effect of mechanical reinforcement by roots under a forest canopy is often limited to surface soil layers (90% of the roots in the first 50 cm of soil depth) [Schmidt et al., 2001; Roering et al., 2003; Bischetti et al., 2005]. Consequently, only lateral roots are considered to contribute to slope stabilization. In this work we report data collected to characterize the triggering mechanisms of a shallow landslide that occurred in Tuscany (Italy) during a rainfall event in November 2000. Motivated by a back analysis of this event, we discuss more general issues related to slope stability analysis of vegetated hillslopes, particularly the application of two different root reinforcement models and the use of slope stability calculations which take into account the role of lateral root reinforcement [Reneau and Dietrich, 1987; Schwarz and Preti, 2007]. In addition, we consider the role of soil moisture on slope stability calculation, either as suction or pore-water pressure at limit equilibrium conditions. We begin by illustrating the primary conceptual differences between the classical model of Wu et al. [1979] for quantifying root reinforcement and the fiber bundle model (FBM) of Kun et al. [2007]. The model introduced by Wu et al. [1979], in the following text denoted as Wu model (WM), provided a pioneering contribution to the quantitative consideration of the mechanical role of vegetation in slope stability. The model considers the dependency of maximal tensile strength on root diameter [Wu et al., 1979].

$$c_{veg.} = \alpha \frac{\sum_{i=1}^{n} T_i n_i a_i}{A} \tag{6.1}$$

where T_i is the maximal root tensile strength (MPa) of the diameter class i, n_i is the number of roots in the diameter class, a_i is the cross-section area of the root diameter class (m^2), α is a correction factor which takes in account the inclination of the roots crossing the shear plane or the tension crack (the value varies between 1 and 1.2), and A is the area of soil occupied by the roots (m^2). Additional studies by Waldron and Dakessian [1981] and others advanced the understanding of the mechanisms for root reinforcement in soils. Incorporating these concepts into simple factor of safety calculations reveal consistent overestimation of the role of root reinforcement of soils based on Wus model [e.g., Pollen and Simon, 2005; De Baets et al., 2008; Docker and Hubble, 2008; Fan and Su, 2008; Mickowski et al., 2007]. A summary of various experimental studies is presented in Table 6.1 showing the magnitude of the overestimation. A "correction factor" (frequently denoted as k") emerged from comparison of experimental data with model predictions and the average value of this factor is about 0.4 [Preti, 2006; Preti and Schwarz, 2006]. The "correction factor" is calculated as the quotient between the measured data value and value estimated with the model of Wu. This overestimation is attributed primarily to Wus assumption that all roots break at the same time regardless of their diameters. The introduction of the FBM to quantify root reinforcement [Pollen and Simon, 2005] allows incorporating mechanical contributions as a function of root diameters and improves understanding of how a bundle of roots with varying mechanical properties breaks. The general formulation of the FBM assumes that at a certain strain (ε) fibers of class j with strength threshold $\sigma_{max_j} < E_j \varepsilon$ are broken (or have a plastic residual strength), while remaining fibers carry a load equal to $E_j \varepsilon$, where E_j is the youngs modulus of the fiber class j. The global behaviour of the bundle is calculated as

$$\sigma(\varepsilon) = \sum_{j=1}^{n} E_j \varepsilon \tag{6.2}$$

In this study we will also summarize the technique used to consider root reinforcement at the slope scale. With reference to a case study, we introduce a potential approach for vegetated slope stability estimation, considering lateral root reinforcement and balancing the burden of detailed and spatially resolved calculations and the relatively large (and practical) scale of the required information.

Table 6.1: Comparison of computed values of correction factor k?? for different studies, where cv is the apparent root cohesion estimated with the Wu model (Wu et al., 1979).

Case Study	**Author**	$\mathbf{c'_{veg.}}$ [**kPa**]	**Method**	**Verified** $\mathbf{c'_{veg.}}$ [**kPa**]	$\mathbf{k'}$
Salix esigua	Pollen [2007]	3	Cumulative displacement - stress curve	1.5	0.5
Grass roots	Pollen et al. [2004]	17.5	Direct shear-box tests	6	0.34
Platanus occidentalis	Pollen et al. [2004]	5.6	Cumulative displacement - stress curve	2.31	0.41
Platanus occidentalis	Pollen et al. [2004]	5.6	Rip Root model	2.48	0.44
Wood Rods	Shewbridge and Sitar [1989]	3.7	Shear tests	1.8	0.49
Reed fibers	Gray and Ohashi [1983]	1.5 [kN]	Laboratory-shear tests	0.6 [kN]	0.4
Copper wires	Gray and Ohashi [1983]	0.72 [kN]	Laboratory-shear tests	0.3 [kN]	0.42

6.3 Materials and Methods

Study area and data collection

The study area (Figure 6.1) is located in a catchment near the village of Vinchiana in the province of Lucca (Tuscany, Italy), where a number of shallow landslides have occurred. One of them resulting in human casualties during a mild rainfall event on 19 - 20 November 2000 after very prolonged rainfall (three weeks duration with a cumulative rainfall of 360 mm of return time period of more than 100 years). The back analysis carried out in this study focuses on a particular landslide that affected a small portion of the slope (area 600 m^2) between the altitudes of 260 and 175 m.a.s.l.. The

mean soil thickness was about 1 m and slope inclination was about 35 ^{o} . The mobilized sediments reached the main stream as a debris flow. Similar scenarios were observed for other shallow landslides in this area.

Figure 6.1: Localization of the Vinchiana (Tuscany, Italy) case study and landslides map: black-lines landslide contours and in dark colour areas with SF 1 estimated by the infinite slope model during the November 2000 event and in (Solco dellAngelo and Piantone basin).

The site has a dominant vegetation cover composed of chestnut trees (*Castanea sativa* Mill.), managed as coppice wood, with the presence of black locust trees (*Robinia pseudoacacia* L.) and clusterpines (*Pinus pinaster* A.). Tree species composition is dominated by chestnut trees (70%). In this region, the fruit chestnut crop lies on terraced slopes while the coppice wood generally lies on steeper slopes (like in our study area). Since the abandonment of land at the end of the 20th century, both types of

tree covers are now present in forms going towards mixed and broad leaves woodland. Today, the fruit chestnut crop is characterized by a stem density of 120 - 150 plants per hectare. The mass of the vegetation on the landslide area was estimated with standard dendrometrical methods considering the neighbour forest stand as reference. The climate is Mediterranean (Köppen classification). Geologically, the study area is a flysch formation (Macigno) composed of quartz and feldspar sandstone alternated with layers of siltstone. Such geologic formations create acid soils which differ as a function of slope angle: soils under fruit chestnut crop are classified according to Soil Survey Staff [U.S.D.A., 1998] as a sandy-clay-loam to a loamy-sand, subgroups *Dystric Eutrochrepts* on weak slope, and *Lithic Eutrochrepts* and *Lithic Udorthents* on steeper slopes. Measured pH values ranged between 4.4 and 4.7 in the A horizon and between 5.6 and 6 in the B horizon. Soil thickness varies between 35 and 110 cm; A horizon thickness varies between 5 and 35 cm. The dry and saturated soil bulk density was measured from undisturbed soil samples. Shear tests in laboratory under saturated-drained conditions for three different confining pressures (50, 100, and 150 kPa) were carried out on rooted samples (root diameter 1 mm) to characterize the mechanical properties of the soil slip surface with and without roots. The friction angle was 33.4^o with no cohesion (Table 6.2). Single root specimens were sampled and tested for tensile strength [Preti and Giadrossich, 2009] for the calibration of the root maximal tensile strength of different root diameter classes. Five infiltration tests with a double ring setup were carried out to characterize the infiltration behaviour of the study area [Hillel, 2004]. Values of saturated hydraulic conductivity range from 10^{-4} to 10^{-5} m/s, typical or sandy soils. Since the soil is well structured, we considered the upper layer of the slope to be well drained. Bulk density of soil is determined on core samples which are taken by driving a metal corer into the soil at the desired depth and horizon. The samples (the volume of which is known) are then oven dried and weighed. In addition to geotechnical data collection, root distributions were mapped for three chestnut trees and the data were used to calibrate the root distribution model. Table 6.2 shows the measured or assessed values.

Table 6.2: Values of the parameters used for the inverse analysis considering three different conditions: saturated profile with basal root reinforcement only, saturated profile with lateral root reinforcement only, and unsaturated condition with lateral root reinforcement only.

Parameters		**Measured values**	**Saturated conditions**		**Unsaturated conditions**
			Calculated basal reinf.	Calculated lateral reinf.	Lateral reinf.
Vegetation overload	$m_{veg.}$ $[t/m^2]$	0.071	0.071	0.071	0.071
Soil bulk density	γ $[t/m^3]$	1.4/2.1	2.1	2.1	1.5
Pore-water pressure	u $[kPa]$	(?)	**10**	**10**	1
Saturation	%	(?)	**100**	**100**	10
Soil cohesion	c $[kPa]$	0	0	0	0
Friction angle	θ $[^o]$	33.4	33.4	33.4	33.4
Slope angle	β $[^o]$	35	35	35	35
Lat. root reinf.	$c_{lat.veg.}$ $[kPa]$	(?)	0	90	14
Bas. root reinf.	$c_{bas.veg.}$ $[kPa]$	(?)	7.4	0	0
Basal area	A $[m^2]$	600	600	600	600
Soil Depth	h $[m]$	1	1	1	1

Scaling of root reinforcement

The positions, dimensions, and species of 54 trees along the scarp of the Vinchiana landslide were recorded. This information was combined with pedological and eco-hydrological data to estimate the root distribution on the slope. In the absence of validation data for different species, we neglected differences between various species. Based on the root distribution information we calculated the maximal tensile strength of the bundle of roots at different distances from tree stem. Considering the different tree dimensions and distances from tree stems, the patterns of root reinforcement were calculated and visualized with a GIS program (ArcGIS from ESRI) on the entire slope. The raster cells have a resolution of 1 m2 . For the final calculation of root reinforcement we used the FBM and considered the peak tensile strength of the bundle of roots as representing the contribution of roots to lateral reinforcement. We extended the fiber bundle model proposed by Pollen et al. [2004] by introducing a strain step loading (instead of stress step loading) and considered variation in the root Youngs modulus as a function of root diameter. An important aspect to keep in mind is that this peak value is reached at different displacements depending on the characteristics of the root distribution. With this method we were able to quantify the variation in the maximum root reinforcement along the scarp (Figures. 6.2 and 6.4) based only on the trees standing on the slope; no information was available to reconstruct the original distribution of vegetation cover that existed prior to the landslide.

Slope stability calculations

We implement limit equilibrium assumptions for an infinite slope to compute slope stability [Coppin and Richards, 1990; Schmidt et al., 2001]. The failure condition was quantified using the MohrCoulomb criterion. The inclusion of lateral root reinforcement in slope stability calculations was achieved by considering an additional stabilizing force proportional to the scarp surface and to the mean root reinforcement (Figure 6.4). Additionally, we computed the force balance for different landslide shapes (varying the ratio between the two principal axes L and l in Figure 6.2) and dimensions. The standard formulation of the limit equilibrium equation for the infinite slope is

$$SF = \frac{A\tau_{bas.}}{F_{par.}} \tag{6.3}$$

where SF is the safety factor, A is the landslide area (m^2), $\tau_{bas.}$ is the

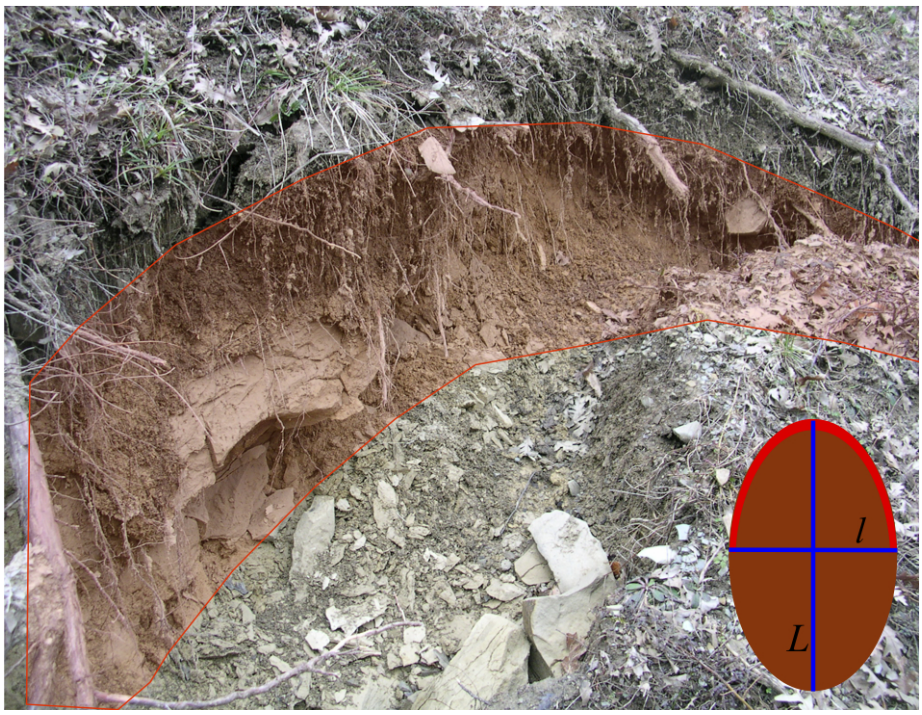

Figure 6.2: Illustration of the lateral area of the scarp (in red) considered to influence the stability of the landslide through tensile root reinforcement. The lateral area is related to an elliptic shape with horizontal and vertical axes l and L, respectively. (For interpretation of the references to color in this figure legend, the reader is referred to the web version of the article).

shear strength at the slip interface (kPa), and $F_{par.}$ is the destabilizing force parallel to slip interface. The modified formulation of the limit equilibrium equation for a safety factor SF considering lateral root reinforcement is

$$SF = \frac{A\tau_{bas.} + F_{tot.veg.}}{F_{par.}} \tag{6.4}$$

including the terms for lateral and basal forces, $F_{lat.veg.}$ and $\tau_{bas.}$, and the driving force $F_{par.}$. Below the expressions for the various forces and strengths are listed:

$$F_{par.} = [(Ah)\,\gamma g sin\beta] + (Am_{veg.} g sin\beta) \quad [kN] \tag{6.5}$$

$$F_{lat.veg.} = \frac{Lateral\,Area}{2} c_{lat.} \quad [kN] \tag{6.6}$$

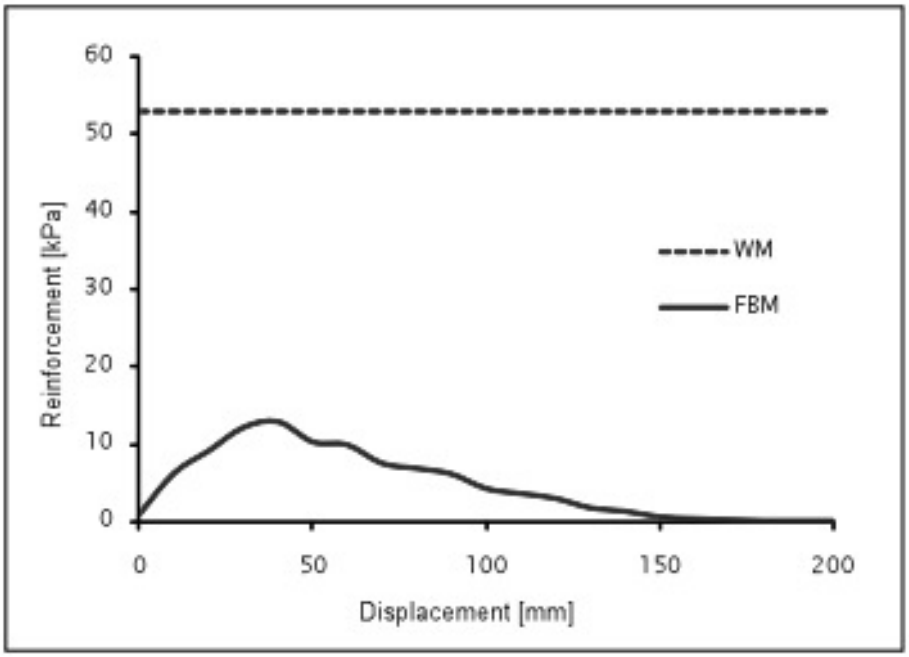

Figure 6.3: Example of tensile strength of a bundle of root as a function of displacement. The graphic shows the difference between the use of the Wu model (Wu) and the fiber bundle model (FBM).

$$\tau_{bas.} = c + \sigma' tan\phi' \quad [kPa] \tag{6.7}$$

$$c = c_s + c_{bas.veg.} \quad [kPa] \tag{6.8}$$

where

$$\sigma' = \sigma - u \quad [kPa] \tag{6.9}$$

is the effective normal stress and
σ = total normal stress [kPa]

u = pore water pressure [kPa]

ϕ' = residual friction angle [^{o}]

A = basal area [m^2]

h = soil depth $[m]$, perpendicular to the slope

γ = soil bulk density $[t/m^3]$

β = slope angle $[^o]$

$m_{veg.}$ = weight of vegetation cover $[t/m^2]$

c_s = residual soil cohesion [kPa]

$c_{lat.veg.}$ = lateral root reinforcement [kPa]

$c_{bas.veg.}$ = basal root reinforcement [kPa]

g = gravitational acceleration $[m/s^2]$

The main assumption for the implementation of root reinforcement in the slope stability calculations is that roots along the scarp were subjected to similar displacement. In reality, roots on the upper part of the scarp are activated before roots located on the sides of the landslide scarp. Figure 6.5 shows how lateral root reinforcement influences the stability of a landslide as a function of the landslide dimension. The FBM was applied considering a series of static strain-controlled loading of a bundle of roots containing roots with different properties (e.g., Youngs modulus and maximum tensile strength, which varies as a function of root diameter) to quantify the bundle stressstrain behaviour. We considered infiltrating water into the profile to have a twofold effect on slope stability: increasing the soil bulk density (from 1.4 g/cm2 in dry condition to 2.1 g/cm2 in saturated condition) and weakening the shear strength of the soil material.

6.4 Results

Root reinforcement

Figure 6.3 shows the value of root reinforcement for a hypothetical root distribution for the Wu model [modified by Wu et al., 1988] and the extended FBM as a function of pullout displacement. The WM estimation results in a constant value of reinforcement of about 3850 kPa, while the result of the modified FBM shows a strong dependence on displacement and a maximal peak value of about 14kPa. The distribution of the maximal root reinforcement calculated with the FBM for the landslide scarp in Vinchiana

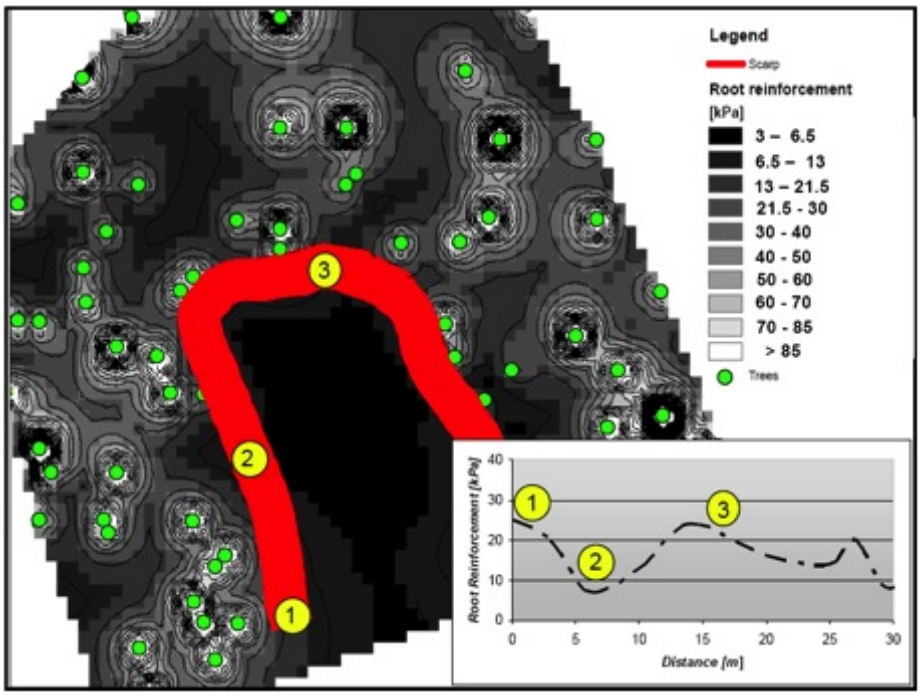

Figure 6.4: Plan view of the root reinforcement distribution along the landslide scarp. Yellow circles help to locate the information in the inset; the inset shows the root reinforcement variability along the scarp calculated with FBM.

is illustrated in Figure 6.4. The values of maximal root reinforcement in the stand range between 0 and 100 kPa and between 5 and 25 kPa along the scarp.

Effects of lateral reinforcement

Figures 6.5 and 6.6 show the results based on the implementation of lateral reinforcement in our model and its influence on slope stability. Results in Figure 6.5 depict the force balance for different dimensions of landslides. The point where the two curves cross defines the dimension at which a slope become unstable. Figure 6.6 presents the same results in terms of variation in the safety factor (SF). This scenario is illustrated by plotting the value of SF versus hypothetical landslide dimension: the slope becomes unstable and a landslide occurs for size with a value of SF below 1.

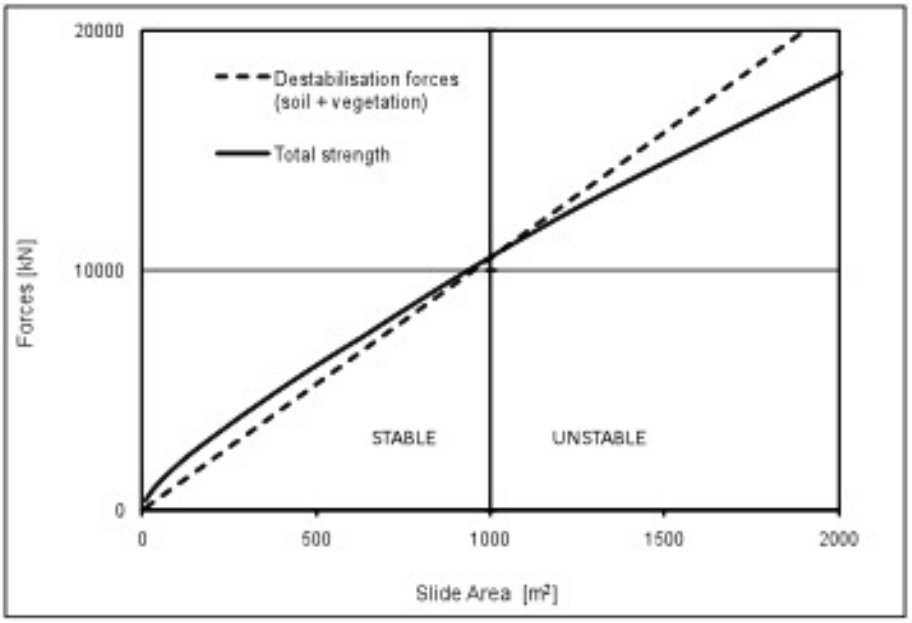

Figure 6.5: Example of a force balance for an elliptical landslide (see Figure 6.2) as a function of landslide dimension. The dotted and continuous lines represent the destabilization and stabilization forces, respectively.

Back analysis of pore-water pressure and root reinforcement

It is not surprising that the most uncertain values of the parameters used for the back analysis were those related to hydrology and root reinforcement. For the calculation we considered two scenarios: (1) and (1bis) complete saturation, and (2) unsaturated conditions using the mean estimated value of lateral root reinforcement (14 kPa). In the first cases 1 and 1bis we assumed that all the entire soil profile was saturated and we estimated (by inversion) the basal and the lateral root reinforcement, respectively, needed to attain the limit equilibrium. In the second case (2), we assumed that no roots crossed the slip surface and only lateral roots contributed to slope stabilization. Table 6.2 (in italics) shows the measured values used for the analysis and the values of basal and lateral root reinforcement obtained from the back analysis. These values likely represent extreme conditions that could have taken place during the landslide. More realistically, the values of the parameters at the time of landslide triggering may have fallen somewhere in between calculated values for saturated and unsaturated conditions. Figure 6.7 shows the critical pore-water pressure (resulting in SF

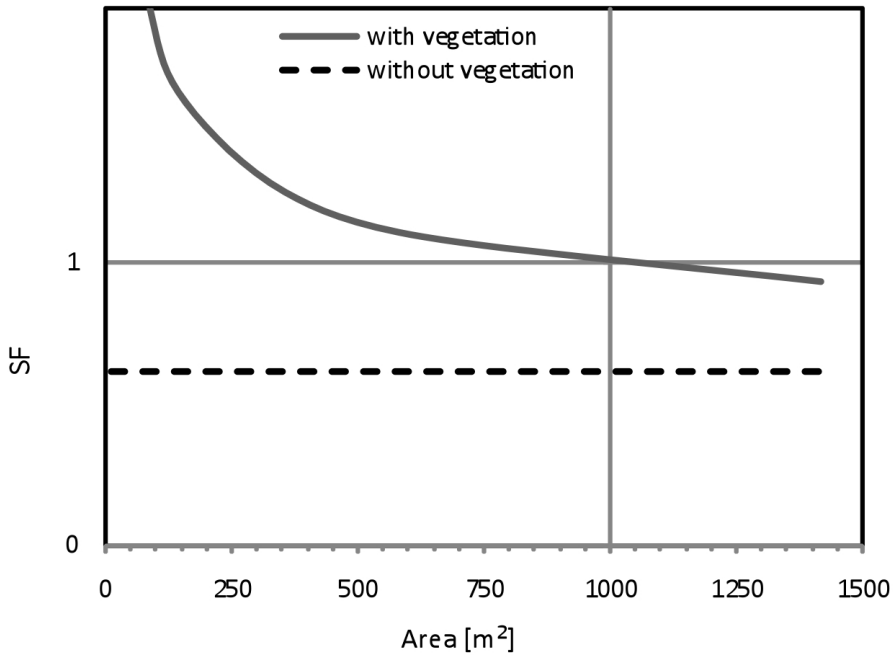

Figure 6.6: Variation in the safety factor (SF) as a function of landslide area for an elliptical landslide assuming pore-water pressure of 1 kPa (saturation 10%), with and without vegetation. SF greater then 1 means stable, while SF smaller then 1 means unstable.

= 1) back calculated for several combinations of parameters (basal and lateral root reinforcement values). Considering low basal root reinforcement because only a few roots crossed the slip surface, with lateral root reinforcement ranging between 10 and 15 kPa, we can identify from the graph a plausible combination of values which suggests pore-water pressures in the range of 0.53 kPa, corresponding to a seepage height of 50300 mm with respect to the slip surface (530% saturation). Table 6.2 values of the parameter used for the back analysis, considering three conditions: saturated profile with basal root reinforcement only, saturated profile with lateral root reinforcement only, and unsaturated condition with lateral root reinforcement only. In bold imposed values and in italics back calculated values.

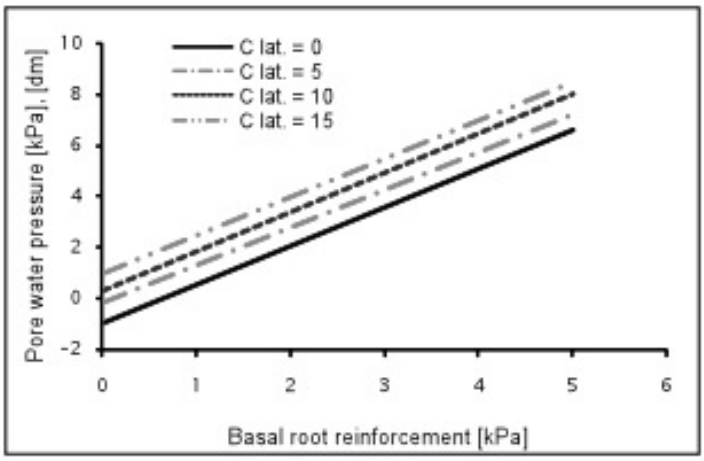

Figure 6.7: Several combinations of back calculated values for root reinforcement and pore-water pressure in limit equilibrium conditions (SF = 1) for the Vinchiana landslide. Clat in the legend is the value of lateral root reinforcement in kPa.

6.5 Discussion

The introduction of the FBM concept for the quantification of root reinforcement in soils [Pollen and Simon, 2005] improved our understanding of the mechanical behaviour of rooted soils during failure. The FBM [Kun et al., 2007] used in this work gives results in accordance with data from literature for the quantification of the correction factor k" (Table 6.1). A longstanding issue for the application of this approach to slope stability is limited availability of root distribution data. Field estimation of root distribution on vegetated slopes is difficult and better techniques are needed. Despite this shortcoming, the root distribution model used here was in good agreement with existing field data and was used to calibrate our model. Neglecting differences between tree species in the estimation of root distribution may have an important influence on calculated root reinforcement in specific situations. In our case study, however, the forest stand was dominated by Chestnut trees (70%) and thus variations among species may not play an important role in these particular slope stability calculations. The absence of data for trees distribution and composition present on the slide area before the event would clearly result in an underestimation of root density along the scarp. This problem could be circumvented by increasing availability of airborne data (LiDAR, aerial photos, DEM, picture, etc.) or other types of inventories often collected in areas susceptible to landslides.

In our case, we should keep in mind that the estimation of lateral root reinforcement is underestimated because we considered only the influence of the vegetation present on the upper part of the landslide scarp, and that the real values of lateral root reinforcement could probably range between 15 and 20 kPa (instead of the calculated value of 14 kPa) if the vegetation on the landslide would be considered too. Thus, pore-water pressure needed to trigger the landslide could reasonably have been as high as 24 kPa. The simplifications made in the slope stability model may, on the other hand, cause an overestimation of the effects of root reinforcement and a consequent increased stability, as was previously discussed in Section 2. Based on the calculations presented herein, about 1 kPa of mean pore-water pressure (saturation 10%) was required to trigger the Vinchiana landslide, a plausible value considering the amount of rain (intensity and cumulative) and the hydrological properties of the soil. The presence of an asphalted road about 100 m above the slide area contributed to the local amount of inflow, increasing the building up of pore-water pressure. Under natural rainfall events, water may accumulate differentially in various locations on the slope resulting in local destabilization of different dimensions (based on subsurface conditions, local topography, etc.). This local hydrologically induced instability may be contained through lateral stabilizing forces to a certain dimension (volume or area) where additional increase results in failure and landslide triggering. The use of the classical WM for estimation of lateral root reinforcement [Wu et al., 1979], would have resulted in overestimated stabilization forces leading to an error of about 10% in the calculation of the safety factor. This error would have increased exponentially for smaller landslides, as illustrated in Figure 6.5. This error would be even higher with Wus estimation for basal root reinforcement, particularly if this parameter exceeded 5 kPa. Not considering root reinforcement or suction, it would have required more than 1 kPa of mean basal cohesion (suction or cementation) to stabilize the landslide footprint. If the lateral effects of root reinforcement or suction were omitted the result would be that the area needed more than 1 kPa of mean basal cohesion (either suction or cementation) to be stable. It is important to point out that the maximum root reinforcement operates in a range of 05 cm of displacement (depending on the root distribution), while cementation or suction act at much smaller displacement (a few millimeters). This scale mismatch implies that root reinforcement acts at different time scales and has effects of different magnitudes compared to suction or cementation. In our case study, root reinforcements at different displacements have values between 0 and 20 kPa. Suction in sandy soils has values between 0 and 2 kPa when (tensile) displacement range is between 0 and 2mm [Richefeu et al., 2007;

Pierrat and Caram, 1997; Goulding, 2006]. For displacement values exceeding 15cm, soil strength imparted by root reinforcement is the primary lateral stabilization mechanism on scarp (see Figure 6.3). On the slip surface the situation is different. The root reinforcement has to be added to the residual shear strength of the soil material and eventually to suction forces in the case of unsaturated conditions (but in the case of rainfall-triggered landslide we often have saturated conditions). Not considering dilatationconsolidation or cementation effects would influence the calculation in the range of small displacement (a few millimeters). In our case these effects do not influence the results because we consider a force balance calculation for displacement between 1 and 5 cm, which is a typical range of displacement at which rooted soils reach their maximum shear and tensile strength [Zhou et al., 1998]. Assuming that the initial few centimeters of soil deformation are slow means we can neglect kinetic energy effects. Considering that natural systems are continuously subjected to cyclic stresses (due to rainfall, snow melt, daily and seasonal temperature oscillations, atmospheric pressure oscillations, etc.) and that they adjust accordingly (at various time scales) to the new equilibrium conditions, we can imagine that different zones on a slope are under particular stressstrain conditions at different times. In the case of the Vinchiana landslide we can hypothesize that less than 2 cm of displacement were needed to reach the critical equilibrium of forces, because, under dry conditions, equilibrium would be reached at a root-soil strength corresponding to a displacement of about 23 cm (depending on local soil characteristics and root distribution).

6.6 Summary

In this work we discussed quantitatively the role of lateral root reinforcement in vegetated slope stability using the FBM formalism. A key outcome of the model is that we can quantify and interpret the overestimation of k?? often observed in calculations based on the well-known Wu model [Wu et al., 1979, 1988; Waldron and Dakessian, 1981]. The results of the slope stability calculations considering lateral root reinforcement show quantitatively the importance of this parameter in relation to the dimension of the landslide area. The stabilization effect of lateral roots was shown to be important for landslides with areas up to 1000 m^2 ($1.8 > SF > 1$) (see Figure 6.6). This information provides guidance concerning the scale at which vegetation can contribute to lateral redistribution of destabilizing forces on the slope. Neglecting lateral root reinforcement would result in safety factors SF in dry conditions of 0.94 for landslides of any size. Another important result of

the model is the quantification of stressstrain behaviours of a bundle of roots. These stressstrain curves elucidate the role of root reinforcement in comparison with other factors such as suction, cementation, or soil friction. We show that root reinforcement acts in a range of a few centimeters of lateral displacement (depending on the root distribution) while suction and cementation act in a much smaller range of a few millimeters.

6.7 Acknowledgements

We thank the CCES [Competence Center Environment and Sustainability] platform of the Swiss Federal Institute of Technology for funding the TRAMM project [Triggering of Rapid Mass Movements], all partners of the project, Manfred Stähli, Christian Rickli and Albert Böll for many constructive discussions.

6.8 References

Anderson, C. J., M. P. Coutts, M. N. Ritchie, and D. J. Cambell (1989), Root extraction force measurements for sikta spruce, *Forestry*, *62(2)*, 127-137.

Bathurst, J. C., G. Moretti, A. El-Hames, S. Begueira, and J. M. Garzia-Ruiz (2007), Modelling the impact of forest loss on shallow landslide sediment yield, Ijuez river catchment, Spanish Pyrenees, *Hydrol. Earth Syst. Sci.*, *11(1)*, 569-583.

Bischetti, G. B., E. A. Chiaradia, T. Limonato, B. Speziali, B. Vitali, P. Vullo, and A. Zocco, A. (2005), Root strength and root area ratio of forest species in Lombardy (Northern Italy), *Plant Soil*, *278*, 11-22.

Casadei, M., and W. E. Dietrich (2003), Controls on shallow landslide width. In: Rickermann, D., Chen, C. (Eds), Debris-Flow Hazards Mitigation: Mechanics, Prediction, and Assessment. Proceedings of the Third International Conference on Debris Flows Hazards Mitigation, Davos, Switzerland. Millpress, Rotterdam, pp. 91-102. http://eps.berkeley.edu/?bill/papers/117.pd

Casadei, M., W. E. Dietrich, and N. L. Miller (2003), Testing a model for predicting the timing and location of shallow landslide initiation in soil

mantled landscapes, *Earth Surf. Process. Land. 28(9)*, 925-950.

Coppin, N. J., and I. G. Richards (1990), Use of Vegetation in Civil Engineering, *Butterworth*, London, p. 272.

De Baets, S., J. Poesen, B. Reubens, K. Wemans, J. De Baerdemaeker, and B. Muys (2008), Root tensile strength and root distribution of typical Mediterranean plant species and their contribution to soil shear strength, *Plant Soil*, *305*, 207-222.

Dietrich, W. E., J. McKean, D. Bellugi, and J. T. Perron (2008), The prediction of shallow landslide location and size using a multidimensional landslide analysis in a digital terrain model. Proceedings of the Fourth International Conference on Debris-Flow Hazards Mitigation. ¡http://www-eaps.mit.edu/ faculty/perron/files/Dietrich08.pdf¿.

Docker, B. B., and T. C. T. Hubble (2008), Quantifying the enhanced soil shear strength beneath four riparian tree species, *Geomorphology*, *100*, 400-418.

Fan, C. C., and C. F. Su (2008), Role of roots in the shear strength of root-reinforced soils with high moisture content, *Ecol. Eng.*, *33*, 157-166.

Goulding, R. B. (2006), Tensile Strength, Shear Strength, and Effective Stress for Unsaturated Sand Dissertation. University of Missouri, Columbia.

Gray, D. H., and H. Ohashi (1983), Mechanics of fiber reinforcement in sand, *J. Geotechnol. Eng.*, *109*, 335. doi:10.1061/(ASCE)0733-9410(1983)109:3(335).

Hillel, D. (2004), Water Dynamics in Plant Production, Book Review. CAB1 Publishing.

Kokutse, N., T. Fourcaud, K.Kokou, K. Neglo, and P. Lac (2006), 3D numerical modelling and analysis of the influence of forest structure on hill slopes stability. In: Marui, H., Marutani, T., Watanabe, N., Kawabe, H., Gonda, Y., Rimura, M., Ochiai, H., Ogawa, K., Fiebiger, G., Heumader, J., Rudolf Miklau, F., Kienholz, H., Mikos, M. (Eds.), Disaster Mitigation of Debris Flows, Slope Failures and Landslides. Universal Academy Press, Inc., Tokyo, Japan, pp. 561-567 (Interpraevent, September 2527 2006, Niigata, Japan).

Kun, F., F. Raischel, R. C. Hidalgo, and H. J. Herrmann (2007), Extensions of fibre bundle models. *Lect. Notes Phys.*, *705*, 57-92.

Mickowski, S. B., A. G. Bengough, M. F. Bransby, M. C. R. Davies, P. D. Hallett, and R. Sonnenberg (2007), Material stiffness, branching pattern and soil matric potential affect the pullout resistance of model root system, *Eur. J. Soil Sci.*, *58*, 1471-1481.

Peires, F. T. (1926), Tensile tests for cotton yarns. v.the weakest link, theorems on the strength of long composite specimens, *J. Textile Inst.*, *17*, T355-368.

Pierrat, P., and H. S. Caram (1997), Tensile strength of wet granular materials, *Powder Technol.*, *91*, 83-93.

Pollen, N., A. Simon, and A. J. C. Collison (2004), Advances in assessing the mechanical and hydrologic effects of riparian vegetation on streambank stability. In: Bennett, S., Simon, A. (Eds.), Riparian Vegetation and Fluvial Geomorphology, *Water Science and Applications*, *8*, AGU, 125-139.

Pollen, N., and A. Simon (2005), Estimating the mechanical effects of riparian vegetation on stream bank stability using a fiber bundle model, *Water Resour. Res.*, *41*, W07025.

Pollen, N. (2007), Temporal and spatial variability in root reinforcement of streambanks: accounting for soil shear strength and moisture, *Catena*, *69*, 197-205.

Preti, F., (2006), Stabilit dei versanti vegetati. Cap. 10, in Manuale 3 dIngegneria Naturalistica Sistemazione dei versanti. Regione Lazio, Roma (in Italian) http://www.regione.lazio.it/web2/contents/ingegneria naturalistica/manuale versanti/Cap 10 10.pdf.

Preti, F., and F. Giadrossich (2009), Root reinforcement and slope bioengineering stabilization by Spanish Broom (*Spartiumjunceum* L.). *Hydrol. Earth Syst. Sci. Discuss.*, *6*, 3993-4033, http://www.hydrol-earth-syst-sci-discuss.net/6/ 3993/2009/hessd-6-3993-2009.html.

Preti, F., and M. Schwarz (2006), On root reinforcement modelling, *Geophysical Research Abstracts*, *8*, EGU General Assembly 2006, 27 April,

ISSN: 1029-7006.

Reneau, S. L., and W. E. Dietrich (1987), Size and location of colluvial landslides in a steep forested landscape. In: Erosion and Sedimentation in the Pacific Rim, Proceed- ings of the Corvallis Symposium, IAHS Publ. no. 165.

Richefeu, V., M. S. El Youssoufi, and F. Radja (2007), Shear strength of unsaturated soils: experiments DEM simulations and micromechanical analysis. In: Schanz, T. (Ed.), Theoretical and Numerical Soil Mechanics. Springer.

Roering, J. J., K. M. Schmidt, J. D. Stock, W. E. Dietrich, and D. R. Montgomery (2003), Shal- low landsliding, root reinforcement, and the spatial distribution of trees in the Oregon Coast Range, *Can. Geotech. J.*, *40*, 237-253.

Schmidt, K. M., J. Roering, J. Stock, J. D. Dietrich, W. E. Montgomery, and D. R. T. Schaub (2001), The variability of root cohesion as an influence on shallow landslide susceptibility in the Oregon, *Coast Range. Can. Geotech. J*, *38*, 995-1024.

Schwarz, M., and F. Preti (2007), The influence of root reinforcement depending on the shape and the dimension of shallow landslides, *Geophysical Research Abstracts*, *vol. 9*, 00257, 2007. The role of vegetation in slope stability, EGU General Assembly 2006, 1520 April 2007, ISSN: 1029-7006.

Sidle, R. C., and W. Wu (2001), Evaluation of the temporal and spatial impacts of timber harvesting on landslide occurrence, *Water Sci. Appl.*, *2*, 179-193.

Shewbridge, S. E., and N. Sitar (1989), Deformation characteristics of reinforced sand in direct shear, *J. Geotech. Eng.*, *115(8)*, 1134-1147.

USDA, 1998. Keys to Soil Taxonomy, 8th ed. U.S. Department of Agriculture, Soil Survey Staff, Natural Resources Conservation Service, Washington, D.C, 326 pp.

Waldron, L. J., and S. Dakessian (1981), Soil reinforcement by roots: calculation of increased soil shear resistance from root properties, *Soil Sci.*, *132*, 427-435.

Wu, T. H., W. P. McKinnell, and D. N. Swanston (1979), Strength of tree roots and landslides on Prince of Wales Island, Alaska, *Can. Geoth. J.*, *16*, 19-33.

Wu, T. H., M. McOmber, R. T. Erb, and P. E. Beal (1988), Study of soilroot interaction *J. Geotech. Eng.*, *114*, 1351-1375.

Zhou, Y., W. D. Li, and Y. X. Cheng (1998), A case study of effect of lateral roots of *Pinusyunnanensis* on shallow soil reinforcement, *Forest Ecol. Manage.*, *103*, 107-120.

Chapter 7

Discussion and Conclusions

The details of the research presented in this work show that the topic of quantification of root reinforcement in vegetated slopes claims big challenges in terms of multidisciplinary (from physics to biology, and from engineering to forest sciences). Moreover, this study represents the first attempt in its field to draw a consistent upscaling of the involved processes over a wide range of spatial scales (from local root-soil interface interactions to hillslope scale). Research presented in Chapters 2 through 6 provide new insights into root mechanics and root reinforcement for vegetated slopes. Results ameliorate and extend earlier work on these topics. Specifically, our work can be discussed considering the two main outcomes: (1) Failure of root bundles is progressive and mobilization of root strength is a strong function of displacement and hence failure is a very displacement dependent process; (2) Spatial characterization of lateral roots at the stand scale is needed for a realistic estimation of the mechanical effects of roots on slope stability.

(1) **Roots in bundles fail progressively**. Our description of root bundles mechanics based on fiber bundle model concepts (the Root Bundle Model) describe with minimal input data the behavior of roots in soil under tensile loading. Our results show that equating root reinforcement to a unique apparent cohesive term valid over all displacements is incorrect. In Chapters 5 and 6 we showed that maximal root reinforcement takes place at a few centimeters of displacement (the exact value depends on the root diameter distribution of the bundle). Thus, root reinforcement cannot simply be added to the soil lateral cohesion, as often done in infinite limit equilibrium calculations. This is because the maximum tensile cohesive strength of soil due to suction and cementation operates at displacements of only a few millimeters, an order of magnitude less than roots.

Our analysis of root bundle mechanics also shows the precise geometrical

and mechanical conditions under which a certain class size of roots is prone to break or slip out of the soil. While Schmidt et al. [2001] report that bigger roots tend to slip out and smaller roots tend to break, Pollen and Simon [2005] show, through simple calculations and pullout experiments, the exact opposite. Our numerical simulations yielded both cases depending on geometrical and mechanical properties of roots and soil. For instance, just considering the non linear relation between the root diameter and the root length (see Figure 3.3), it is possible to demonstrate that both conditions are plausible (fine roots slip and coarse roots break, versus fine roots break and coarse roots slip).

For the first time our study quantified experimentally the influence of soil water content on the root-soil interface friction, showing that pullout forces of roots are low influenced by the water content of the tested soil (loamy soil). These results may differ a lot considering different types of soil. Further research is needed to quantify this aspect. Considering the outcomes of our experiments it can be argued that the wetting process during rainfalls and the related weakening effects on root reinforcement is not the dominant factor that causes the triggering of a shallow landslide. More realistically it is the change in the strength and plasticity of the soil matrix that causes the triggering of the shallow landslides. For instance, studies on the compression strength of soil aggregates show that the maximum rupture energy does change one order of magnitude with water content [Munkholm et al., 2007], and similar behaviour is observed for the residual and maximal shear strength of soil [Lu and Likos, 2006]. However, even a small variation in soil moisture can lead to a change in the type of failure of a single root (slipping instead of breaking). The combination of abrupt failures of breaking roots and the residual reinforcement imparted by slipping roots results in different macroscopic behavior of a bundle, depending mainly on root size distribution and soil matrix conditions. Variation of soil moisture may lead in this case to big differences in the global pull out behaviors of a bundle of roots, particularly when small roots outnumber coarse roots (as is the case in real situations). Generally speaking, roots in wet soil (60% to 100% degree of saturation) slip out instead of breaking, show a smaller resistance to pullout and a higher displacement at maximal pullout force. These effects of soil moisture on the global behavior of a bundle are strongly influenced by root size distribution: it is possible that the maximal pullout resistance is slightly higher in wet soil than in dry soil because of the residual strength of small roots (see chapter 3). These different types of macroscopic behaviors have an important meaning to landslide triggering dynamics in which the activation or failure of certain classes of roots across a tension crack may slow down and suppress a landslide or abrupt

failure.Further investigations are needed, however, in order to more fully test this hypothesis.

A possible limitation of the presented RBM is due to the consideration of conditions where roots are pulled out of a soil mass. In reality, there are cases where in certain zones of a slope, it is the soil mass that moves apart from fixed root bundles (as in the case of a tree standing on the upper side of a tension crack). No previous studies have considered this scenario and further research is needed to clarify this aspect. From field observations and considering the volumetric strain of failing soil mass, it is possible to formulate the hypothesis that root bundles pulled out from stable soil matrix have higher maximum strength than root bundles slipping out from failing soil matrix.

Another limitation of the RBM model is that it considers only a quasi-static strain load. This condition may be realistic for zones of vegetated slope where the propagation of tension cracks starts in the early stages of the failure of a landslide. The application of the RBM in the case of fast loading rates, like in the case of zones in the bottom part of a landslide, may lead to false estimations. Considering the behavior of root reinforcement under different loading rates represents and important field of research also for other processes influencing tree stability like wind solicitation [Vanomsen, 2006] and the impact of rockfall [Jonsson, 2007]. The study of these processes represents a big challenge for the future research. Moreover, the influence of combined stresses due to landslide and wind solicitations on the root bundles and consequently on the stability of a slope remains to be studied.

In practical applications, a simplified version of the RBM that avoids complications due to slip out of roots may be sufficient (see Chapter 6). The estimation of root distribution still remains a challenge and must be addressed in future studies as it has a large influence on the predicted magnitude of root reinforcement. The root distribution model presented in this work (Chapters 3 and 6) is based on simple assumptions, but has the important advantage of considering only the maximum root size as a function of tree size, and the distance from it. Both quantities (tree size and tree position) are easily measurable, possibly by means of light detection and ranging (LIDAR). Moreover, the model may be easily calibrated for different locations and tree species using only two parameters (pipe coefficient and mean root branching distance). Despite this simplification, more field data and case studies are desired for further validation of the model and for future model extensions.The modeling of root distribution at different scales represents an important element for the spatial characterization of root reinforcement and it is one of the most promising research topics for

improving model results and capabilities. For instance, only few quantitative data are available to show the influence of soil depth and compaction on the rooting depth of different types of trees. Moreover, few studies were undertaken to study and quantify the intra- and interspecific competition of neighbor root systems. In this context, there are no studies that consider the effects of biodiversity in terms of increased root reinforcement due to the spatial niche differentiation of root distribution of different tree species. Furthermore, the fact that the mass distribution of fine roots depends on growth and death of individual root tips with relatively high turnover rate [Majdi et al., 2005; Borja et al., 2008] depending on local conditions [Johnsen et al., 2005] and season, may also represent an important research area relevant to root reinforcement quantification. Finally, data on rate of root decay after thinning measures are needed to implement the time evolution of root strength for different scenarios of forest management.

(2) **Spatial characterization of lateral roots at the stand scale is needed for a realistic estimation of the mechanical effects of roots on slope stability**. Our study focused on lateral roots instead of basal roots because numerous field evidences indicate that the majority of roots on landslide scarps are oriented roughly parallel to the ground surface and located within the upper 0.5–1 m of the colluvium [Schmidt et al., 2001; Roering et al., 2003]. Based on this observations, our modeling framework presented in Chapter 1 and 6 represents a new methodology for the spatial characterization of lateral root reinforcement that can be upscaled at the hillslope scale. The limitation of the proposed framework lies in the parameterization and computational burden; hence it would be limited to small-scale applications (forest stand or hillslope) and would not be suitable for an entire catchment. Nevertheless, coupling information on soil thickness, topography and hydrology would make it possible to better define mass and shape of potentially unstable zones.

As discussed in Schmidt et al. [2001], assessing shallow landslide susceptibility in forested hillslopes with different land-use histories requires knowledge of the spatial variability of root cohesion and vegetation age. However, studies on the influence of vegetation cover on the pedological evolution of the soil are still missing. In slope stability models, spatial and temporal variability of root cohesion greatly affect the outcome. When comparing predictions of regional slope stability to mapped landslides resulting from a given storm, site-specific variations of not only root reinforcement but also variations in soil depth, material properties, and hydrologic routing, strongly influence the outcome of the results. Hence, a detailed spatial characterization of root distribution will yield a better estimation of the

location and the magnitude of the landslide event. These results are also needed because they are fundamental inputs to other dynamic models that consider the runout of debris flow which are strongly influenced by the initial triggered volume [Christen et al., 2007; Beguería et al., 2009].

Rickli et al. [2002] showed that the volumes of landslides are usually bigger in forest stands than in open meadows because of the effect of root reinforcement. Calculations in Chapter 6 explain and confirm quantitatively the results of Rickli et al. [2002]. However, the number of landslides in forests or in meadows can vary depending on catchment characteristics and on the rainfall event. Rickli and Graf [2009] showed that shallow landslides in forests occur generally on steeper slopes ($>35^o$) than in meadows (25–35^o). Moreover, Rickli et al. [2002] also showed that within a forest, the susceptibility to landslides strongly depends on the condition of the forest structure: the probability to have a landslide in a well-structured forest with a canopy cover larger than 80% is 10 times less than in a poorly-structured forest with a canopy cover that is less than 30%. The application of the methodology presented in Chapters 5 and 6 for typical conditions of vegetated hillslopes, such as described by Rickli and Graf [2009], gives, for the first time, the possibility to quantitatively define the limits of lateral root reinforcement. The results show that in the best cases forests with a minimal lateral root reinforcement of 5 kPa may stabilize landslides with volumes up to 1000 m^3.

The results shown in Chapters 5 and 6 indicate that the variability of root reinforcement within a forest stand is high but that a simplified calibrated model can yield a good estimation of root distribution. The simplified version of the Root Bundle Model also gives a good spatial characterization of the dynamics of root reinforcement at the scale of a forest stand. These results make apparent that a simple infinite slope equilibrium approach for estimating slope stability is limited because that approach fails to include the dynamic of the failure process. However, while research should pursue this path to obtain a better description of the triggering mechanisms of shallow landslides, for practical application the classic infinite slope approach still represents a simple suitable method that needs to consider the variability and dynamic of root reinforcement, at least from a conceptual point of view (as shown in chapter 6). In particular, it is important to highlight how the results presented in this work and the field observation suggest that maximum root reinforcement represent only part of the contribution of roots to slope stability and that the change in stiffness of the rooted soil could have a large influence on the triggering mechanisms of shallow landslides. For instance, the application of simple fracture mechanics principles shows that even large root reinforcement may trigger

small landslides if the stiffness of the rooted soil is low; vice versa, if the rooted soil is suffiently stiff, even low values of maximum root reinforcement may stabilize big volumes of soil. The implementation of this aspect in new modeling approaches represents a big challenge for further research.

In conclusion, this thesis investigated in details the triggering mechanisms of shallow landslides in vegetated hillslopes with specific emphasis on the mechanical effects of root reinforcement. The approaches used in this research to quantify and understand triggering mechanisms are based on physically-based models that strike a compromise between too much complexity that require large input data sets difficult to obtain, and over simplification of physical processes. The presented modeling framework considers a fully spatial distributed approach for the upscale of root reinforcement quantification from single root to hillslope scale. In this regard we agree with the statement of van Asch et al. [2007] , which suggest that physically-based models do not have to be complete and perfect, they only have to be adequate for the purpose of hazard assessment. Our work represents a good example of how physical models may be used to understand the mechanics of the fundamental processes and how accurate model simplifications may be applied in practice. We believe that the results of this work will contribute to a better understanding of the triggering mechanisms of shallow landslides and will help practitioners for assessing shallow landslides, manage protection forests, and plan bioengineering measures. For instance, the use of extended slope stability models that consider the spatial distribution of vegetation will allow not only a better estimation of the timing, location and dimension of shallow landslides, but it also will allow a quantitative evaluation of the protection function of forests, thus a cost/benefit analysis too. This kind of quantitative instrument represents today an important tool for decision makers to justify strategic political decisions. Furthermore, the combination of such slope stability analysis for vegetated slope with forest growth models would allow to extend the predictions to longer time scales. The possibility to simulate the evolution of future slope stability scenarios in vegetated slopes represents a powerful tool for efficient planning in forest and landscape management.

7.1 References

Beguería, S., Th. W. J. Van Asch, J.-P. Malet, and S. Gröndahl (2009), A GIS-based numerical model for simulating the kinematics of mud and debris flows over complex terrain, *Nat. Hazards Earth Syst. Sci.*, *9*, 1897-1909.

Christen, M., P. Bartelt, and U. Gruber (2007), RAMMS - a Modeling System for Snow Avalanches, Debris Flows and Rockfalls based on IDL, *Photogrammetrie Fernerkundung Geoinformation*, *4*, 289-292.

Lu, N., and W. J. Likos (2006), Suction stress characteristic curve for unsaturated soil, *Journal of geotechnical and geo-environmental engineering*, *2*, 131-141.

Jonsson, M. J. O. (2007), Energy absorption of trees in a rockfall protection forest, Diss. ETH Nr. 17214, Zrich, 222 pp.

Munkholm, L. J., E. Perfect, and J. Grove (2007), Incorporation of Water Content in the Weibull Model for Soil Aggregate Strength, *Soil Sci. Soc. Am. J.*, *71*, 682-691. doi:10.2136/sssaj2006.0038

Pollen, N., and A. Simon (2005), Estimating the mechanical effects of riparian vegetation on stream bank stability using a fiber bundle model *Water Resources Research*, *41*, w07025. doi: 10.1029/2004WR003801.

Rickli, C., K. Zürcher, W. Frey and P. Lüscher (2002), Wirkungen des Waldes auf oberflächennahe Rutschprozesse, *Schweiz. Z. Forstwes.*, *153(11)*, 437-445.

Rickli, C., and F. Graf (2009), Effects of forests on shallow landslides case studies in Switzerland, *For. Snow Landsc. Res.*, *82 (1)*, 3344.

Roering, J. J., K. M. Schmidt, J. D. Stock, W. E. Dietrich, and D. R. Montgomery (2003), Shallow landsliding, root reinforcement, and the spatial distribution of trees in the Oregon Coast Range, *Can. Geotech. J.*, *40*, 237253.

van Asch, T. W. J., J. Malet, L. P. H. van Beek, and D. Amitrano (2007), Techniques, issues and advances in numerical modelling of landslide hazard, *Bull. Soc. géol. Fr.*, *178 (2)*, 65-88.

Vanomsen, P. (2006), Der Einfluss der Durchforstung auf die Verankerung der Fichte hinsichtlich ihrer Sturmresistenz, Diss. ETH Nr. 16532, Zrich, 246 pp.

Schmidt, K. M., J. J. Roering, J. D. Stock, W. E. Dietrich, D. R. Mont-

gomery, and T. Schaub (2001), The variability of root cohesion as an influence on shallow landslide susceptibility in the Oregon Coast Range, *Can. Geotech. J.*, *38*, 995-1024.

Curriculum Vitae

1980
Born in Florence, Italy (August 30th)

1986-1991
Primary School, Scandicci (FI), Italy

1991-1994
Secondary School, Scandicci (FI), Italy

1994-1999
High School, Liceo Scientifico *I. Newton*, Scandicci (FI), Italy

1999-2006
Universitá Statale degli studi di Firenze. Degree in Forest and Environmental Science. Thesis: *Development of plants and soil within the scope of soil bioengineering measures.* Advisor Prof. F. Preti and Dr. F. Graf.

2006
Collaborator at the "*Amt für Wald Graubünden*", Zuoz, Switzerland

2006-2008
Doctoral student in the Laboratory of Soil and Environmental Physics (LASEP) of Prof. D. Or, EPFL, Lausanne, Switzerland.

2008-2010
Doctoral student in the Soil and Terrestrial Environmental Physics (STEP), Institute of Terrestrial Ecosystems (ITES) of Prof. D. Or, ETHZ, Zürich, Switzerland.